

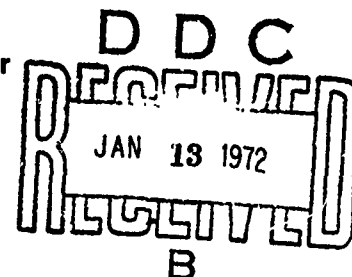
AD743978

CHARACTERIZATION OF WIRE-WOUND TUNGSTEN COMPOSITE

J. G. Hill

F. L. Banta

United Technology Center



TECHNICAL REPORT AFML-TR-71-245

January 1972

Contract No. F33615-70-C-1484

Air Force Materials Laboratory

Wright-Patterson Air Force Base, Ohio

Reproduced by
NATIONAL TECHNICAL
INFORMATION SERVICE
U S Department of Commerce
Springfield VA 22151

DISTRIBUTION STATEMENT A

Approved for public release;
Distribution Unlimited

UTC 2380-FR

196

NOTICES

When U. S. Government drawings, specifications, or other data are used for any purpose other than a definitely related Government procurement operation, the Government thereby incurs no responsibility nor any obligation whatsoever, and the fact that the Government may have formulated, furnished, or in any way supplied the said drawings, specifications, or other data, is not to be regarded by implication or otherwise, or in any manner licensing the holder or any other person or corporation, or conveying any rights or permission to manufacture, use, or sell any patented invention that may in any way be related thereto.

ACCESSION for		
CPSTI	WHITE SECTION	<input checked="" type="checkbox"/>
ROC	DIFF SECTION	<input type="checkbox"/>
IF ANNOUNCED		<input type="checkbox"/>
JUSTIFICATION		
BY		
DISTRIBUTION/ACCOMMODATION CODES		
QST.	AVAIL.	and/or SPECIAL
7		

Don Telleman

CHARACTERIZATION OF WIRE-WOUND TUNGSTEN COMPOSITE

J. G. Hill
F. L. Banta

FOREWORD

This report was prepared by the Materials and Process Branch of United Technology Center, a Division of United Aircraft Corporation, Sunnyvale, California. The work was performed under USAF Contract F33615-70-C-1484. The contract was initiated under Project 7381, "Materials Application," Task No. 738102, "Space and Missile and Propulsion Systems Material and Component Evaluation," and was administered by the Air Force Materials Laboratory, Wright-Patterson Air Force Base, Ohio, Mr. William H. Wheeler (AFML/LAS), Project Engineer.

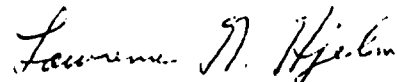
This report covers the work conducted from 1 May 1970 through 30 September 1971 under management of Mr. F. L. Banta, Chief, Metallurgical Engineering, and Mr. J. G. Hill, Project Engineer, Materials and Process Branch. Final preparation of this report is a joint authorship and the major contributors, in addition to Messrs. Banta and Hill, were: J. F. Lagedrost, K. E. Wilkes, and E. A. Eldridge, Thermal Property Testing, Battelle Memorial Institute, Columbus, Ohio; and S. A. Bortz and Y. Harada, Mechanical Property Testing, Illinois Institute of Technology Research Institute.

The authors wish to acknowledge the contribution of the following persons who participated in this program: J. Coy, Applied Space Products, Palo Alto, California and Dr. K. Williams, Stanford University, Palo Alto, California for their aid in the scanning electron microscope and electron microprobe analysis; P. O'Driscoll and P. Henderson, United Technology Center, for structural and thermal analysis; R. Sweig, United Technology Center, for nondestructive test analysis; and D. Trimble, United Technology Center, for metallurgical evaluation.

The contractor's report number is UTC 2380-FR.

The report was submitted by the authors in November 1971.

This technical report has been reviewed and is approved.



LAWRENCE N. HJELM, Chief
Space & Missiles Systems Sup Branch
Materials Support Division
AF Materials Laboratory

ABSTRACT

✓
This program was conducted to determine and extend the potential of wire-wound tungsten composites for analysis, design, and fabrication of rocket hardware through characterization of its mechanical, thermal, chemical, and physical properties.

Specimens, designed specifically for desired structural and thermal analytical properties, were fabricated by previously developed rocket nozzle techniques of plasma-spraying and filament reinforcement. Thermal and mechanical properties were determined for the temperature range of 70° to 4,000°F (21° to 2,210°C). Residual test specimen material was evaluated to characterize physical and chemical properties of both as-composited and elevated temperature exposed wire-wound tungsten. Suitable test methods for nondestructive examinations were determined, and a material specification was prepared based on the program results.

CONTENTS

Section	Page
I INTRODUCTION	1
II SUMMARY	2
III RESULTS AND DISCUSSION	5
1. Specimen Preparation	5
a. Specimen Design	5
b. Raw Materials	11
c. Specimen Fabrication	11
d. Nondestructive Testing	22
2. Thermal Property Tests	37
a. Thermal Test Methods and Results	39
3. Mechanical Property Tests	69
a. Experimental Procedures	69
b. Results and Discussion	80
c. Test Observations	114
4. Physical and Chemical Characteristics	120
a. Density Measurements	120
b. Chemical Analysis and Composition	121
c. Optical and Electron Metallography	125
d. Observations	140
5. Material Specification	144
IV CONCLUSIONS	145
REFERENCES	147
APPENDIX I: Procedures for Preparation of Mechanical and Thermal Property Specimens	148
APPENDIX II: Thermal Conductivity Measurement by the Self-Guarding Disk Technique	169
APPENDIX III: Thermal Diffusivity Measurement	172
APPENDIX IV: Specific Heat Measurement	177
APPENDIX V: Thermal Expansion Measurement	179
APPENDIX VI: Wire-Wound-Tungsten Composite	182

ILLUSTRATIONS

Figure		Page
1	Design of THE Specimen	6
2	Design of Thermal Property Specimen	7
3	Design of Tension Specimen	8
4	Design of TIP Specimen	9
5	Design of IP Specimen	10
6	Setup for Wire-Wound Tungsten Tension Specimen	12
7	Wire-Wound Tungsten Tension Specimen Receiving Helical Reinforcement	13
8	Specimen Blanks for THE Tests	15
9	Thermal Property Specimens	18
10	Completed Wire-Wound Tungsten Tension Specimens	19
11	Wire-Wound Tungsten IPC Specimens	20
12	TIP Specimens	21
13	3,000-Rhm Cobalt 60 Radiograph of THE Specimens	29
14	THE Specimen After 13-Min Neutron Exposure	32
15	THE Specimens Impregnated with Grain Alcohol After 13-Min Neutron Exposure	33
16	Conductivity vs Wall Thickness for Specimens T-5, T-7, THE-1, THE-2, and THE-5	35
17	Conductivity vs Wall Thickness for All Specimens	36
18	Appearance of Tested Wire-Wound Tungsten Specimen	38
19	Steady-State Thermal Conductivity Specimen Assembly	41
20	Thermal Conductivity of Unsintered Wire-Wound Tungsten Composite (Steady-State Measurement)	43
21	Thermal Diffusivity of Unsintered Wire-Wound Tungsten Composite Normal to Wire Direction (Sample 1)	44
22	Thermal Diffusivity of Three Unsintered Wire-Wound Tungsten Composite Specimens Normal to Wire Direction	48
23	Thermal Diffusivity of Wire-Wound Tungsten During Isothermal Anneal at 1,645°C (Sample 2)	50
24	Thermal Diffusivity of Wire-Wound Tungsten During Isothermal Anneal at 1,986°C (Sample 3)	51
25	Enthalpy of Wire-Wound Tungsten Composite in Sealed Container	53

ILLUSTRATIONS

Figure		Page
26	Specific Heat of Wire-Wound Tungsten Composite in Sealed Container	54
27	Specimen and Fixture Assembly for Thermal Expansion Measurement in Axial Direction	56
28	Specimen and Fixture Assembly for Thermal Expansion Measurement in Radial Direction	57
29	Linear Thermal Expansion of As-Composited Tungsten Composite Axial Direction (Specimen 2A)	59
30	Linear Thermal Expansion of As-Composited Tungsten Composite Axial Direction (Specimen 1A, Two Cycles)	60
31	Linear Thermal Expansion of Presintered Tungsten Composite Axial Direction (Specimen 3A)	61
32	Linear Thermal Expansion of As-Composited Tungsten Composite Radial Direction (Specimen 1R)	62
33	Linear Thermal Expansion of As-Composited Tungsten Composite Radial Direction (Specimen 2R, Two Cycles)	63
34	Linear Thermal Expansion of Presintered Tungsten Composite Radial Direction (Specimen 3R)	64
35	Thermal Conductivity of As-Composited Wire-Wound Tungsten Normal to Wire Direction	68
36	Configuration of Tension Test Specimen	71
37	Configuration of IP Test Specimen	72
38	Configuration of Compression Test Specimen	73
39	Configuration of Tension-IP Test Specimen	74
40	Apparatus for Room Temperature Uniaxial Tension Test	75
41	Exploded View of IP Test	77
42	Apparatus for Room Temperature IP Test	78
43	Fixtures for Room Temperature TIP Test	78
44	Diagram of Apparatus for High-Temperature Compression Tests	79
45	Apparatus for High-Temperature Testing	81
46	Apparent Cracks in Tension (Specimens T-1 and T-2)	82
47	Exposed Wires and Surface Defects in Internal Pressurization (Specimen IP-5)	82
48	Chips, Gouges, and Apparent Cracks in Compression Specimens	83

ILLUSTRATIONS

Figure		Page
49	Weibull's Theory of Strength for Biaxial Stresses for Hydrostone Plaster ($m=12$)	86
50	Stress-Strain Behavior Showing Data Obtained From Three Strain Gages	87
51	Stress-Strain Behavior in Tension	89
52	Load-Lateral Strain Behavior in Tension	90
53	Tension Specimen Tested at Room Temperature	91
54	Stress-Strain Behavior in Compression	92
55	Load-Lateral Strain Behavior in Compression	93
56	Compression Specimens Tested at Room Temperature	94
57	Stress-Strain Behavior in Internal Pressurization	95
58	Load-Axial Strain Behavior in Internal Pressurization	96
59	IP Specimen Tested at Room Temperature	97
60	Stress-Strain Behavior in Internal Pressurization to 80% for Biaxial Test in Tension-Tension Mode	98
61	Load-Axial Strain Behavior in Internal Pressurization to 80% for Biaxial Test in Tension-Tension Mode	99
62	Stress-Strain Behavior in Tension for Biaxial Test Tension-Tension Mode	100
63	Load-Lateral Strain Behavior in Tension for Biaxial Test in Tension-Tension Mode	101
64	Stress-Strain Behavior in Tension-IP Test	102
65	TIP Specimen Tested at Room Temperature	103
66	Disassembled View of Fixturing for High-Temperature Tests	105
67	Partially Assembled View	105
68	Assembled View	105
69	Diagram of Apparatus for High-Temperature IP and CIP Tests	106
70	Tension Specimen Tested at 4,000°F	109
71	Tension Specimen Tested at 3,000°F with Failure in Gage Section	109
72	Tension Specimen Tested at 4,000°F Showing Deformation and Melting of Stainless-Steel Inserts	110
73	Stress-Strain Behavior in Compression at 3,000°F	111

ILLUSTRATIONS (Continued)

Figure		Page
75	Compression Specimens Tested at 4,000°F	113
76	Compression Specimen Tested at 3,000°F	113
77	Stress-Strain Behavior in Internal Pressurization at 3,000°F	115
78	Stress-Strain Behavior in Internal Pressurization at 4,000°F	116
79	Stress-Strain Behavior During Compressive Loading in CIP Test at 3,000°F	117
80	Stress-Strain Behavior in CIP Test at 4,000°F	118
81	IPC Specimens Tested at 3,000° and 4,000°F	119
82	Typical Fracture Section Transverse to the Material Thickness (Specimen TIP-1)	126
83	Typical Fracture Section Through Specimen T-1	127
84	Typical Fracture Section Exposed to 3,000°F for 5 Min (Specimen T-4)	128
85	Carbon and Oxygen Distribution in a Typical Fracture Section Exposed to 4,000°F (Specimen T-7)	129
86	Metallographic Longitudinal Section (Specimen T-1)	131
87	Optical Micrographs of a Transverse Section (Specimen T-1)	132
88	Optical Micrographs of Metallographic Sections (Specimens TIP-1 and IP-1)	133
89	Optical Micrographs (Specimens C-3 and T-4)	134
90	Optical Micrographs (Specimens THE-1A and THE-3A)	135
91	SEM Micrographs of Metallurgical Sections (Specimens IP-1 and T-4)	137
92	SEM Micrographs of Fracture Sections (Specimens T-1 and IP-2)	138
93	SEM Micrographs of a Fracture Section	139
94	SEM Micrographs of a Fracture Section Containing a Partially Exposed Filament	141
95	SEM Micrographs of a Fracture Section (Specimen T-7)	142
96	SEM Micrographs of a Fracture Section (Specimen T-7)	143

TABLES

Table		Page
I	Tungsten Powder	14
II	TH-55 1%-Thoriated Tungsten Wire	16
III	Tantalum Powder	17
IV	NDT Test Sequence and Area of Interest	23
V	Tungsten Specimens Dimensional Data	26
VI	Wire-Wound Tungsten Specimens Conductivity Results	28
VII	Steady-State Thermal Conductivity Data for Unsintered Wire-Wound Tungsten Composite	42
VIII	Thermal Diffusivity of Unsintered Wire-Wound Tungsten Composite for Sample No. 1	45
IX	Thermal Diffusivity of Wire-Wound Tungsten for Sample No. 2	46
X	Thermal Diffusivity of Wire-Wound Tungsten for Sample No. 3	47
XI	Experimental Enthalpy Values for Wire-Wound Tungsten Composite In a Sealed Container Under Helium	52
XII	Thermal Conductivity Data for Wire-Wound Tungsten Composite Normal to Wire Direction	67
XIII	Visible Damage to Test Specimens	84
XIV	Summary of Room Temperature Data	85
XV	Summary of High-Temperature Data	108
XVI	Measured Densities	122
XVII	Chemical Analyses	124

AFML	Air Force Materials Laboratory
AIME	American Institute of Mechanical Engineers
AR	as-received
ASTM	American Society for Testing Materials
CIP	combined compression/internal pressurization
FSSS	Fischer sieve size
IACS	International Association of Copper Standards
ID	inside diameter
IP	internal pressurization
IPC	internal pressurization/uniaxial compression
LOR	loss on reduction
NDT	nondestructive testing
OD	outside diameter
SEM	scanning electron microscope
S/N	serial number
THE	thermal expansion
TIP	combined uniaxial tension/internal pressurization
UTC	United Technology Center

SECTION I

INTRODUCTION

A unique composite material, commonly known as wire-wound tungsten, has been developed by UTC over the past several years. The primary objective has been to produce rocket nozzle throat inserts capable of withstanding long-duration multi-restart high-pressure firings in solid propellant and hybrid motors.

The composite essentially consists of a reinforced tungsten filament, plasma-sprayed tungsten matrix. Nozzle throat inserts are produced by winding the high-strength reinforcing wires over a properly shaped mandrel in a pre-arranged order of helical and hoop sequences. After each winding, a layer of plasma-sprayed tungsten is used to encapsulate the wires and to provide a laminate base for the next wire-winding sequence. Fabrication by this method ensures a good balance of hoop and longitudinal strength in the insert and also provides for interruption of stress paths and attendant retardation of crack propagation.

Results of test firings for several Air Force sponsored programs^(1,2) using throat inserts fabricated of wire-wound tungsten have been very encouraging. In the initial design of these inserts, UTC used data for thermal and stress analysis derived from properties of pure wrought tungsten adjusted to conform with estimated properties of an 85.7% theoretically dense tungsten composite system.

To "design" a throat insert has, however, been extremely difficult because of the paucity of thermal and mechanical properties data for this unusual composite material. It had been recognized by both the Air Force and UTC that an extensive characterization of the properties of wire-wound tungsten would be required to permit use of standard nozzle design procedures. Also, because of the complex nature of the material, it was decided that much of the data should be derived from actual nozzle inserts or from specimens geometrically similar to such components, e.g., hollow cylinders.

The program objective was to characterize wire-wound tungsten's mechanical, thermal, chemical, and physical properties over a temperature range from room temperature to 4,000°F (2,200°C). Specimens were to be designed and tested so that the data derived could be used for rocket nozzle hardware design analysis. The specimens were to be fabricated to simulate current rocket nozzle techniques. Data from the completed characterization tests were to be analyzed and processed as input information for computer analysis. Other task objectives were (1) to conduct an NDT inspection to screen specimens for defects that could adversely affect test results, (2) to provide an evaluation of the uniformity or reproducibility of test specimens, and (3) to prepare a material specification including the necessary procurement, destructive testing, and NDT inspection requirements to assure production of reproducible and predictable wire-wound tungsten components.

This report discusses all design, fabrication, and test functions performed to accomplish the program objectives. Because of a change in work scope, structural data (mechanical properties and thermal expansion) were not analyzed to determine design failure modes nor were the data processed as input information for UTC's finite element computer program L177ZZZ.

SECTION II

SUMMARY

Wire-wound-tungsten, a composite material of plasma-arc-sprayed tungsten reinforced with tungsten filaments, has been characterized by an evaluation of its mechanical, thermal, physical, and chemical properties. These properties were determined on specially designed specimens which were fabricated in specified quantities as bodies-of-revolution in the manner of rocket nozzle throats.

An NDT program conducted prior to property testing determined that the specimens were free of gross defects which might adversely affect test results. The NDT study also demonstrated that photon and neutron radiography could detect defects in the composite and that eddy current inspection could identify cracks and provide a measure of the composite's uniformity or reproducibility. Ultrasonic test methods were shown to be unacceptable because of sound wave attenuation characteristics.

Thermal expansion, thermal conductivity, specific heat, and thermal diffusivity properties were determined for the temperature range from room temperature to 4,000°F (2,200°C). Fixtures and test procedures were developed to perform the required tests. Conductivity, diffusivity, and specific heat were determined on as-composited material, and thermal expansion was measured in both the as-composited and presintered condition. No appreciable difficulties occurred during the tests, and the data generated are considered typical of wire-wound tungsten composites and useful for rocket nozzle design application.

Axial tension, axial compression, internal pressurization (hoop tension), TIP, and CIP properties (including stress-strain relationships) were determined for room temperature, 3,000°F (1,650°C), and 4,000°F (2,200°C). Fixtures and test procedures were developed for performing tension and biaxial tests at elevated temperature. Water-cooled pull rods with wedge grips were developed for tension testing of cylindrical specimens, and tantalum foil pressure bags were developed for elevated temperature internal pressurization and biaxial tests.

Room temperature testing was straightforward and the resultant data were essentially consistent and reproducible. Elevated temperature tests were considerably more difficult. While the CIP tests were performed and the desired data were obtained, problems with excessive thermal stresses and the low strength of wire-wound tungsten at elevated temperatures caused premature fracture of tension and TIP specimens during heatup. As a result, the 4,000°F (2,200°C) axial tension data point was not attained, and the TIP test technique had to be modified for CIP. The data indicate that wire-wound tungsten behaves in a nonlinear elastic manner at room temperature and as an elastic-plastic material at elevated temperature.

The physical and chemical characteristics of wire-wound tungsten were investigated on material from the tested thermal and mechanical property specimens. The complete range of test temperature (room temperature to 4,000°F (2,200°C)) was examined. Microstructure and fracture characteristics were evaluated by optical metallography and scanning electron microscope techniques. Pycnometric and immersion methods were used to determine and compare density. Chemical composition was determined by a combination of spectrographic, conductometric, vacuum fusion, X-ray diffraction, and electron microprobe analysis techniques.

Based on these results, a preliminary material specification was prepared. The specification is intended to assure the production of reproducible wire-wound tungsten composites so that the property data obtained has general utility for design purposes.

SECTION III

RESULTS AND DISCUSSION

1. SPECIMEN PREPARATION

Preparation of specimens for characterizing the thermal, mechanical, physical, and chemical properties of wire-wound tungsten consisted of (1) designing specimen configurations consistent with desired test techniques and apparatus, (2) procuring raw materials, (3) fabricating specimens according to previously demonstrated nozzle throat techniques, and (4) evaluating specimens for defect criteria by NDT inspection.

a. Specimen Design

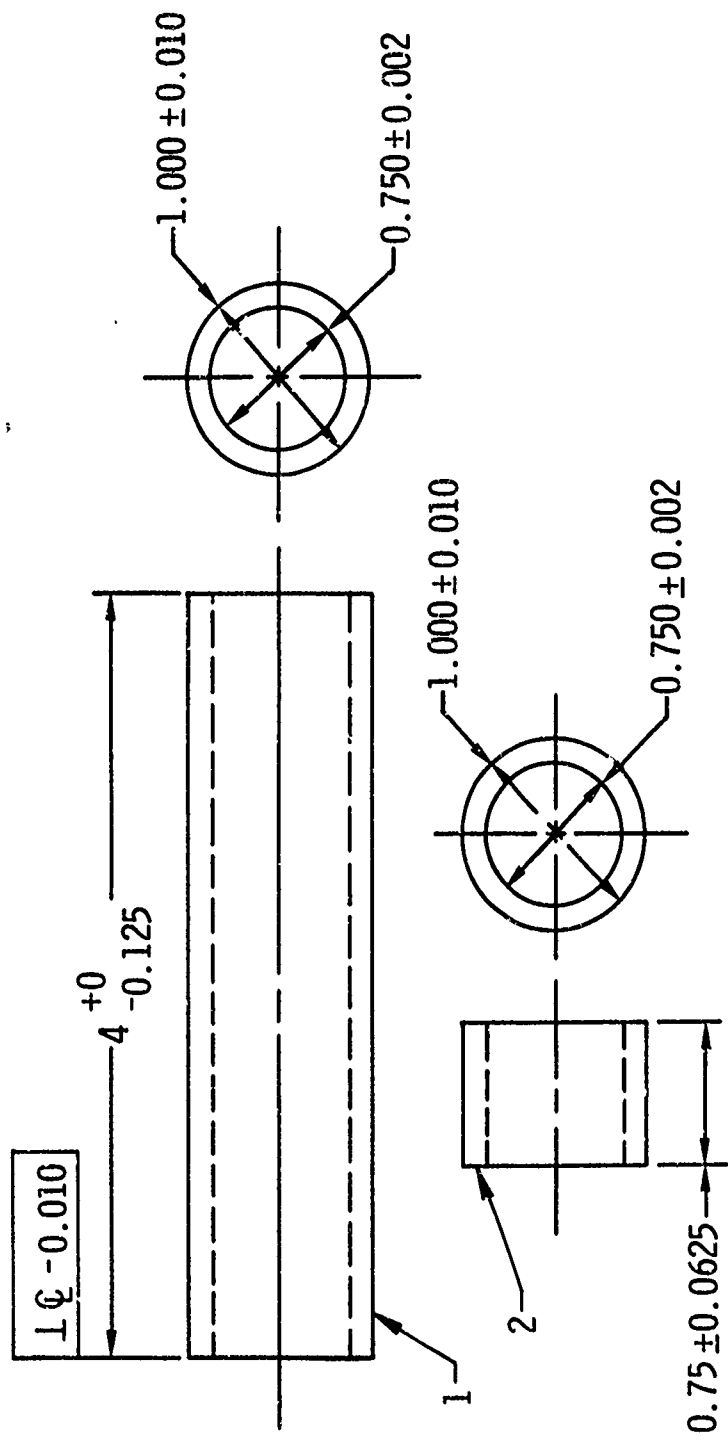
The specimens had to provide property requirements for adequate design data input. The specimens also had to be compatible with state-of-the-art elevated temperature testing technology and be of a configuration which was fabricable by UTC nozzle throat cylinder-of-revolution techniques. The thermal properties desired were:

- A. Thermal expansion from room temperature to 4,000°F (2,200°C) (4,500°F, if possible)
- B. Thermal conductivity from room temperature to 1,500°F (815°C)
- C. Thermal diffusivity from 1,500° to 4,000°F (4,500°F, if feasible)
- D. Specific heat from room temperature to 4,000°F (2,200°C)

Thermal expansion data were to be determined in the axial and radial directions; conductivity and diffusivity in the radial or through the thickness direction. Figure 1 shows the design configurations for the thermal expansion specimens, and figure 2 shows the thermal diffusivity, conductivity, and specific heat specimens. These configurations represented the best fit to the subcontractor's (Battelle Memorial Institute) test apparatus capability.

The design of specimens for mechanical property testing was considerably more difficult than for thermal specimens. The properties required for adequate design input were axial tension, axial compression, hoop tension, and biaxial characteristics including elastic modulus and Poisson's ratio for each mechanical test property. These properties were required over the range from room temperature to 4,000°F (2,200°C).

Design configurations for the specimens are shown in figures 3, 4, and 5. Compression specimens (not shown) were 1-in.-long, simple, hollow, right cylinders having a 1.750 in. ID and a 2.00 in. OD. All envelope dimensions were selected to comply with the subcontractor's (Illinois Institute of Technology Research Institute, Chicago, Illinois) test apparatus capability using diameters large enough to satisfy UTC's fabrication constraints.



NOTE: ALL DIMENSIONS ARE IN INCHES

LEGEND:
 1 = AXIAL THE SPECIMEN
 2 = RADIAL THE SPECIMEN

Figure 1. Design of THE Specimen

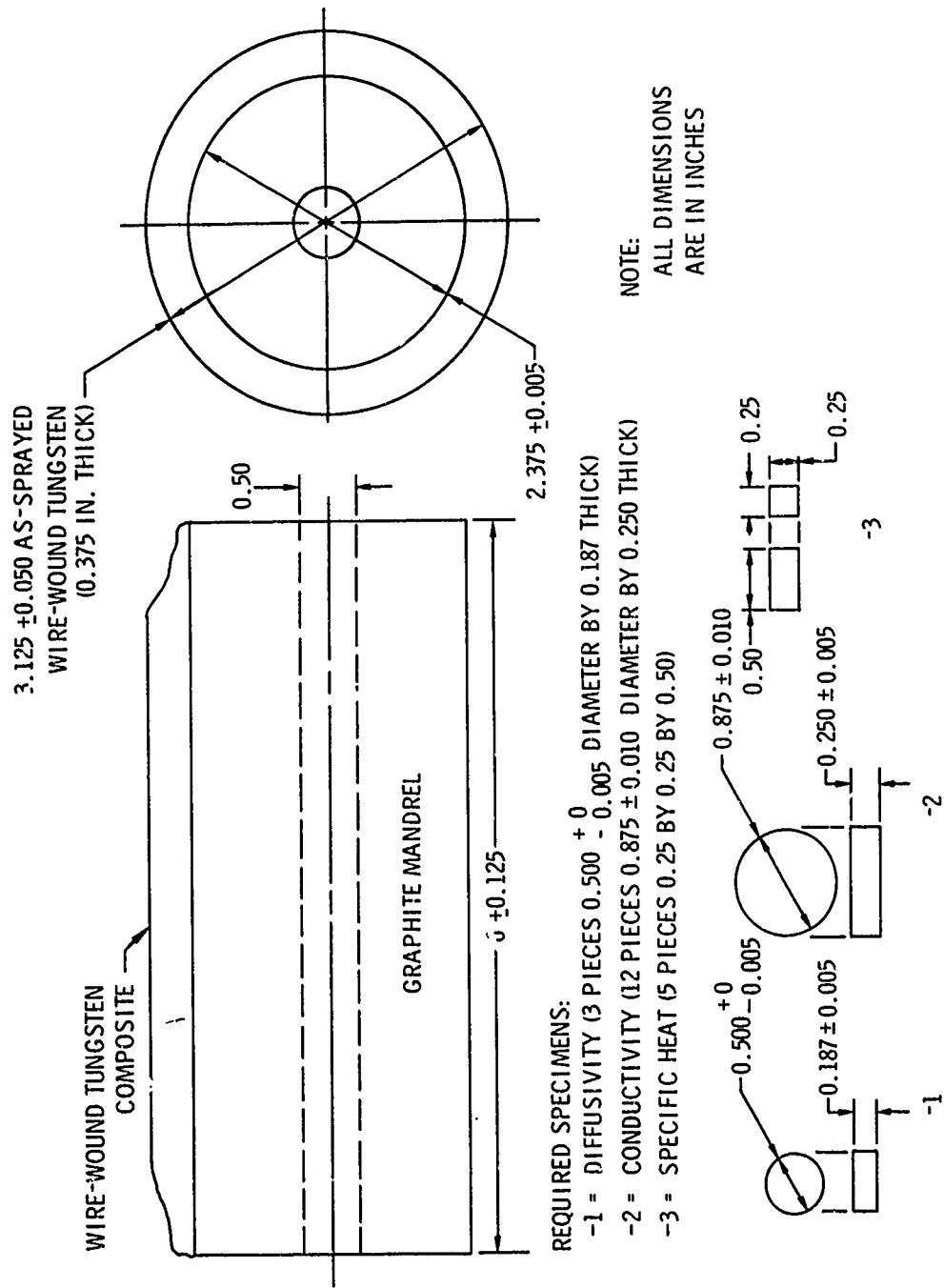
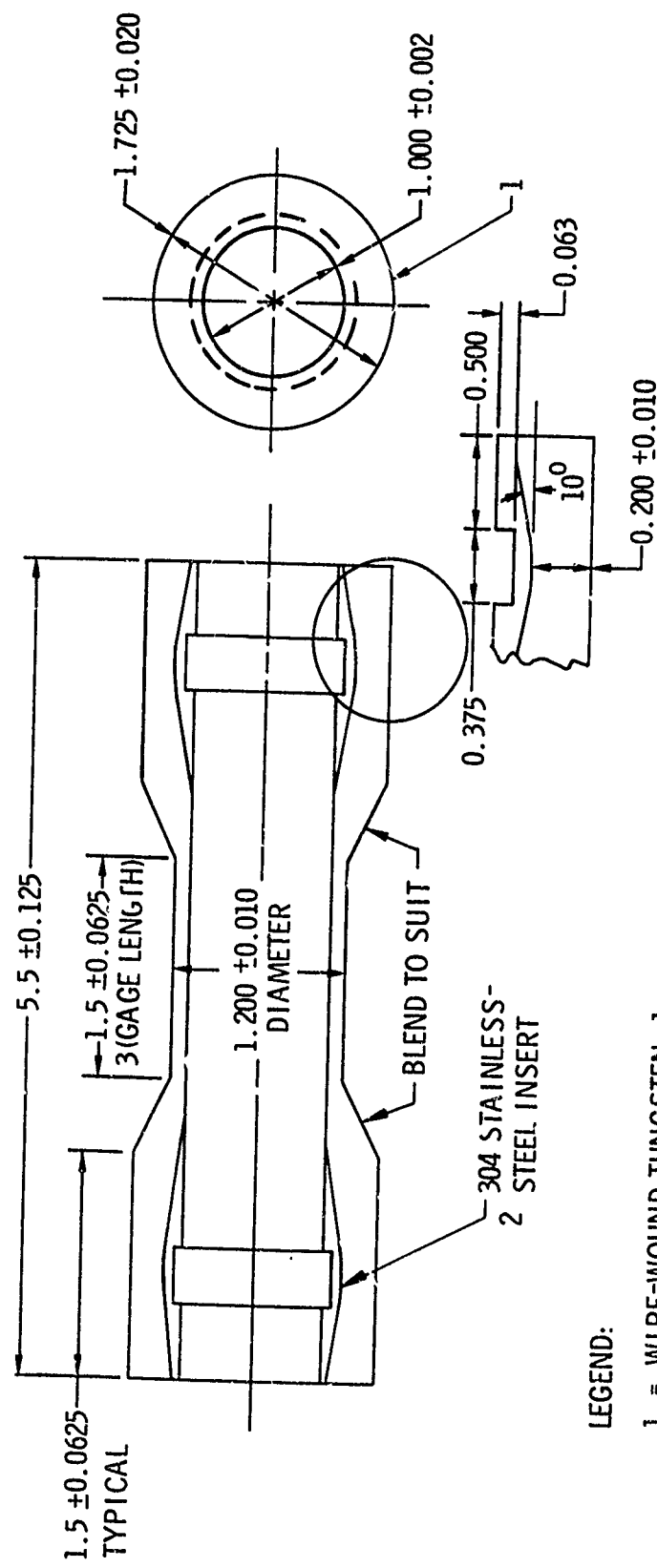


Figure 2. Design of Thermal Property Specimen

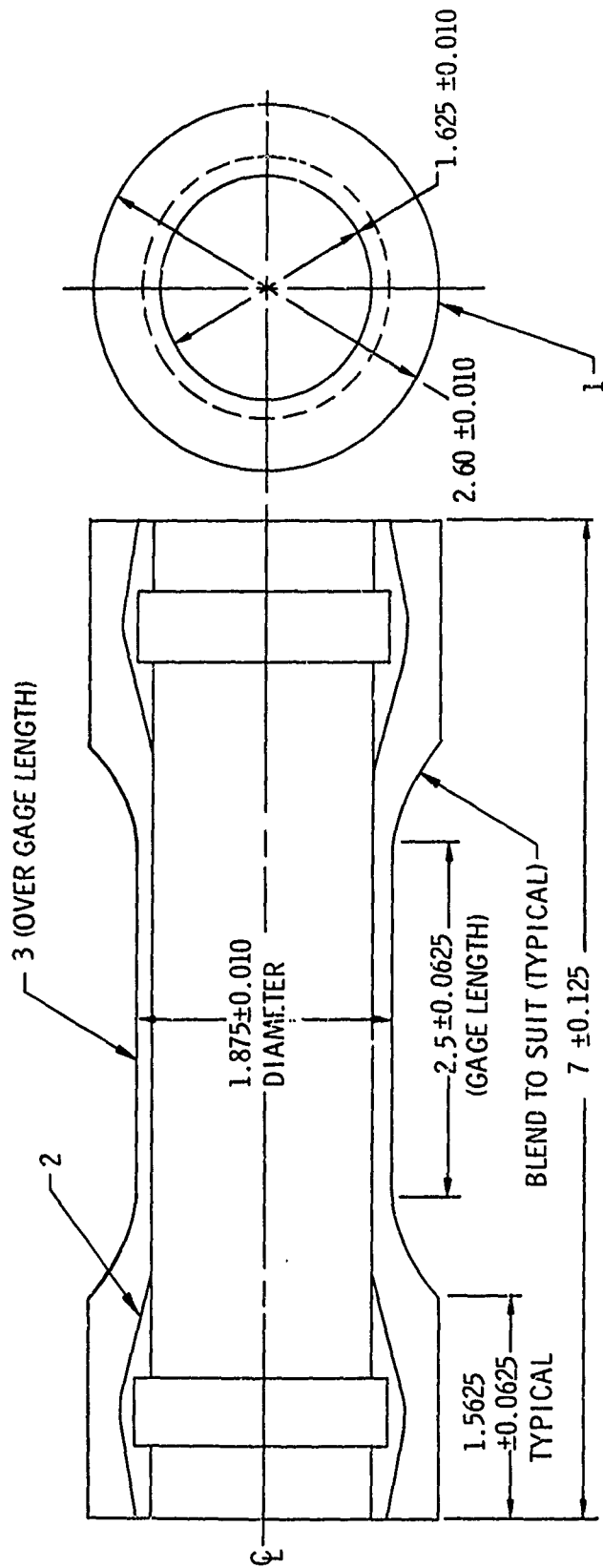


LEGEND:

- 1 = WIRE-WOUND TUNGSTEN, 1
- 2 = GRIP END INSERT (M&P DWG. JH-8281, 2
- 3 = PLASMA-SPRAYED TAN/ALUM COAT (0.010), AR

NOTE: ALL DIMENSIONS ARE IN INCHES.

Figure 3. Design of Tension Specimen



LEGEND:

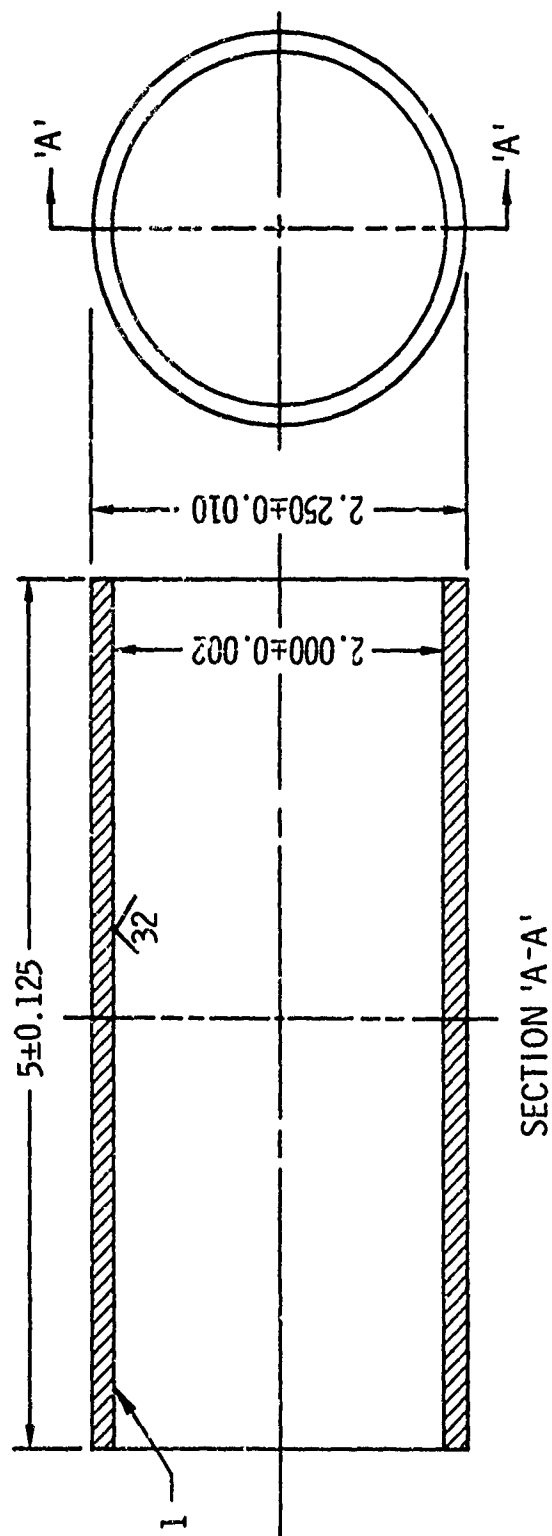
1 = WIRE-WOUND TUNGSTEN, 1

2 = GRIP END INSERT [M & P DWG. JH-828], 2

3 = PLASMA-SPRAYED TANTALUM COAT (0.010) GAGE LENGTH, AR

NOTE: ALL DIMENSIONS ARE IN INCHES.

Figure 4. Design of TIP Specimen



LEGEND:

1 - GRIP END MAY BE THICKENED TO ACCOMMODATE
TEST TOOLING

NOTE:

APPARENT BULK DENSITY = $85^{+2}_{-5}\%$

ALL DIMENSIONS ARE IN INCHES.

Figure 5. Design of IP Specimen

The tension and TIP specimens, figures 3 and 4, respectively, were designed with stainless-steel grip inserts to enable tension load application. Preliminary laboratory evaluation showed that normal tension gripping techniques (such as threads or serrated fixtures) would fracture the as-composited wire-wound tungsten material so it was decided to use internal wedge grips. In this manner, the grip load would be applied on a structurally adequate material and would be transmitted radially to the wire-wound tungsten through a 10° ramp angle and large shear area. Specimen grip areas were thickened sufficiently to assure fracture in the gauge length. Stainless steel was selected for compatibility with the test fixtures.

b. Raw Materials

Raw materials utilized in specimen preparation were tungsten powder, 1%-thoriated tungsten wire, and tantalum powder; graphite was used as the mandrel material. The program did not include an evaluation of the effect of raw material variables on property characteristics; therefore, the specimens were produced using material conforming to specifications identical to those used in the previous manufacture of wire-wound tungsten nozzle throat inserts.

Tungsten powder, plasma-spray grade (-200, +325 mesh) and 0.004-in.-diameter 1%-thoriated tungsten wire were supplied by Sylvania Electric, Chemical and Metallurgical Division. Graphite bars (type 8882) for mandrels were supplied by Airco Speer Carbon Products. Plasma-spray grade tantalum powder (-200, +325 mesh) was purchased from Teledyne-Wah Chang. The appropriate physical and chemical characteristics of the raw materials are listed in tables I, II, and III.

c. Specimen Fabrication

Thermal and mechanical property specimens, whose designs were described in the subsection entitled, "Specimen Design," were fabricated by procedures developed for the manufacture of wire-wound tungsten nozzle throat inserts. The basic procedure consisted of layers of plasma-sprayed tungsten powder alternated with helical and hoop windings of 0.004-in.-diameter 1%-thoriated tungsten wire. The desired configuration was achieved by spraying and winding over a precision machined graphite mandrel which conformed to the internal dimensions of the specimen. After building up suitable thicknesses, the outer surfaces were machined to meet design requirements. Typical examples of the process are shown in figures 6 and 7. Figure 6 shows the mandrel and grip inserts in place prior to the first plasma spray layer; figure 7 shows a 45° helical reinforcement winding operation prior to an intermediate plasma spray layer. Note in the example (of a tension specimen) that the spraying and winding operations are contoured to approximate the external configuration and minimize machining requirements.

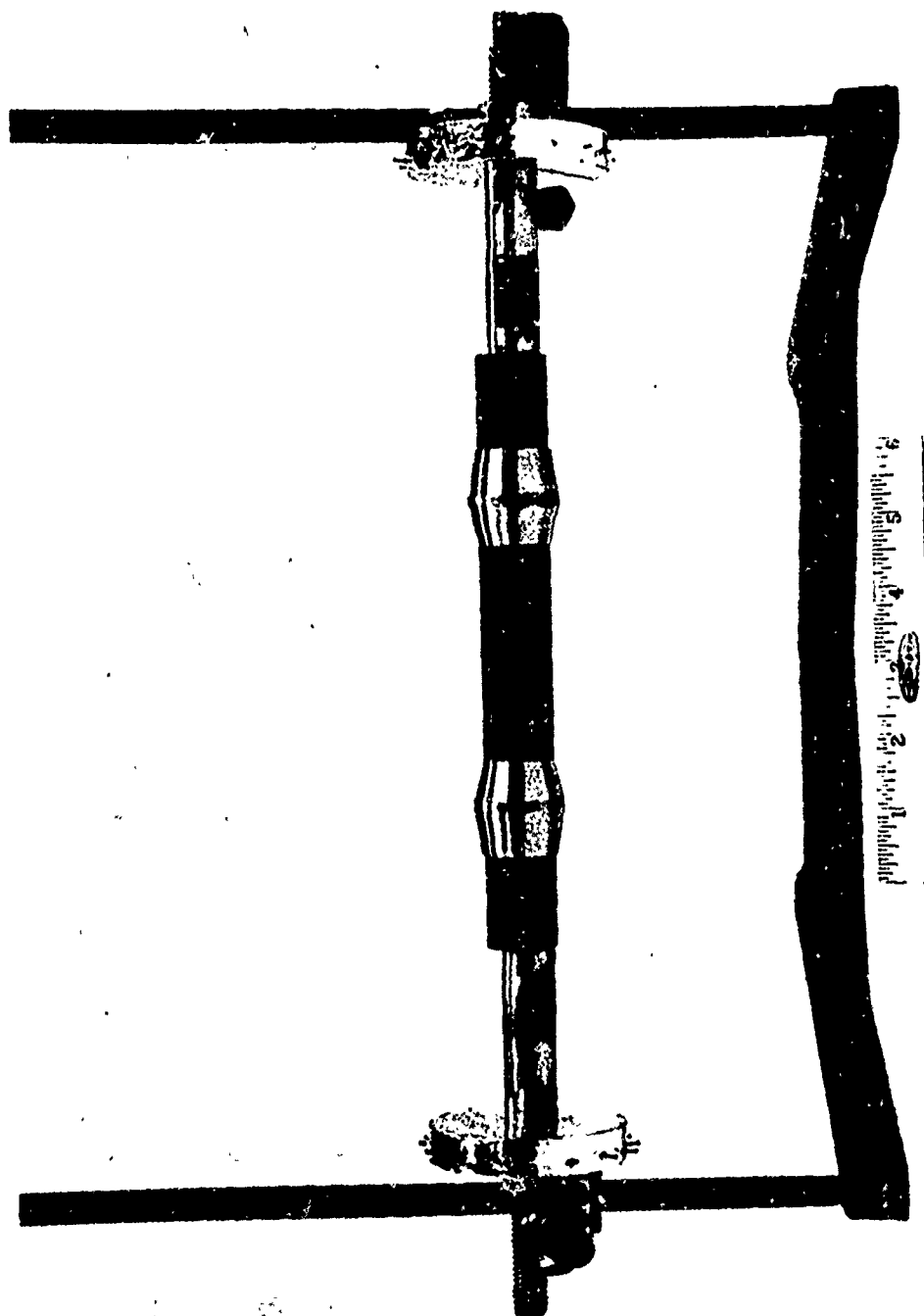


Figure 6. Setup For Wire-Wound Tungsten Tension Specimen

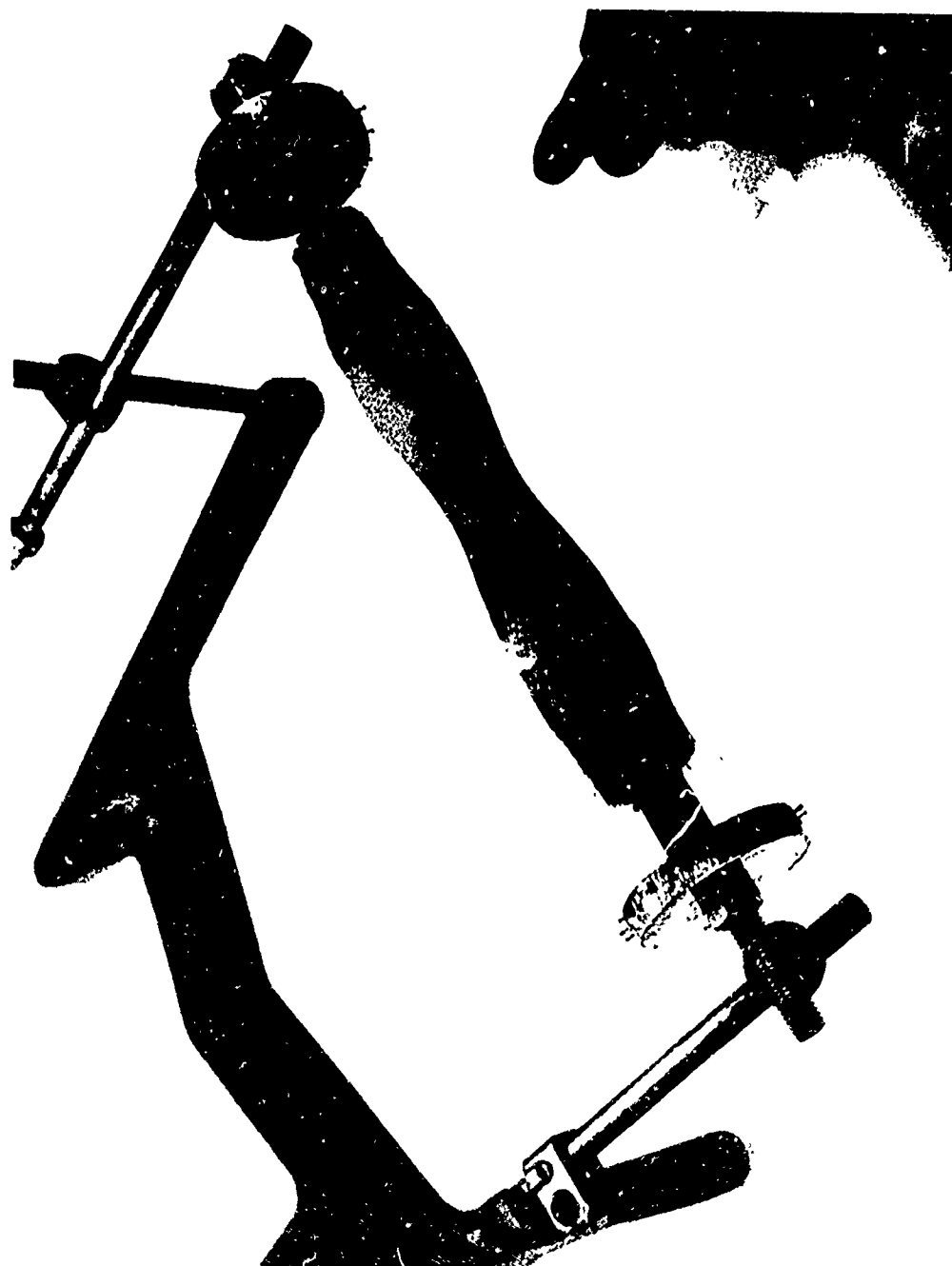


Figure 7. Wire-Wound Tungsten Tension Specimen
Receiving Helical Reinforcement

TABLE I
TUNGSTEN POWDER
Lot No. C-200-115-C

Chemical Analysis

<u>Element</u>	<u>Amount, ppm</u>
Cr	10 to 100
Cu	1
Fe	5 to 50
Mg	0.5 to 5
Mn	0.5 to 5
Mo	5 to 50
Ni	10 to 100
Si	5 to 50
Ti	1 to 10
Fe	17
Mo	32
W	Balance

Powder Characteristics

FSSS, micron	44.0
Bulk density, g/in. ³	163.5
LOR, ppm	100
Hall flow, sec	8

Screen Size

<u>Mesh</u>	<u>%</u>
-200, +325	60
-325	39

(1) Thermal Property Specimens

Five 5-in.-long wire-wound tungsten blanks with a 1-in. OD and 3/4 in. ID were fabricated for thermal expansion specimens (figure 8). Each blank was machined according to drawing requirements (figure 1) and was sectioned to provide an axial (4 in. long) and radial (3/4 in. long) specimen. The thermal expansion specimens were identified as THE-1A through THE-5A and THE-1R through THE-5R. (A denotes axial direction test and R denotes radial direction test). The graphite mandrel was removed from the ID by boring on a lathe. The specimens were inspected visually for surface irregularities and dimensions and were given a bulk density determination. All specimens met

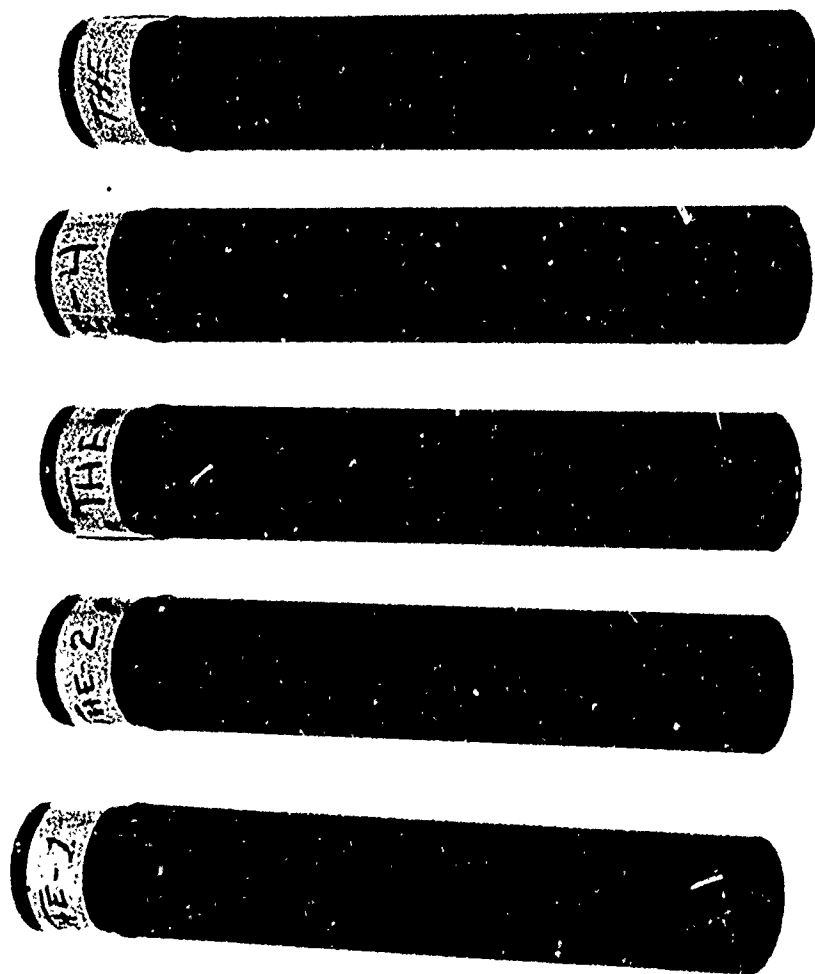


Figure 8. Specimen Blanks for THE Tests

drawing requirements and were within the normal as-composited bulk density range of $85 \pm 2\%$. Specimens 3A and 3R were sintered in argon for 1 hr at $3,600^{\circ}\text{F}$ ($1,982^{\circ}\text{C}$) as required by the test plan.

Component reproducibility was ensured during fabrication by following a written procedure which detailed subcomponent requirements, step-by-step spraying and winding operations, and postspraying fabrication. Sample procedure forms, indicating the type of operator and in-process inspection controls, are contained in Appendix I.

TABLE II

TH-55 1%-THORIATED TUNGSTEN WIRE
30.15 mg/200 mm (0.004-in. diameter)

Tensile strength, psi	70,000
End-to-end wire tolerance, %	1 maximum
Out of round, %	4 maximum

Typical Chemical Analysis

<u>Element</u>	<u>Amount, ppm</u>
Ca	1.0
Cu	1.0
Cr	1.0
Fe	6.0
Mg	1.0
Mn	1.0
Si	5.1
Sr	1.0
Al	1.0
Ni	11.0
Na	6.0
K	25.0
Mo	51.0
C	16.0
Thoria as tungsten metal powder	0.99%
W	Balance

Specimens for thermal diffusivity, conductivity, and specific heat tests were obtained from a 6-in.-long, 3.125-in.-OD, 2.375-in.-ID hollow cylinder (figure 2), which was prepared using fabrication procedures identical to those used for the thermal expansion specimens. From the wire-wound tungsten log, the following specimens were obtained:

- A. Thirteen disks 0.875 in. in diameter and 0.500 in. thick for thermal conductivity tests.

B. Four disks 0.500 in. in diameter and 0.187 in. thick for thermal diffusivity tests.

C. Six blanks 1/4 by 1/4 by 1/2 in. for specific heat tests.

Diamond core drills were used to trepan the specimen material from the log. The completed specimens are shown in figure 9. All specimens were produced so that the diffusivity and conductivity test measurements could be obtained in the through-the-thickness direction.

TABLE III

TANTALUM POWDER
-200, +325 Mesh - Type 228
Heat No. Lot T2-228

Chemical Analysis

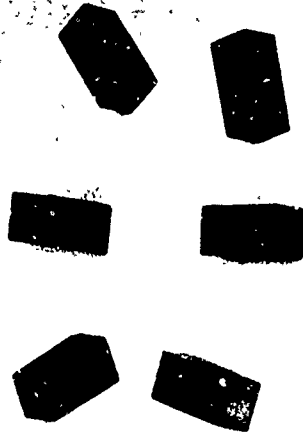
<u>Element</u>	<u>Amount, ppm</u>
Al	20
B	1
C	30
Cb	50
Cd	1
Co	20
Cr	20
Cu	40
Fe	69
Mg	20
Mn	20
Mo	20
N	30
Ni	20
O	1,320
Pb	20
Si	30
Sn	20
Ti	50
V	20
W	10
Zn	20
Zr	50
Scott density	103 g/in. ³

(2) Mechanical Property Specimens

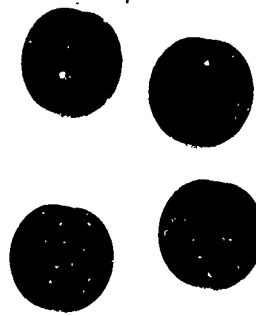
Mechanical property specimens, fabricated for the test program, are shown in figures 10, 11, and 12. Seven tension, 6 IPC, and 6 TIP specimens were prepared. Each type was fabricated according to a



CONDUCTIVITY



SPECIFIC HEAT



DIFFUSIVITY



Figure 9. Thermal Property Specimens

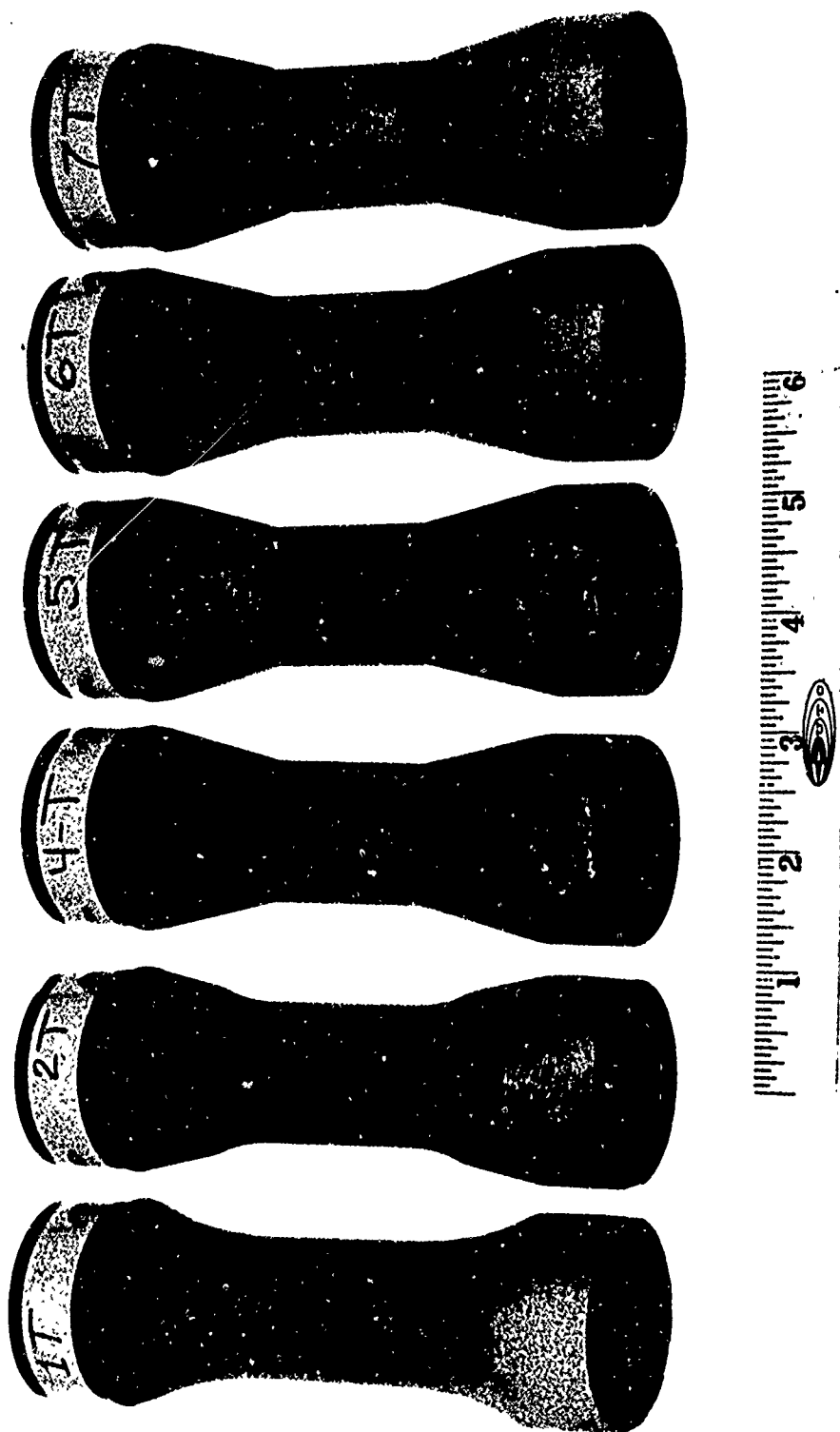
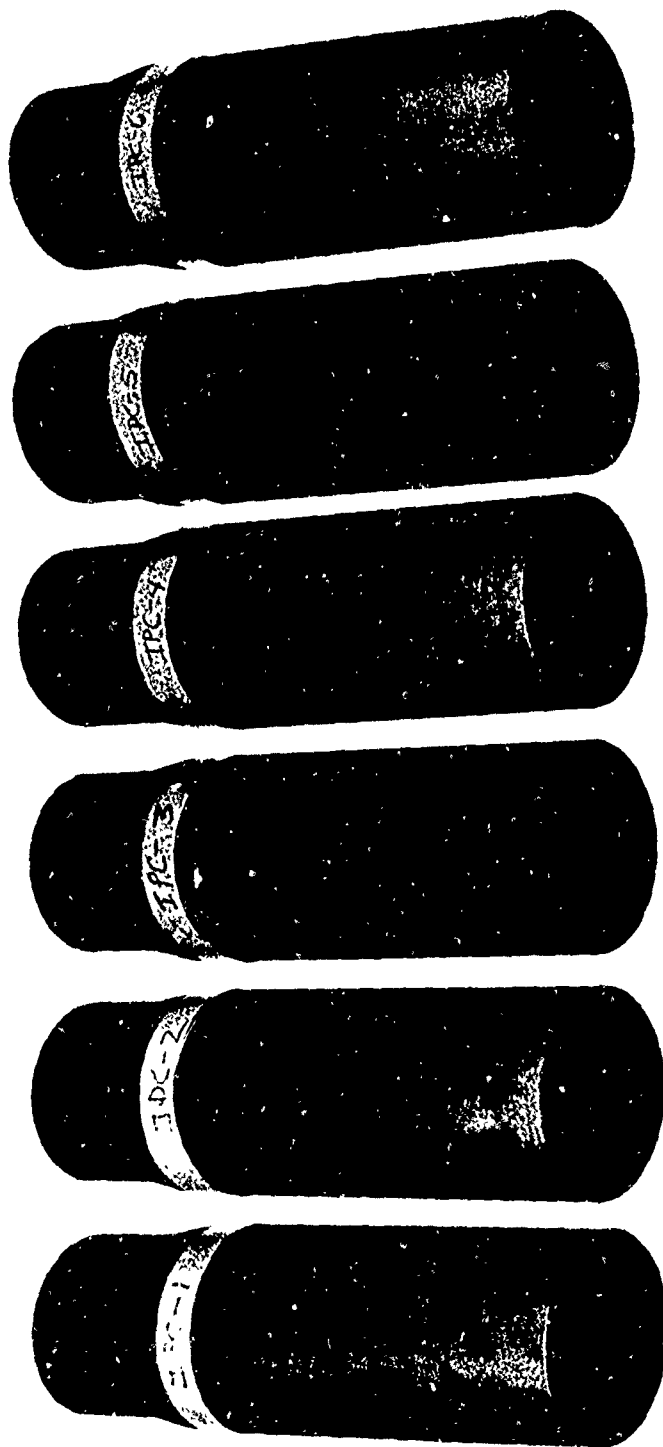


Figure 10. Completed Wire-Wound Tungsten Tension Specimens



1 2 3 4 5 6

Figure 11. Wire-Wound Tungsten IPC Specimens

Reproduced from
best available copy.

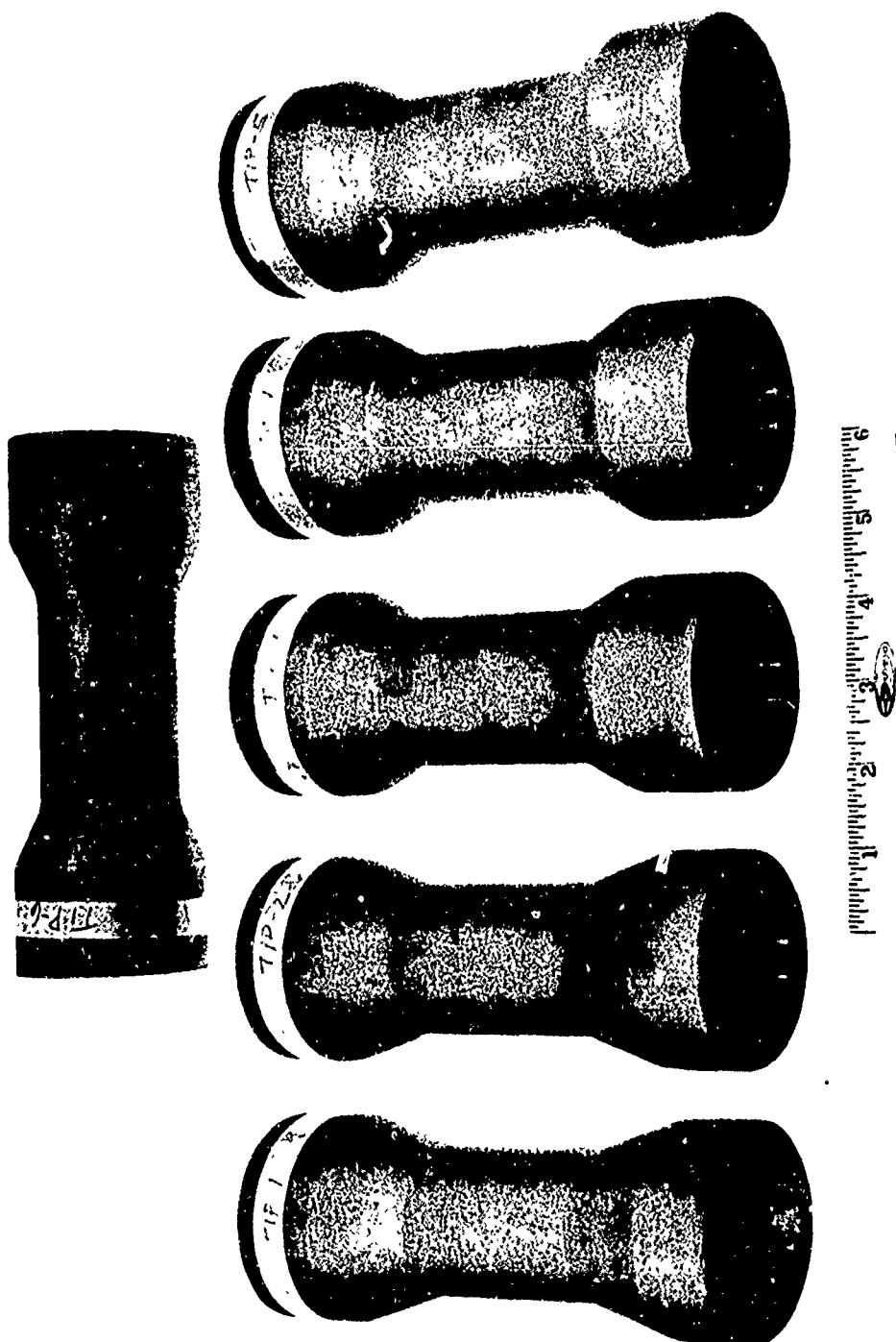


Figure 12. TIP Specimens

definite procedure, detailing layer thicknesses, and winding requirements. The procedures specifications 2380-IT, 2380-TIP, and 2380-IPC are contained in Appendix I. No problems were encountered during fabrication and the resultant bulk density measurements showed that each specimen was within the desired $85 \pm 2\%$ of theoretical density, the typical value for as-composited wire-wound tungsten nozzle throat inserts. After removal of the graphite mandrels, 1-in.-long compression specimens were sectioned from the IPC blanks with an abrasive cut-off saw. No specimens were fabricated for the physical and chemical characterization phase of the program; material from specimens tested in the mechanical and thermal property characterization was used. In this manner, as-composited material and material exposed to elevated temperature could be examined on a common basis.

Approximately 500 lb of tungsten powder and over 10,000 ft of 0.004-in.-diameter tungsten filament were used to fabricate these thermal and mechanical property specimens. Tantalum powder was used as a final overspray of each specimen in accordance with nozzle throat insert standard fabrication practice. The tantalum layer provides a barrier in the throat between the tungsten and carbon back-up materials to prevent a low-temperature eutectic reaction. For the elevated temperature tests, the tantalum was ground off of the specimens because it would spall if left on during exposure to high temperature due to differences in thermal expansion.

d. Nondestructive Testing

The NDT evaluation portion of this program was added after the initial contract negotiations to further define the characteristics of wire-wound tungsten. The NDT objectives were to:

- A. Screen out specimens with gross defects that could adversely affect thermal and mechanical test results.
- B. Identify discrete defect indications and record their type, size, and location.
- C. Provide evaluation/measurement of uniformity/reproducibility of test specimens by relating NDT results to physical performance.
- D. Provide NDT inspection technique input for materials specification.
- E. Provide NDT inspection discrete defect input for selection of accept/reject criteria.
- F. Recommend advanced NDT as appropriate based on experience gained.

(1) NDT Techniques and Evaluation

NDTs were conducted on specimens after fabrication and final machining with the exception of the IPC specimens which were fabricated on the same mandrel and tested intact prior to sectioning the compression

specimens. Six TIP, six IPC, seven tension, and five THE specimens were evaluated with the test sequence and areas of interest shown in table IV. One specimen (THE-4) was dropped on a concrete floor while in dimensional inspection. This cracked specimen was used as a standard for eddy current crack detection.

TABLE IV
NDT TEST SEQUENCE AND AREA OF INTEREST

<u>Type of Test</u>	<u>Purpose of Test*</u>	<u>Characteristic or Area of Interest</u>
Identification	D and U	Uniform frame of reference
Visual	D	Defects in end surface
Eddy current	D	Location of all cracks indicate areas of accumulative microfractures
Dimensional	U	Reference data for other NDT tests
Audiosonics	U	An index of reproducibility between repetitive geometries
Eddy current conductivity	U	An index of specimen uniformity by indicating distribution of resistivity
Ultrasonic velocity	U	An index of specimen uniformity by indicating distribution of elasticity
Photon radiography	D	Detection of large voids, cracks, and wide delaminations
Neutron radiography	D and U	Possible enhancement over photon radiography for crack and void resolution. Mesh pattern of wire.
Ultrasonic flaw	D	Defines all delaminations
Posttest visual	D and U	Reference data for analysis

* D = locate discrete defects

U = gage uniformity/reproducibility

With the exception of the audiosonic natural frequency test (which was conducted after neutron radiography), the NDT tests listed in table IV were performed in the sequence indicated. Neutron radiography and ultrasonic flow tests were subcontracted; the balance of NDT tests were conducted by UTC.

(a) Identification

After fabrication, the specimens were identified with a plastic marking tape. To perform neutron radiography, it was necessary to remove the plastic tape to prevent specimen masking by neutron absorption in this hydrogenous material. In removal of the tape, several areas of the tantalum overspray were removed by the tape's adhesive.

The specimens were reidentified with the assigned serial number by a felt marking pen. The orientations of 0° , 120° , and 240° and the required data reference points were plotted on each specimen.

(b) Visual

Identifying discrepant conditions was difficult by visual inspection. Delaminations were observed in the TIP specimens which did not correlate with photon or neutron radiographic results. This was primarily due to the masking effect of the protective coating of tantalum sprayed on the specimens. Even on a sectioned specimen (with the end not tantalum coated), it was difficult to delineate between a delamination and an area where a wire has been pulled from the matrix.

A 0.25-in.-long crack was observed on the end of compression specimen IPC-5. Neutron and photon radiography showed delaminations at the end of all the compression specimens; however, none of these were reported by visual inspection. Eddy current indications confirmed the visually reported crack on IPC-5.

(c) Eddy Current

Eddy current inspection for crack detection was conducted on all specimens. UTC fabricated a special test probe for the inspection of specimen inside surfaces. Full-scale instrument meter deflections were obtained when scanning the cracked specimen (THE-4). Greater than half-scale instrument meter deflections were obtained on other specimens, which indicates the presence of minute cracks. A Magnaflux ED 510 instrument was used at the highest operating frequency available. A major problem in the use of eddy currents for crack detection is the abrasive effect of the surface on the test probe. Since it is unnecessary for the probe to touch the surface during testing, special tooling can be designed to align the probe for production hardware testing.

(d) Dimensional Inspection

Dimensional inspection was performed according to the NDT plan for each specimen. Specimen dimensions are shown in table V. The wall thickness is reported as minimum-maximum; however, only three readings were taken (0° , 120° , and 240°).

(e) Audiosonic Natural Frequency

Audiosonic natural frequency results were obtained on all specimens. There appears to be a correlation between physical characteristics of the specimens and the frequencies obtained. Specimen IPC-5, visually reported as cracked, had the lowest natural frequency of all the IPC specimens. Specimen THE-4, which had several cracks, was well below the other four THE specimens in natural frequency. Two suspect TIP specimens, having eddy current crack-like indications, had the lowest frequencies of their group.

(f) Eddy Current Electrical Conductivity Measurements

Electrical conductivity of the specimens was measured with a Sigmatest Model 2.067 instrument. Special extrapolation techniques were used to measure conductivities below 1%. While the Magnaflux ED 510 eddy current instrument is used for defect detection, the Sigmatest Model 2.067 is designed to quantitatively measure electrical conductivity. The instrument is calibrated by placing the probe on a calibration test block of known conductivity which causes a change in the inductance of the probe. This change in probe inductance produces an unbalance in the instrument wherein rebalancing the circuit through a variable capacitor gives a measure of conductivity. The variable capacitor has a meter graduated in IACS conductivity. The change in inductance of the test probe is directly proportional to the resistivity or electrical conductivity of the metal using 100% for commercial pure copper.

Conductivity readings can be measured directly on the scale for values above 1% and can be computed by special means to values as low as 0.61% IACS. The conductivity of the wire-wound tungsten specimens ranged from 0.71% to 2.33% IACS. Conductivity measurements were made at the midpoint of each specimen at 0° , 120° , and 240° with the minimum and maximum conductivity points being located and recorded for postphysical test analysis.

Conductivity readings measured on specimen TIP-1 ranged from 0.855% to 1.981% IACS (variation of 224%). This variability was not a result of test or instrument application since all values were repeatable.

TABLE V
TUNGSTEN SPECIMENS DIMENSIONAL DATA

<u>Specimen S/N</u>	<u>OD (Center) Minimum/Maximum</u>	<u>ID (Center) Minimum/Maximum</u>	<u>Wall Thickness Minimum/Maximum</u>
Length = 1.0 in.			
C-1	2.0270/2.0270	1.7501/1.7498	0.1370/0.1380
C-2	2.0285/2.0310	1.7504/1.7506	0.1365/0.1405
C-3	2.0220/2.0230	1.7502/1.7504	0.1360/0.1385
C-4	2.0260/2.0280	1.7500/1.7504	0.1350/0.1395
C-5	2.0250/2.0265	1.7494/1.7500	0.1370/0.1390
C-6	2.0300/2.0310	1.7499/1.7503	0.1385/0.1410
Length = 5.5 in.			
T-1	1.2135/1.2160	0.9998/1.0002	0.1060/0.1175
T-2	1.2135/1.2145	0.9997/0.9999	0.1105/0.1130
T-4	1.2130/1.2130	0.9998/1.0002	0.1080/0.1110
T-5	1.2080/1.2085	1.0000/1.0004	0.1050/0.1160
T-6	1.2060/1.2065	0.9995/1.0000	0.1040/0.1095
T-7	1.2085/1.2100	0.9989/0.9994	0.1085/0.1110
IP-1	---	2.0005/2.0010	0.1385/0.1390
IP-2	---	2.0001/2.0008	0.1360/0.1385
IP-3	---	2.0002/2.0006	0.1320/0.1410
IP-4	---	---	0.1330/0.1390
IP-5	---	---	0.1335/0.1370
IP-6	2.2830/2.2850	---	0.1375/0.1385
Length = 6 in.			
THE-1	0.9995/0.9995	0.7500/0.7507	0.1109/0.1219
THE-2	1.0015/1.0020	0.7498/0.7504	0.1142/0.1223
THE-4	1.0010/1.0013	0.7502/0.7506	0.1126/0.1226
THE-5	1.0000/1.0005	0.7504/0.7506	0.1160/0.1231
Length = 7.125 in.			
TIP-1	1.8615/1.8630	1.6262/1.6264	0.1110/0.1210
TIP-2	1.8750/1.8760	1.6258/1.6260	0.1210/0.1275
TIP-3	1.8810/1.8820	1.6248/1.6253	0.1250/0.1300
TIP-4	1.8770/1.8775	1.6255/1.6265	0.1220/0.1270
TIP-5	1.8850/1.8860	1.6256/1.6261	0.1275/0.1300
TIP-6	1.8885/1.8895	1.6241/1.6242	0.1260/0.1300

It has been established that thickness variability affects the eddy current electrical conductivity measurement. Since wire-wound tungsten has an extremely low conductivity, the thickness variation effect on electrical conductivity is not known. The conductivity values for the specimens are shown in table VI.

(g) Ultrasonic Velocity

Ultrasonics was considered as an NDT for detecting delaminations. Due to the material's extreme porosity, complex matrix, and anticipated high attenuation, the only ultrasonic method considered feasible was through transmission ultrasonics. Ultrasonic velocity was measured by the pitch and catch technique. A signal could not be transmitted through the material. Several modifications were attempted including applying coatings, compensating for change in sound velocity, and using different transducers and more powerful equipment. It was concluded that ultrasonic velocity measurements are not practical for this material.

(h) Photon Radiography

Previous experience with wire-wound tungsten composite throat inserts indicated excellent radiographic results using a single-wall technique and a 300-kv source. Radiographs of the wire-wound samples were not readable and indicated that the thicknesses were beyond the capability of this X-ray facility. Therefore, a practical limit for a 300-kv source X-ray of wire-wound tungsten appears to be a thickness of 0.125 to 0.150 in. The radiation absorption of the 0.200-in.-thick specimen was so pronounced that test results were meaningless.

The specimens were inspected with a 3,000-rhm cobalt 60 source at a film-to-source distance of 30 ft. This distance was necessary to achieve maximum sensitivity since the source has a 1-cm-diameter focal spot. Figure 13 shows the THE specimens and a calibration standard of various thicknesses. The light areas in the radiograph indicate low density. Note the clearly visible cracks in specimen THE-4 and the principal voids in the ends of the other specimens. Resolution sensitivity was at the threshold level for the wire mesh pattern. A greater film focal distance on this source could achieve comparable sensitivity to that of neutron radiography. However, a Linac or Betatron (small focal spot) could result in even greater line resolution than for neutron radiography.

Defects detected by cobalt radiography were large granular voids, chips at the ends of the parts, large cracks, and delaminations near the end of the compression specimens. The contrast in the radiograph was not good enough to reveal the small tubular voids accompanying the wire mesh. An advantage of the cobalt radiography method is detection of gross defects without the masking effect of the wire mesh pattern.

TABLE VI
WIRE-WOUND TUNGSTEN SPECIMENS CONDUCTIVITY RESULTS

Specimen S/N	% IACS		
	At 0°	At 120°	At 240°
T-1	0.688	0.663	0.703
T-2	0.942	0.980	1.000
T-4	0.820	0.830	0.760
T-5	1.120	1.182	1.150
T-6	1.212	1.210	1.263
T-7	1.112	1.119	1.140
IP-1	0.914	0.934	0.871
IP-2	0.960	0.957	1.051
IP-3	0.805	0.830	0.813
IP-4	0.842	0.902	0.815
IP-5	0.938	1.032	0.945
IP-6	0.663	0.648	0.673
C-1	0.815	0.842	0.780
C-2	0.800	0.755	0.785
C-3	0.830	0.847	1.010
C-4	0.968	0.934	0.873
C-5	0.805	0.790	0.830
C-6	0.757	0.805	0.790
TIP-1	0.938	1.981	1.000
TIP-2	1.268	1.000	1.120
TIP-3	0.772	0.811	0.830
TIP-4	1.172	1.130	1.143
TIP-5	0.740	0.788	0.711
TIP-6	0.813	0.870	0.830
THE-1	1.290	1.325	1.172
THE-2	1.179	1.168	1.157
THE-5	1.500	1.496	1.425

Reproduced from
best available copy.

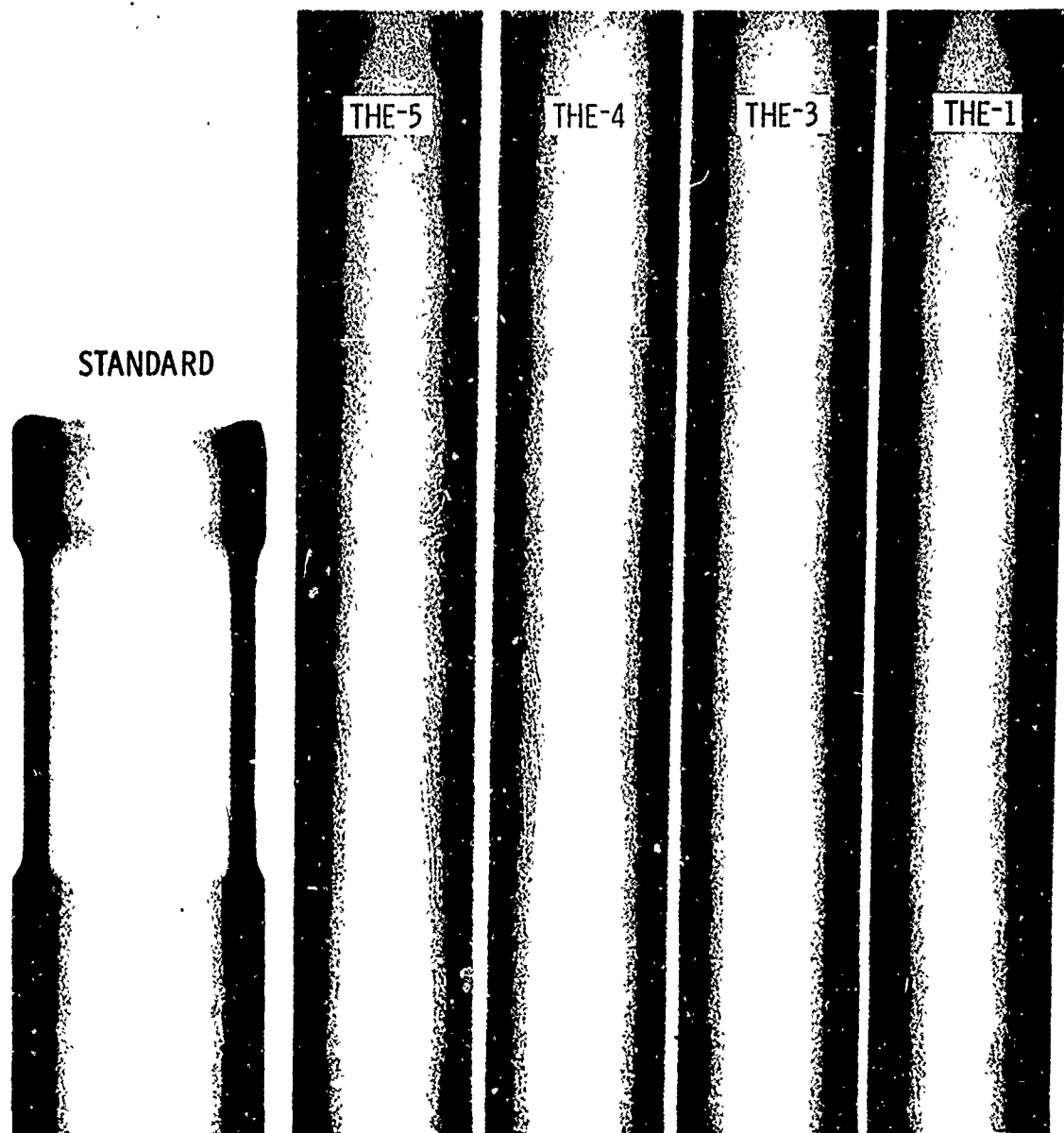


Figure 13. 3,000-Rhm Cobalt 60 Radiograph of THE Specimens

(i) Neutron Radiography

Neutron radiography was conducted by Aerotest Operations of San Ramon, California, under a service contract. The reactor used was a swimming pool type having zirconium hydride moderation and licensed for 250-kw (t) maximum operating power. The reactor core was housed in a tank 23 ft deep and 10 ft in diameter. Neutrons were gathered by a shaft (rectangular aluminum tube) running from the core to the surface. Stray neutrons from the core traversed the tube to the shooting area which accommodates two 14 by 17-in. film cassettes. Additional shielding was built around this area to allow setup of the next exposure during operation, thus providing production-line neutron radiography. By use of specially constructed vacuum cassettes and a laminar flow film change area, maximum film process quality is obtained. The neutron radiographs produced were of a film process quality comparable to those in a conventional radiographic inspection setup.

The objectives of the NDT plan were achieved for neutron radiography. The original concern was that the wire matrix image, so pronounced in thin wall X-rays of the tungsten composite, would mask defects such as cracks. Techniques were proposed to enhance the contrast between defects and matrix wire patterns. The proposed enhancement methodology was not feasible; however, a contrast enhancement technique was accomplished.

The reactor produced a neutron flux of 3.5×10^9 . Exposure technique is merely a matter of determining exposure time, since the available neutrons per unit of time is a fixed quantity. The first exposures made at 8-1/2 min (normal time) resulted in a film density of 2.02 H & D units. The contrast was not considered adequate. The remaining exposures made at 13 min resulted in a film density of 2.59 H & D units. Neutron radiographs were made at 0° and 120° for all specimens.

As experienced with photon radiography, film density increases with exposure time due to object and beam scattering. Using a contrast, resolution, and scatter indicator, calculations were made to determine the percentage of the total film density usable in contrasting variations in the test object. For the 8-1/2-min exposure, 74.1% of the film density was computed to be usable, while for the 13-min exposure, the percentage is 76.4.

A visual comparison was made of the films exposed at 8-1/2 and 13 min. Line resolution (sensitivity) was greatly enhanced in the 13-min exposure making the wire mesh pattern clearly visible, wherein the 8-1/2-min exposures resulted in no visible wire mesh pattern.

Enhancement techniques were considered, such as hydrogen gas infiltration or liquid impregnation with high cross-section neutron absorbers (boric acid, gadolinium nitrate, solvents). Hydrogen gas was ruled out by the test facility because the volume of gas required and the anticipated loss of neutrons would result in an underexposure. Boric acid and other similar liquid impregnants were not used because of potential contamination.

The enhancement test media selected was neutral grain alcohol which completely evaporates without a residue. The specimens were soaked in alcohol for 20 min, placed in an aluminum container, sealed with zinc chromate putty to prevent surface evaporation of the alcohol, and immediately radiographed at an exposure time of 13 min. The resultant radiographs (figure 14 and 15) were completely void of the wire mesh pattern. The annular voids remained in the overspray near the ends of the specimens.

Chips, annular voids, delaminations, cracks, and wire matrix patterns (where associated tubular voids are large enough) are clearly detectable by neutron radiography. A disadvantage of this test method is residual radioactivity in the material after irradiation which requires at least 48 hr to dissipate.

Neutron radiography can disclose discrete defects in wire-wound tungsten composites in thicknesses less than $3/4$ of an in. This is the distance the beam must travel through the part to reach the film, hence single-wall radiographic techniques (film at center of part) must be used on large components. Wire-wound tungsten throat inserts should be neutron radiographed before assembly since low-density components such as graphite or ablative materials exhibit a high neutron absorption capability.

(j) Ultrasonic Flaw Testing

As noted previously, wire-wound tungsten attenuates sound at a very high rate. A commercial test laboratory, using all available instruments produced by Sperry including the Reflectroscope Models UM700 through Model 821, was unable to penetrate the sample specimen. A pulse echo signal could not be obtained through the material at frequencies from 15 through 0.2 MHz. The specimens were tested with transducers of very high sensitivity by Branson Instruments. Specimens with wall thicknesses of 0.130 to 0.140 in. could not be penetrated by their instruments.

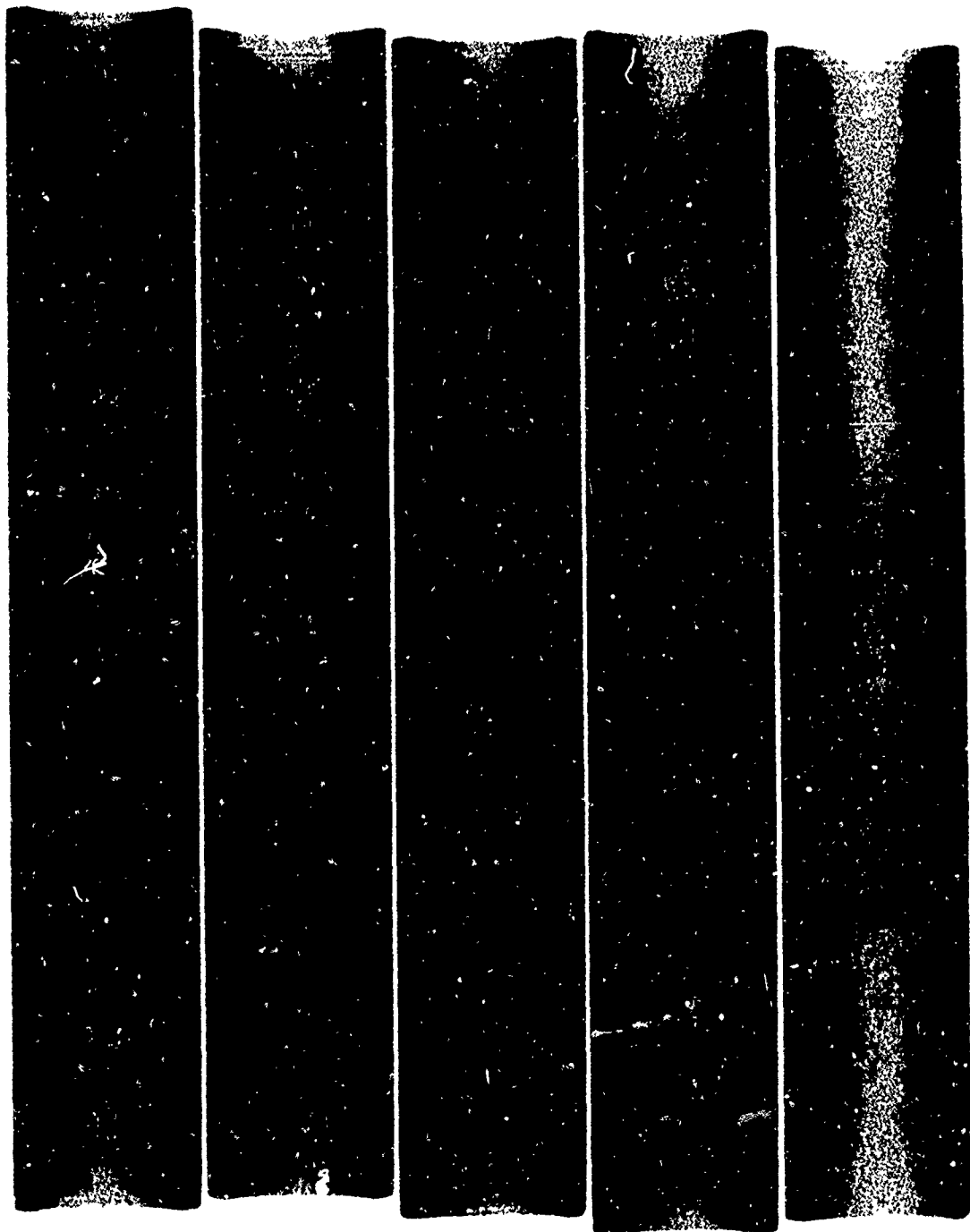


Figure 14. THE Specimen After 13-Min Neutron Exposure

Reproduced from
best available copy.

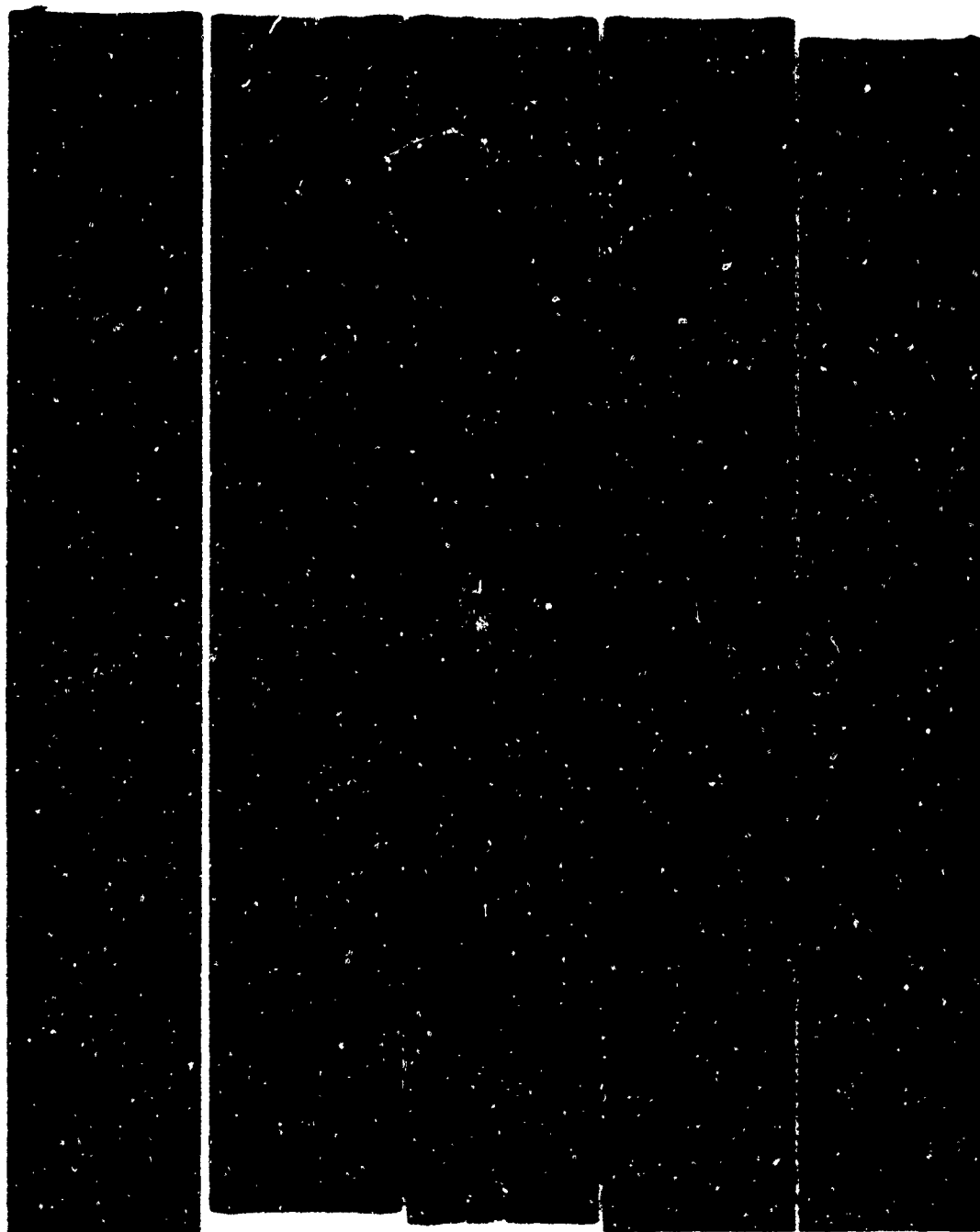


Figure 15. THE Specimens Impregnated with Grain Alcohol
After 13-Min Neutron Exposure

(2) Evaluation/Measurement of Uniformity/Reproducibility

The neutron radiographic study has shown that a small channel or void remains behind the tungsten wire as a result of the wire eclipsing the subsurface from the oncoming plasma spray. Ultrasonic and radiographic results indicate that a void is present for the entire length of the wire between the plasma-sprayed surface and the wires. The diameter of this tubular void is a function of the variable determining neutron radiographic sensitivity. Every wire in the composited system appears ultrasonically to be a long void. These tubular voids result in sufficient sound scatter centers to prevent reception of sound reflection or sound transmission through the wire-wound tungsten composite material at ultrasonic frequencies.

Natural frequency analysis of the specimens indicated a relationship between structural strength and frequency in that specimens containing discrete defects exhibited the lowest frequencies.

Eddy currents provide a gauge of product local variability by a quantitative measurement of the electrical conductivity measured in percent IACS. Conductivity varied from specimen to specimen and within each specimen. A study was made of the thickness effect on conductivity. The results are shown in figure 16 which plots conductivity versus wall thickness at the center reference point of each specimen. The curves for specimens T-5 and T-6 show the typical response encountered when variations in thickness affect the electrical conductivity. However, T-7 shows a reversing trend of having higher conductivity for thinner sections. The THE-2 specimen shows the type of correlation which occurs if thickness affects the conductivity reading below the reversal knee, since the thinner location has the lower conductivity and the thicker location the higher conductivity. The curves for THE-5 show no correlation to thickness. The tension specimens (T-5, -6, and -7) were 1.208-in. in diameter in the area studied, while the thermal expansion specimens were 1.001-in. in diameter showing that the variability was not due to a combination of edge effect and thickness variation. Conductivity versus thickness for all specimens is shown in figure 17. The pattern shows that the threshold of thickness interference with true material conductivity is below 0.100 in. for wire-wound tungsten.

(3) Discussion of NDT Results

(a) Screening of Specimens

The majority of defects in the specimens were in areas to be removed prior to mechanical and thermal property testing. Some annular voids were detected by photon and neutron radiography in the heavy grip areas of the tension specimens and would not affect physical testing. Two of the specimens (TIP-5 and 2) had crack-like indications detected by eddy currents. No visual, photon radiographic, or neutron radiographic inspection methods

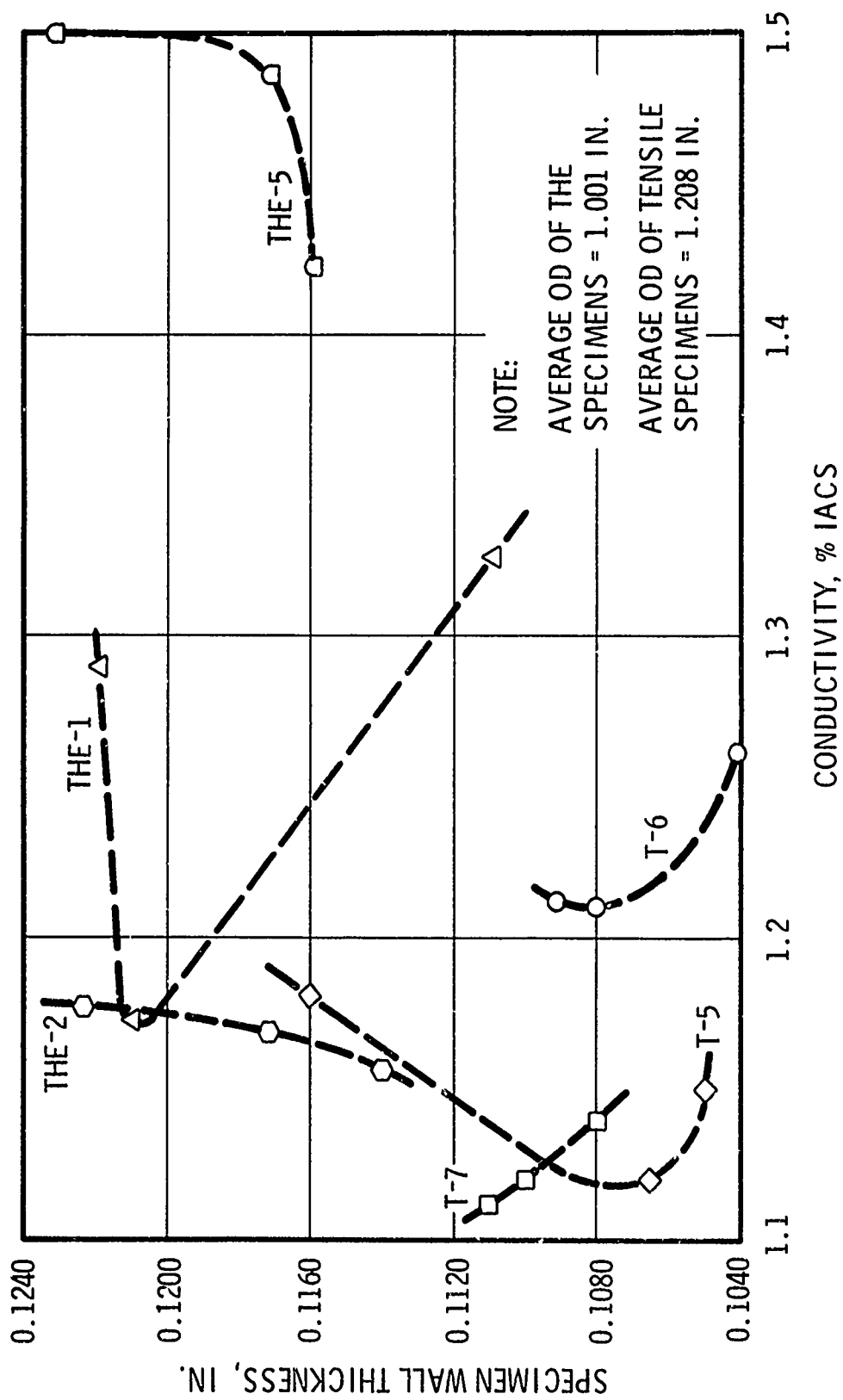


Figure 16. Conductivity vs Wall Thickness for Specimens T-5, T-6, T-7, THE-1, THE-2, and THE-5

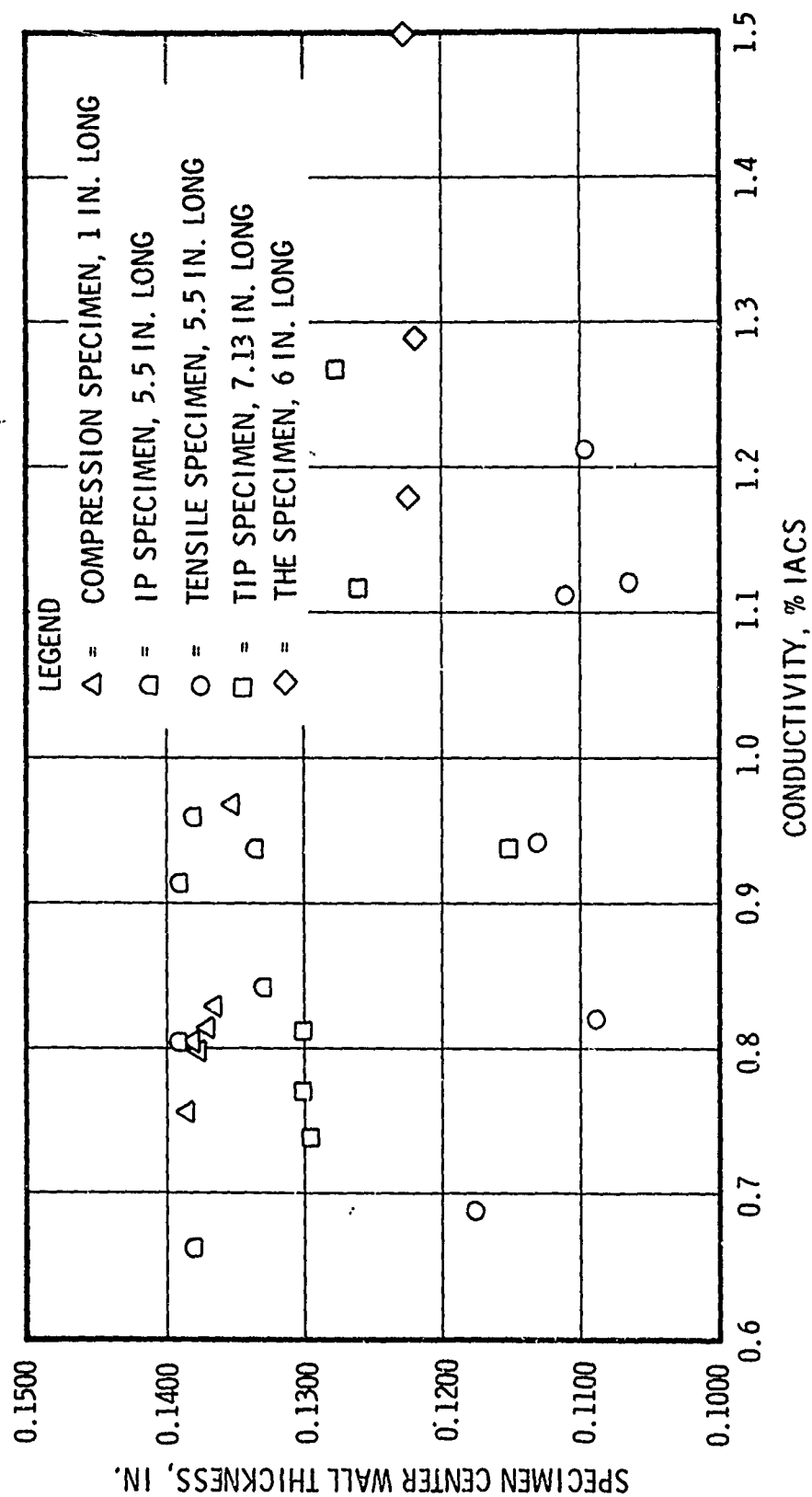


Figure 17. Conductivity vs Wall Thickness for All Specimens

could corroborate these eddy current indications. The eddy current response could have been caused by separation of the tungsten wire hoop windings. Since one objective of the NDT study was to determine reject criteria based on correlation of discrete defects to performance, these specimens could provide meaningful data. Therefore, these specimens were included in the test phase.

(b) Capability to Identify Discrete Defects

The capability of the various NDT inspection methods to detect defects in wire-wound tungsten was evaluated. Ultrasonics are unsatisfactory for inspection of discrete defects. The properties of wire-wound tungsten are such that no sound wave can penetrate the porous composite. Eddy current techniques have a high sensitivity for crack detection. Photon radiography is satisfactory below 0.100 in. for wire-wound tungsten material.

(4) Posttest Evaluation with NDT Results

An evaluation of the tested specimen's appearance and properties, compared with pretest NDT results, proved inconclusive. The elevated temperature test conditions erased any evidence of the effect of suspected defects and their correlation to failure or property variations. Specimens tested at room temperature showed no correlation to suspected defects. Specimens TIP-2, TIP-5, and IP-5 had cracks. The properties of TIP-2 agreed favorably with those of TIP-1, a specimen supposedly defect free. Specimens IP-1 and IP-2 were considered identical in NDT quality and defect free; however, a large difference in elastic modulus indicates the possibility of internal delaminations. Finally, there was no evidence that the specimen test fractures originated at prior defects in the composite. The fracture appearances shown in figure 18 were typical for the type of test conducted.

2. THERMAL PROPERTY TESTS

Thermal property testing was performed on test specimens fabricated and inspected by UTC, by Battelle Memorial Institute, Columbus, Ohio, as described in the subsection entitled, "Specimen Fabrication." The task objectives of this study included evaluation of:

- A. Thermal conductivity (direct, steady-state) - 70° to 1,500°F (21° to 815°C)
- B. Thermal diffusivity - 1,500° to 4,000°F (815° to 2,200°C)
- C. Specific heat - 1,500° to 4,000°F (815° to 2,200°C)
- D. Thermal expansion - 70° to 4,000°F (21° to 2,200°C)

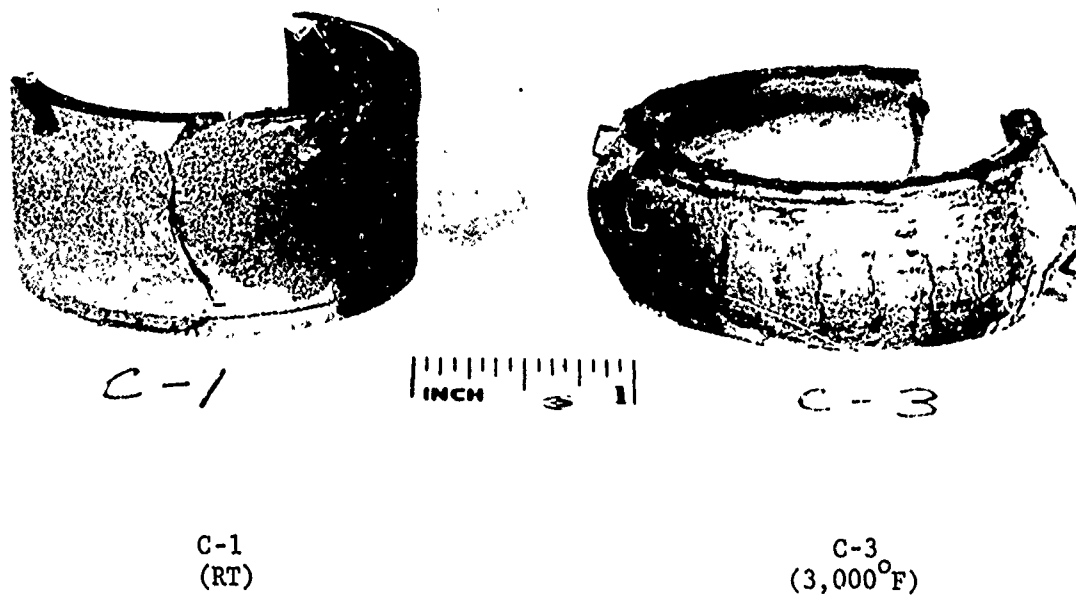
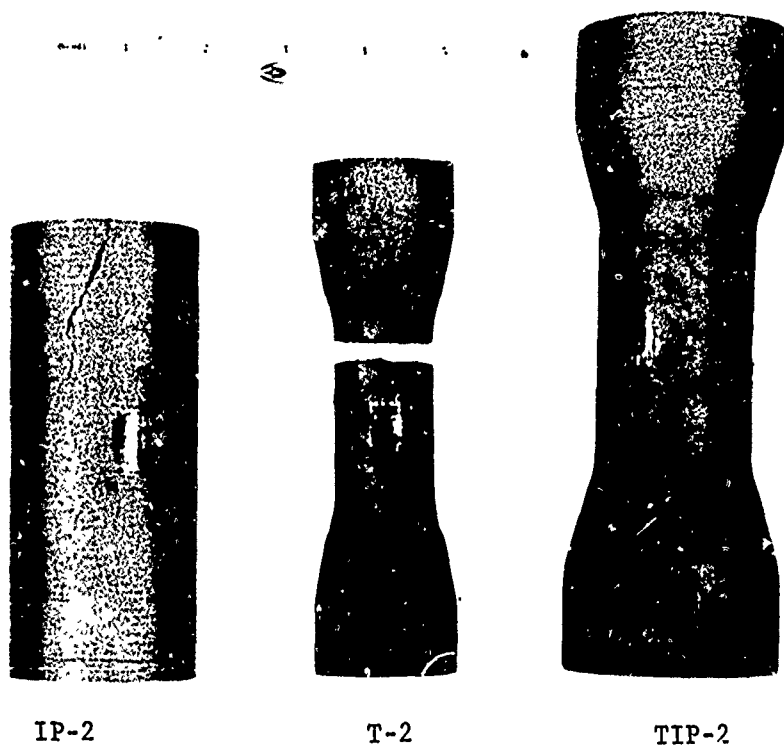


Figure 18. Appearance of Tested Wire-Wound Tungsten Specimen

Specimen materials for items A, B, and D were furnished with geometries in a direction normal to the reinforcing filaments. Items A and B involved evaluation of material not presintered; item D involved studies of material in both the as-composited and presintered conditions and in the axial and radial (through-the-thickness) directions. Item C evaluation was made on as-composited material. The desired maximum test temperature of 4,500°F (2,482°C) was not attained because of test apparatus capabilities.

Samples of the as-composited material were analyzed by spectrographic and vacuum fusion techniques to aid in interpretation of the thermal property measurement data. The results were:

<u>Element</u>	<u>Content, ppmw</u>
Fe	10
Ni	5
Mo	30
Cu	1
Ca	1
O	2,350
H	10
N	260
W	Balance

No studies were made to determine the form of the oxides present in the material.

a. Thermal Test Methods and Results

Detailed test methods, fixtures, and apparatus used to determine thermal conductivity, thermal diffusivity, specific heat, and thermal expansion properties for wire-wound tungsten are discussed in Appendixes II through V. A brief description of the specific tests and the resulting property data are presented in the following subsections.

(1) Thermal Conductivity Studies (Direct Measurement)

Thermal conductivity in the range from room temperature to 1,500°F (815°C) was measured by the steady-state longitudinal heat flow technique described in Appendix II.

This approach is a variation of the cut-bar technique, which usually requires a bar specimen with a length-to-diameter ratio of at least 4. Since this configuration was not practical for the material available to this study, specimens were assembled by joining three groups of four 3/4-in.-diameter 1/4-in.-long tungsten composite by indium soldering. The faces of the specimen disks were ground flat and parallel prior to being joined. The three 1-in.-long specimens were then joined alternately between four 1-1/2-in. lengths of Type 347 stainless steel which served as the heat flowmeter. Thermocouples were located in the meters; specimen temperatures at meter

interfaces were determined by extrapolation. The assembled specimen and meter components are shown in figure 19 after removal from the insulated apparatus chamber.

During measurement, the assembly was loaded axially at about 50 psi to maintain good contacts at all the interfaces. Pressure in the chamber was held high enough to avoid evaporation of the indium and low enough to avoid problems of convective heat transfer (approximately 40×10^{-3} mm Hg).

Table VII lists the conductivity data in the order recorded. Since there were three specimen segments in the assembly, three data points were obtained at each thermal equilibrium. The data are plotted in figure 20.

The good agreement of values for different segments of the specimen assembly at approximately the same temperatures (at different equilibria) promotes confidence in the data and the measurement technique.

At low temperatures (below 300°C), conductivity appears to be relatively insensitive to temperature. As the temperature is increased above approximately 400°C , conductivity increases and remains at the higher levels on subsequent cooling. Some sintering of the material apparently takes place at these temperatures. This was also observed in the thermal diffusivity measurements.

(2) Thermal Diffusivity Studies

Thermal diffusivity measurements in the range from 932° to $3,812^{\circ}\text{F}$ (500° to $2,100^{\circ}\text{C}$) were made by the technique described in Appendix III. Diffusivity was measured on three unsintered specimens approximately 0.16 in. thick in a direction normal to the laminae under argon at atmospheric pressure.

Specimen No. 1 was studied throughout this temperature range to accumulate data on the effects of sintering as well as temperature. Table VIII lists these data in the order measured. These values, plotted in figure 21, illustrate the significant irreversible effects of sintering on the diffusivity. Table VIII also shows accumulated time for the specimen at the various temperature levels.

Measurements on specimen Nos. 2 and 3 were directed toward an investigation of sintering rate effects at two elevated temperatures. The first sintering temperature was approximately $3,000^{\circ}\text{F}$ ($1,645^{\circ}\text{C}$), which was chosen to coincide with the maximum thermal diffusivity on the heating curve for sample No. 1. Specimen No. 2 was heated rapidly to $3,000^{\circ}\text{F}$ ($1,645^{\circ}\text{C}$), and diffusivity measurements were made as a function of time over a period of approximately 2 hr. Following this heat treatment, the sample was heated to $3,270^{\circ}\text{F}$ ($1,800^{\circ}\text{C}$) and was held for 1/2 hr during which time measurements were made. Data on cooling were then obtained. The time and diffusivity data are given in table IX.

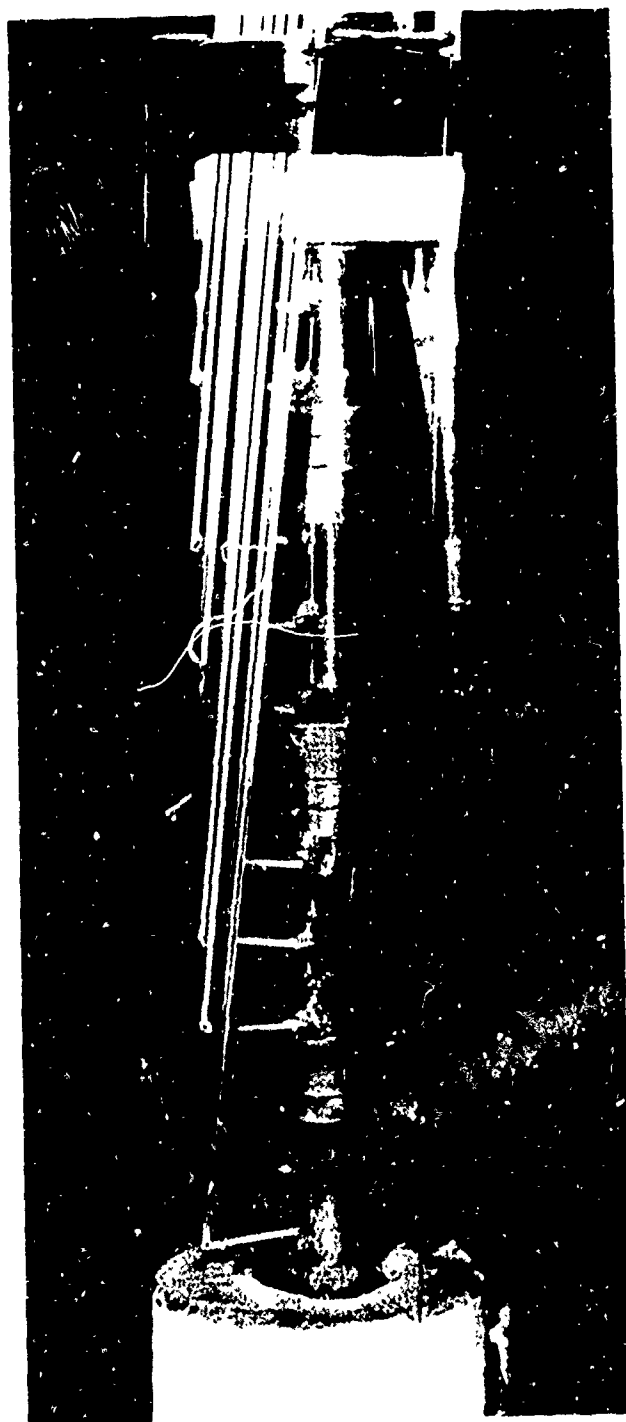


Figure 19. Steady-State Thermal Conductivity Specimen Assembly

TABLE VII
STEADY-STATE THERMAL CONDUCTIVITY DATA FOR UNSINTERED
WIRE-WOUND TUNGSTEN COMPOSITE

Thermal Equilibrium	Temperature °C	Thermal Conductivity $\text{W cm}^{-1} \text{K}^{-1}$
1	60	0.060
	135	0.061
	211	0.058
2	109	0.063
	244	0.061
	376	0.061
3	191	0.058
	404	0.070
	583	0.087
4	284	0.062
	587	0.090
	835	0.104
5	315	0.089
	1621	0.081

The next sintering temperature chosen was the highest temperature considered safe over an extended time period, or approximately 3,630°F (2,000°C). Sample No. 3 was heated rapidly to 3,600°F (1,986°C) and measurements were made as a function of time over a 30-min period. After cooling, data were obtained. Time and diffusivity values are shown in table X.

Figure 22 includes curves for the three samples plotted from the data in tables VIII, IX, and X. It is obvious that sintering becomes pronounced above 1,472°F (800°C) and results in the maximum increase in diffusivity at about 2,912°F (1,600°C) (with adequate time). The increase is permanent, and the data on cooling illustrate a pronounced change in the character of the property curve.

Sintering is obviously both time and temperature sensitive. After fairly rapid heating to 3,000°F (1,645°C), specimen No. 2 continued to show an increase in diffusivity for 2 hr, then further increased on heating to 3,270°F (1,800°C). Specimen No. 3 apparently reached saturation in approximately 30 min at 3,600°F (1,986°C).

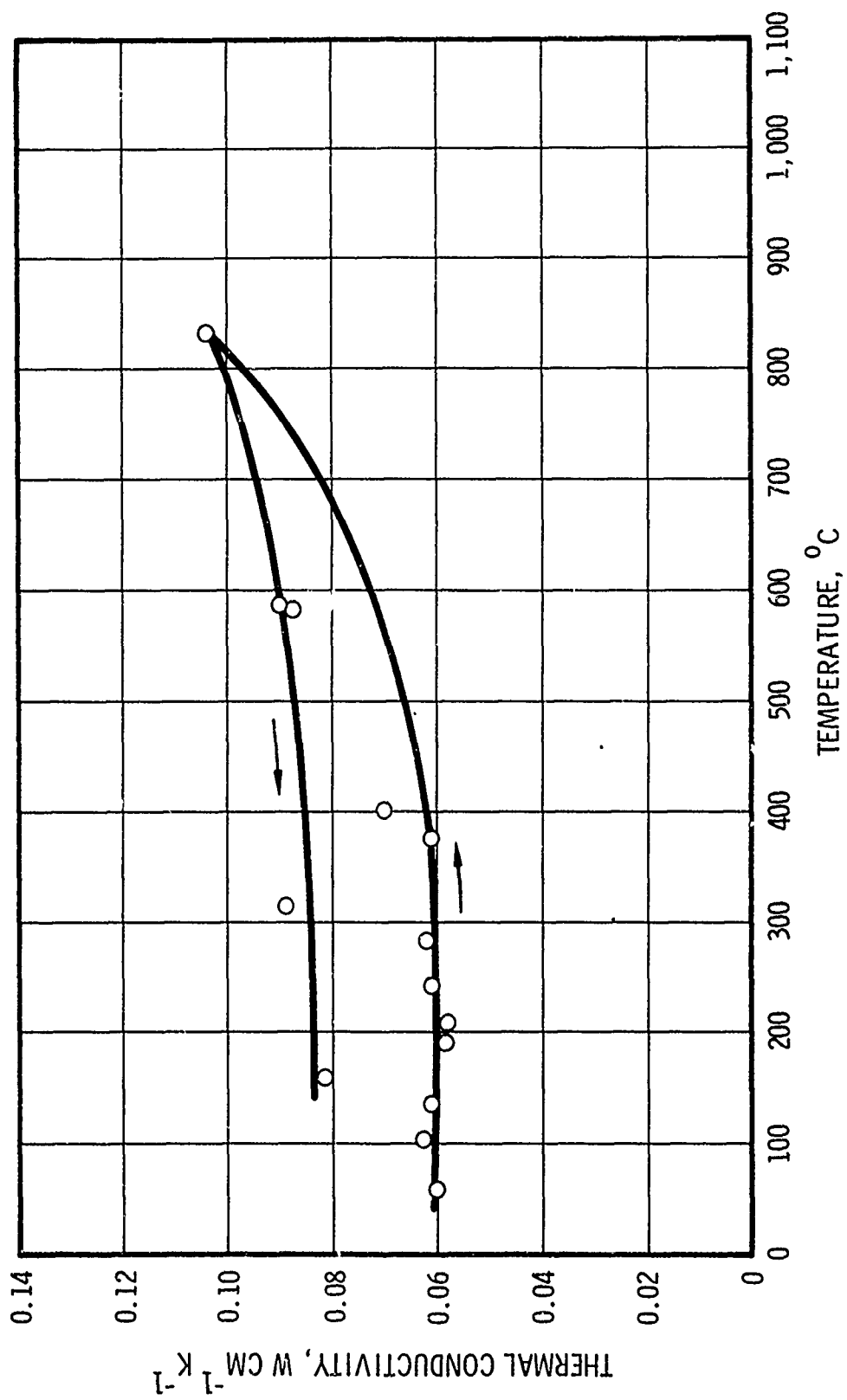


Figure 20. Thermal Conductivity of Unsintered Wire-Wound Tungsten Composite
(Steady-State Measurement)

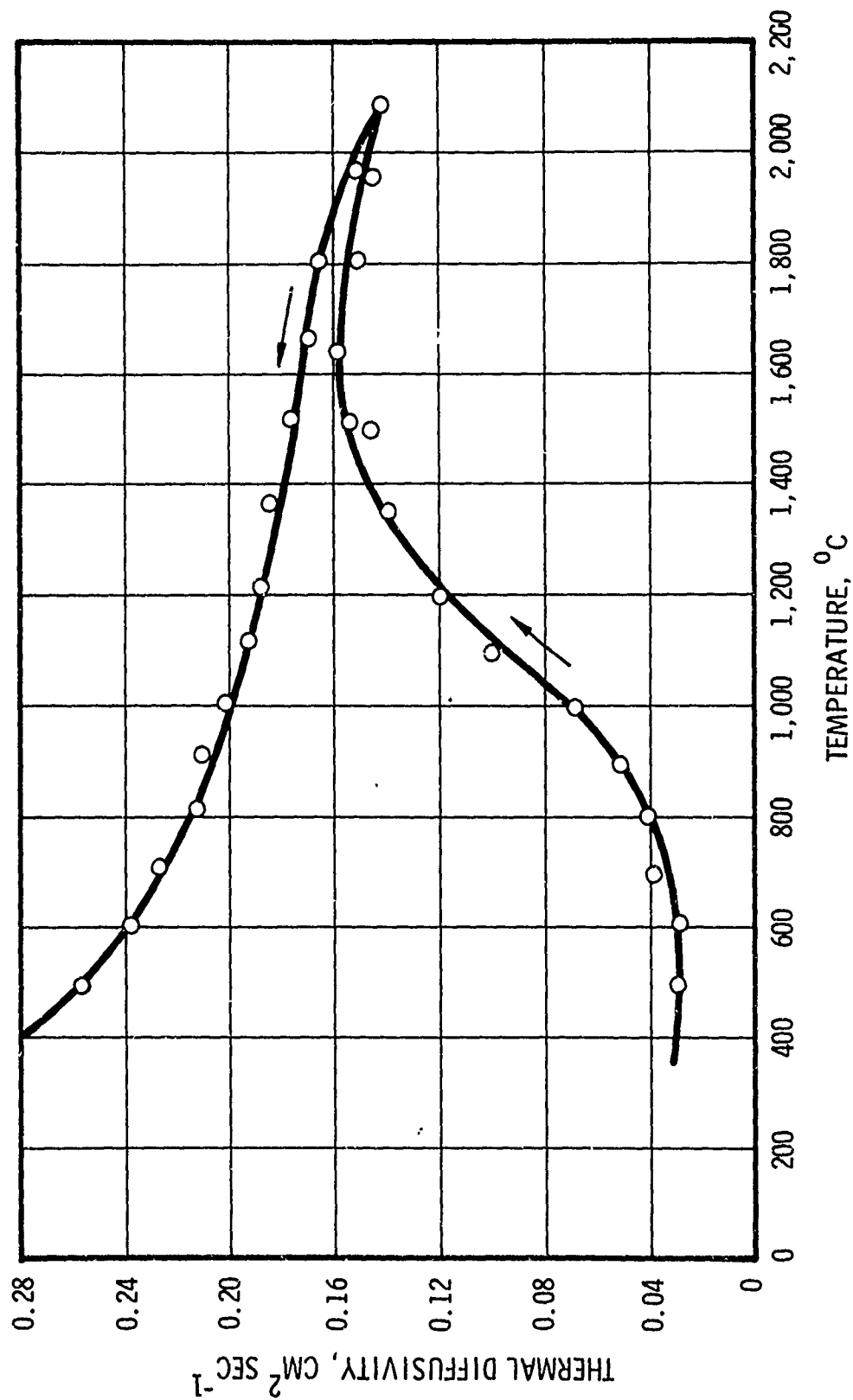


Figure 21. Thermal Diffusivity of Unsintered Wire-Wound Tungsten Composite
Normal to Wire Direction (Sample 1)

TABLE VIII

THERMAL DIFFUSIVITY OF UNSINTERED WIRE-WOUND
TUNGSTEN COMPOSITE FOR SAMPLE NO. 1*

Accumulated Time, min	Temperature °C	Thermal Diffusivity cm ² sec ⁻¹	Accumulated Time, min	Temperature °C	Thermal Diffusivity cm ² sec ⁻¹
0	499	0.0294	695	2,090	0.143
2		0.0297	697		0.143
4		0.0299	699		0.142
50	606	0.0295	715	1,968	0.152
52		0.0294	717		0.152
54		0.0293	719		0.151
133	697	0.0386	732	1,804	0.170
135		0.0385	734		0.162
137		0.0387	736		0.165
155	801	0.0407	765	1,662	0.173
157		0.0412	767		0.167
159		0.0407	769		0.170
207	899	0.0516	788	1,519	0.174
210		0.0506	790		0.180
212		0.0518	792		0.176
240	999	0.0676	825	1,369	0.185
243		0.0689	827		0.186
245		0.0701	829		0.183
307	1,098	0.0994	842	1,216	0.186
309		0.0993	844		0.188
311		0.1010	846		0.189
343	1,202	0.113	929	1,120	0.195
345		0.120	931		0.191
348		0.121	933		0.193
401	1,351	0.141	954	1,007	0.202
403		0.140	956		0.203
405		0.140	958		0.201
424	1,500	0.146	985	918	0.213
426		0.151	987		0.212
428		0.143	989		0.206
556	1,517	0.154	1,014	813	0.217
558		0.153	1,016		0.213
560		0.154	1,018		0.209
585	1,640	0.157	1,068	710	0.227
587		0.157	1,070		0.230
589		0.160	1,072		0.223
609	1,810	0.153	1,122	604	0.237
611		0.150	1,124		0.237
613		0.149	1,126		0.240
683	1,957	0.148	1,186	495	0.256
685		0.152	1,188		0.256
687		0.144	1,190		0.259

* Specimen bulk density is 15.87 g cm⁻³ before diffusivity measurement and 15.97 g cm⁻³ after diffusivity measurement.

TABLE IX

THERMAL DIFFUSIVITY OF WIRE-WOUND TUNGSTEN FOR SAMPLE NO. 2*

Accumulated Time, min	Temperature °C	Thermal Diffusivity cm ² sec ⁻¹	Accumulated Time, min	Temperature °C	Thermal Diffusivity cm ² sec ⁻¹
4.5	1,645	0.1155	150	1,800	0.142
6.5		0.1158	158		0.136
8.5		0.1078	166		0.150
11		0.1126	173		0.142
15		0.1159	182		0.144
20		0.1180			
25		0.1216	192	1,652	0.149
30		0.1226	201		0.154
			208		0.156
35	1,647	0.1232			
40		0.1243	233	1,391	0.164
45		0.1325	248		0.163
50		0.1341	255		0.159
55		0.1341			
60		0.1337	274	1,098	0.177
72		0.1284	284		0.169
80		0.1358	291		0.173
90		0.1325			
100		0.1303	372	796	0.192
			375		0.190
			378		0.192
110	1,646	0.1316			
120		0.1352			
125		0.1352	411	504	0.228
130		0.1383	413		0.224
			415		0.228

* Specimen bulk density is 15.83 g cm⁻³ before diffusivity measurement and 15.71 g cm⁻³ after diffusivity measurement.

TABLE X

THERMAL DIFFUSIVITY OF WIRE-WOUND TUNGSTEN FOR SAMPLE NO. 3*

Accumulated Time, min	Temperature °C	Thermal Diffusivity cm ² sec ⁻¹	Accumulated Time, min	Temperature °C	Thermal Diffusivity cm ² sec ⁻¹
4.3	1,986	0.0825	95	1,398	0.136
6.3		0.0906	97		0.134
8.3		0.0983	99		0.132
11.3		0.1002			
15		0.0998	115		0.138
18.5		0.1062	117		0.139
22.5		0.1027	119		0.141
26		0.1082			
30		0.1082	209		0.159
33		0.1058	211		0.156
			213		0.152
60	1,696	0.122		792	
62		0.121	248		0.180
64		0.123	250		0.175
			252		0.173

* Specimen bulk density is 15.63 g cm⁻³ before diffusivity measurement and 15.69 g cm⁻³ after diffusivity measurement.

If it is assumed that the process responsible for the increase in diffusivity obeys first-order kinetics, the diffusivity at any time (t) during an isothermal anneal is given by

$$\alpha(t) = \alpha_f - (\alpha_f - \alpha_i) \exp \left[(-At) \exp \left(-\frac{E}{kT} \right) \right] \quad (1)$$

where

α_f = final value of thermal diffusivity after annealing for infinite amount of time at temperature T

α_i = thermal diffusivity at start of anneal at temperature T

A = frequency factor (7.5×10^{13} sec⁻¹)

t = time counted from start of isothermal anneal

E = activation energy for process responsible for diffusivity change

k = Boltzmann's constant

T = absolute temperature, °K.

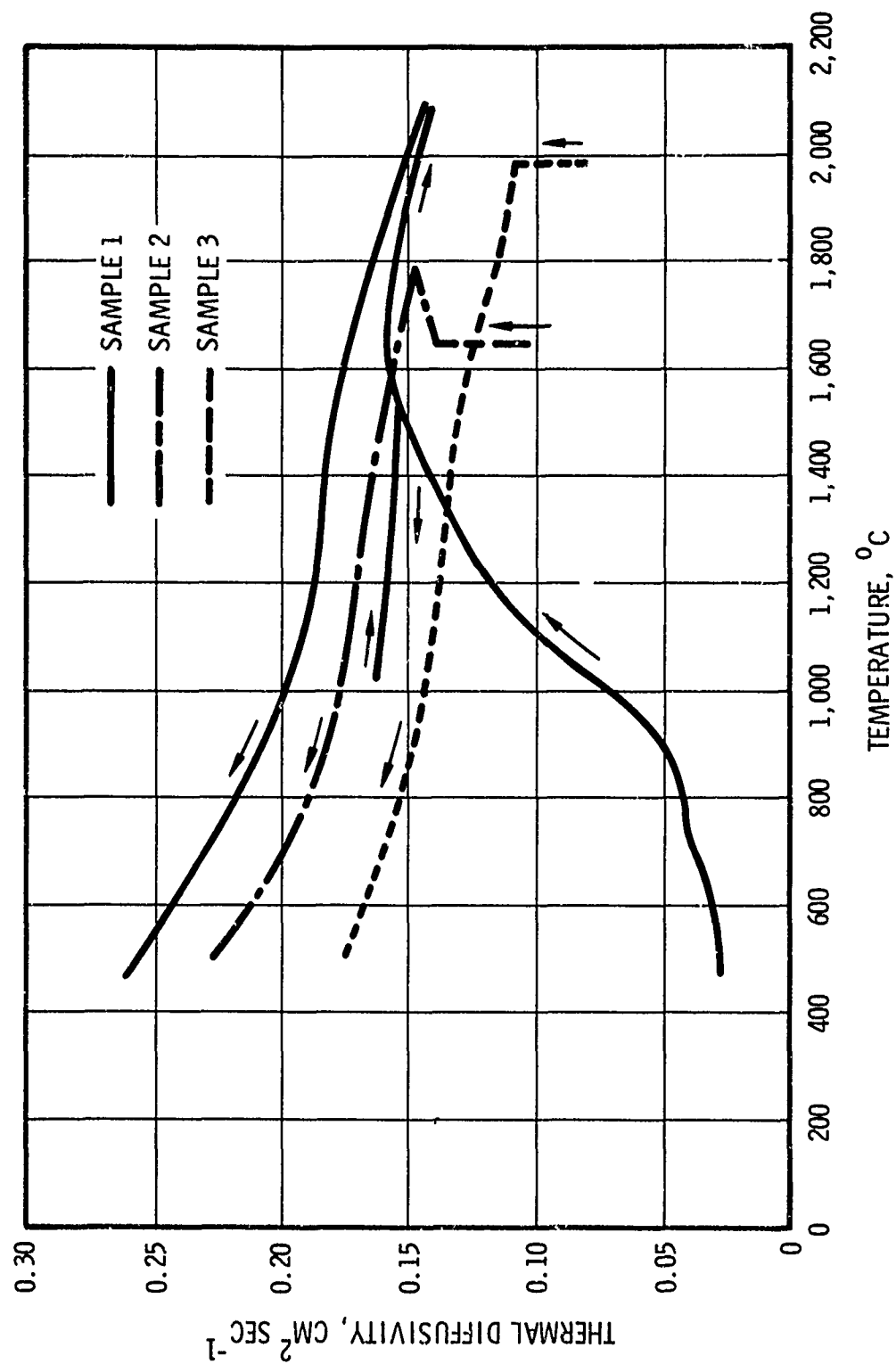


Figure 22. Thermal Diffusivity of Three Unsintered Wire-Wound Tungsten Composite Specimens
Normal to Wire Direction

Figures 23 and 24 show the results of thermal diffusivity measurements made during isothermal anneals at 3,000°F (1,645°C) and 3,600°F (1,986°C), respectively. The smooth curves through the data points are of the form of equation 1, chosen to give an approximate best fit to the data points. The activation energies were found to be approximately 6.5 and 7.4 eV at 3,000°F (1,645°C) and 3,600°F (1,986°C), respectively. For comparison, the activation energy for self-diffusion in tungsten has been reported from 4.05 to 6.65 eV⁽³⁾, while the heat of vaporization is approximately 8.0 eV.⁽⁴⁾ From the present study, it was not possible to determine the mechanisms responsible for the sintering effects.

The large differences in cooling curves for the three specimens are believed to be due to the presence of delaminations within the material either present initially or produced as a result of high heating rates, particularly for sample Nos. 2 and 3.

(3) Specific Heat Studies

Specific heat was determined from enthalpy measurements by the technique described in Appendix IV. Enthalpy was measured over the range from 1,470°F (800°C) to 4,000°F (2,200°C) on one sample of as-composited material in a sealed tantalum capsule.

Table XI lists enthalpy values in the order measured. A plot of these values (figure 25) illustrates changes in the material at approximately 2,010°F (1,100°C) on first heating and near 2,900°F (1,600°C) on heating and cooling. The order of measurements and location of the points describes the heat effects associated with these changes. It is not possible to determine the nature of the changes from this data, but it seems probable that the apparently large amounts of oxides indicated by the chemical analyses were involved in transfer reactions which are partially reversible in this closed system.

The specific heat-temperature relation which would normally be assumed from these enthalpy data is illustrated in figure 26. These curves describe the radically changing heat effects normally associated with transfer reactions which probably occurred in this case. If the reaction products had been allowed to escape during the enthalpy measurements, the specific heat curve probably would assume a shape and location similar to that of pure tungsten, also illustrated in figure 26. However, this should not be considered conclusive.

Specific heat values for wire-wound tungsten at various temperatures as determined from the enthalpy measurements and comparison of these values with those for pure tungsten follow.

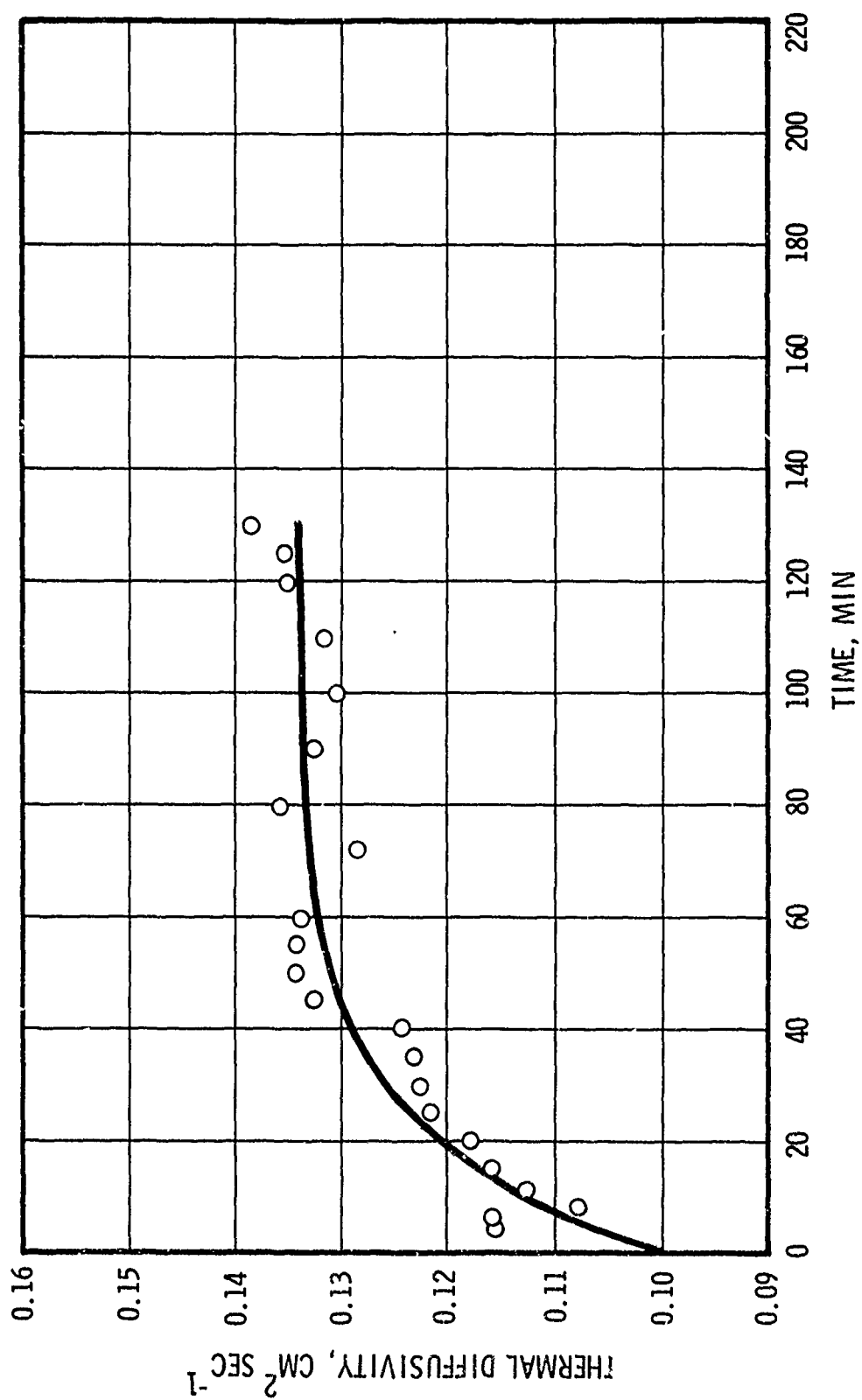


Figure 23. Thermal Diffusivity of Wire-Wound Tungsten During Isothermal Anneal at 1,645°C (Sample 2)

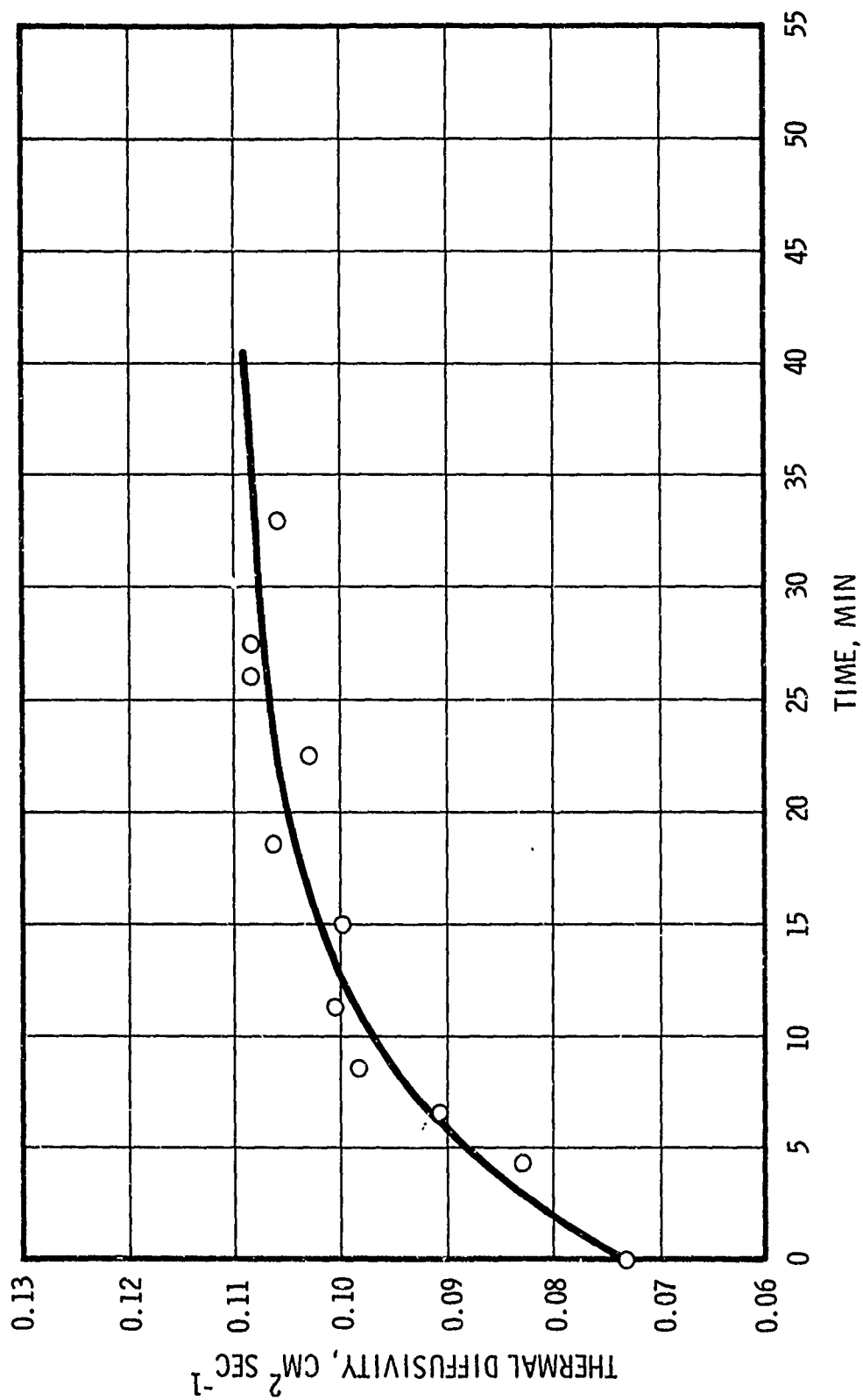


Figure 24. Thermal Diffusivity of Wire-Wound Tungsten During Isothermal Anneal at 1,986°C (Sample 3)

TABLE XI
EXPERIMENTAL ENTHALPY VALUES FOR WIRE-WOUND TUNGSTEN COMPOSITE
IN A SEALED CONTAINER UNDER HELIUM*

Temperature °C	Enthalpy $_{-1}^{(H_o^t)}$ cal g ⁻¹
845	29.3
951	33.0
1,071	37.7
1,301	46.3
1,595	58.8
1,078	38.3
1,131	39.9
1,308	46.6
1,100	38.8
1,075	37.8
1,904	69.5
1,598	59.3
1,864	67.9
1,699	61.3
1,647	59.1
2,049	75.1
2,201	80.7
1,552	55.9
1,575	55.9
910	30.7
1,200	41.4

* In the order measured.

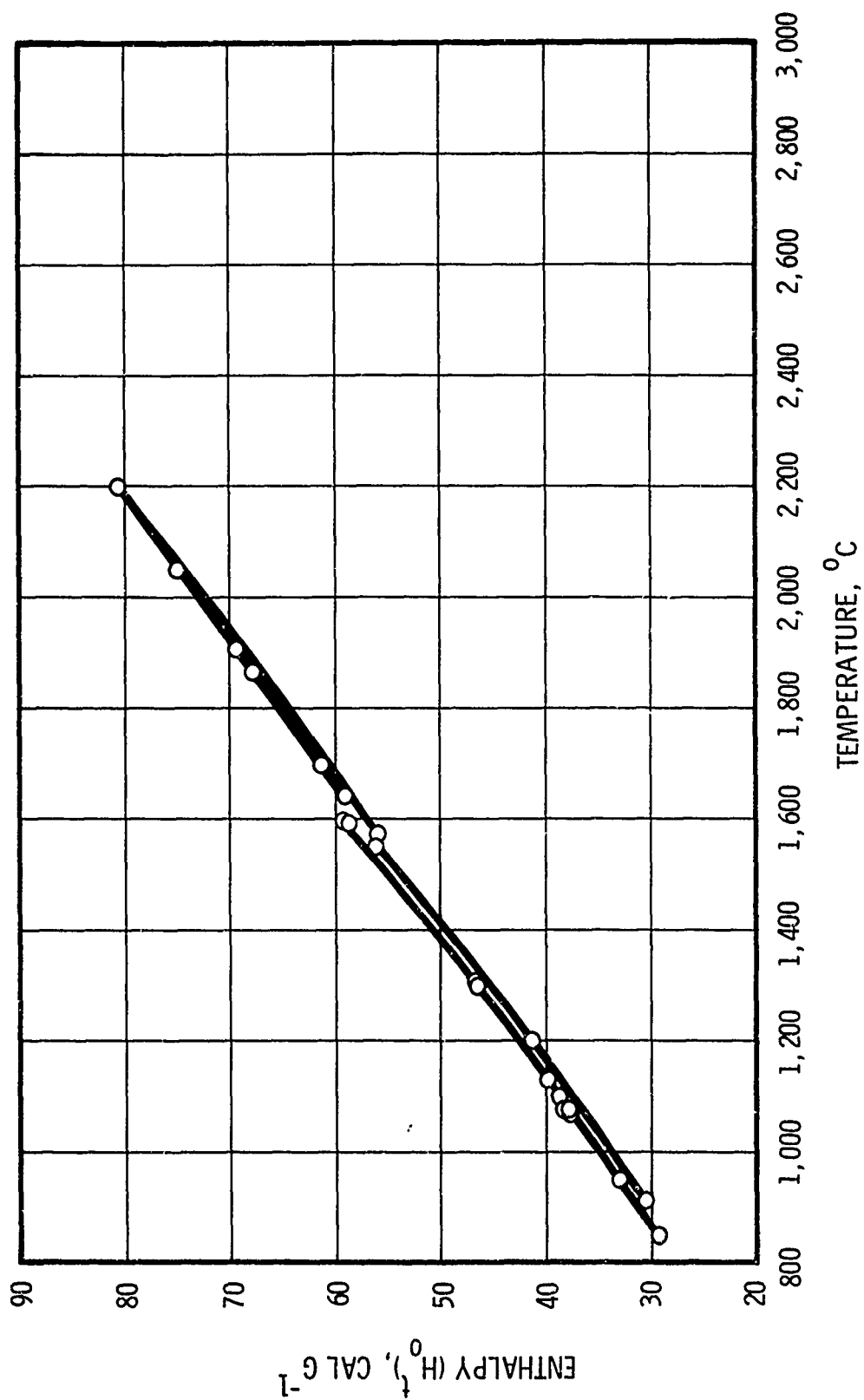


Figure 25. Enthalpy of Wire-Wound Tungsten Composite in Sealed Container

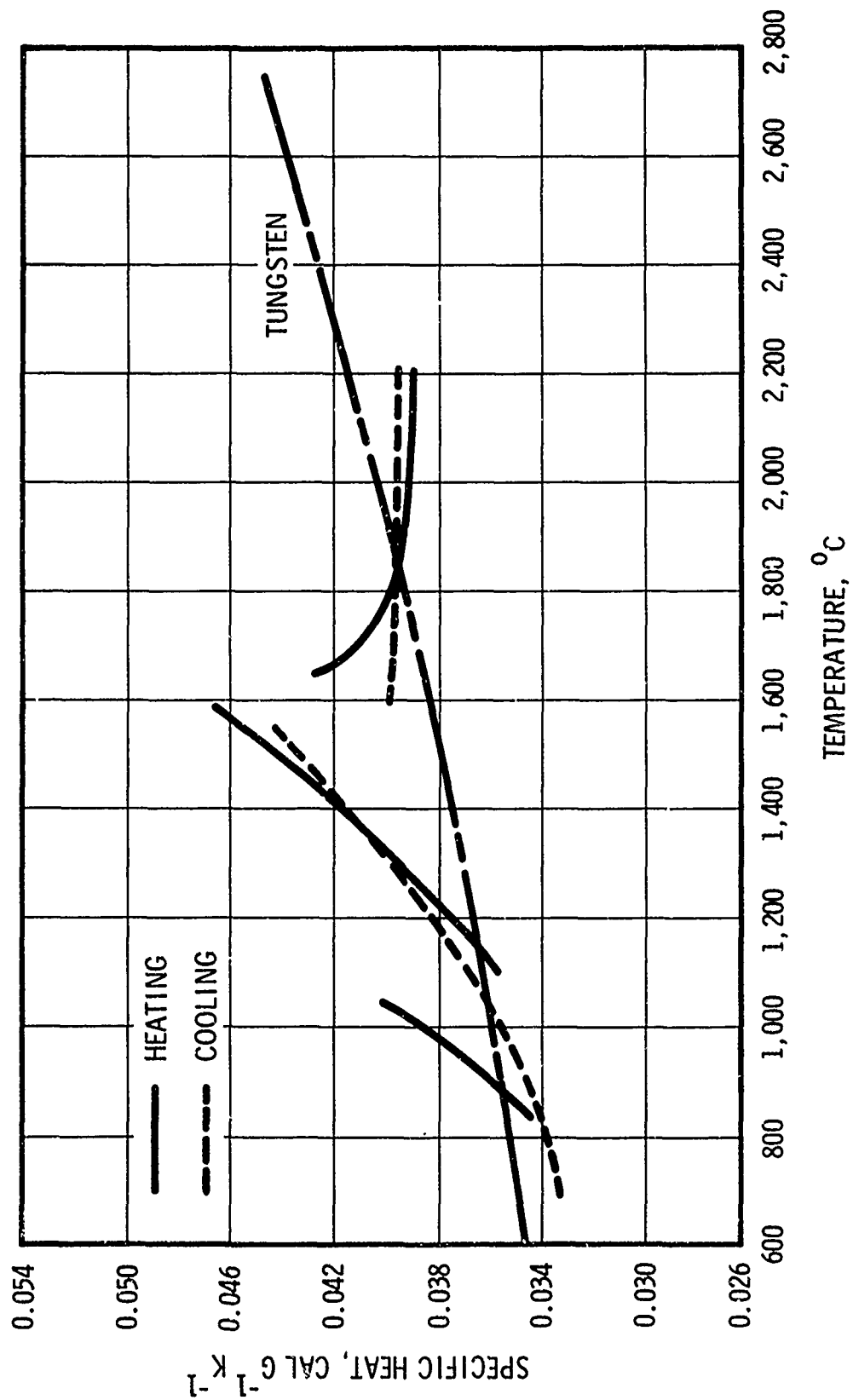


Figure 26. Specific Heat of Wire-Wound Tungsten Composite in Sealed Container

Temperature °F (°C)	Specific Heat, cal/gm/°K	
	Wire-Wound Tungsten	Pure Tungsten
1,470 (800)	0.0340	0.0350
2,190 (1,200)	0.0380	0.0365
2,550 (1,400)	0.0415	0.0375
3,270 (1,800)	0.0395	0.0395
3,990 (2,200)	0.0390	0.0415

(4) Thermal Expansion Studies

Linear thermal expansion over the range from room temperature to approximately 4,000°F (2,200°C) was measured on six samples by the technique described in Appendix V. Expansion of tubular material was measured in both axial and radial directions in the presintered condition (at 2,000°C for 1 hr) and the as-composited condition. Data were recorded on both heating and cooling; one sample each of axial and radial direction specimens was cycled two times, the others, one time. The samples and experiment conditions follow:

Specimen S/N	Condition	Measurement Direction	No. of Cycles
THE-2A	As-composited	Axial	1
THE-1A	As-composited	Axial	2
THE-3A	Sintered	Axial	1
THE-1R	As-composited	Radial	1
THE-2R	As-composited	Radial	2
THE-3R	Sintered	Radial	1

Special fixtures were required to obtain measurements of these specimen materials in the direct-view dilatometer. The texture of the composited tungsten made it impractical to inscribe suitable fiducial marks in the specimen surfaces for tracking. Therefore, tantalum fixtures, on which it was possible to inscribe fiducial marks at appropriate distances apart, were fabricated and used in this study. Figures 27 and 28 illustrate these fixture assemblies with specimens. Figure 27 shows a typical axial direction specimen which is nominally 2-5/8 in. long.¹ It is supported and capped at each end by square tantalum tube sections in which fiducial marks are located nominally 1/16 in. from the specimen and in windows which are backlighted. Figure 28 shows a typical radial direction specimen in the vertically supported tantalum fixture. Expansion or contraction of the 3/4-in.-ID specimen was monitored by tracking

1. The original specimen length of 4 in. proved unacceptable for Battelle's apparatus.

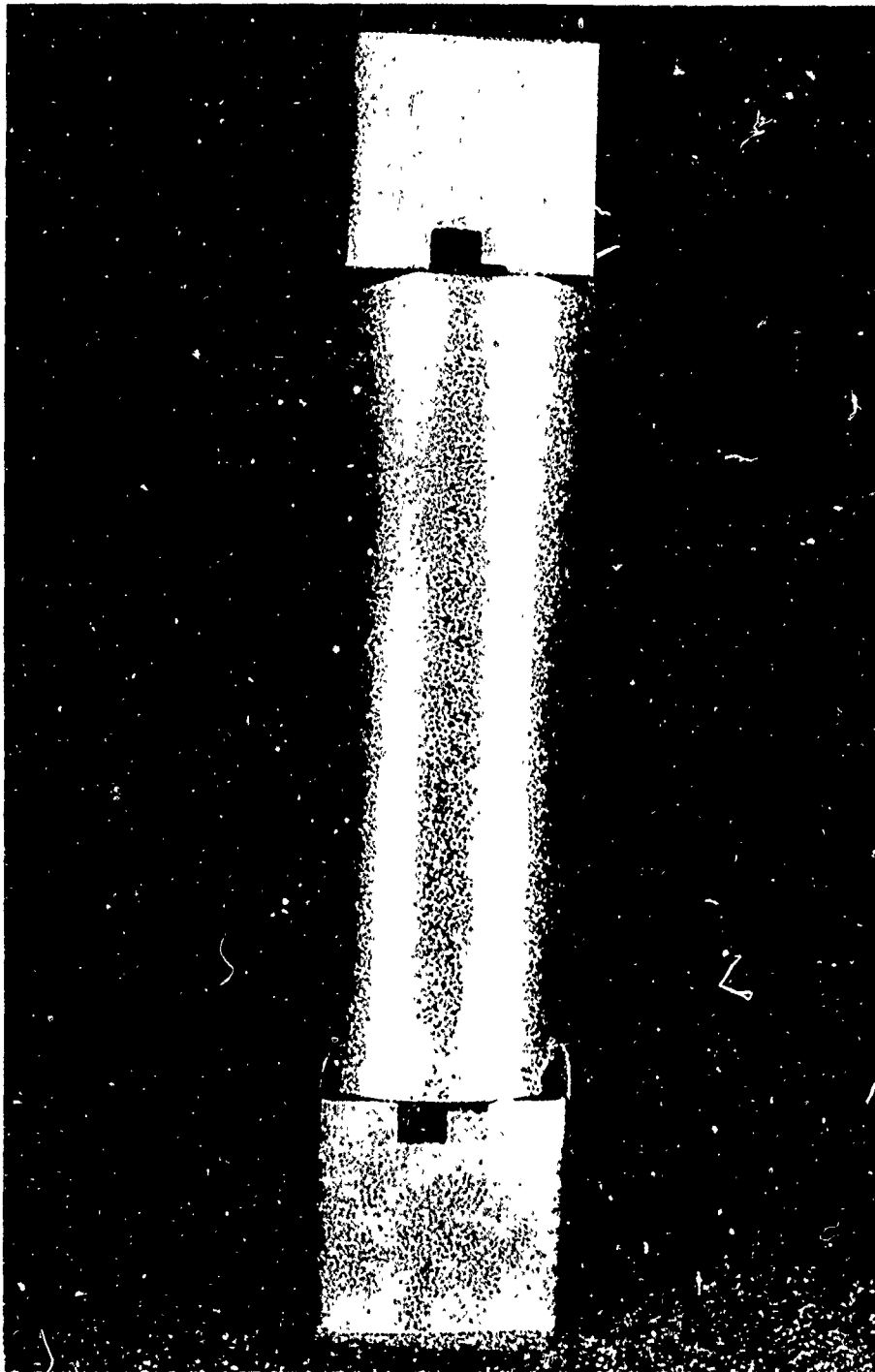


Figure 27. Specimen and Fixture Assembly for
Thermal Expansion Measurement in Axial Direction



Figure 28. Specimen and Fixture Assembly for Thermal Expansion Measurement in Radial Direction

the fiducial marks located in the 1-in.-OD tantalum tubes through the windows located approximately 2-3/4 in. apart. Corrections for tantalum expansion were applied in both cases.

Considerable trouble was encountered in the early phases of this task because (1) the tantalum coating material on the specimens sloughed off and cracked irregularly on heating causing distortion of the supporting attitude in the fixtures, and (2) the specimens released a constituent, possibly an oxide, on heating which resulted in a hard metallic deposit on neighboring parts usually clogging the fiducial marks on the specimen fixtures. Evidence of this deposit is visible near the radial specimen in figure 28. These deposits occurred when passing through the temperature ranges where unusual thermal effects were noted in the enthalpy measurements, i.e. between 1,832°F (1,000°C) and 2,000°F (1,100°C) and between 2,730°F (1,500°C) and 3,090°F (1,700°C). For the expansion measurements, it was frequently necessary to discontinue the run, clean the fixtures, and restart. To eliminate the coat-sloughing problem, 10 to 20 mils of material were ground from the specimen's outside surfaces.

Data for the thermal expansion measurements are illustrated in figures 29 through 34 with smooth curves visually fitted. In reviewing these data it is important to note that they generally do not fit on smooth curves, and that the sum of potential experimental errors associated with each point is generally less than ±1% of the indicated value. Therefore, the materials expand somewhat erratically, possibly due partially to mechanical (stress relief, etc.) phenomena.

Figures 29 and 30 indicate similar behavior for the two as-composited axial specimens on the first heating cycle. Expansion up to about 2,900°F (1,600°C) is typical of tungsten. Contraction indicative of sintering begins above 2,900°F and is confirmed by posttest measurements. Measurement during the second thermal cycle shows additional contraction at the higher temperatures, even though stable conditions appeared to have been reached at each of the high-temperature points in the first cycle, i.e., there was no change in dimension over a period of approximately 15 min after thermal equilibrium was reached.

Expansion of the presintered axial specimen (figure 31) is typical of tungsten. The slightly lower values after cooling probably indicate some additional sintering since the presinter temperature was exceeded.

Figures 32 and 33 indicate behavior for the radial specimens less stable than for the axial direction as-composited material. In these tests the specimens, supported during the measurement as shown in figure 28, sagged when passing through the 2,100°F (1,200°C) to 2,900°F (1,600°C) range, assuming a permanent shape more elliptical than round. This is not surprising since the total weight supported

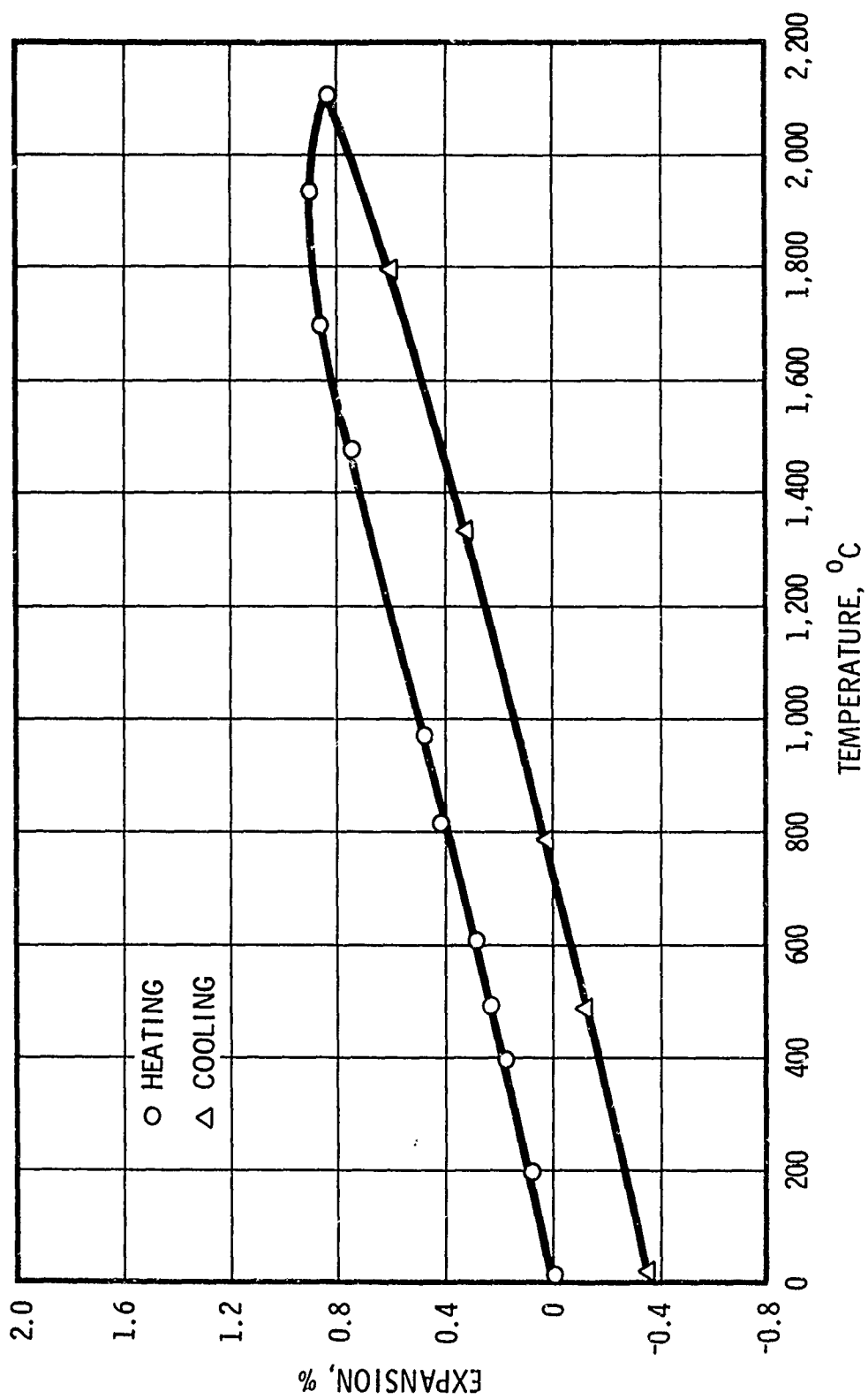


Figure 29. Linear Thermal Expansion of As-Composited Tungsten Composite Axial Direction (Specimen 2A)

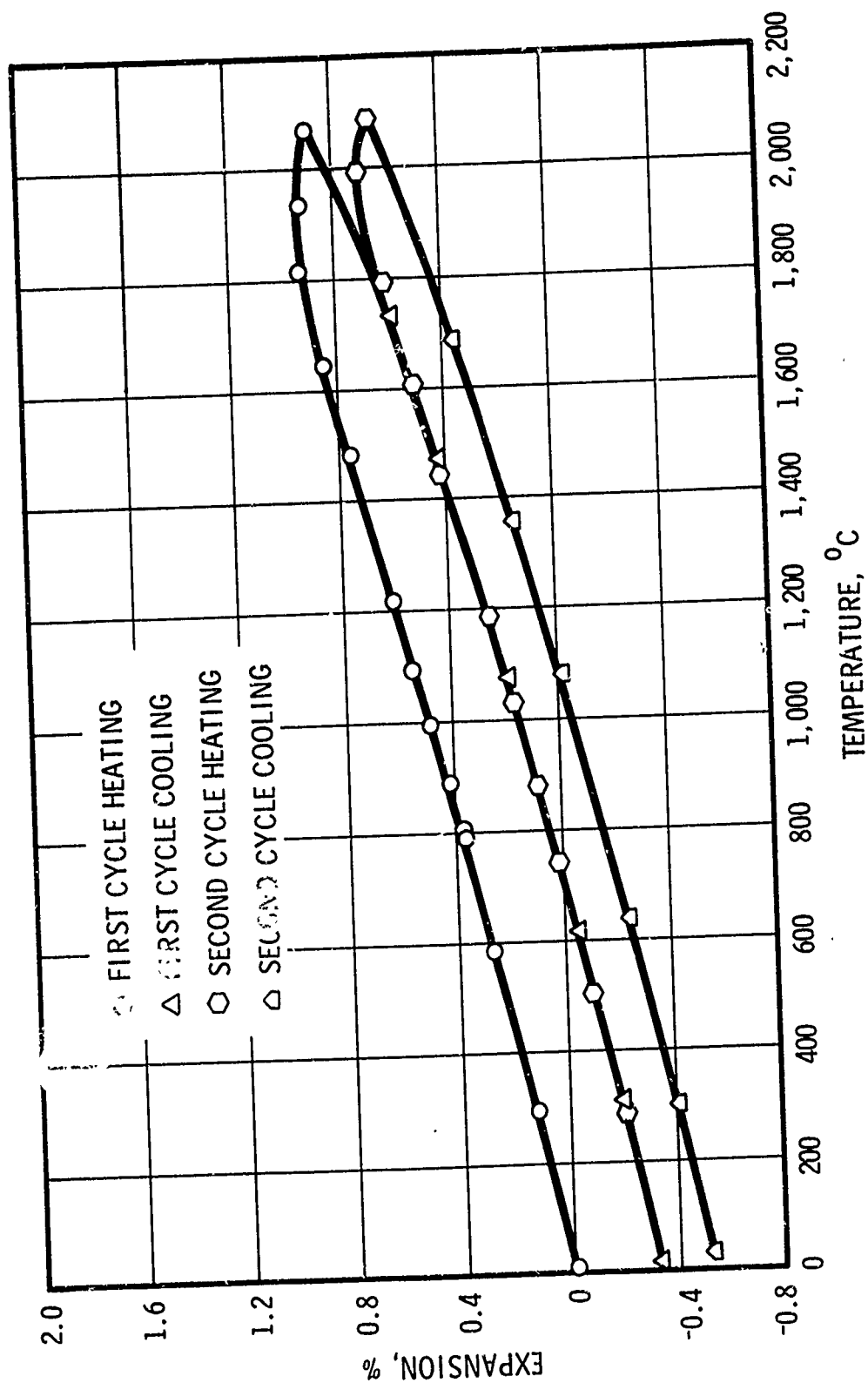


Figure 30. Linear Thermal Expansion of As-Composited Tungsten Composite
Axial Direction (Specimen 1A, Two Cycles)

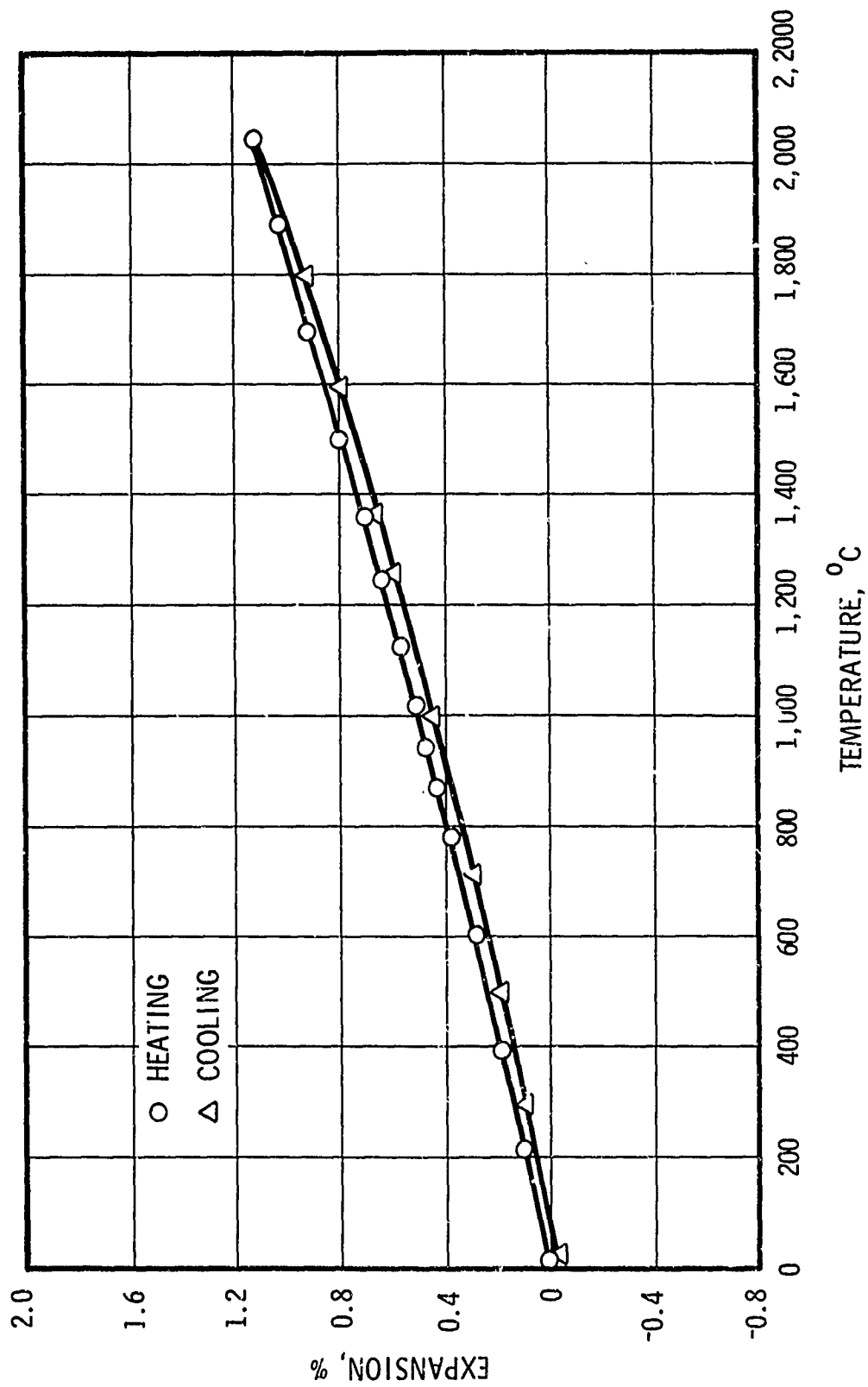


Figure 31. Linear Thermal Expansion of Presintered Tungsten Composite Axial Direction (Specimen 3A)

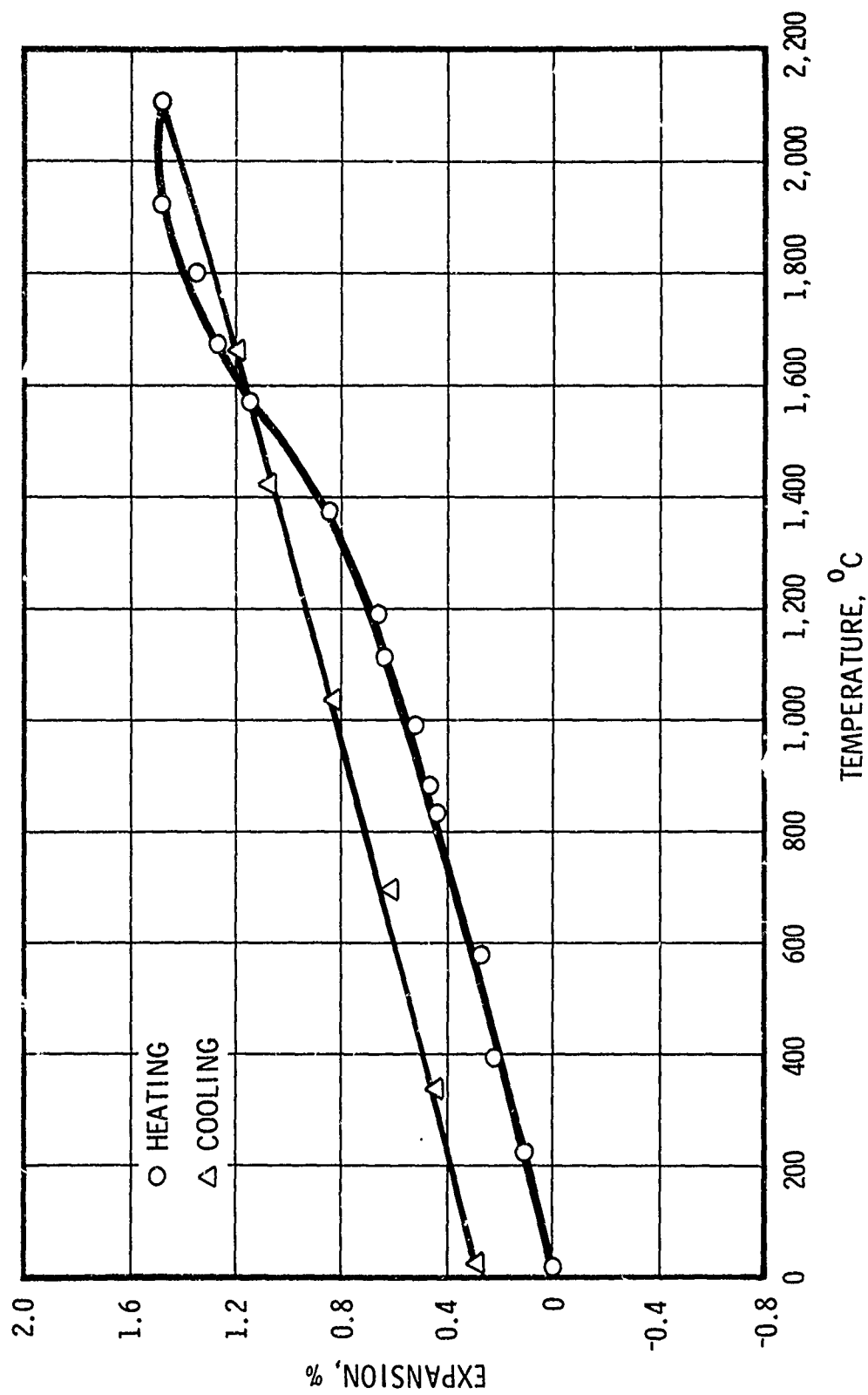


Figure 32. Linear Thermal Expansion of As-Composited Tungsten Composite
Radial Direction (Specimen 1R)

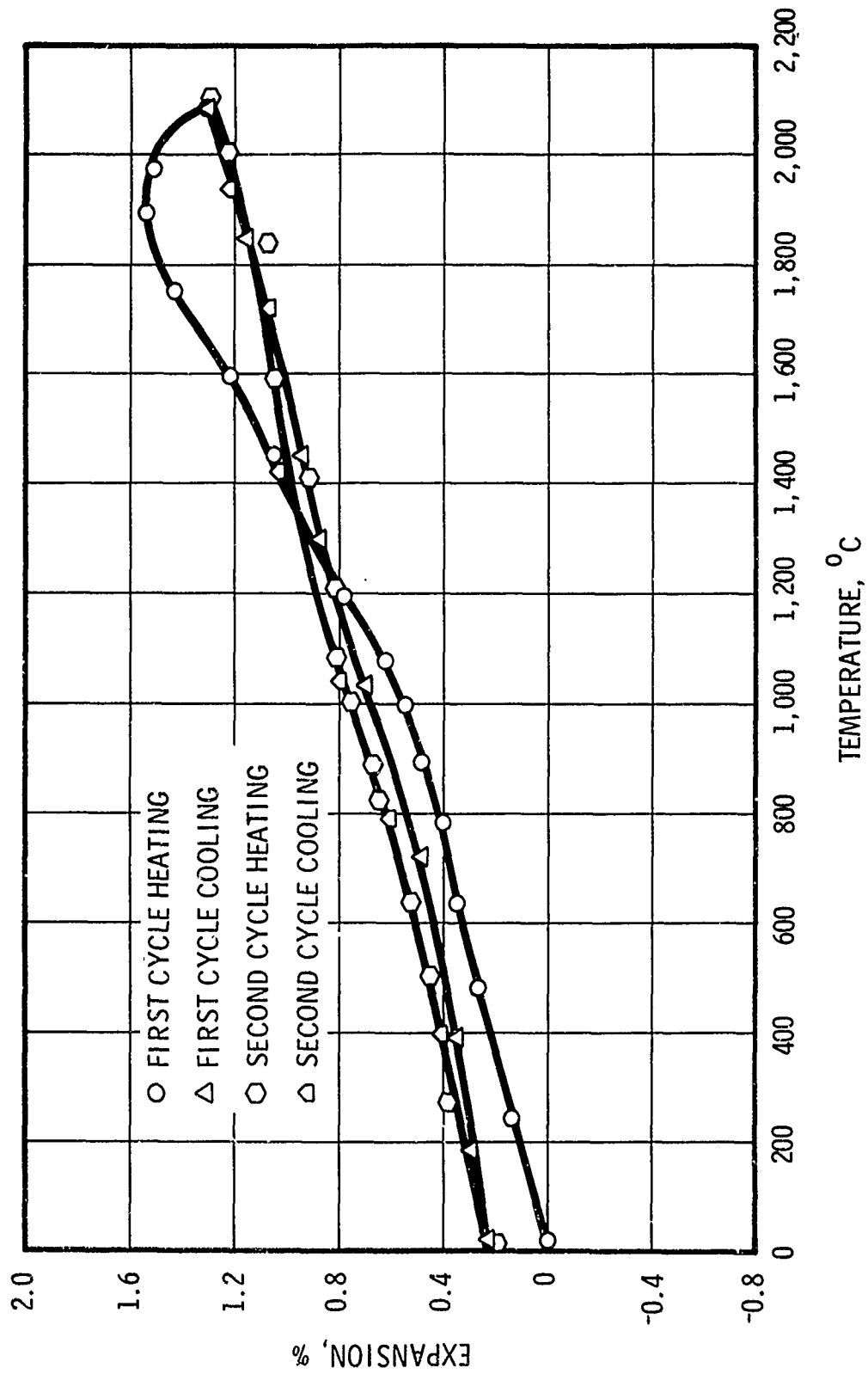


Figure 33. Linear Thermal Expansion of As-Composited Tungsten Composite
Radial Direction (Specimen 2R, Two Cycles)

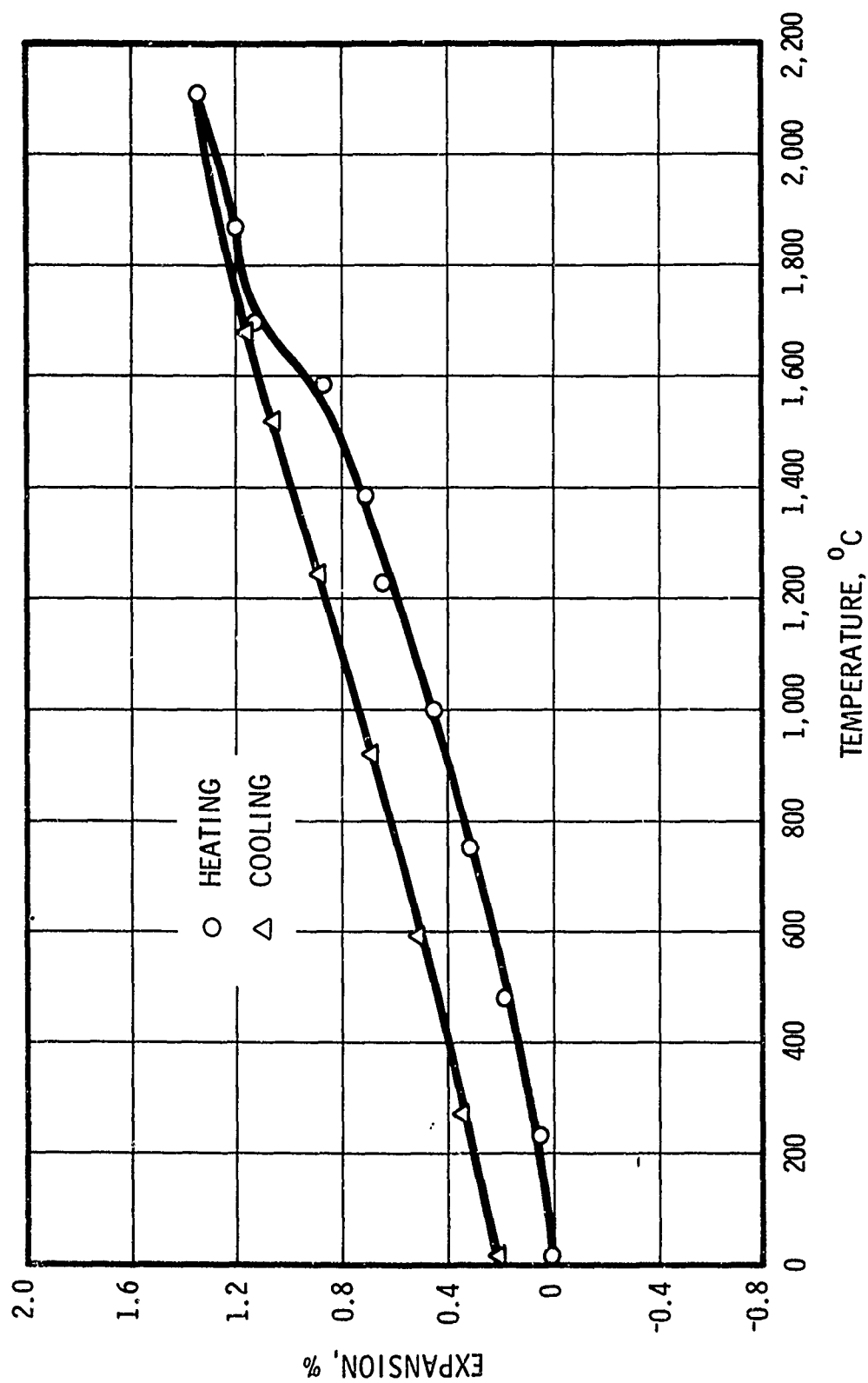


Figure 34. Linear Thermal Expansion of Presintered Tungsten Composite
Radial Direction (Specimen 3R)

by the upper 3/16-in.-diameter Ta pin (i.e., specimen, lower tantalum fixture, and pin) was slightly over 100 g. In addition, these specimens slowed sintering effects above approximately 3,090°F (1,700°C).

Figure 34 illustrates expansion characteristics for a presintered specimen in the radial direction. Again, sagging occurred similar to that for the as-composited specimens. Also, there was an indication of some additional sintering above 3,630°F (2,000°C).

The data generated in this study provide a reliable illustration of the thermal expansion performance of the tungsten composite. However, sagging and slight distortion of the radial direction specimens apparently was a result of the hanging attitude necessary in the measurements. The erratic expansion of all specimens with temperature is noteworthy.

A valid comparison of expansion in the axial and radial direction can be achieved by comparing the cooling curves of the two presintered specimens (figures 31 and 34). These indicate that expansion on heating from room temperature to 3,630°F (2,000°C) is about 1.08% in the axial direction and about 1.11% in the radial direction, i.e., about 3% greater in the radial direction. Comparison of values on heating to 1,832°F (1,000°C) using heating curves indicated approximately 3% greater expansion for axial than for radial direction. In view of the erratic expansion behavior which makes curve locations difficult, these differences probably should be considered negligible. In the absence of this erratic expansion and the sintering and sagging effects, expansion in both directions would be very close to that of pure commercial tungsten.

(5) Thermal Conductivity Summary

The thermal conductivity-temperature relation for the wire-wound tungsten composite material in the direction of the reinforcing wire is given directly in the low-temperature range by the steady-state measurement results and may be calculated from diffusivity, density, and specific heat data for the higher temperatures. Values representing material in unsintered, partially sintered, and completely sintered conditions may be derived after approximately 1 hr at 3,632°F (2,000°C).

The relationship for calculating conductivity is

$$k = \alpha \rho C_p \quad (2)$$

where

k = thermal conductivity
 α = thermal diffusivity
 ρ = density
 C_p = specific heat.

With the possible exception of specific heat, these properties were well defined up to 3,632°F (2,000°C). The specific heat would apply to the case when the material is heated and cooled in a sealed container. However, in use the products resulting from heat-effected reactions might be allowed to escape, and the specific heat curve might be different from that illustrated for the composite as shown in figure 26.

The greatest difference between specific heat values for tungsten for the specimen material and specific heat values from literature⁽⁵⁾ is about 20%, as illustrated by figure 26. The average difference would be between 5% and 10%. For convenience and because the specific heat studies could not be expanded to resolve these differences within the scope of the program, the literature values were used to calculate conductivity with the understanding that this source of potential error exists.

Table XII lists values of diffusivity, density, and specific heat as well as conductivity at appropriate intervals in the temperature range of interest. Values of conductivity are calculated for cooling as well as heating data to illustrate the effect of sintering on conductivity of the composite material.

Figure 35 illustrates the resulting conductivity-temperature relationship, again illustrating the significant effect on the as-composited material of sintering after starting. The curve is irreversible once any sintering has commenced. This means that the cooling for any as-composited sample heated above 1,100°F (600°C) would not retrace the heating curve but would be higher and would approach a shape approximately parallel to that in figure 35.

TABLE XII

THERMAL CONDUCTIVITY DATA FOR WIRE-WOUND
TUNGSTEN COMPOSITE NORMAL TO WIRE DIRECTION

Temperature C(1)	Thermal Diffusivity cm ² sec ⁻¹ (2)	Density g cm ⁻³ (3)	Specific Heat cal g ⁻¹ K ⁻¹ (4)	Thermal Conductivity W cm ⁻¹ K ⁻¹ (5)
20	---	15.87	0.0322	0.062
200	---	15.83	0.0328	0.060
400	0.030	15.79	0.0335	0.066
600	0.029	15.75	0.0341	0.065
800	0.040	15.71	0.0349	0.092
1,000	0.069	15.67	0.0358	0.162
1,200	0.120	15.63	0.0365	0.286
1,400	0.146	15.59	0.0373	0.355
1,600	0.157	15.55	0.0382	0.390
1,800	0.151	15.51	0.0392	0.384
2,000	0.144	15.47	0.0402	0.374
1,800	0.166	15.52	0.0392	0.423
1,600	0.173	15.57	0.0382	0.430
1,400	0.180	15.62	0.0373	0.439
1,200	0.189	15.67	0.0365	0.451
1,000	0.201	15.72	0.0358	0.473
800	0.217	15.77	0.0349	0.500
600	0.240	15.82	0.0341	0.541
400	0.281	15.87	0.0335	0.624

Note: Parenthetical numbers denote the order of measurement of the as-composited material.

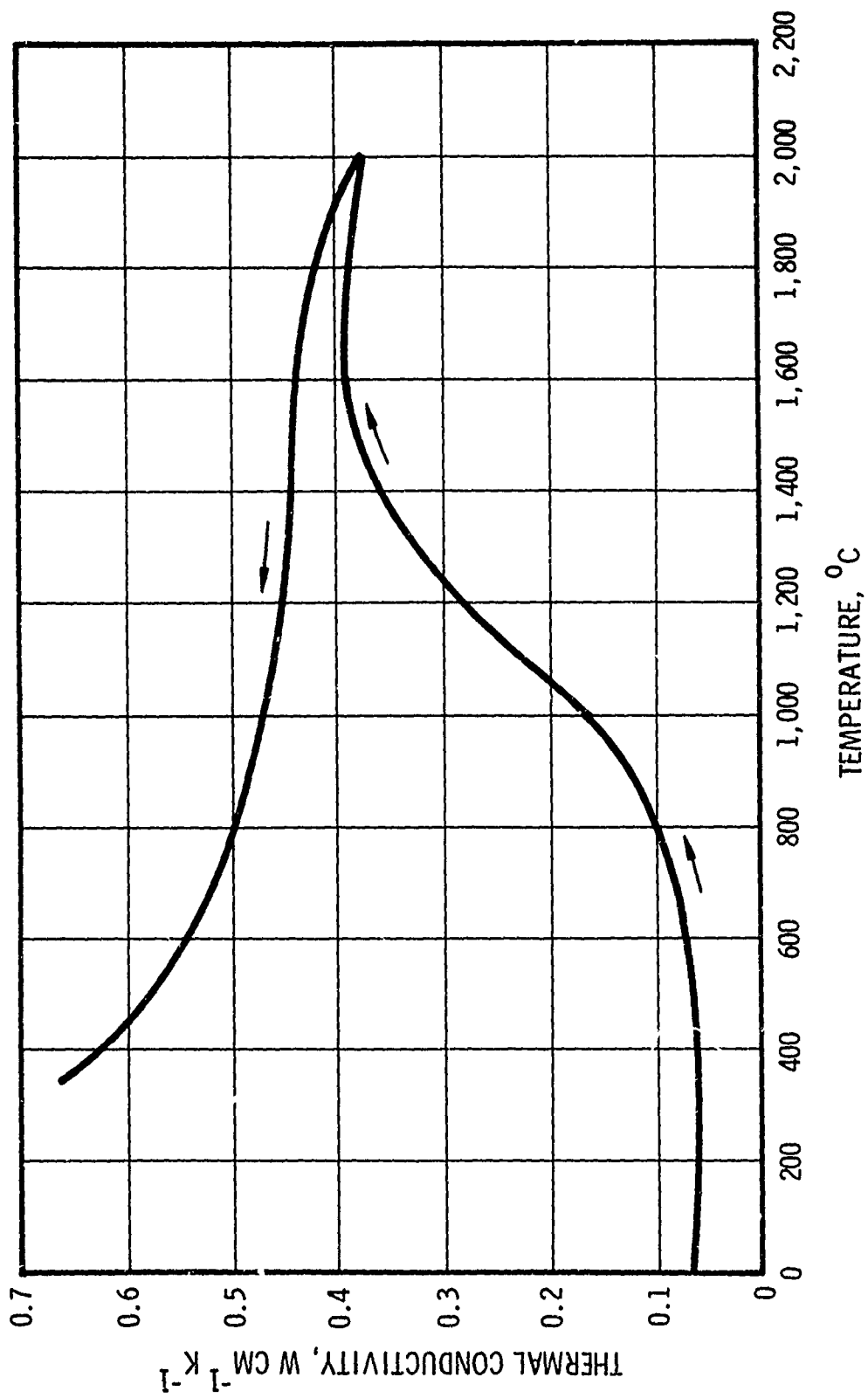


Figure 35. Thermal Conductivity of As-Composited Wire-Wound Tungsten
Normal to Wire Direction

3. MECHANICAL PROPERTY TESTS

Mechanical property testing was performed on test specimens fabricated and inspected by UTC by Illinois Institute of Technology Research Institute (IITRI), Chicago, Illinois. The task objectives of this study were to determine tension, compression, biaxial, elastic, and stress-strain properties of wire-wound tungsten at room temperature, 3,000°F (1,650°C), and 4,000°F (2,200°C). Secondary task requirements were to design and fabricate test fixtures and to develop procedures for the elevated temperature tension and biaxial tests.

Considerable difficulty was encountered in performing the elevated temperature tension and biaxial tests. Three tension specimens (type T) and two biaxial specimens (type IIP) were destroyed during the test without determining data points. Since these difficulties occurred late in the program and considerably in excess of the original schedule, replacement specimens could not be made available. Although specimen breakage prevented determination of the axial tensile strength at 4,000°F (2,200°C), a good estimate of this value may be obtained by analysis of the internal pressurization results and comparison with the respective room temperature test values.

Elevated temperature biaxial tests were modified from a TIP to an CIP stress field application because of anticipated specimen fracture in the grip ends due to thermal expansion stresses. At the time of the specimen design and fabrication, elevated temperature tensile strengths of wire-wound tungsten were estimated to be higher (by a magnitude of 10) than the actual determined values. When computed for the specimen configuration, this low strength and the thermal expansion differential between the hot (3,000° to 4,000°F) gauge section and the cool (1,000°F) grip ends would cause a radial fracture in the tapered portion of the grip without any applied load.

The following subsections describe the subcontractor's test effort to characterize the mechanical properties of wire-wound tungsten.

a. Experimental Procedures

A condition of the program was that heating rates be rapid and consistent with the test apparatus and that the total time to reach temperature and perform the mechanical tests be under 15 min, preferably less than 5 min. Various methods of heating, i.e., radiation, resistance, and induction, were analyzed. Induction heating was chosen as the method consistent with the requirements of the program and the type of test specimens used. A series of experiments was performed using dense tungsten rods to determine the feasibility of coupling wire-wound tungsten to the induction heating units. Having established that induction heating could be used for rapid heating for elevated temperature tests, it was possible to proceed with designing test fixtures around the test samples.

(1) Test Samples

Test samples of wire-wound tungsten were fabricated by UTC using the previously described procedures. The wire-wound tungsten process involves winding high-strength tungsten wire (0.004 in. in diameter)

over a removable mandrel and simultaneously bonding the wires together with plasma-arc-sprayed tungsten powder. In this concept, the wire acts as a reinforcement for the plasma-sprayed tungsten matrix. The wire is wound (in alternate hoop and helical layers) to provide hoop and longitudinal strength and to minimize the effects of crack propagation.

Test samples are shown in figures 36 through 39. A wedge fixture was developed to grip the uniaxial tension specimens (figure 36), and the specimen was loaded biaxially (figure 39) to eliminate stress concentration or overstressing of the specimen in the hoop direction when loaded. Stainless-steel inserts were used to provide a bearing shoulder for the wedge grips. Only one spare specimen was provided for preliminary tests, which complicated development of test procedures. Carbon dummy samples were substituted for wire-wound tungsten samples for most preliminary tests.

(2) Test Procedures

The following properties were measured:

- A. Uniaxial tension strength
- B. Internal pressure burst strength
- C. TIP burst strength
- D. Uniaxial compression strength
- E. CIP burst strength

Uniaxial and internal pressure tests were performed under room temperature and elevated temperature conditions. TIP testing was performed only at room temperature, while CIP testing was performed at elevated temperatures. By cutting off the grip ends of the TIP samples, cylinders were obtained which could be tested in an CIP mode.

(a) Uniaxial Tension Tests

Six hollow cylindrical specimens (figure 36) were tested to determine tensile properties, modulus of elasticity, Poisson's ratio, and stress-strain relationships. Two tests each were performed at room temperature, 3,000°F (1,650°C), and 4,000°F (2,200°C). Elevated temperature tests were conducted in an inert argon atmosphere. Figure 40 shows the setup for room temperature uniaxial tension tests. Fixturing for elevated temperature testing is similar except for the addition of a Vycor tube to retain an inert atmosphere, an induction coil to produce temperature, and water-cooled pull rods (figure 36).

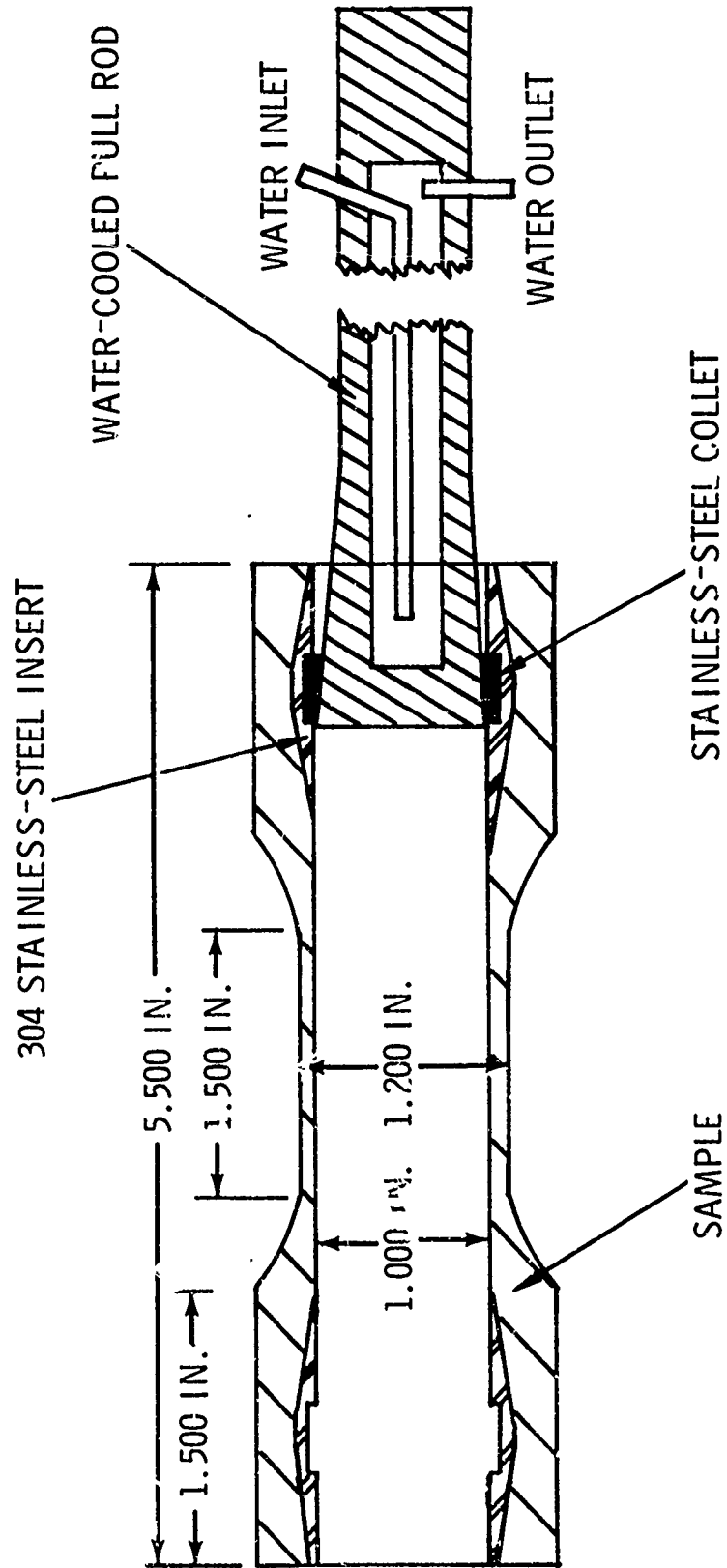


Figure 36. Configuration of Tension Test Specimen

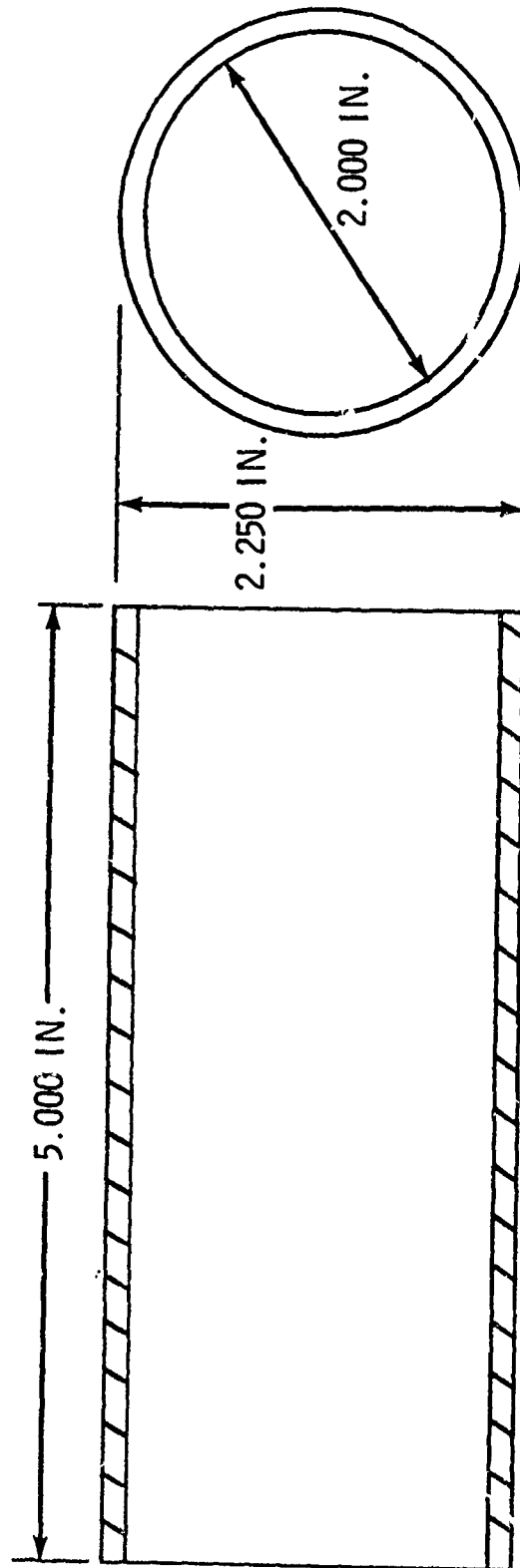


Figure 37. Configuration of IP Test Specimen

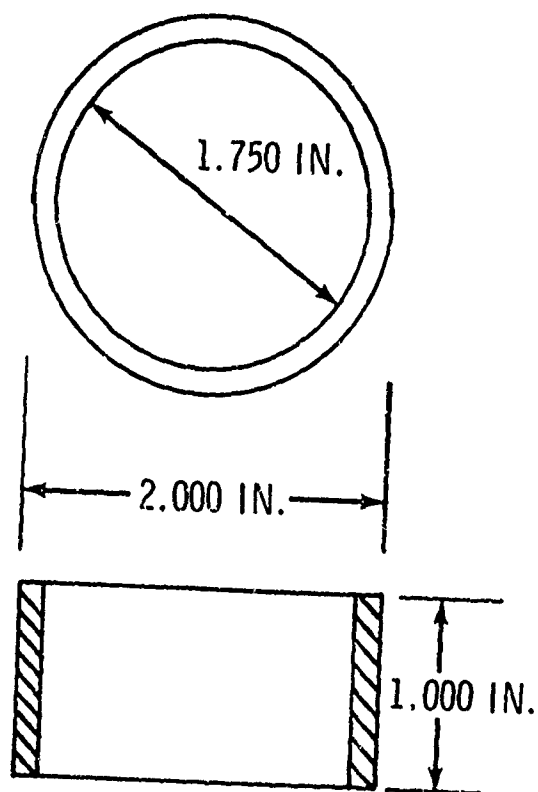


Figure 38. Configuration of Compression Test Specimen

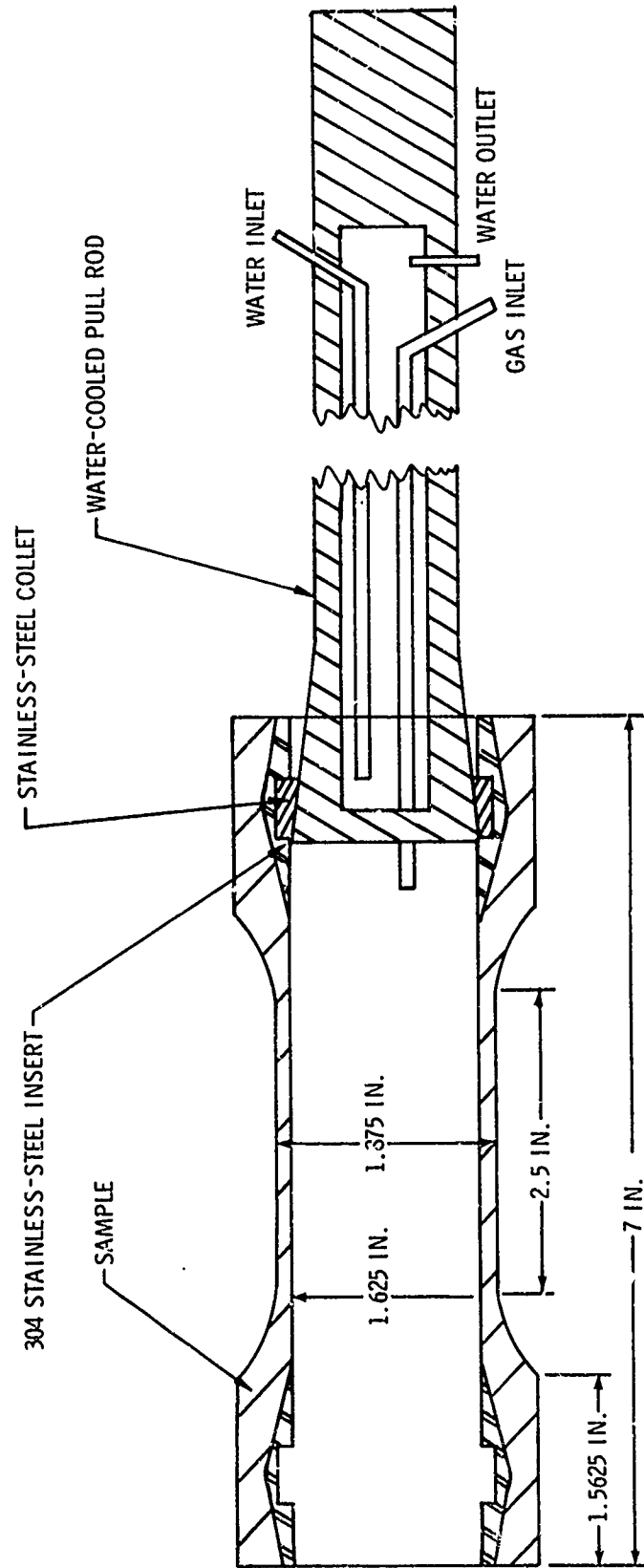


Figure 39. Configuration of Tension-IP Test Specimen

Reproduced from
best available copy.

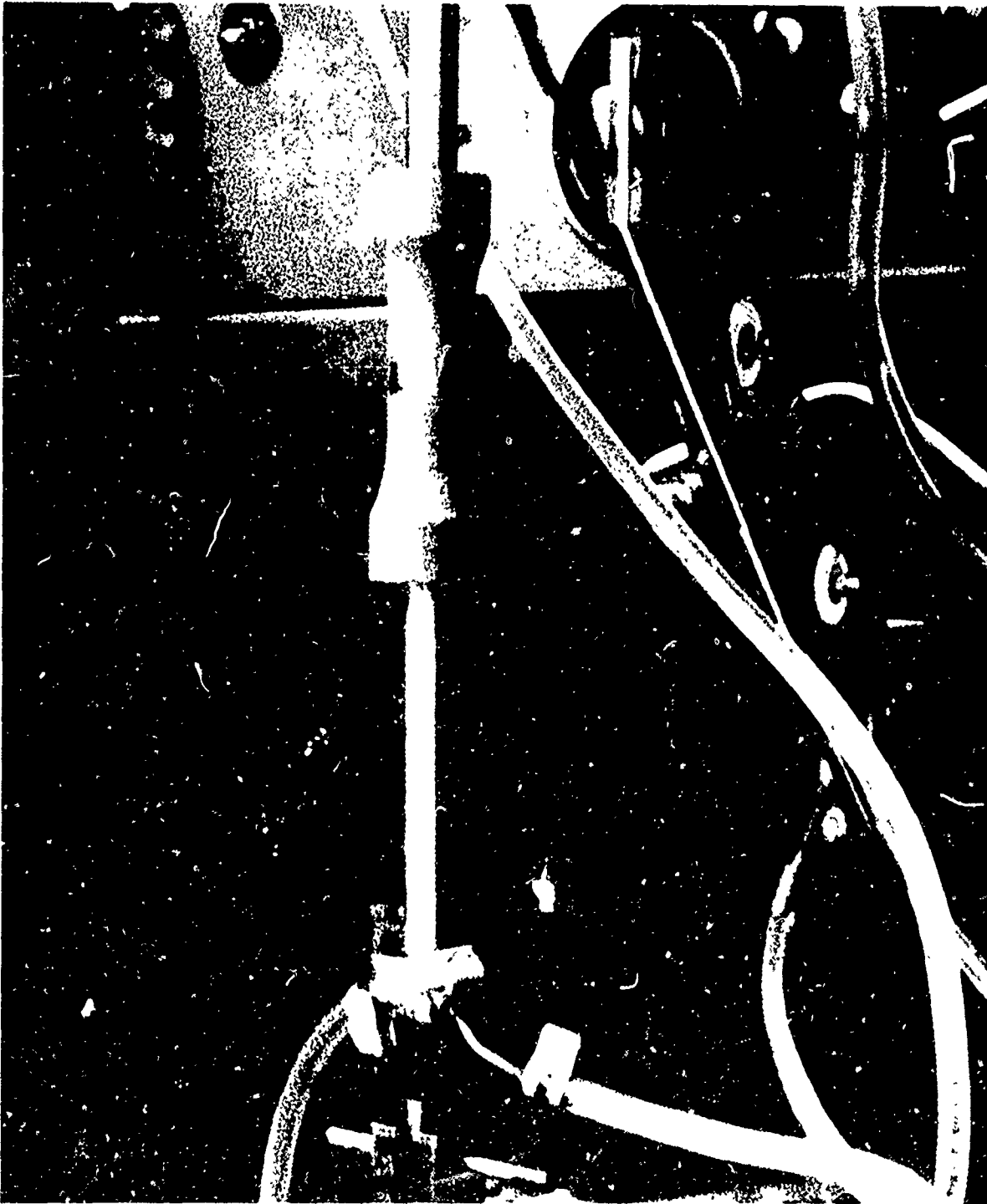


Figure 40. Apparatus for Room Temperature
Uniaxial Tension Test

(b) Internal Pressurization Tests

Six cylindrical specimens (figure 37) were pressurized to determine ultimate tension strength from internal pressurization loading. A schematic of the room temperature internal pressurization apparatus is shown in figure 41 and the actual device is presented in figure 42. For the high-temperature internal pressurization tests, a one-mil tantalum foil bag-inert gas system pressurized with argon was developed to substitute for the rubber bag-hydraulic oil system; this is described in the subsection entitled, "Results and Discussion."

(c) Biaxial Tests

Six hollow cylindrical specimens (figure 39) were to be loaded by internal pressurization to 80% of the burst strength and then loaded to failure in uniaxial tension. Ultimate strength, modulus of elasticity, and stress-strain relationship were obtained. Figure 43 presents a disassembled view of the room temperature test setup showing the pull rods, silicone elastomer bag and cushions which prevent bag failure due to abrasion, and test specimen in relation to the fixture parts. Tests were to be made at room temperature, 3,000°F (1,650°C), and 4,000°F (2,200°C). However due to problems of thermal stress failures at high temperature, biaxial CIP tests were conducted at 3,000°F (1,650°C) and 4,000°F (2,200°C) instead.

(d) Uniaxial Compression Tests

Six hollow cylindrical specimens (figure 38) were tested to determine ultimate compression strength, modulus of elasticity, and stress-strain relationships. Tests were performed at room temperature, 3,000°F (1,650°C), and 4,000°F (2,200°C). Elevated temperature tests were performed in an inert argon atmosphere using the test setup shown in figure 44

(e) Internal Pressurization and Compression Tests

Two of the tension biaxial test specimens (figure 39) were modified by cutting off the end hubs to make compression biaxial samples. One test each was made at 3,000°F and 4,000°F. Each sample was loaded to 80% of the yield stress in compression and then internally pressurized to failure.

Elevated temperature tests were performed in an inert argon atmosphere using the tantalum pressure bag and compression test procedures.

(3) Strain Determinations

SR-4 electric strain gages used to measure static strain at room temperature were Micro-Measurements Co. 90° "Tee" Rosettes, so that Poisson's ratio could be obtained at the same time that

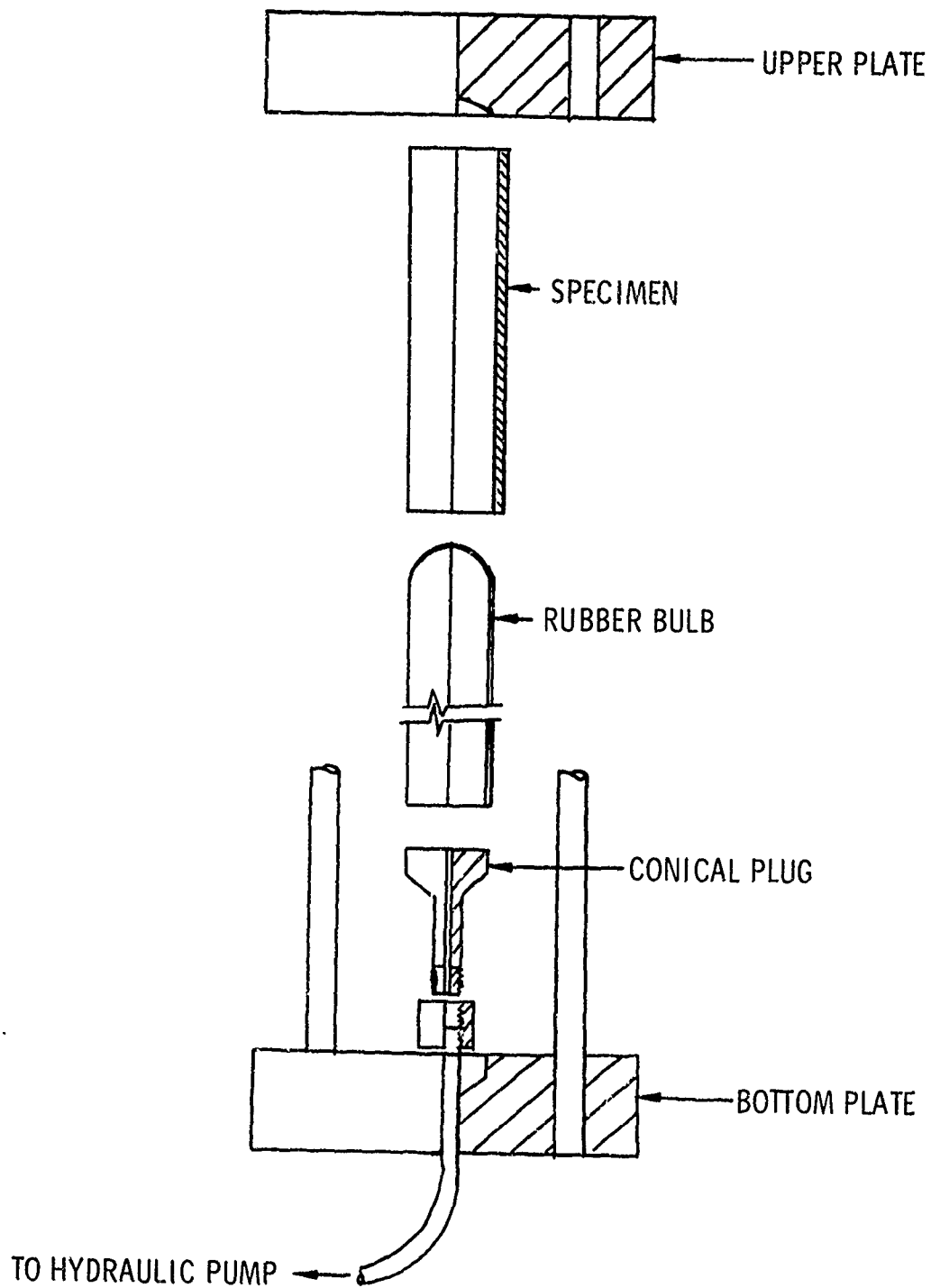


Figure 41. Exploded View of IP Test.

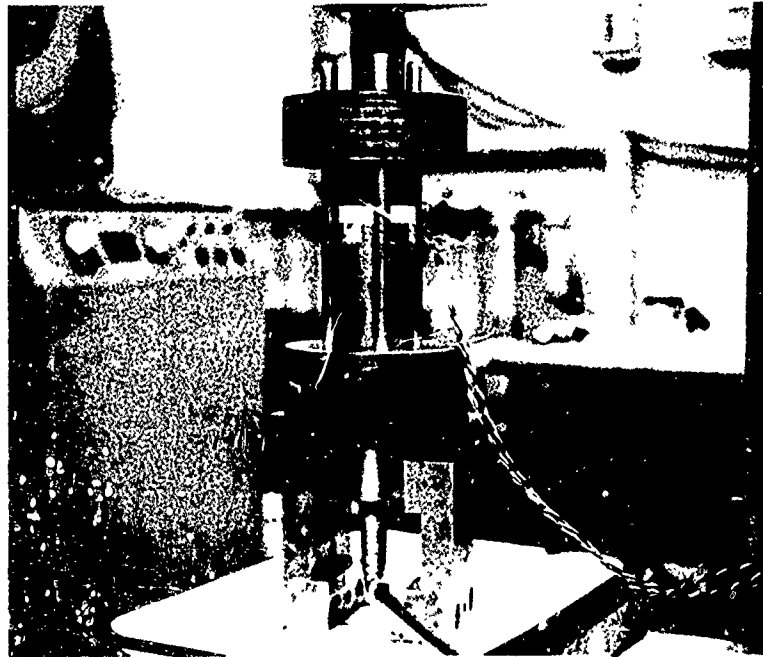


Figure 42. Apparatus for Room Temperature IP Test

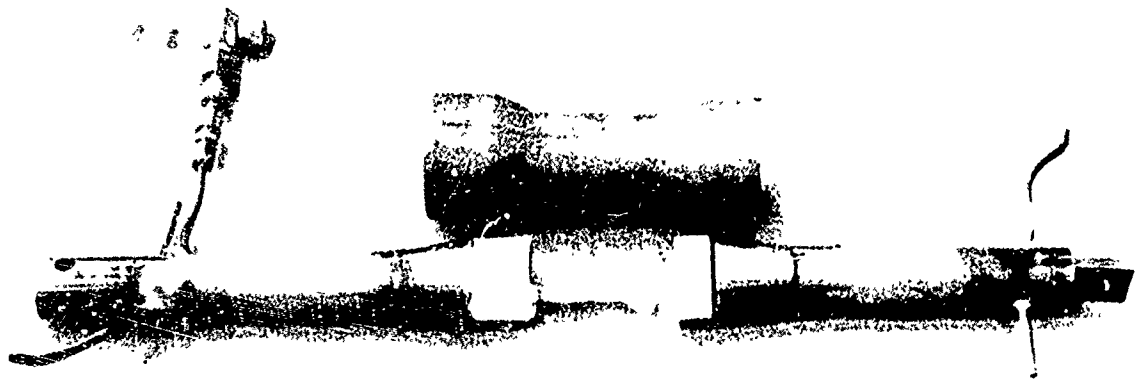


Figure 43. Fixtures for Room Temperature TIP Test

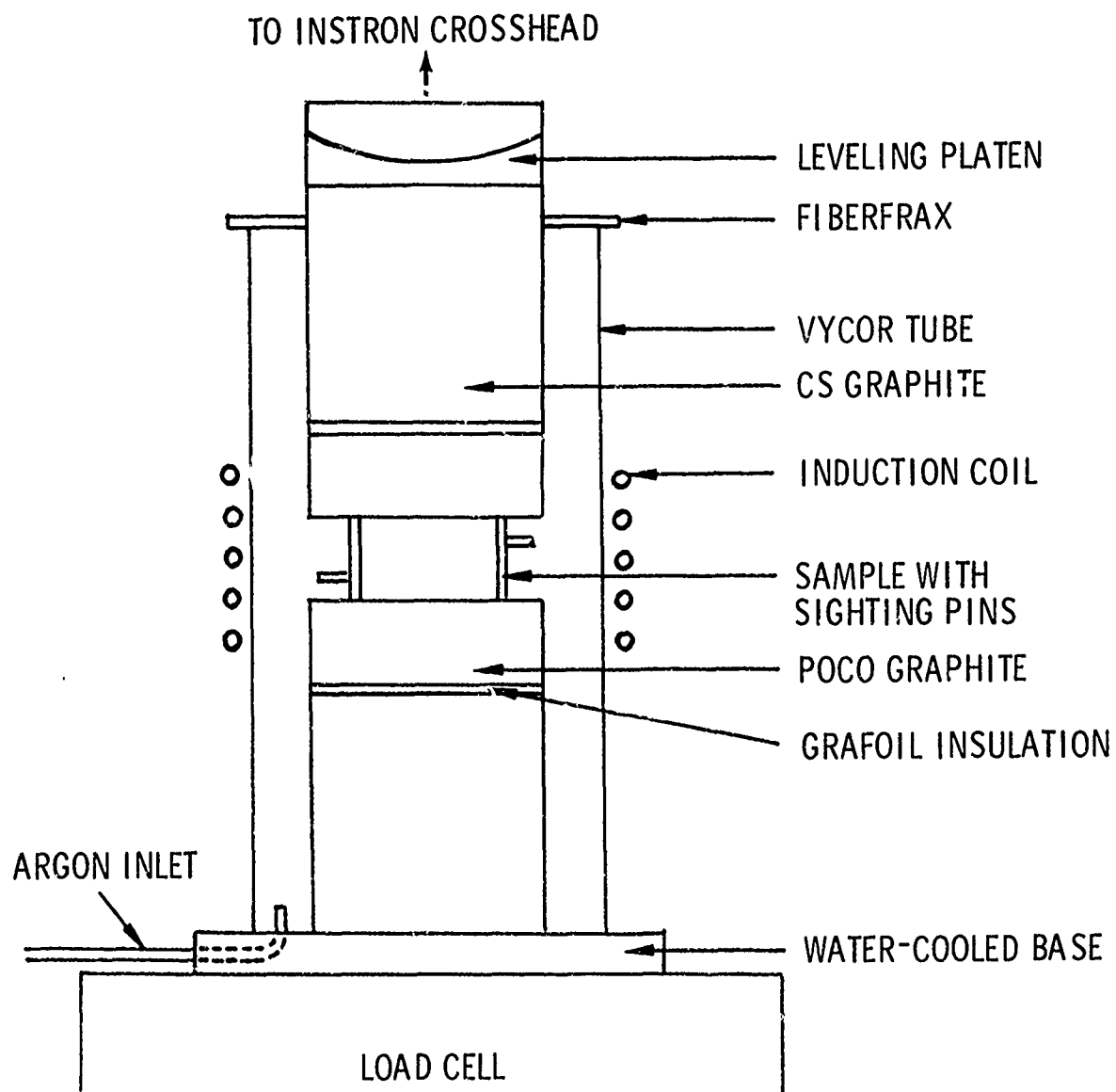


Figure 44. Diagram of Apparatus for High-Temperature Compression Tests

uniaxial measurements were obtained. At elevated test temperatures, an optical strain measuring device, the Physitech 440 x-y optical extensometer, was used. Figure 45 displays a typical elevated temperature setup, exhibiting the Instron machine used to make all the measurements, the Physitech unit for high-temperature strain measurements, and a 80-kva induction unit and control panel for activating the induction coils to heat the test specimen. Both the electrical and optical systems have rapid readouts which can be monitored on an x-y recorder.

b. Results and Discussion

The following subsections provide details and data pertaining to fixture development and the test program. Figures 46 through 48 exhibit conditions typical of the as-received specimens. Table XIII provides the as-received observations made on the samples. Results of the NDT evaluation performed earlier indicated that the observed irregularities would not adversely affect test properties.

(1) Room Temperature Tests

Table XIV presents a summary of data for tests performed at room temperature. Note the approximate 10:1 ratio between compression strength and tensile strength and the 1.35:1 ratio between the uniaxial tension strength and the internal burst tests. The relationship between compression and tension properties is normal for a brittle-acting material. The latter ratio is probably due to wire-reinforcement anisotropy. Also note that the biaxial stressed specimen exhibits a lower stress than the uniaxially stressed specimen. This is expected if biaxial stress failure theory is applied. A modified biaxial failure stress curve⁽⁶⁾ is shown in figure 49. Theories predict that tensile strength increases as compressive stress in the normal direction increases. The biaxial tensile strength is lower than the uniaxial tensile strength.

The elastic properties and Poisson's ratio cluster closely, except for data obtained from sample IP-1. This difference in properties may be real due to variations in fabrication processes. Nonlinear behavior appears to occur at approximately 50% of ultimate strength.

Tension testing of brittle-behaving material is difficult because of the problem of producing uniaxial loading. All room temperature tests were monitored by three strain gages placed at 120° intervals around the center of the test cylinder. Figure 50 presents the results of all three gages monitoring the tensile specimen under load. There was a spread of approximately 10% among the three gages through the linear elastic range of the test. Since the gages are accurate to ±5 micro-in., the readings obtained are considered satisfactory for the strain ranges observed. Similar results were obtained for the compression, internal pressurization, and biaxial tests.

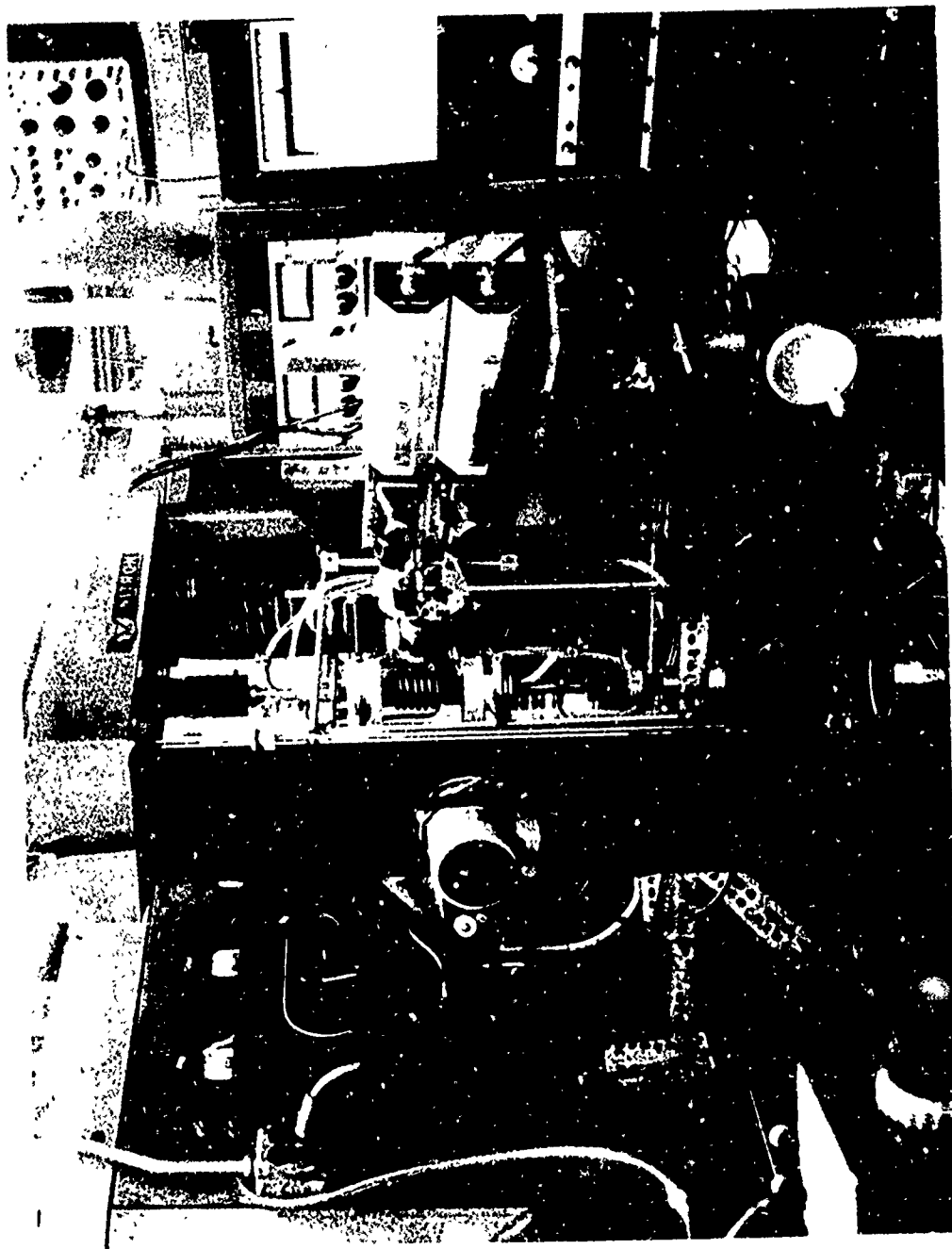
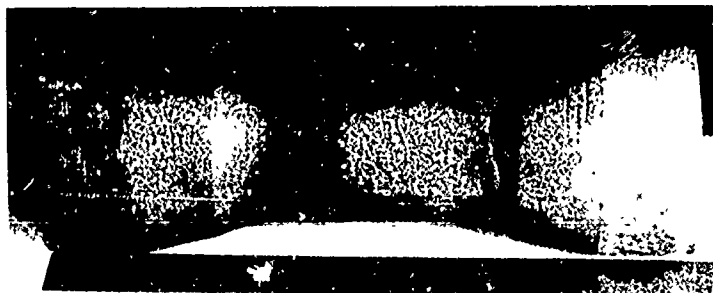


Figure 45. Apparatus for High-Temperature Testing



T-1



T-2

Figure 46. Apparent Cracks in Tension
(Specimens T-1 and T-2)

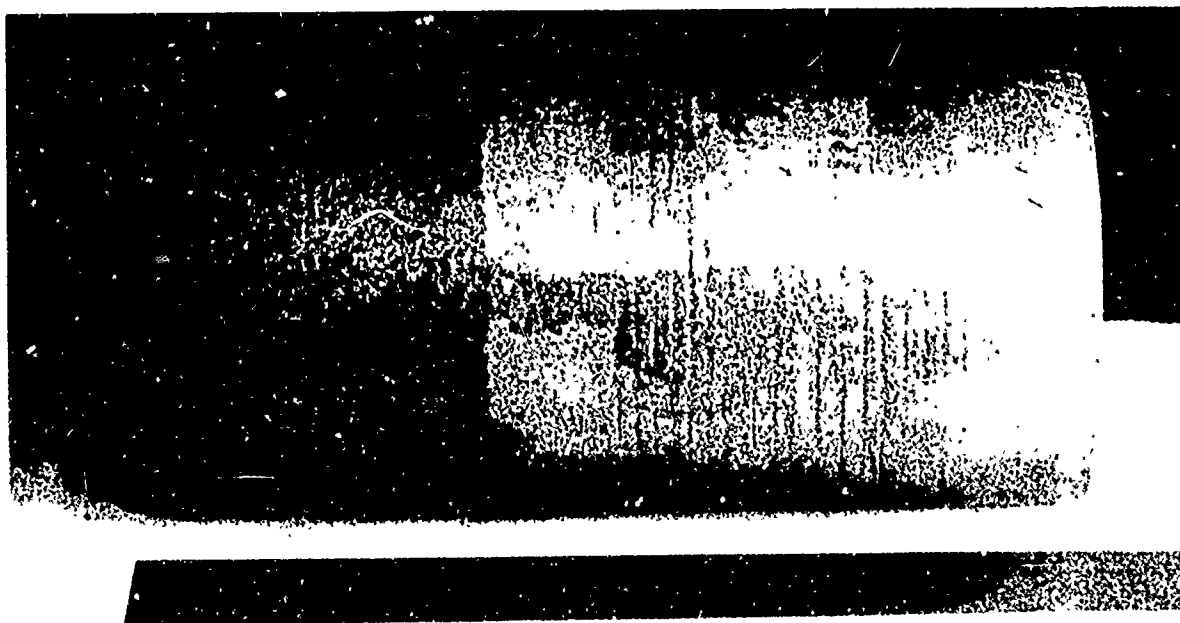
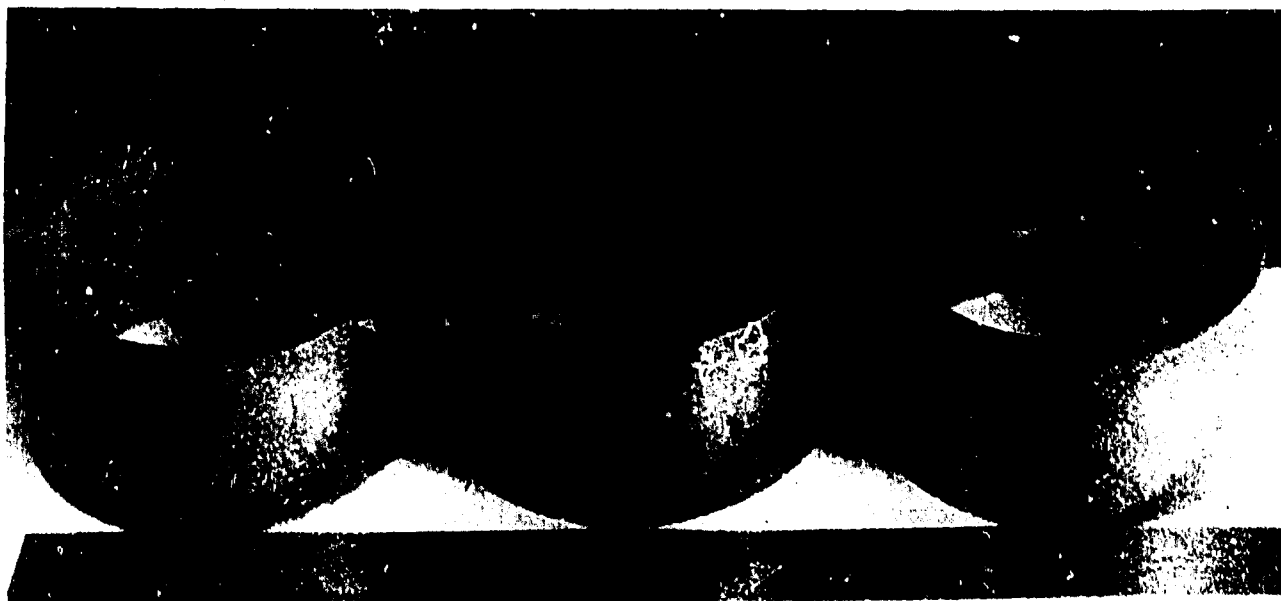


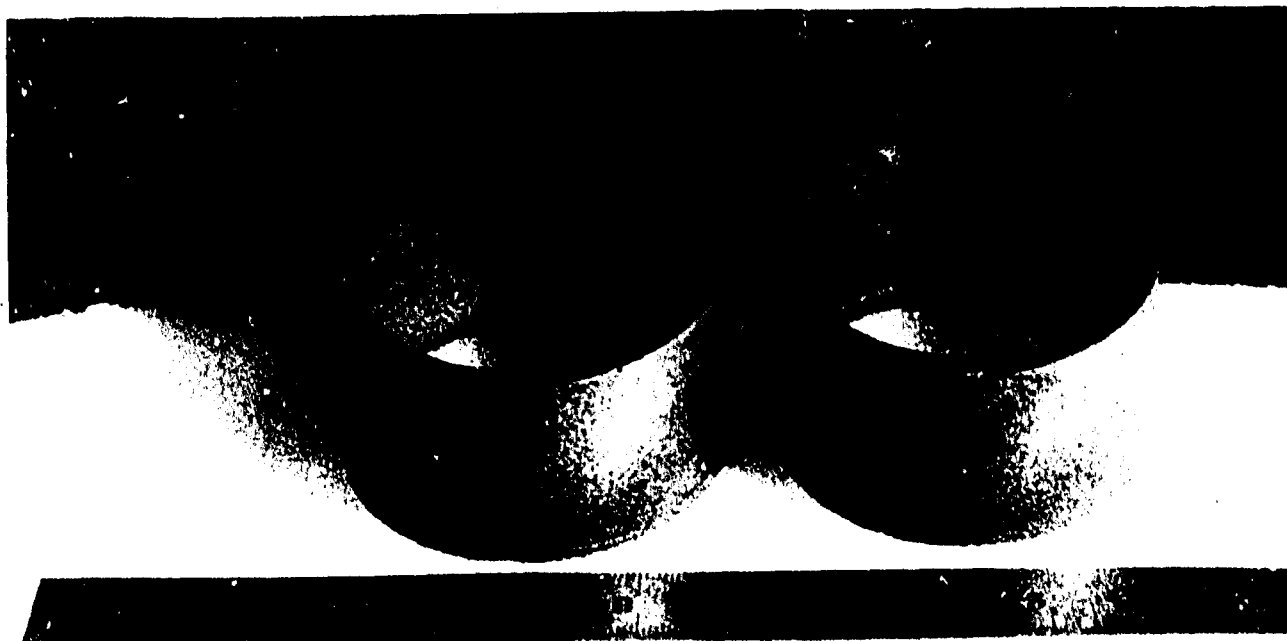
Figure 47. Exposed Wires and Surface Defects in
Internal Pressurization (Specimen IP-5)



C-1

C-2

C-3



C-5

C-6

Figure 48. Chips, Gouges, and Apparent Cracks
in Compression Specimens

TABLE XIII
VISIBLE DAMAGE TO TEST SPECIMENS

<u>Tension</u>	
<u>Specimen Number</u>	<u>Apparent Damage</u>
T-1	Crack in necked down area
T-2	Small chips Repaired cracks
T-4	<div style="text-align: center;"> Acceptable ↑ ↓ Acceptable </div>
T-5	
T-7	
Unmarked	

Internal Pressurization

All specimens appeared to be all right, except for IP-4 and IP-5 which had exposed wires where outer coating has flaked off.

<u>Compression</u>			
<u>Specimen Number</u>	<u>Chips</u>	<u>Gouge</u>	<u>Circular Cracks</u>
C-1	---	---	X
C-2	---	X	---
C-3	X	---	X
C-4	Acceptable	---	---
C-6	X	---	X

TABLE XIV
SUMMARY OF ROOM TEMPERATURE DATA

Sample	Stress, psi	E x 10 ⁶ psi		Poisson's Ratio	Ultimate Stress, %
		<u>tan</u>	<u>sec (0.5σ)</u>		
T-1	2,800	6.0	4.5	0.12	50
T-2	2,900	6.1	4.5	0.05	50
C-1	31,770	6.2	4.5	0.07	20
C-2	30,360	6.0	3.2	0.08	20
IP-1	3,690	11.8	10.9	0.04	50
IP-2	3,730	6.6	6.3	0.10	50
TIP-1	2,740*	5.6	4.4	---	---
TIP-2 (at 80% burst)	2,720*	6.6	5.8	---	---

*Includes stress component from internal pressurization

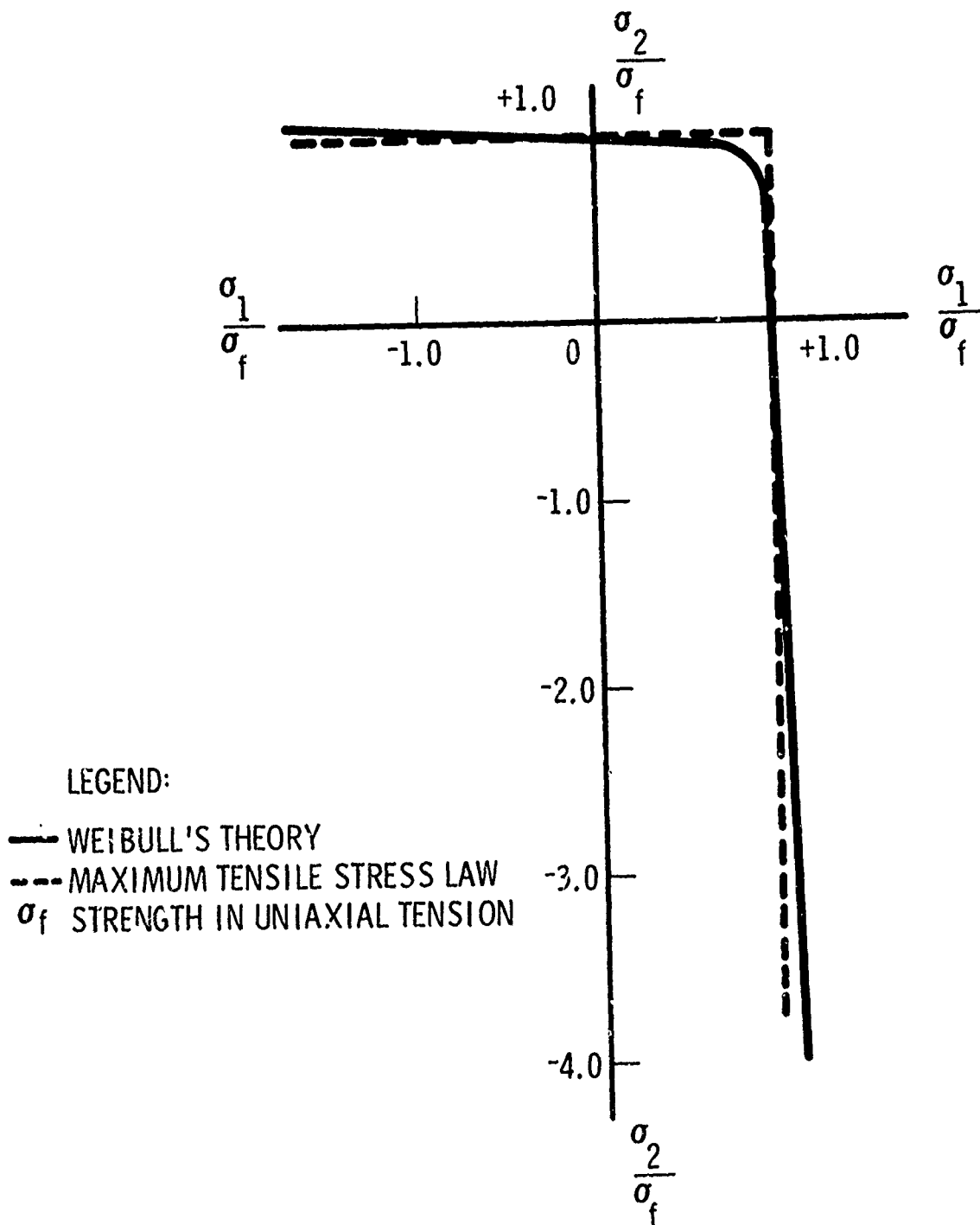


Figure 49. Weibull's Theory of Strength for Biaxial Stresses for Hydrostone Plaster ($m=12$)

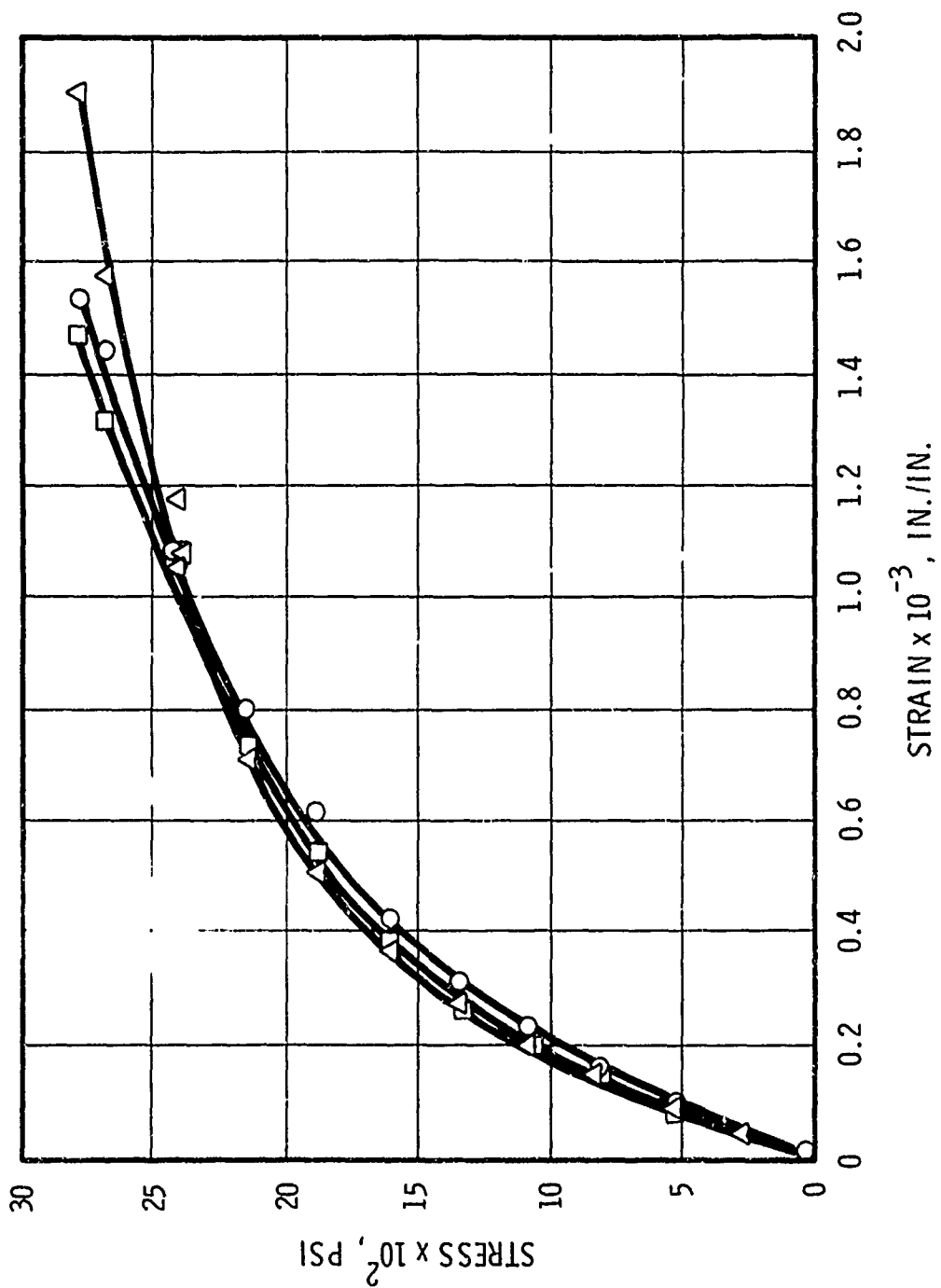


Figure 50. Stress-Strain Behavior Showing Data Obtained From Three Strain Gages

Tensile stress-strain curves for the two room temperature tests are presented in figure 51. Lateral strains from the same tests are presented in figure 52. At room temperature, the specimens failed in a brittle manner (figure 53) indicating that the wire-wound tungsten material behaves as a nonlinear elastic material at room temperature.

The material behaved in a similar manner under compression loading (figures 54 and 55). Figure 56 presents photographs of the tested compression specimens. Note the local crushing and delamination which occurred at failure.

Stress-strain data for the internally pressurized samples are presented in figures 57 and 58. Hoop stresses were calculated using the relationship

$$\sigma_t = \frac{p_i r_i^2}{r_o^2 - r_i^2} \left(1 + \frac{r_o^2}{r_i^2} \right)$$

where σ_t = hoop stress

p_i = internal pressure, psi

r_i = inner radius, in.

r_o = outer radius, in.

Figure 59 is a photograph showing the longitudinal cracks which occurred at failure. The fracture appearance is typical for this type of loading.

Stress-strain data for biaxial tension-tension loading are exhibited in figures 60 through 64. The specimen was loaded using internal pressurization to 80% of the burst strength and then was loaded to failure in tension. Figures 60 and 61 display the stress-strain behavior for the internal pressurization. Figures 62 and 63 present the stress-strain behavior exhibited for the uniaxial loading of the specimens. Each of these measurements was obtained independently of the other. Using the lines of superposition, the results were combined to present the actual stress-strain behavior shown in figure 64. Figure 65 demonstrates the typical fracture for the biaxially loaded specimens.

(2) Elevated Temperature Tests

While it was possible to obtain 3,000°F (1,650°C) in the small compression specimens, it was difficult to obtain test temperatures for the larger tension, burst, and biaxial test specimens. A series of experiments was conducted to determine whether the two available RF generators (15-kw Lepel and 25-kw Lindberg) would provide the power required for obtaining 4,000°F (2,200°C). These experiments included using different coil designs to optimize coupling efficiency.

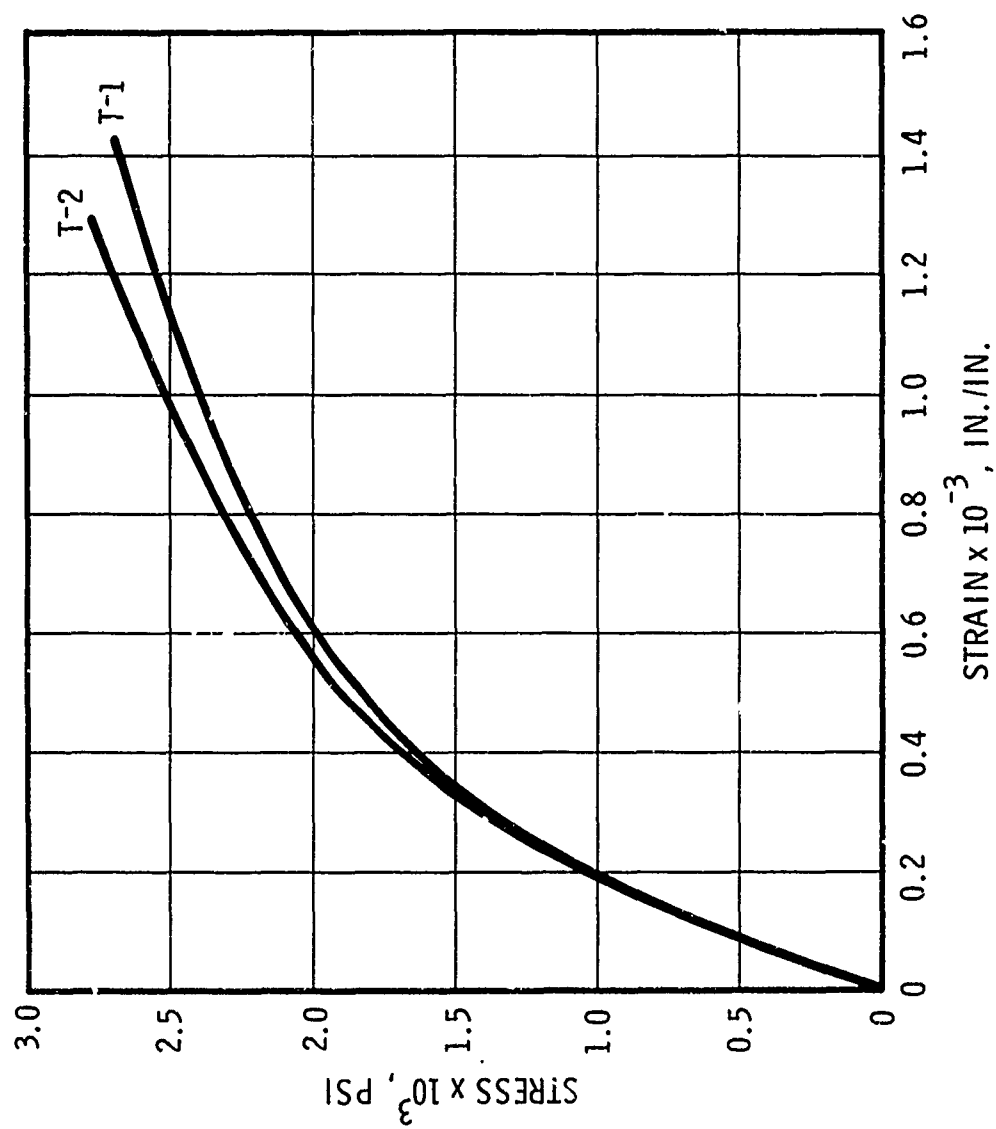


Figure 51. Stress-Strain Behavior in Tension

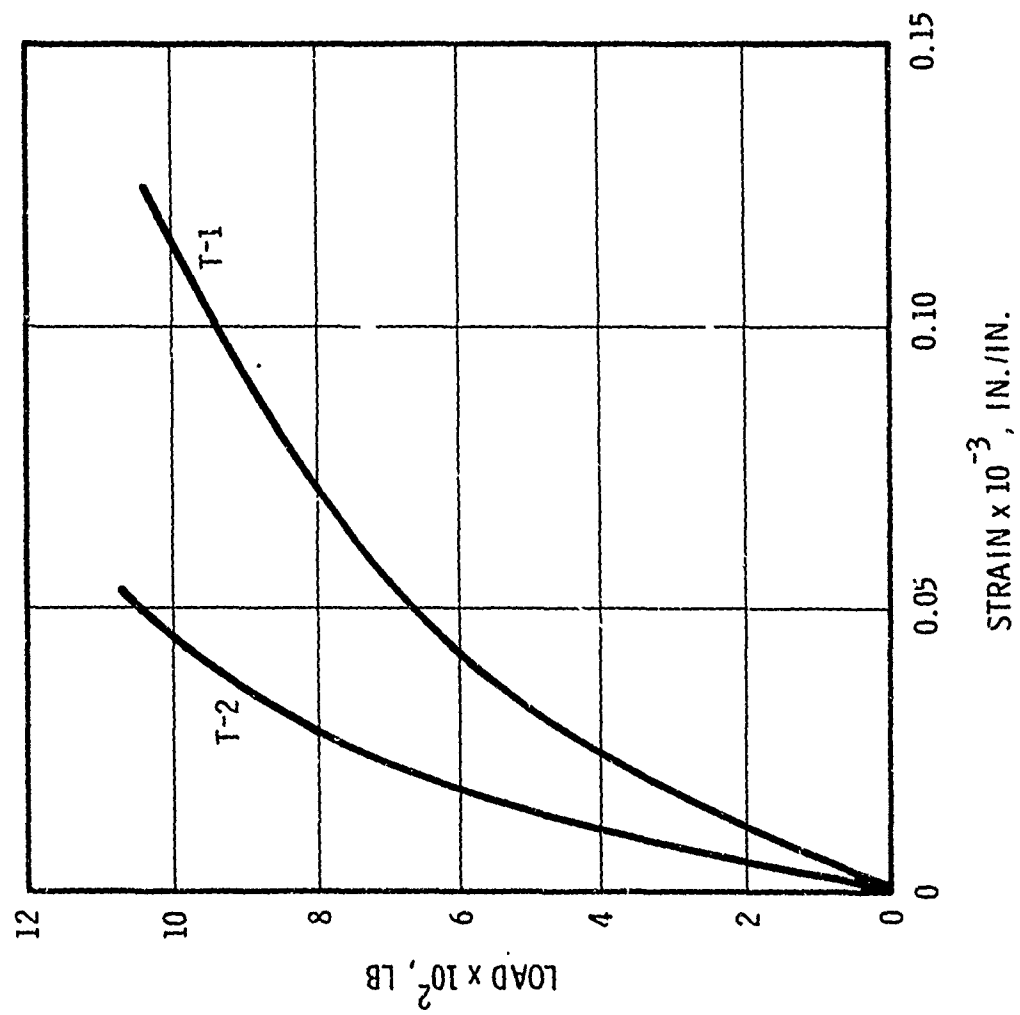


Figure 52. Load-Lateral Strain Behavior in Tension

Reproduced from
best available copy.

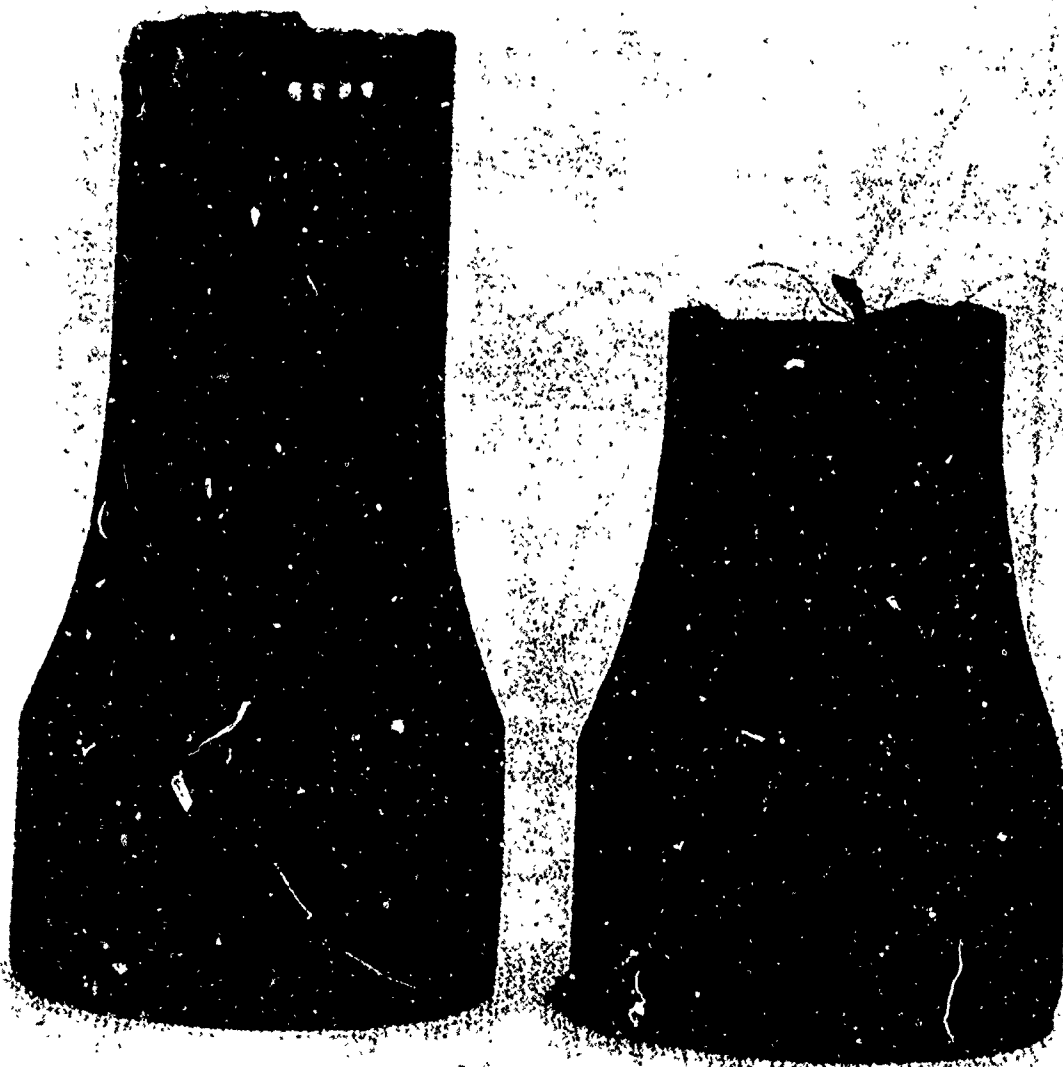


Figure 53. Tension Specimen Tested at Room Temperature

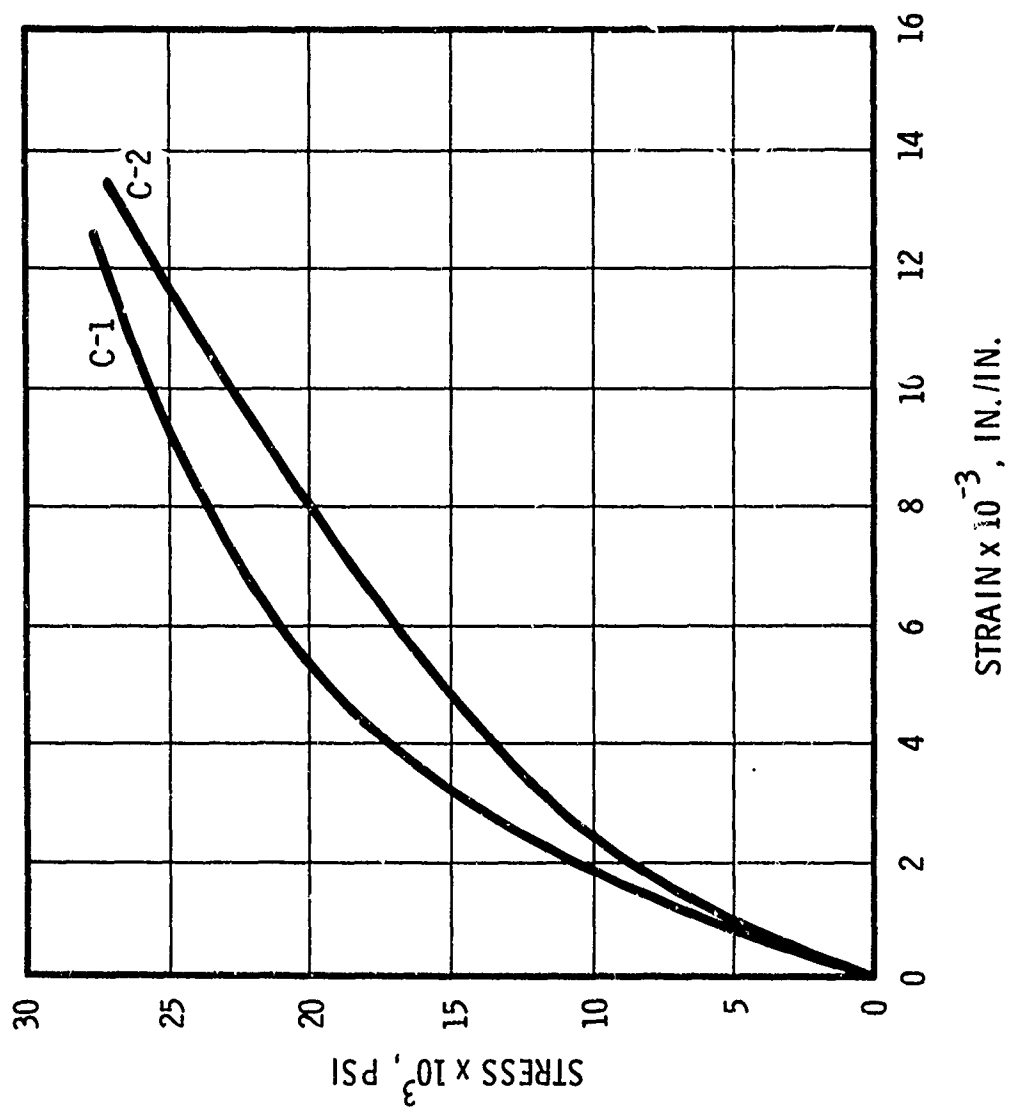


Figure 54. Stress-Strain Behavior in Compression

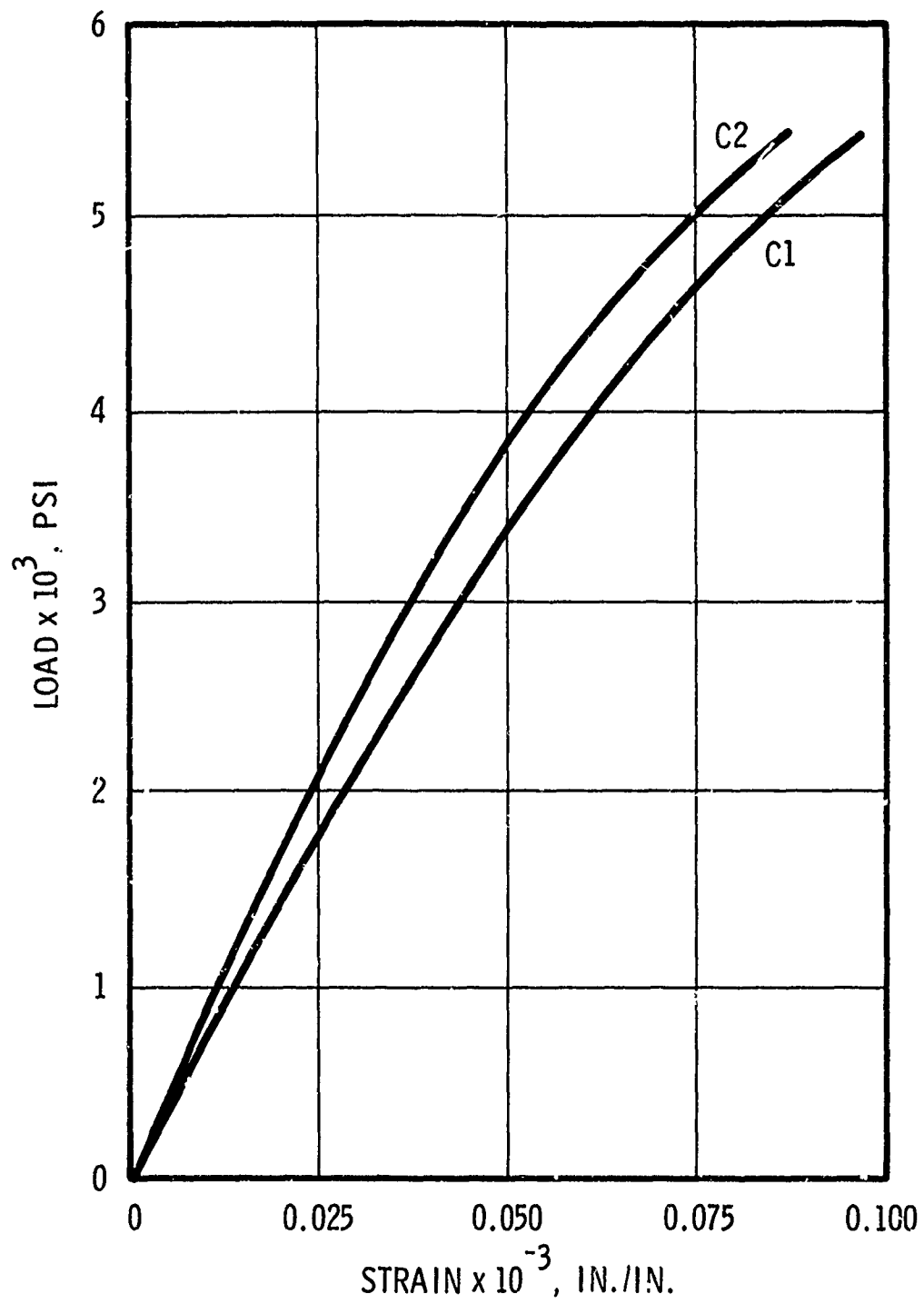


Figure 55. Load-Lateral Strain Behavior in Compression



Sample C-1



Sample C-2

Figure 56 Compression Specimens Tested
at Room Temperature

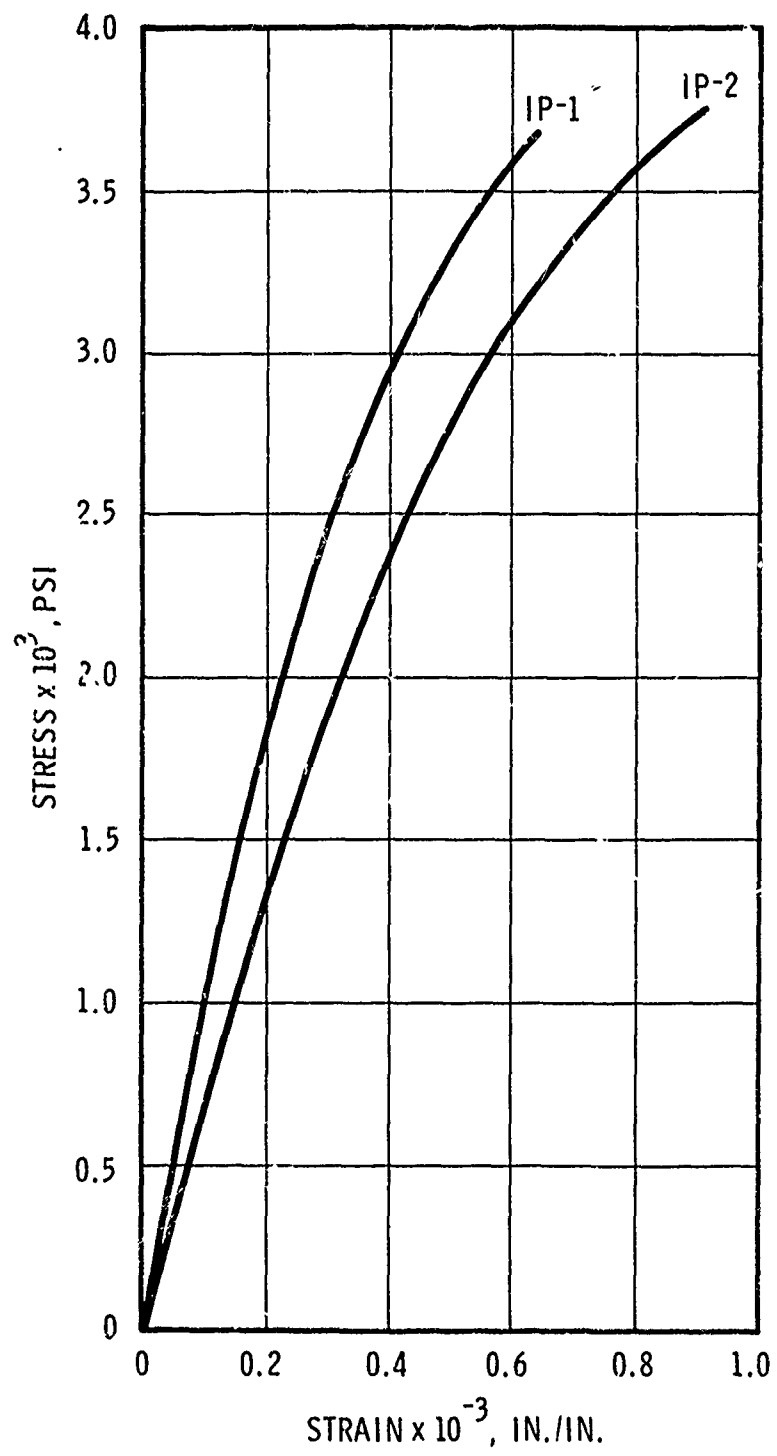


Figure 57. Stress-Strain Behavior in Internal Pressurization

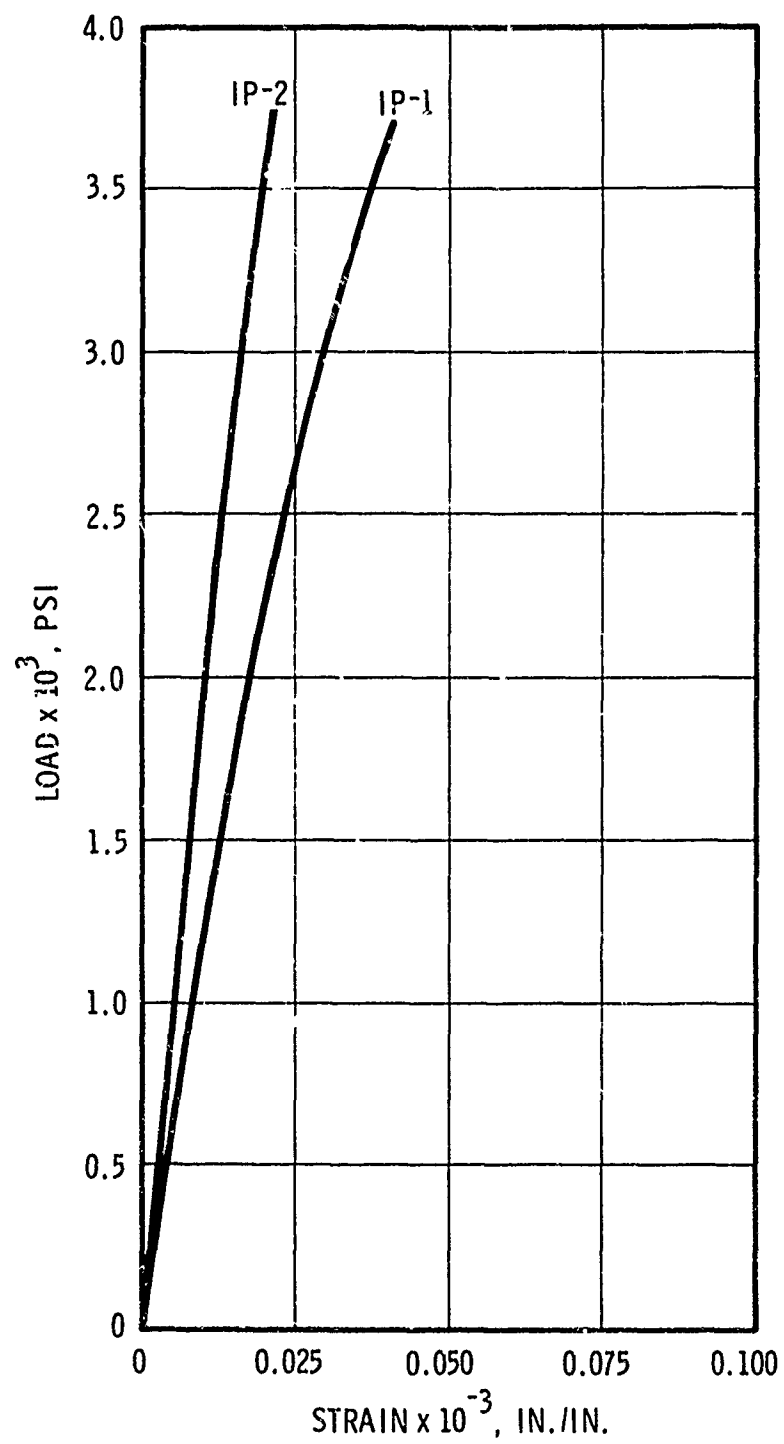


Figure 58. Load-Axial Strain Behavior in Internal Pressurization

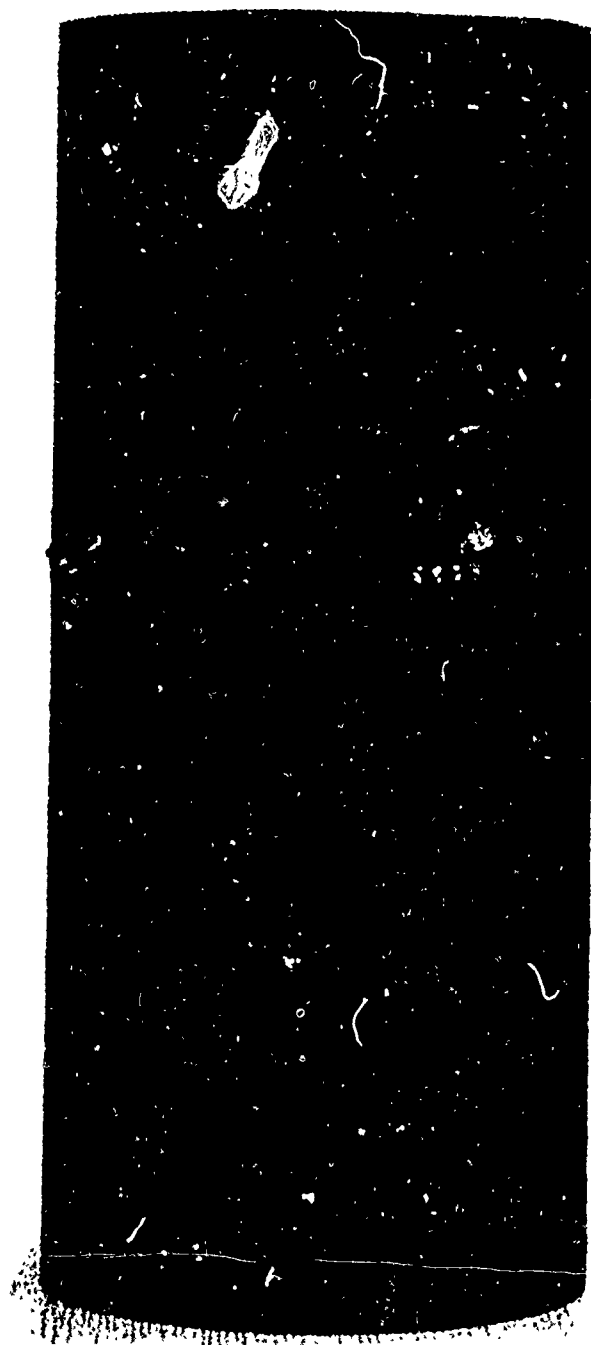


Figure 59. IP Specimen Tested at Room Temperature

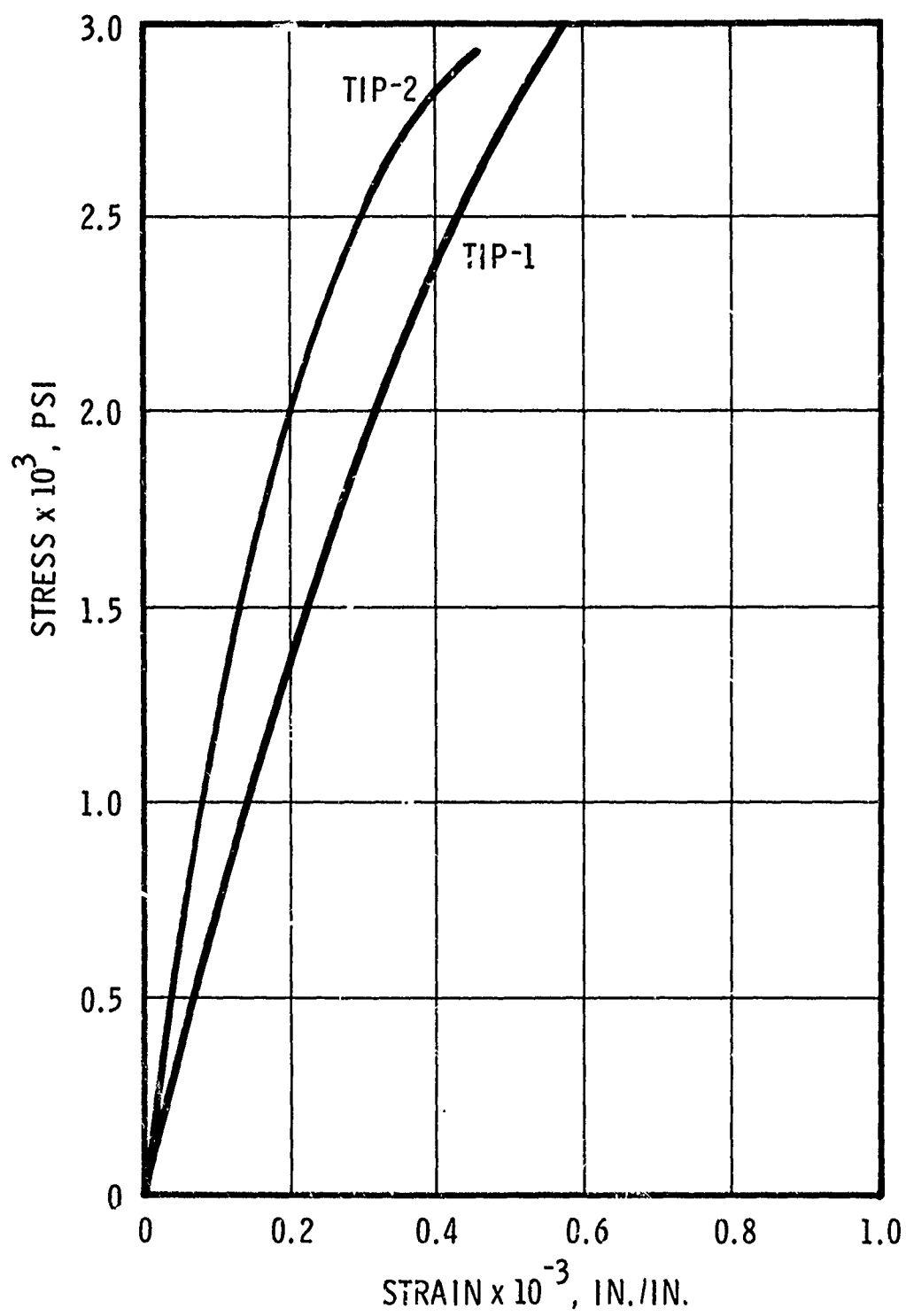


Figure 60. Stress-Strain Behavior in Internal Pressurization to 80% for Biaxial Test in Tension-Tension Mode

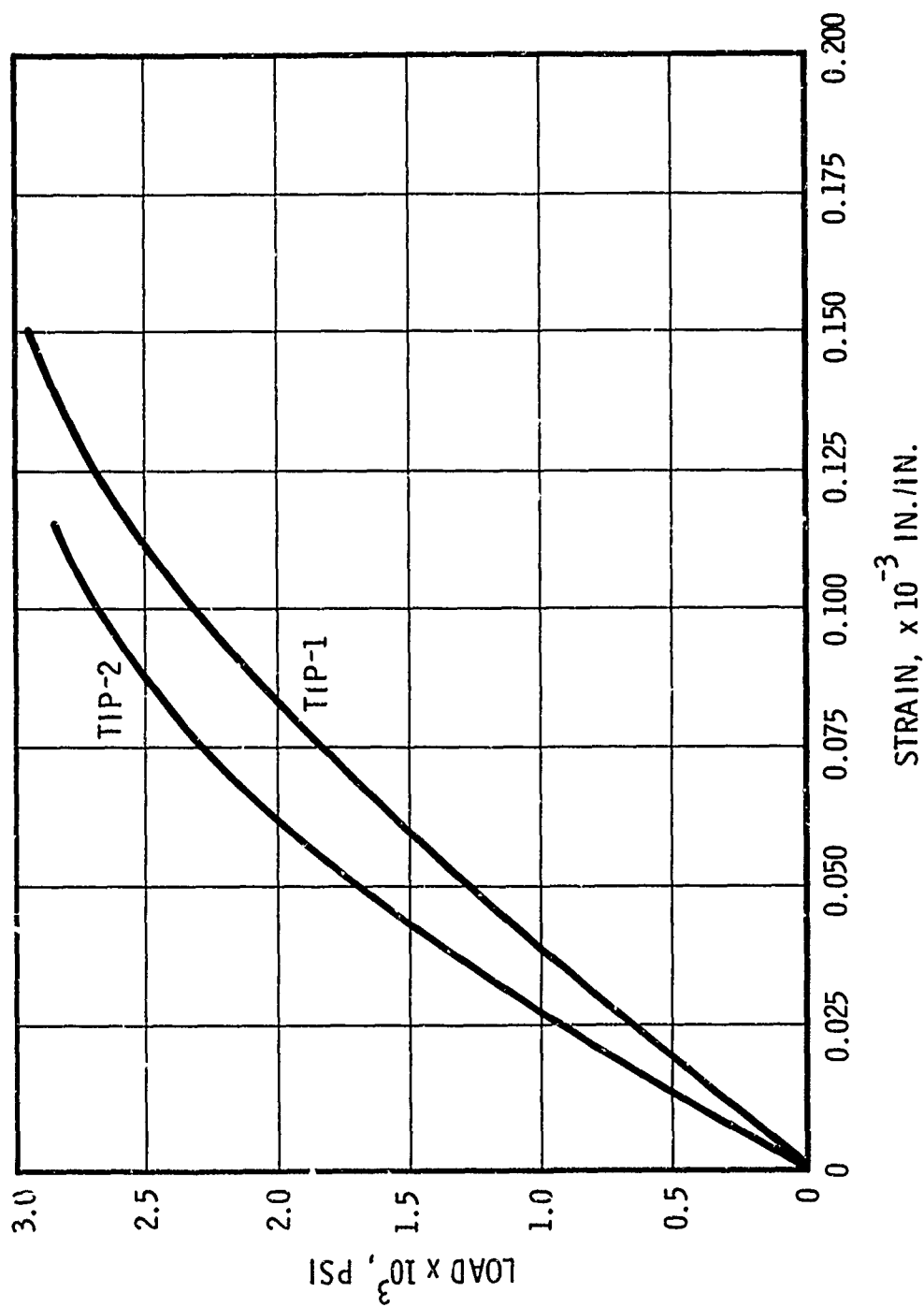


Figure 61. Load-Axial Strain Behavior in Internal Pressurization to 80%
for Biaxial Test in Tension-Tension Mode

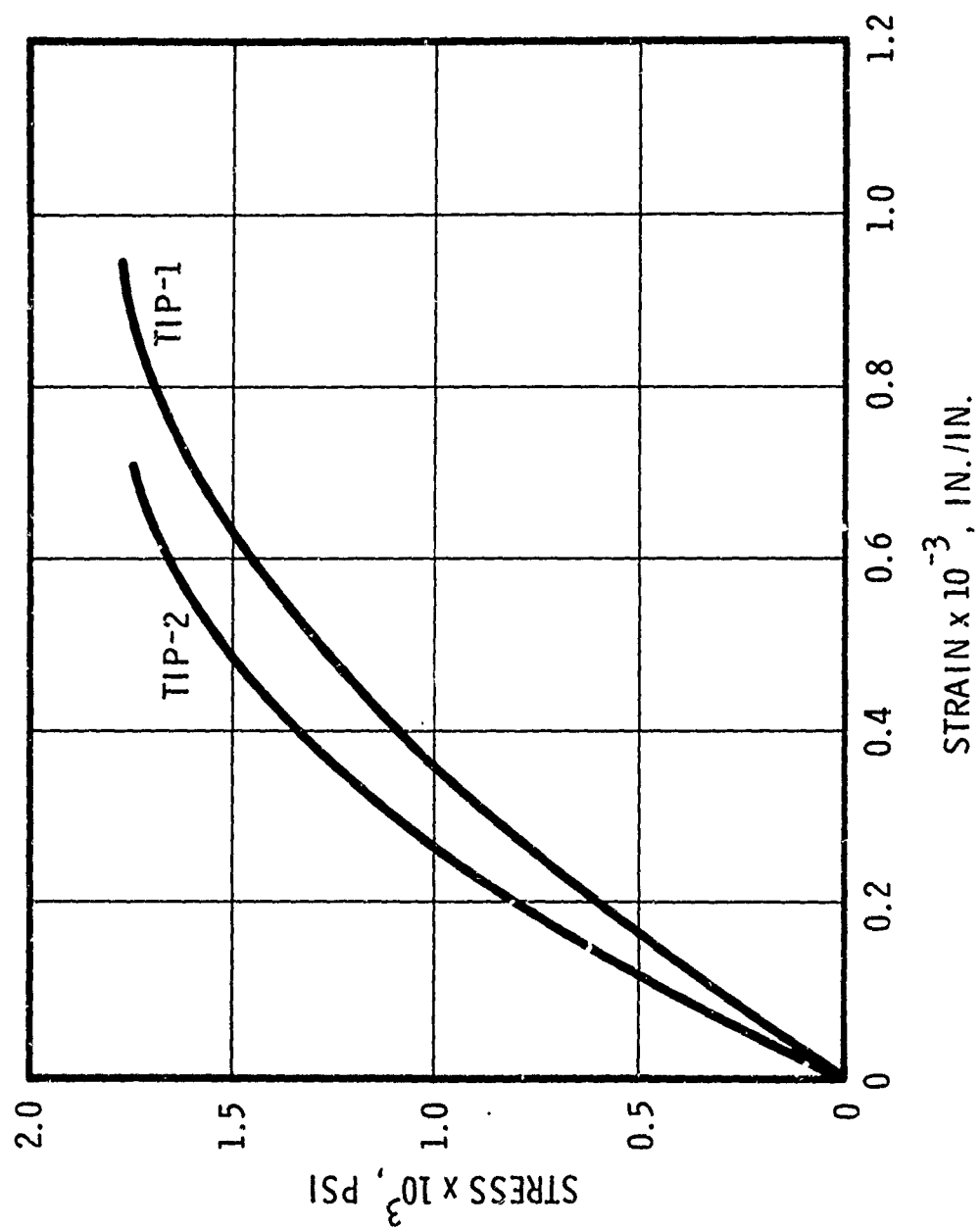


Figure 62. Stress-Strain Behavior in Tension for Biaxial Test in Tension-Tension Mode

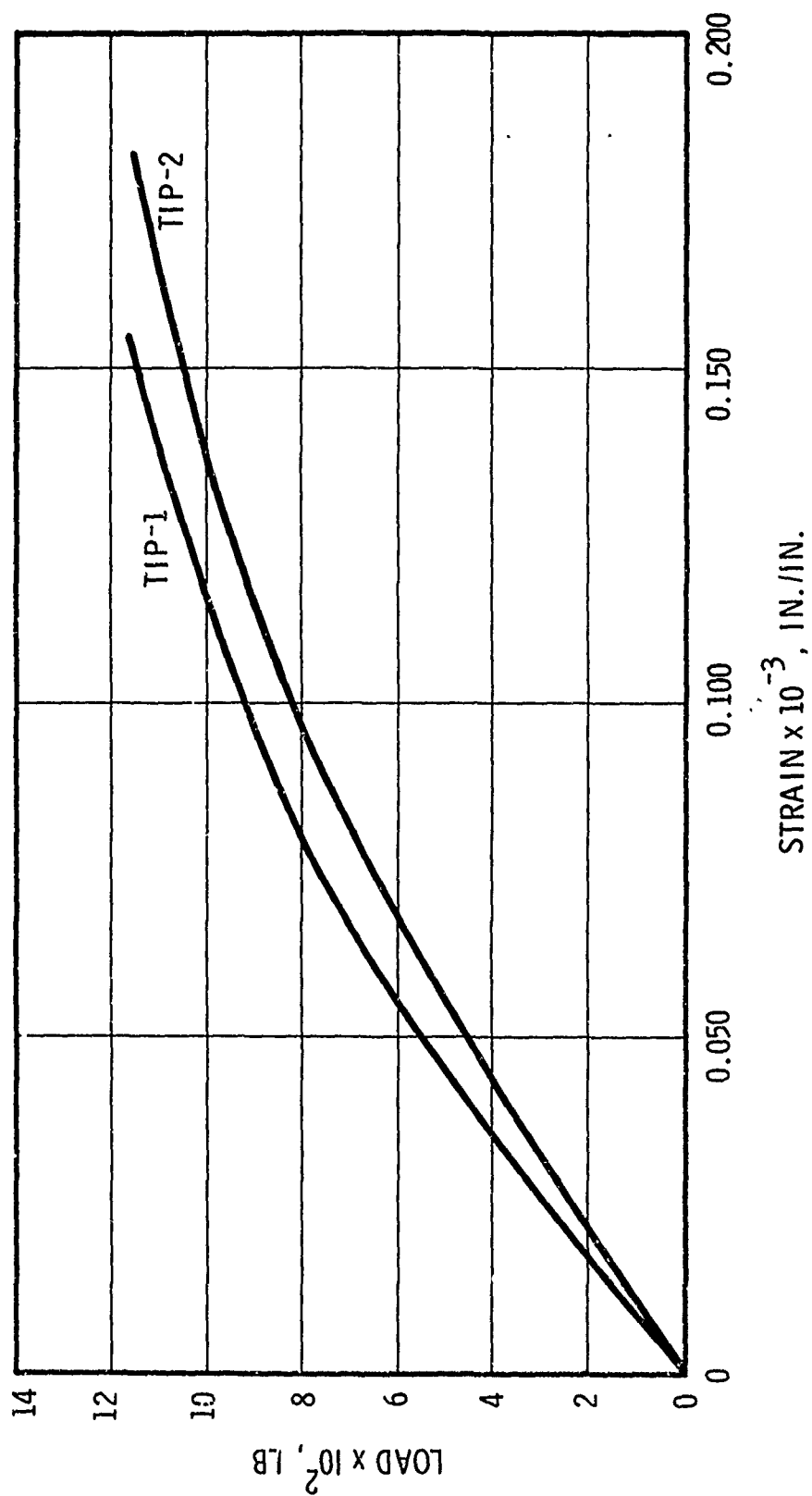


Figure 63. Load-Lateral Strain Behavior in Tension for Biaxial Test in Tension-Tension Mode

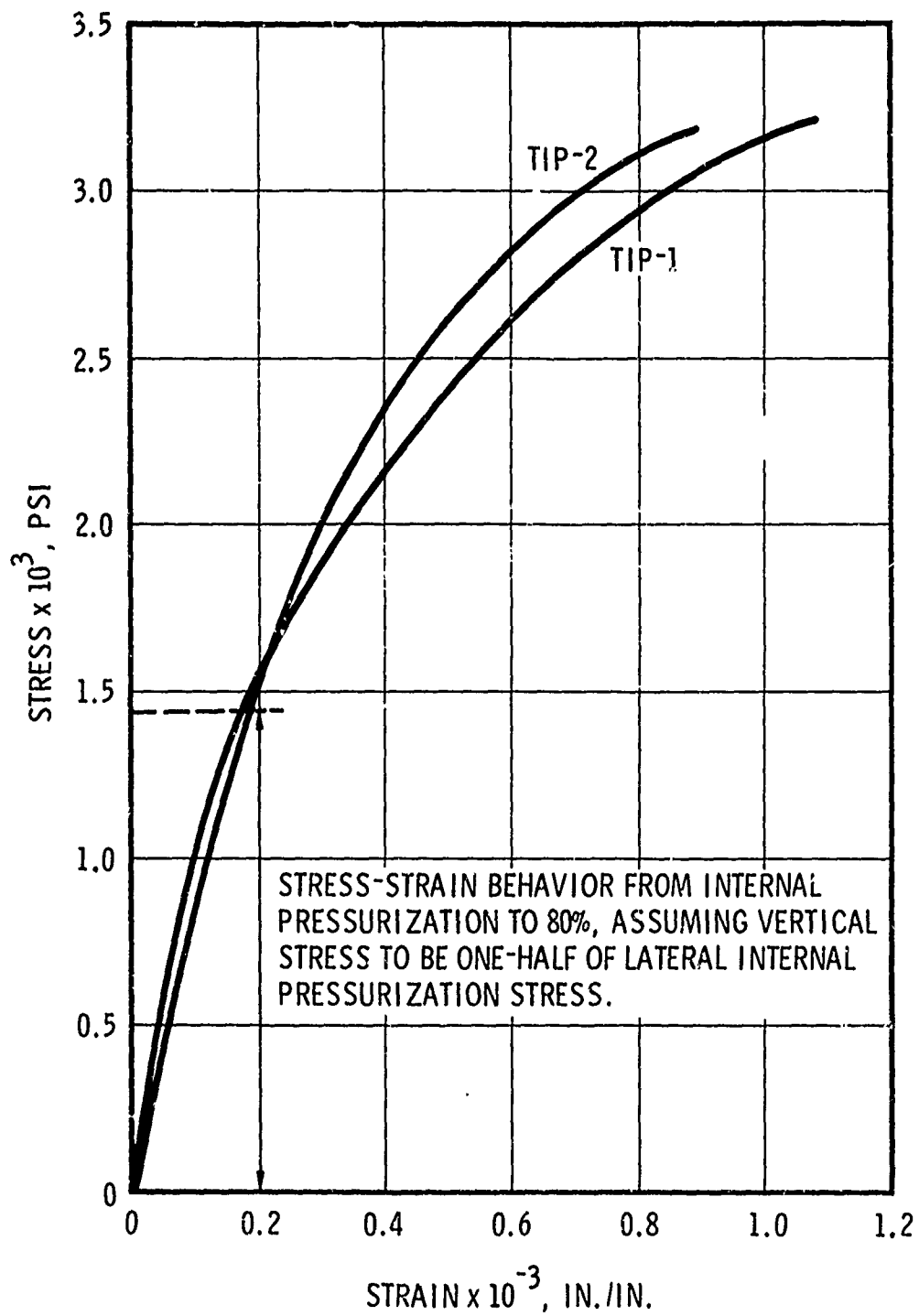


Figure 64. Stress-Strain Behavior in Tension-IP Test



Figure 65. TIP Specimen Tested at Room Temperature

(Size and shape changes were made which included using rectangular cross-sections, varying the number of turns, and varying the spacing of the coils and overall height of the coils.) Attempts also were made to use direct resistance heating or radiation heating to attain the required temperature. These attempts were not successful because of excessive heat loss from the sample or excessive time needed to reach the required test temperature. Finally, the entire test apparatus was moved to another location with a 80-kw 10,000-cps power source. Using this facility, there was no difficulty in obtaining the required test temperatures and rapid heatup times (3,000°F (1,650°C) could be achieved in less than 1 min).

A second problem was encountered when test temperatures were approached. Various species outgassed from the samples causing deposits on the walls of the Vycor tube chamber. These deposits fogged the tube making it difficult to obtain strain readings during elevated temperature testing. The problem was partially solved by rapid preheating of the specimen before testing to drive off some of the gases.

(a) High-Temperature Pressure Bag Development

A major objective of this program was the high-temperature biaxial testing of the wire-wound tungsten material and the containment of a pressurization media. Since there had been little or no experimental background information available, it was necessary to develop a new technique.

It was determined that tantalum metal would be ductile at the test temperatures required so 0.001-in.-thick tantalum foil was fabricated into the pressure bags. Cylinders to fit inside the test specimens were fabricated by spot welding a folded seam along one side. Attempts to seal the top and bottom of the cylinder by welding 1/16-in. tantalum caps were not successful due to the extreme sensitivity of the thin 1-mil foil to burn through.

A tantalum foil cylinder longer than the specimen was formed, and the tantalum foil cap was fitted into an ATJ-graphite cap which would fit over the test specimen. The graphite caps were adjusted so that the tantalum did not fit into the test specimen but only into the tantalum cylinder. When the assembly was heated to temperature, the higher expansion of the tantalum (4×10^{-6} in./in./°F) as compared to that of the graphite (3×10^{-6} in./in./°F) caused a pressure seal. Figure 66 displays the spot welded tantalum pressure cylinder, the tantalum caps and gas inlet, and the graphite pressure caps. Figure 67 shows how the tantalum cylinder extends beyond the specimen and how the graphite and tantalum caps fit onto the specimen. Figure 68 exhibits an assembled high-temperature burst specimen ready for testing. A diagram of high-temperature tests involving internal pressurization is shown in figure 69. This system proved to be successful and was used for all internal burst and biaxial tests.



Figure 66. Disassembled View of Fixturing for High-Temperature Tests

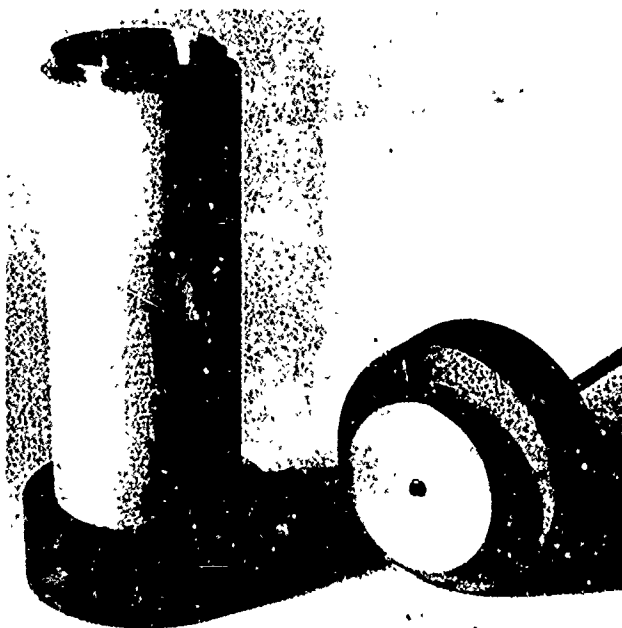


Figure 67. Partially Assembled View

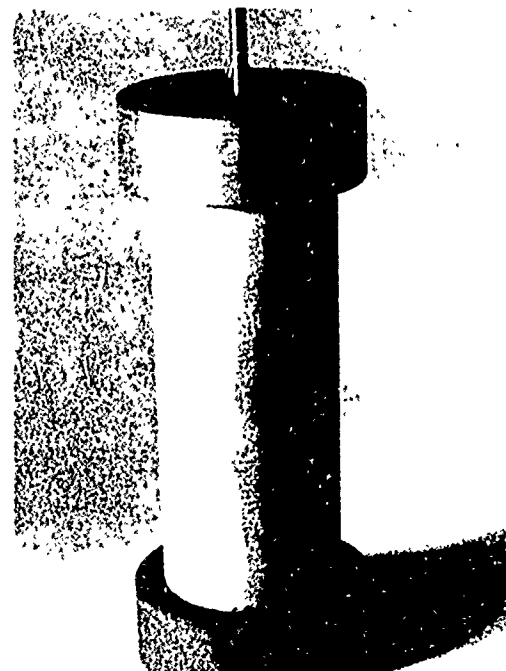


Figure 68. Assembled View

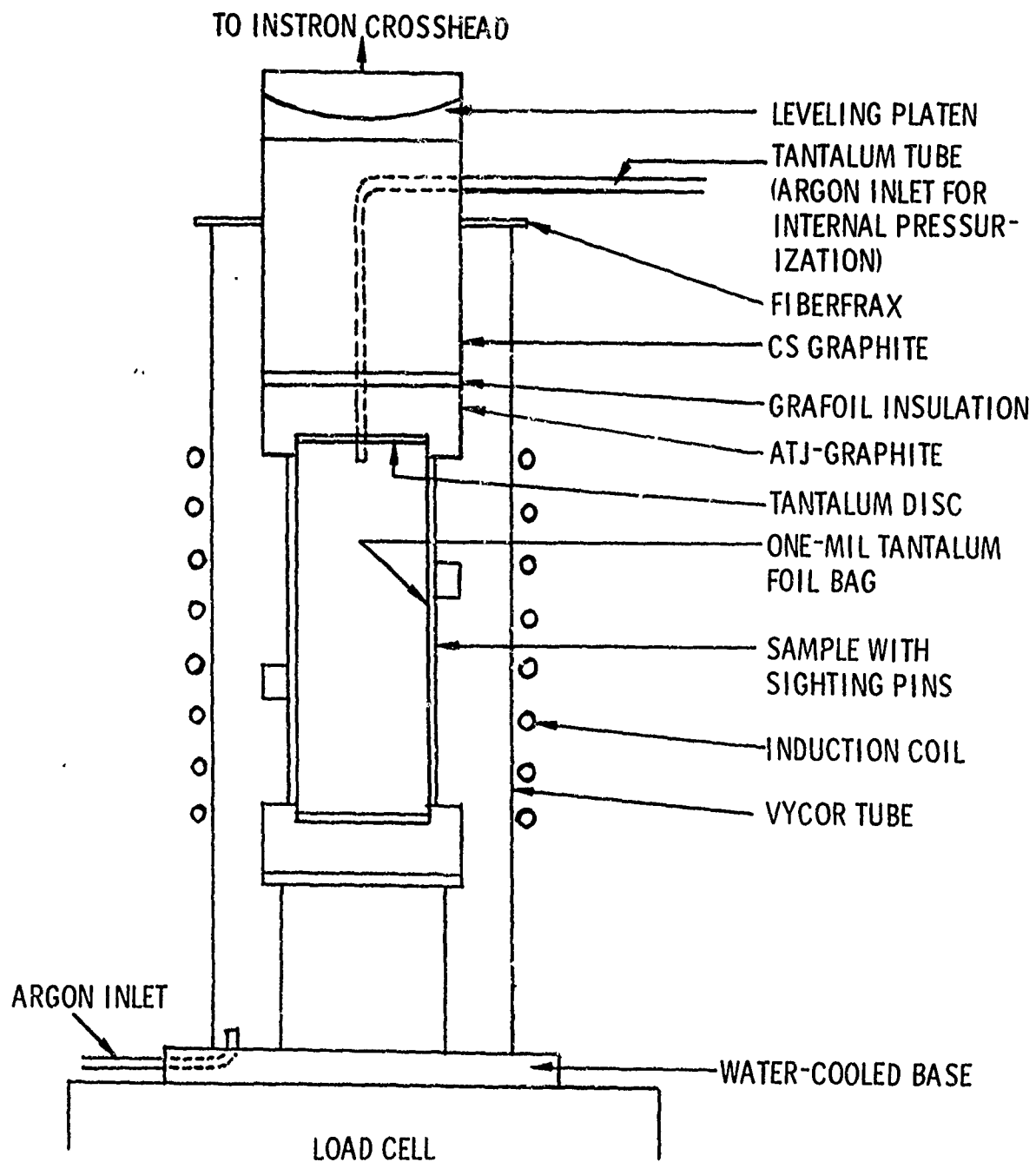


Figure 69. Diagram of Apparatus for High-Temperature
IP and CIP Tests

(b) High-Temperature Test Data

The high-temperature test data are summarized in table XV. It was impossible to obtain all the required tension data because of premature fractures (figure 70).

Two factors contributed to these fractures:

- A. The aforementioned high thermal stress induced by differences in thermal expansion between the heated gage section of the specimens and the cooler grip ends.
- B. The proximity of the induction coil to the grip ends, which in turn allowed heating of the stainless-steel inserts by conduction and radiation. The thermal expansion differences between materials induced a radial stress in the grip area. The induction coil was never intended to cover more than 1 in. of the gage length. However, heating difficulties required the use of a longer coil.

Since the fractures were primarily circumferential and occurred in the tapered grip area factor, item A was determined to be the major cause.

The condition of specimen T-4 tested at 3,000°F (1,650°C) is shown in figure 71. Note the cracks at the hub. However, this specimen held together during the test and a fracture in the gage section was obtained. No stress-strain data could be obtained because of severe outgassing from the specimens. It was observed during the tests that outgassing from the larger tension and TIP samples was much greater than for the much smaller volume compression and internal pressurization samples. Figure 72 exhibits the breakup of a specimen heated to 4,000°F (2,200°C) without a load being applied. Both circumferential and axial cracking occurred in the grip area.

Data for maximum compression exhibit little spread and are consistent for each test temperature. Stress-strain data are presented in figures 73 and 74. Note the well-defined yield point and leveling off of the curve at maximum strains. Tested compression specimens are displayed in figure 75. The target pins for making optical strain measurement can be observed still adhering to the specimens. Permanent barreling of the specimen can be visually observed, confirming that the sample yielded. If the specimen continued to be loaded, it would flatten out as shown in figure 76.

Test results for the internally pressurized specimens appear consistent when compared to the results obtained for the direct tensile test at 3,000°F (1,650°C). These data provide

TABLE XV
SUMMARY OF HIGH-TEMPERATURE DATA

Specimen S/N	Temperature, °F	Stress, psi		E x 10 ⁶ , psi tan
		Yield	Maximum	
T-4	3,000	---	310	---
C-3	3,000	---	9,240	---
C-5	3,000	7,000	8,370	0.45
C-6	4,000	2,000	4,690	0.16
C-4	4,000	---	3,370	---
IP-3	3,000	300	---	0.63
IP-4	3,000	500	---	0.58
IP-5	4,000	250	---	0.35
IP-6	4,000	150	---	0.35
IPC-5	3,000	---	---	0.65*
IPC-6	4,000	650	---	0.20* 0.80 [†]

*Compressive component

[†]Burst component

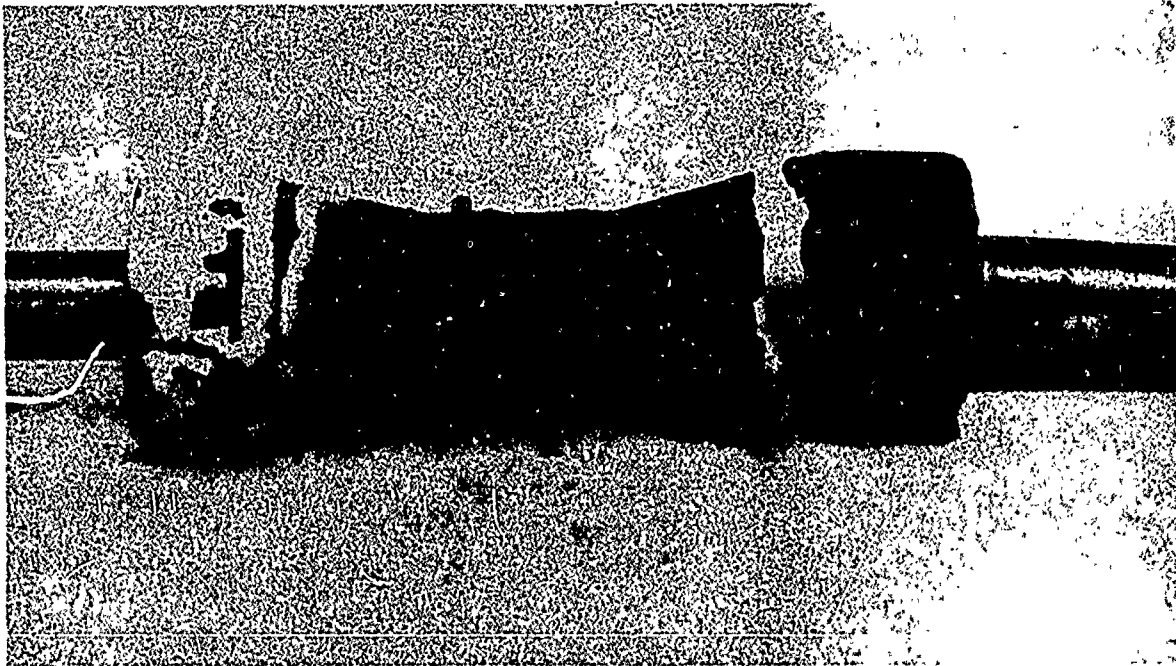


Figure 70. Tension Specimen Tested at 4,000°F

Reproduced from
best available copy.



Figure 71. Tension Specimen Tested at 3,000°F
with Failure in Gage Section

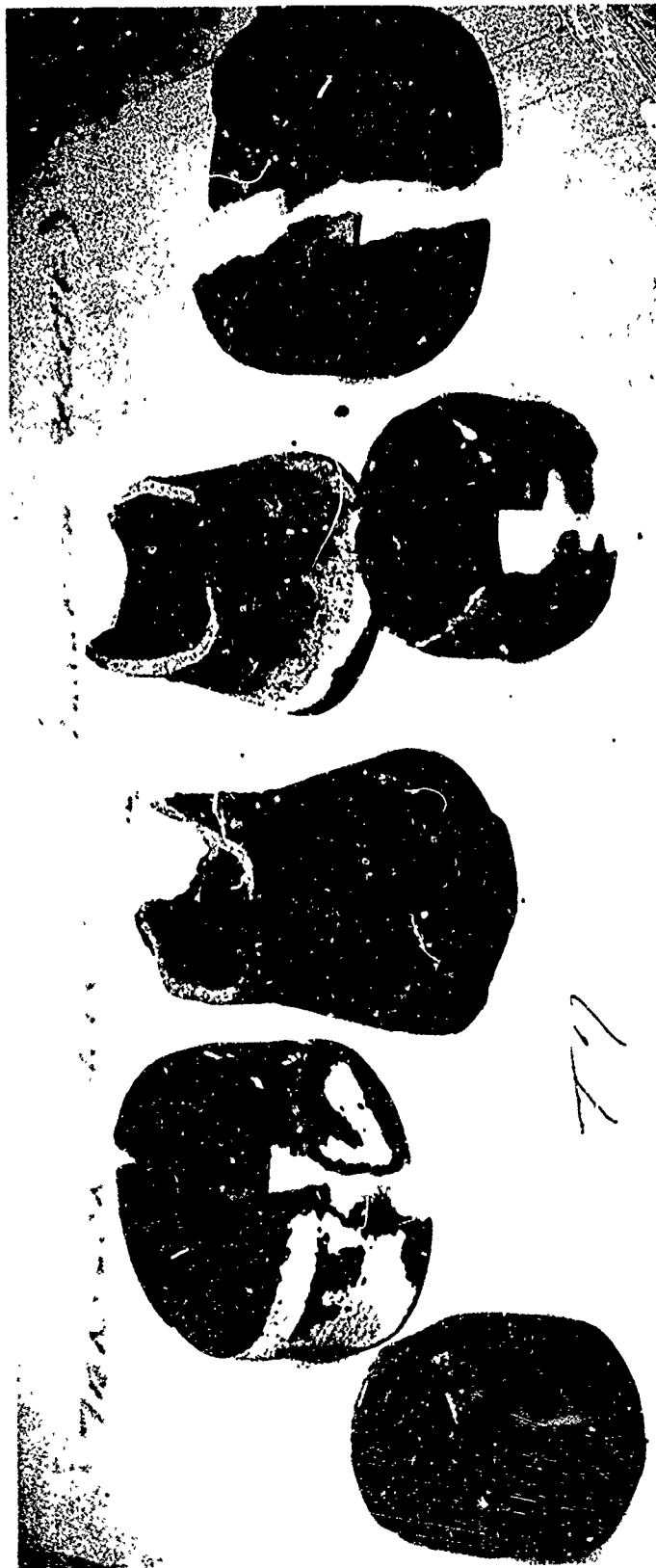


Figure 72. Tension Specimen Tested at 4,000°F Showing Deformation and Melting of Stainless-Steel Inserts

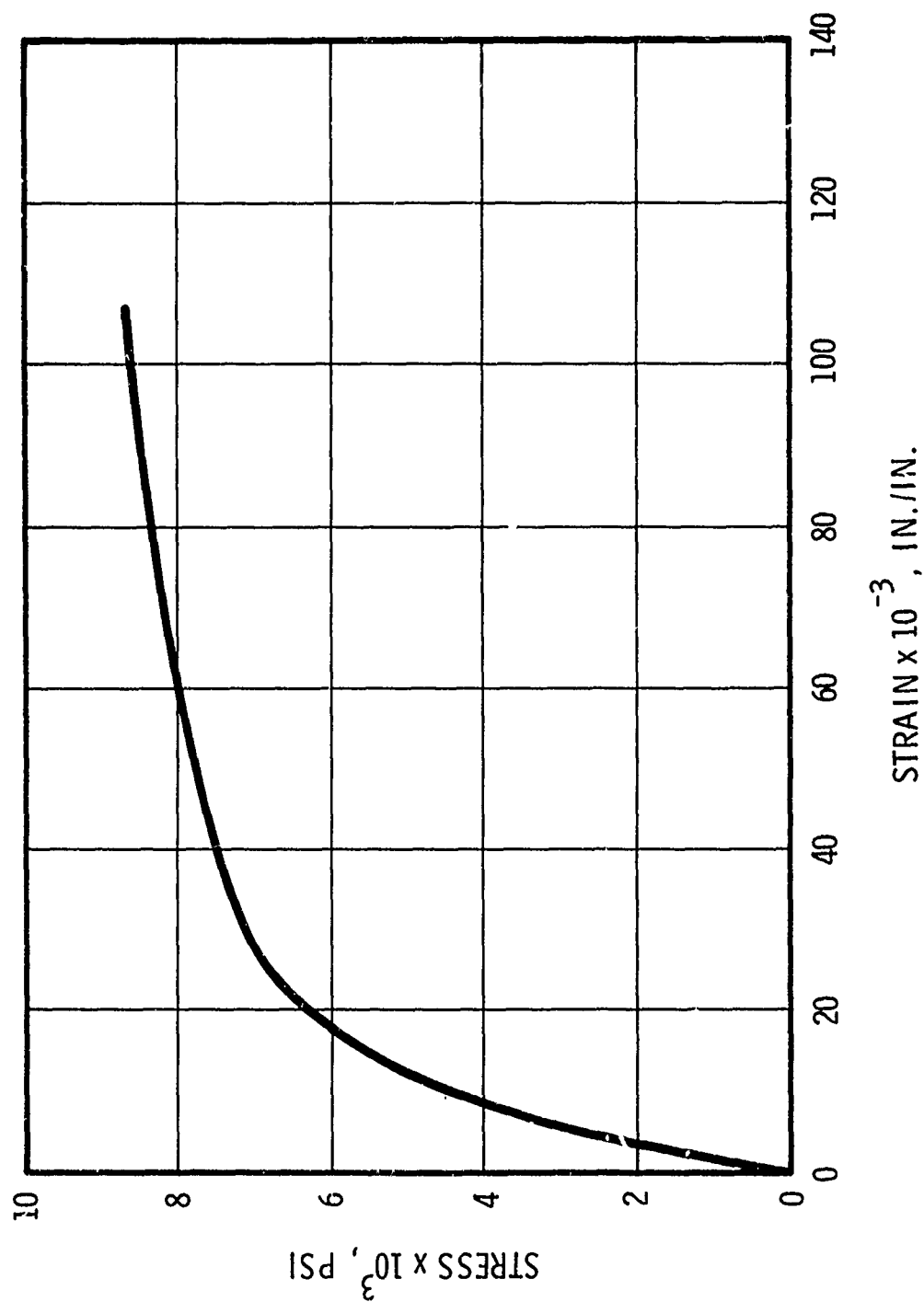


Figure 73. Stress-Strain Behavior in Compression at 3,000°F

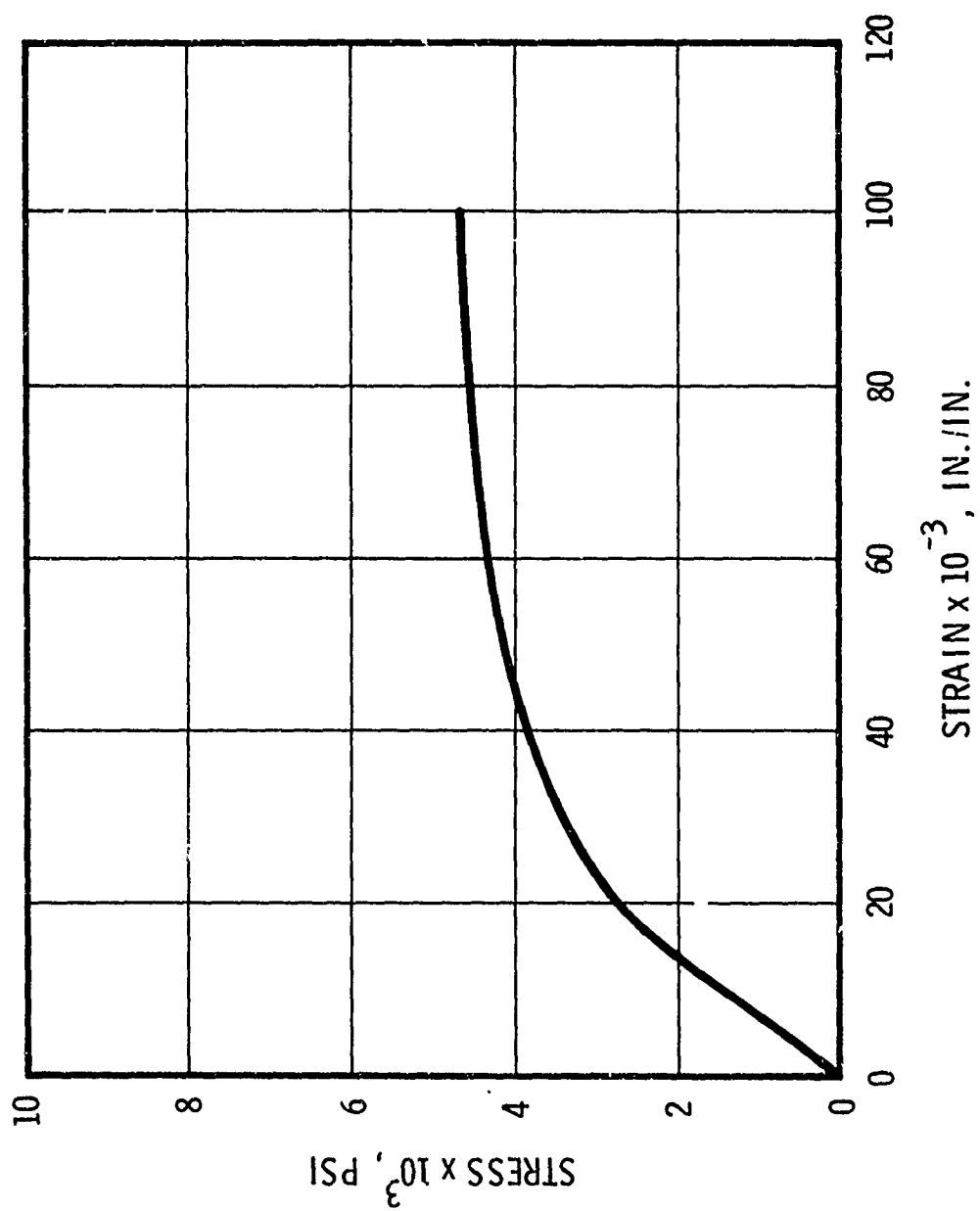


Figure 74. Stress-Strain Behavior in Compression at 4,000°F

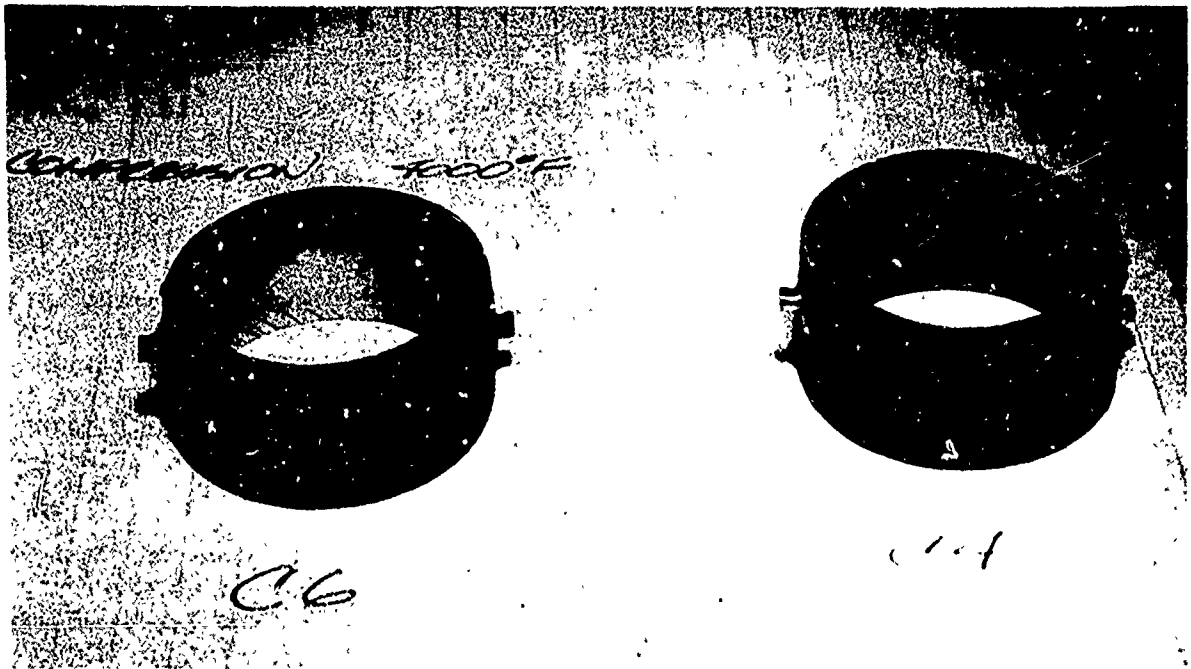


Figure 75. Compression Specimens Tested at 4,000°F

Reproduced from
best available copy.

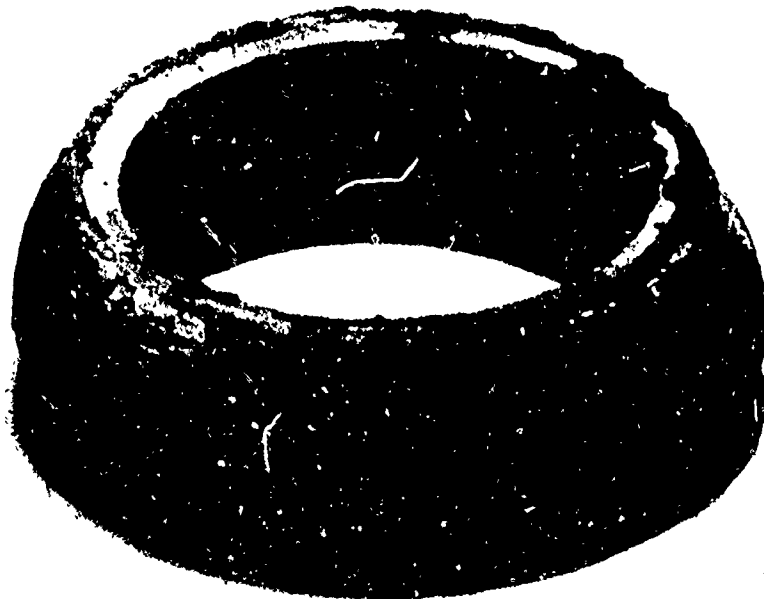


Figure 76. Compression Specimen Tested at 3,000°F

confidence for the tensile data presented for both temperature levels, 3,000°F (1,650°C) and 4,000°F (2,200°C). These specimens did not exhibit brittle failure but yielded in a manner similar to aluminum. No maximum stress could be obtained from these tests because the tantalum metal bag would fail after the test specimen yielded. Figure 77 displays the stress-strain behavior of the internally pressurized samples tested at 3,000°F (1,650°C). Each sample exhibits a definite yield point. Test specimen IP-4 displays somewhat higher strengths because it was heated to temperature and held there for a total of approximately 15 min before testing, thus undergoing sintering. Stress-strain data for test specimens measured at 4,000°F (2,200°C) are presented in figure 78. These curves present a somewhat different situation than the curves shown in figure 77. There is still a hook in the data suggestive of yielding; however, the curve is more typical of work hardening than those obtained at 3,000°F (1,650°C). No explanation can be given at this time for this phenomena.

Biaxial testing was performed in the compression tension mode instead of the tension-tension mode because of the aforementioned premature fractures due to thermal expansion stresses. For these tests, the grips of the test samples were removed to provide for an acceptable compression specimen configuration. Stress-strain data are displayed in figures 79 and 80. The specimens after test are shown in figure 81. Specimen CIP-5 was loaded to 80% of the ultimate compressive strength and then internal pressure was applied. The stress-strain behavior in compression (figure 79) indicates that plastic deformation had occurred. These specimens were at least three times longer than the short uniaxial compression specimens, and buckling occurred at this load (figure 81). The buckling which occurred at 3,000°F (1,650°C) precluded obtaining internal pressurization data. A buckling analysis based on height-to-wall thickness was made, and the compression load of 80% yield at 4,000°F (2,200°C) was determined to be 600 psi, the value used in the test on specimen CIP-6.

c. Test Observations

Test results indicate that wire-wound tungsten behaves in a non-linear elastic manner under room temperature conditions. The material behaves as an elastic-plastic material at temperatures of 3,000°F (1,650°C) and 4,000°F (2,200°C) in an inert gas environment. This behavior offers an explanation as to why wire-wound tungsten resists failure under the severe thermal shock conditions which would fracture other types of high-temperature materials.

The high-temperature biaxial test procedures developed during the program appear to be a satisfactory test procedure which can result in a standard high-temperature test method. For rapid heatup of large specimens, induction heating of the specimen itself is feasible.

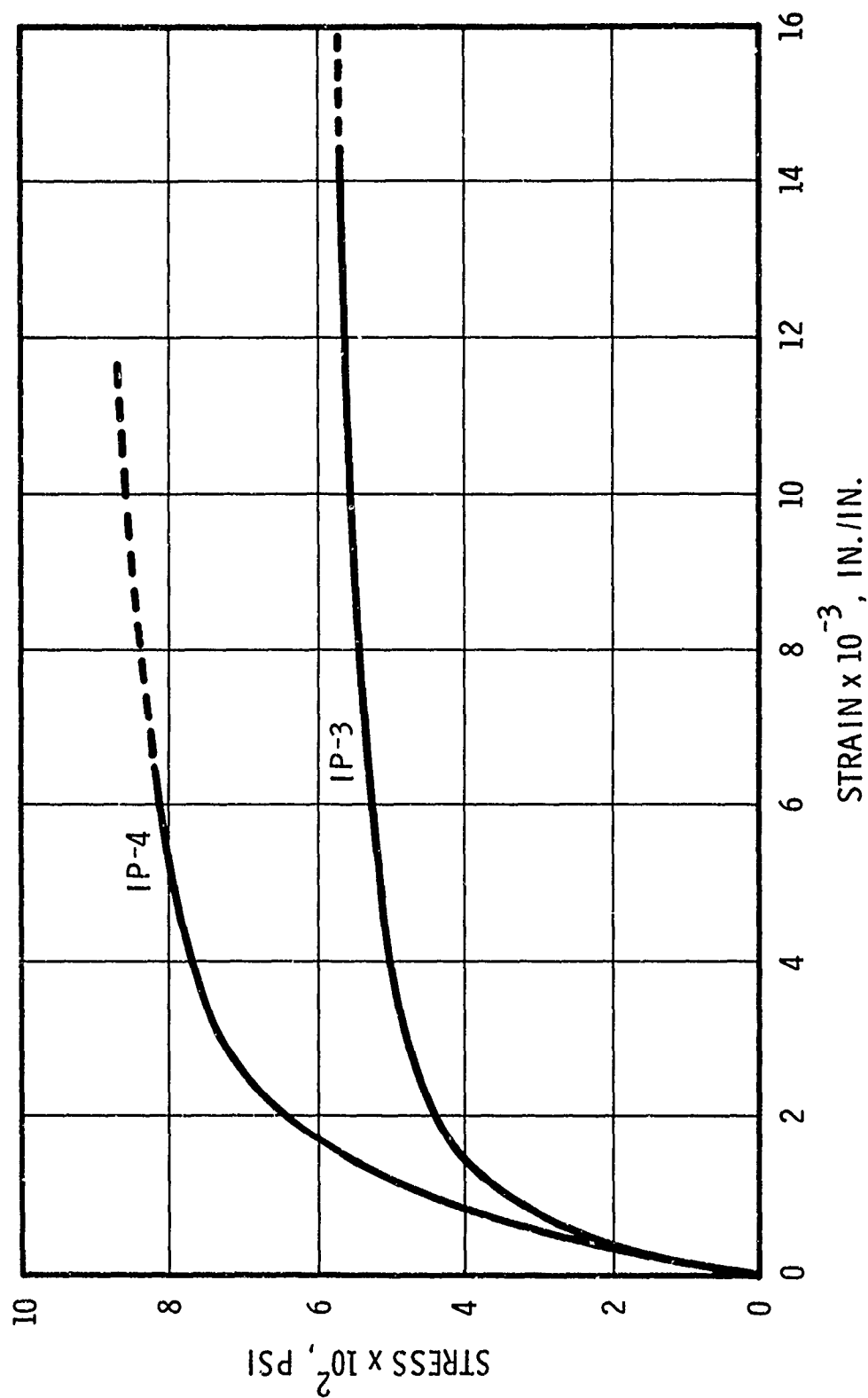


Figure 77. Stress-Strain Behavior in Internal Pressurization at 3,000°F

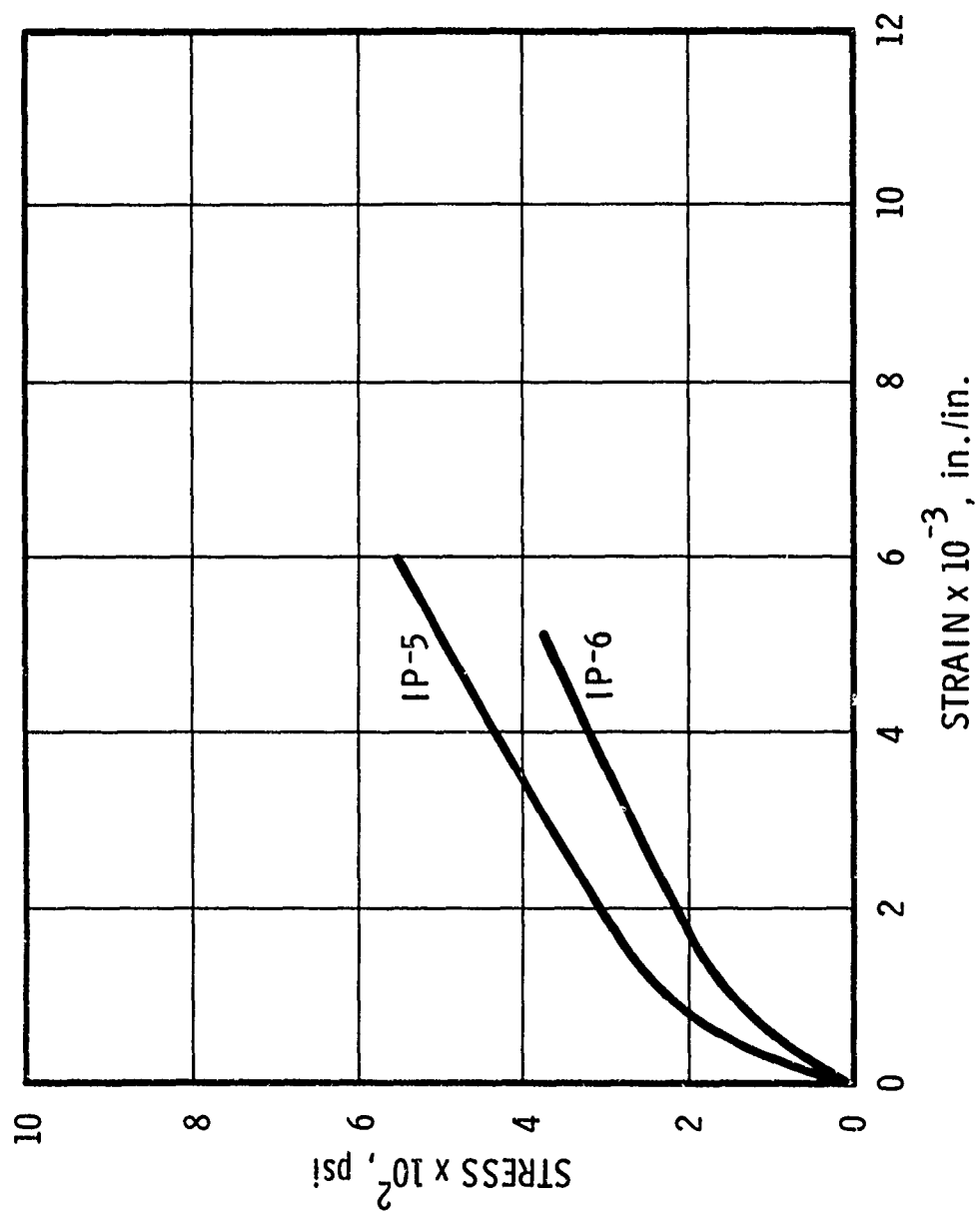


Figure 78. Stress-Strain Behavior in Internal Pressurization at 4,000°F

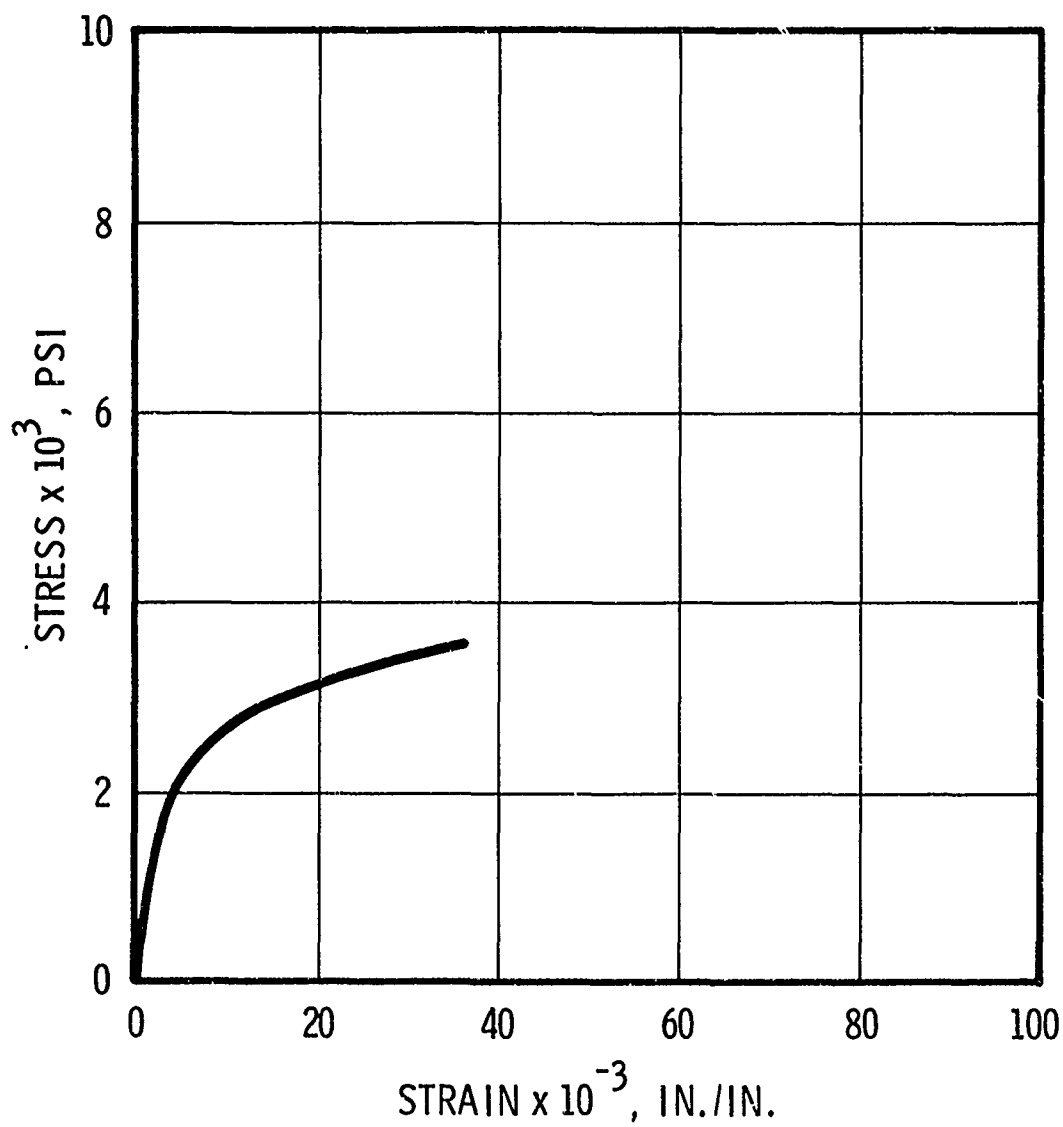


Figure 79. Stress-Strain Behavior During Compressive Loading in CIP Test at 3,000°F

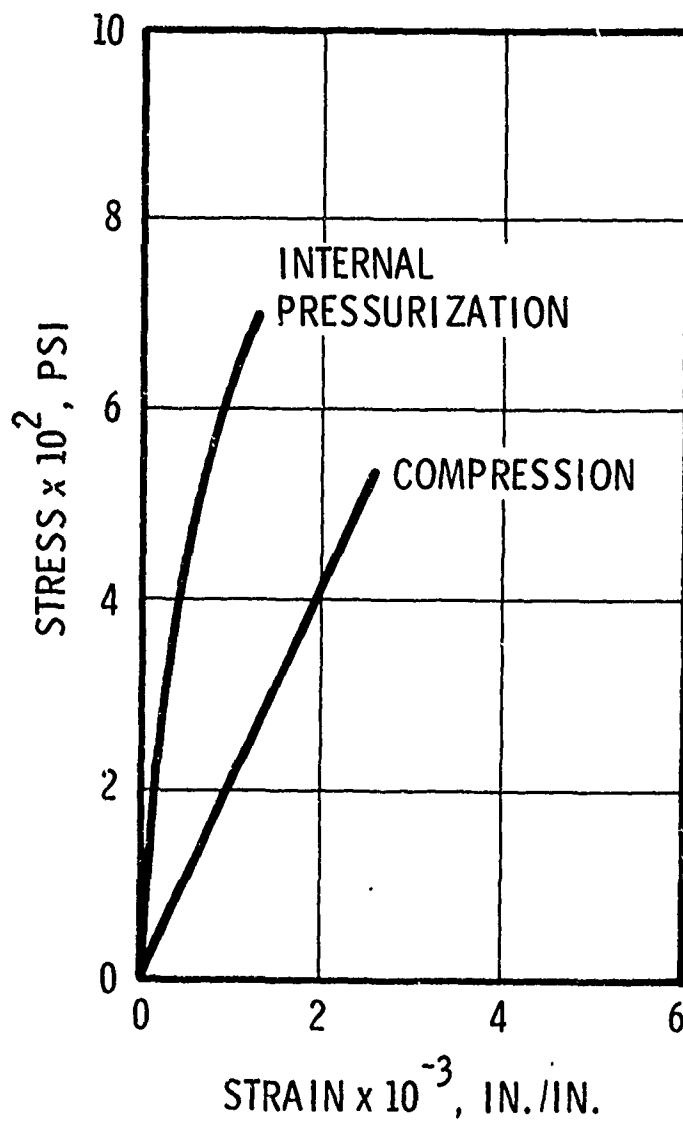


Figure 80. Stress-Strain Behavior in CIP Test at 4,000°F

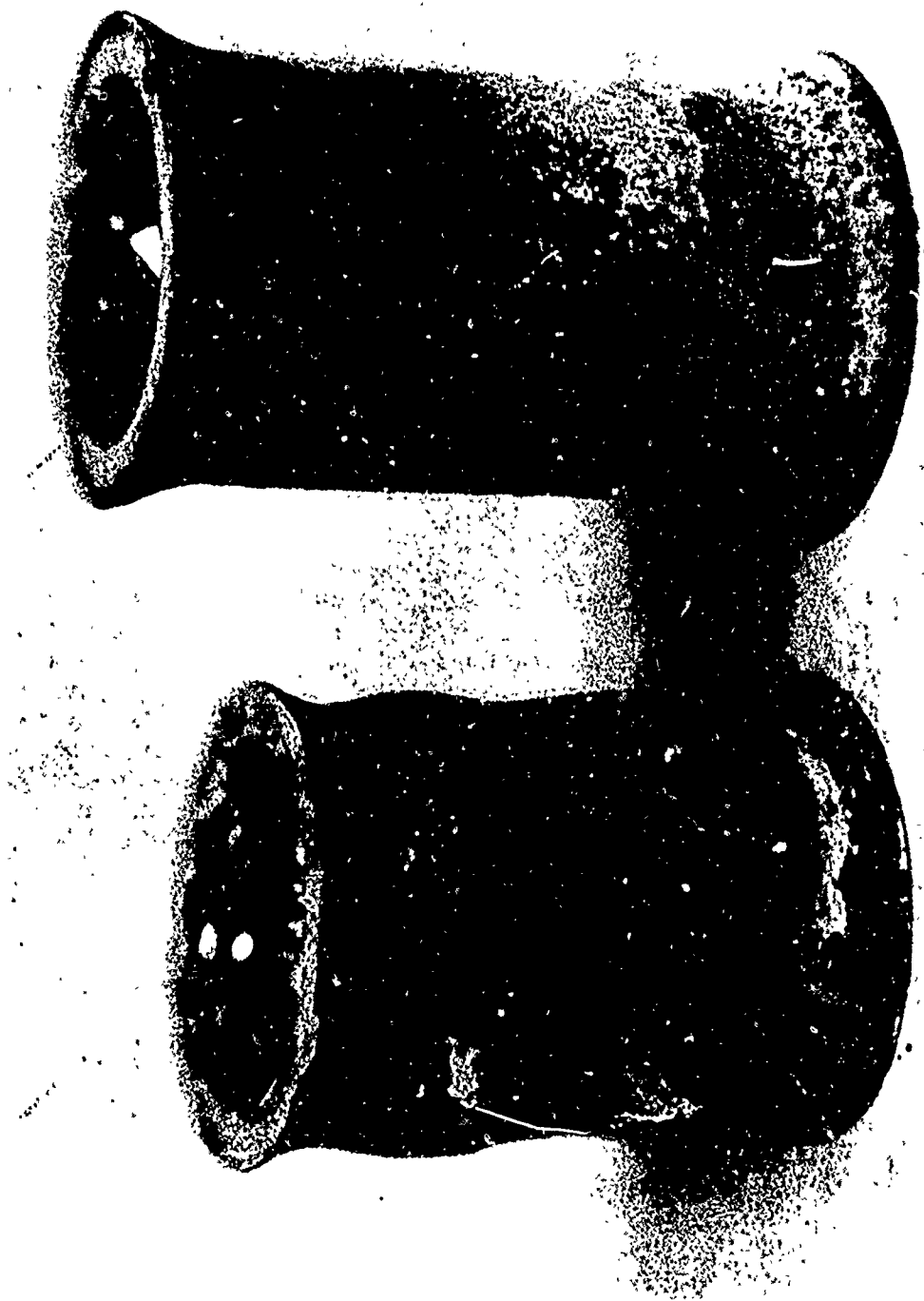


Figure 81. IPC Specimens Tested at 3,000° and 4,000°F

Radiation heating can be used if slower heating rates are used. A tantalum pressure bag is an acceptable method of high-temperature loading a cylindrical sample for a burst test. The data indicate that for a material which exhibits plastic behavior, the yield point can be obtained, but the bag will fail before the sample will rupture. Additional research is required to improve this aspect of the test procedure.

4. PHYSICAL AND CHEMICAL CHARACTERISTICS

The physical and chemical characteristics of wire-wound tungsten were investigated on material obtained from the tested thermal and mechanical property specimens. Conditions representing the complete range of test temperature (from room temperature to 4,000°F (2,200°C)) were evaluated. The following subsections describe the techniques and results used to evaluate the composite's density, chemical composition, and microstructure.

a. Density Measurements

(1) Procedure

The density of wire-wound tungsten specimens in various conditions of thermal exposure was measured using two techniques: water immersion and pycnometric. Density samples were cut to size with an abrasive cut-off wheel. Immersion samples were approximately 1 in. by 1 in. by 0.15 in. Pycnometer samples were 1/8 in. by 1/8 in. by 1/2 in.

The immersion density measurements were conducted in accordance with ASTM-B-311, "Standard Method of Test for Density of Cemented Carbides." This method is a normal water immersion test for bulk density. Pycnometric density measurements were performed with a calibrated pycnometer of known volume using tridecane, a hydrocarbon oil with low viscosity and vapor pressure. For this technique, the samples were weighed in the pycnometer, covered with tridecane, and vacuum degassed. The pycnometer was then filled with tridecane and weighed. Knowing the volume of the pycnometer, tridecane's density, and the sample weight, the density is calculated as

$$\rho_S = \frac{W_S \times \rho_T}{W_T - (W_{S+T} - W_S)}$$

where ρ_S = desired density

W_S = weight of sample when dry

ρ_T = density of tridecane

W_T = weight of tridecane to fill known volume of pycnometer

W_{S+T} = weight of sample plus tridecane to fill pycnometer.

(2) Results

The test specimens used for density measurements and their resultant densities are presented in table XVI. The identity corresponds to the respective mechanical or thermal property test, e.g., IP = internal pressurization, TIP = tension/pressurization, and C = compression. The water immersion measurements showed theoretical densities of 82.5% to 84.0% for as-composited material and 90.8% to 94.4% for elevated temperature exposed material. The pycnometer measurements yielded theoretical densities of 89.7% to 93.4% for as-composited material and 97% for elevated temperature exposed material.

An examination of the as-composited water immersion bulk densities shows the uniformity and reproducibility of the fabrication process. The four samples measured were within the $85 \pm 3\%$ bulk density value established for wire-wound tungsten. Comparing pycnometric densities with the water immersion bulk densities indicates, in some measure, the magnitude of the shadows (void spaces) behind the filament reinforcement. For both the as-composited and elevated temperature exposed material, the difference in density was 5% to 7%. Since the neutron radiography results indicated that these shadows were continuous and since the sintered pycnometric density of 97% is about the maximum to be expected for plasma-arc-sprayed material⁽⁷⁾, it is reasonable to assume that the density difference is a measurement of the void space behind the filaments. This sponginess of wire-wound tungsten is a primary factor of the material's capability to withstand the severe thermal shock environments of rocket nozzle throats.

b. Chemical Analysis and Composition

(1) Procedure

The chemical composition of wire-wound tungsten was evaluated by spectrographic, conductometric, and vacuum fusion analyses. For additional comparison, X-ray diffraction and electron microprobe analyses were performed.

An applied research laboratory instrument was used for film spectrography to yield semiquantitative determinations (in ppm) of the metallic elements present in the composite. A LECO vacuum fusion analyzer was used for quantitative detection of absorbed and adsorbed oxygen, hydrogen, and nitrogen; carbon content was detected and measured by a LECO conductometric analyzer. X-ray diffraction analysis for oxides, nitrides, etc. was performed by the Debye-Scherrer rotating crystal technique with a Norelco X-ray generator using nickel-filtered copper K_{α} radiation. Specimens were exposed at 40 kv and 20 Ma for 3 hr. Because of the large atomic number of tungsten and, consequently, its great X-ray absorption ability, X-ray diffraction could only detect significant amounts ($>3\%$) of the higher nitrides and oxides.

TABLE XVI
MEASURED DENSITIES

Specimen	Thermal History	Density			
		Water Immersion		Pycnometer	
		g/cc	Theoretical, %	g/cc	Theoretical, %
IP-1	RT*	16.1	83.5	16.5 [†]	85.6
IP-2	RT*	16.0	83.0	18.0	93.4
TIP-1	RT*	16.2	84.0	17.3	89.7
C-1	RT*	15.9	82.5	---	---
TD-380	3,000°F	17.5	90.8	---	---
TD-381	4,000°F	18.2	94.4	---	---
THE-2A	3,800°F	18.2	94.4	---	---
THE-3A	Sintered 3,800°F	17.7	91.8	18.7	97.0
C-5	3,000°F	17.8	92.3	18.7	97.0

* Room temperature or as-composited material

[†] This measurement is judged a test anomaly

[‡] Sintering process, 1 hr at 3,600°F in argon

Electron microprobe examinations were made with an ARL-EMX-SM electron microprobe/scanning electron microscope. The element's characteristic spectra produced as the specimens were bombarded by electrons were identified using the instrument's dispersive X-ray spectrometers. The electron beam scanned the specimens in a raster mode, allowing the characteristic spectra of a given element to be displayed on an oscilloscope. Also, secondary electrons were used to form scanning electron images of the specimen surface. Photographs were taken of the oscilloscope patterns to record these observations.

(2) Results

(a) Chemical Analysis

Results of the chemical analyses are given in table XVII, which include the chemistries for the raw tungsten powder used in fabricating the specimens and the specimens in the as-composited and elevated temperature exposed conditions.

Spectrographic analyses results indicate little or no change in the basic element content of the wire-wound tungsten matrix as compared to the tungsten powder for either as-composited or elevated temperature exposed condition. The variations observed are within the $\pm 30\%$ accuracy level for spectrography. Boron in specimen 3-A (20 ppm) and nickel in specimen C-5 (70 ppm) are apparently contaminants picked up during handling and/or testing. The spectrographic results essentially corroborate the material certification chemistry.

Vacuum fusion analyses of specimens T-1 and THE-2 (as-composited material) show a substantial amount of absorbed oxygen and nitrogen as compared to the virgin powder samples (A and B). Exposure to test temperature ($3,000^{\circ}$ and $4,000^{\circ}\text{F}$) in argon appears to drive off all but minor amounts of oxygen which are probably trapped within the plasma-sprayed matrix.

The conductometric analyses of selected specimens revealed no significant amount of carbon. Variation between samples is believed to be caused by contaminants introduced during sample preparation.

(b) X-ray Diffraction

Samples from specimens T-1 (as-composited), 1-A, 3-A, C-5 (temperature exposed), and virgin powder were evaluated by the Debye-Scherrer rotating crystal technique. Powder patterns revealed evidence of tungsten only. This technique, as previously described, is not considered capable of detecting oxides or nitrides in amounts less than 3% because of the masking from tungsten.

TABLE XVII
CHEMICAL ANALYSES

Element	Powder Cert ppm	Spectrographic Analyses Results, ppm				
		Raw Powder	T-1	C-5	1-A	3-A
Al	---	< 3	10	30	20	3
B	---	5	5	10	5	20
Ba	---	<10	<10	<10	<10	10
Be	---	< 1	< 1	< 1	10	5
Ca	---	<10	<10	<10	<10	<10
Cd	---	<100	<100	<100	<100	<100
Co	---	< 5	< 5	< 5	< 5	< 5
Cr	10 to 100	<10	<10	<10	<10	<10
Cu	1	5	5	5	1	5
Fe	17	10	15	15	5	5
Mg	0.5 to 5	1	5	5	2	5
Mn	0.5 to 5	< 3	< 3	< 3	< 3	< 3
Mo	32	<30	<30	<30	<30	<30
Ni	10 to 100	30	30	70	10	20
Pb	---	<10	<10	<10	<10	<10
Si	5 to 50	10	10	15	10	20
Sn	---	< 5	< 5	< 5	< 5	< 5
Ti	1 to 10	< 5	50	< 5	5	< 5
V	---	< 3	< 3	< 3	< 3	< 3
Zr	---	10	10	20	10	10

GAS ANALYSIS

	Powder		THE-2	T-1	C-5	1-A	3-A	T-4	T-7	3A(2)	C-6
	A	B									
Oxygen*	130	180	2,350	2,690	490	40	1,310	750	560	700	1,700
Hydrogen*	4	8	10	33	15	1	13	8	6	14	24
Nitrogen*	<50	30	260	210	<50	<50	<50	30	30	30	<30
Carbon†	---	---	---	11	51	---	---	---	---	---	142

Legend: T-1 = as-composited 3-A = sintered, then exposed to 4,000°F
THE-2 = as-composited T-4 = exposed to 3,000°F for 10 min
C-5 = exposed to 3,000°F for 10 min T-7 = exposed to 4,000°F for 3 min
1-A = exposed to 4,000°F C-6 = exposed to 4,000°F for 10 min

* Vacuum fusion analysis, ppm
† Conductometric analysis, ppm

(c) Electron Microprobe

Samples of wire-wound tungsten were removed from tested mechanical property specimens and were examined by an electron microprobe to identify composition and impurity levels. Specimens T-1 and TIP-1 represent as-composited material, T-4 material exposed to 3,000°F (1,650°C) in a tension test and T-7 material exposed to 4,000°F (2,000°C) in a tension test.

Fresh fracture faces were prepared for each specimen and were evaluated for the full spectrum of radiation. Lithium fluoride, ammonium dihydrogen phosphate, rubidium acid phthalate, and lead stearate dispersion crystals were used for covering the spectrum. Excluding tungsten, only the oxygen and carbon spectra were identified.

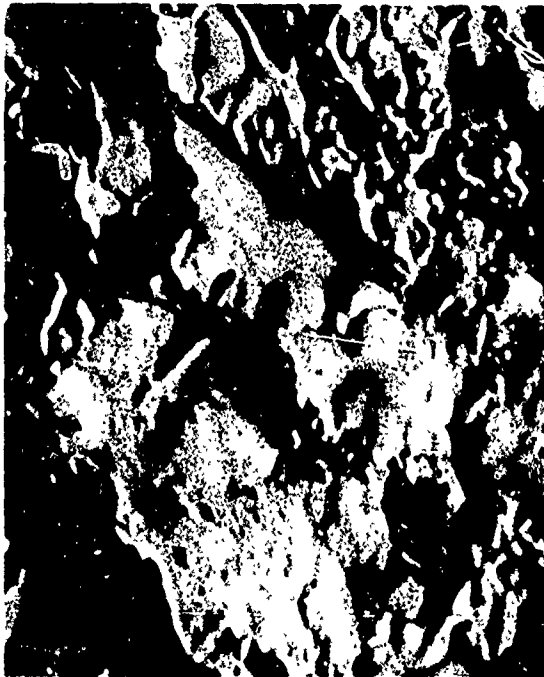
The specimens were then examined in detail to identify and evaluate the distribution of oxygen and carbon. Figures 82 through 85 show these microprobe distributions along with the scanning electron microscope images of the same surfaces. Elemental content of a specific distribution is indicated by the relative concentrations of white dots. An even distribution of white dots indicates that none of the element was detected.

Samples from specimens TIP-1 and T-1 (the as-composited material) show substantial amounts of carbon and oxygen (figures 82 and 83). Distribution was observed on the plasma-sprayed layers rather than through the matrix. Using scheelite as a standard, the oxygen areas were calculated to be 15 to 16 wt-% oxygen, which would indicate the presence of tungsten dioxide. Comparisons of the wavelength shifts in carbon K_{α} radiation using graphite, diamond, and tungsten carbide led to the conclusion that the carbon form was similar to graphite, which was probably picked up from the mandrels used to fabricate the specimens. Little or no oxygen or carbon was evident in the distributions made of samples from specimens T-4 and T-7 (figures 84 and 85). This indicates that the impurities were driven off in the elevated temperature exposure.

c. Optical and Electron Metallography

(1) Optical Metallography

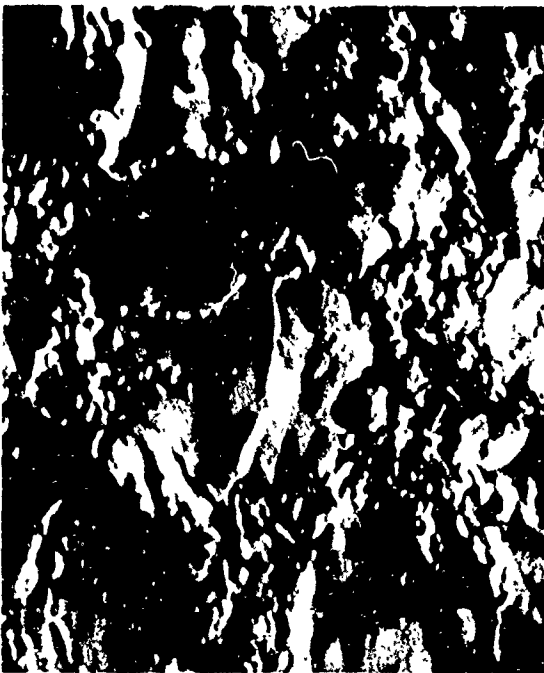
Metallographic specimens were sectioned with an abrasive cut-off wheel and were mounted in bakelite. The mounts were then prepared by surface grinding on wet paper through 240, 320, 400, and 600 grit. Rough polishing was done on 6-micron and 1-micron diamond wheels with final polishing done on a syntron vibratory polisher using 0.3-micron alumina. Some specimens were etched by immersion in a solution of 30% acetic acid, 30% nitric acid, 10% hydrofluoric acid, and 30% water. Etching was at room temperature for 1 to 3 min.



a. SEM Micrograph at 270 Magnification



b. Oxygen Distribution in a.



c. SEM Micrograph at 200 Magnification



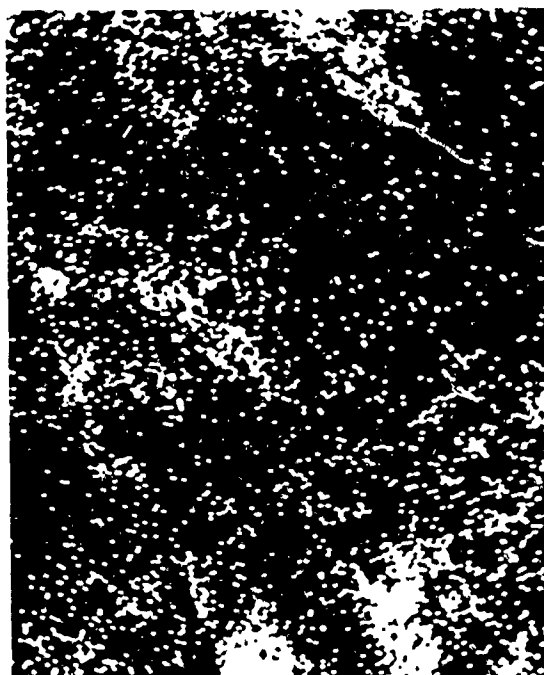
d. Carbon Distribution in c.

Figure 82. Typical Fracture Section Transverse to the Material Thickness (Specimen TIP-1)



a. SEM Micrograph at
1,000 Magnification

b. Oxygen Distribution in a.



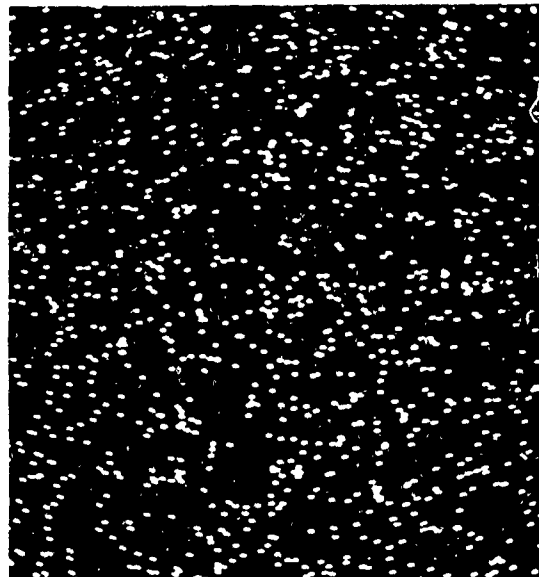
c. Carbon Distribution in a.

Figure 83. Typical Fracture Section Through Specimen T-1

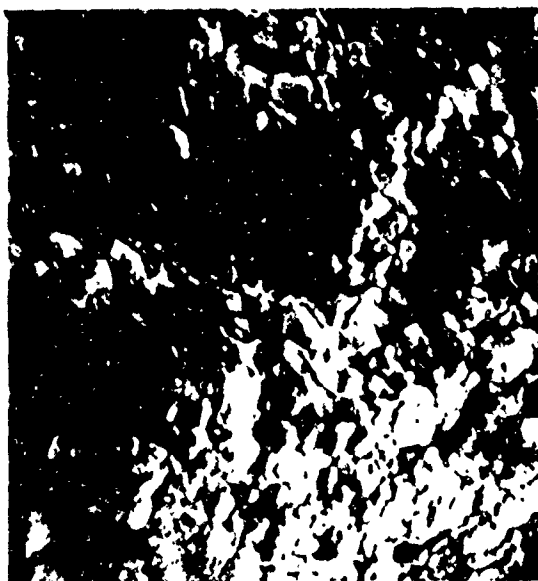
Reproduced from
best available copy.



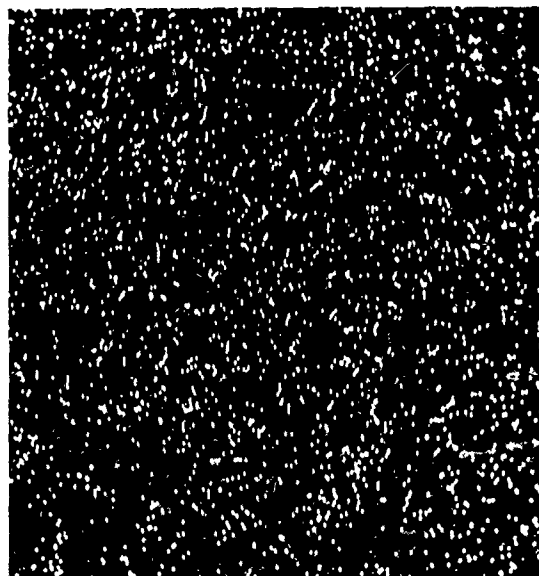
a. SEM Micrograph at
350 Magnification



b. Oxygen Distribution in a.

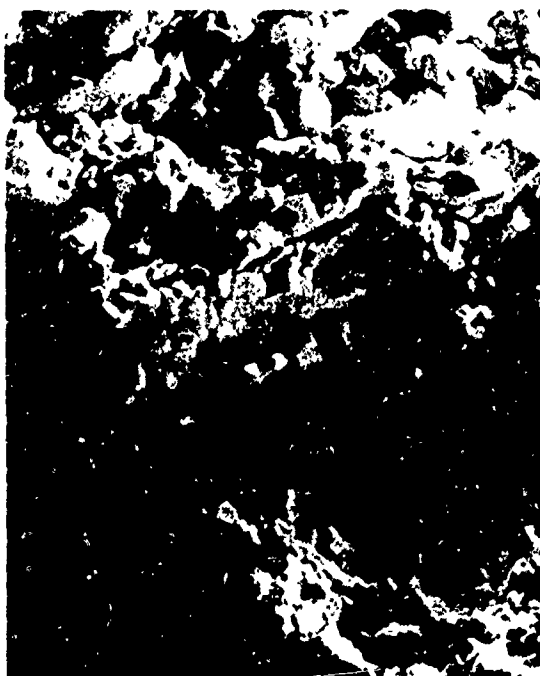


c. SEM Micrograph at
350 Magnification



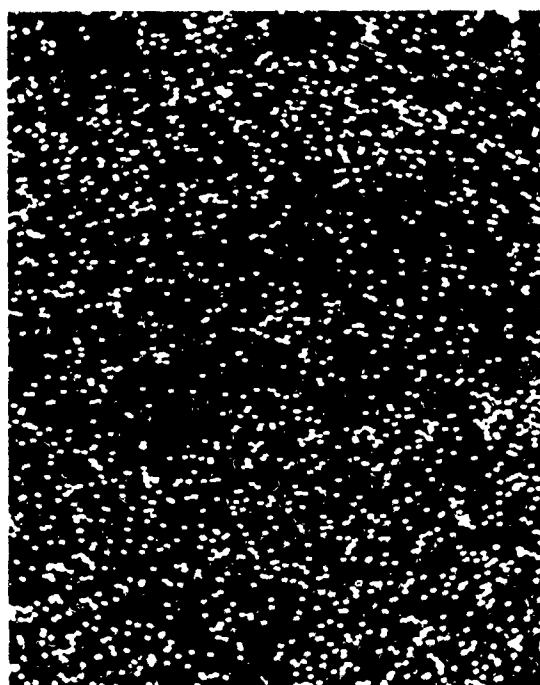
d. Carbon Distribution in c.

Figure 84. Typical Fracture Section
Exposed to 3,000°F for 5 Min (Specimen T-4)



a. SEM Micrograph at
350 Magnification

b. Carbon Distribution in a.



c. Oxygen Distribution in a.

Figure 85. Carbon and Oxygen Distribution in a Typical
Fracture Section Exposed to 4,000°F (Specimen T-7)

Transverse and longitudinal sections through specimens T-1, T-4, T-7, TIP-1, IP-1, C-1, C-3, C-4, C-5, THE-1A, THE-2A, and THE-3A were prepared and examined. Optical examinations were performed on a Reichert model Me F metallograph at magnifications of 50 to 1,000 diameters. Photomicrographs of the typical microstructures observed for individual specimen are shown in figures 86 through 90.

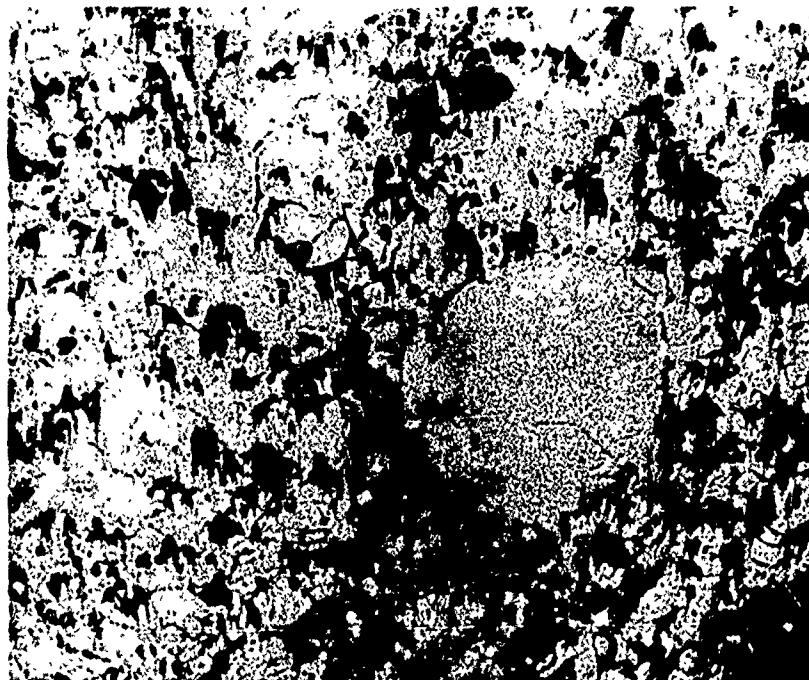
The specimens (T-1, TIP-1, and IP-1) tested at room temperature in tension and/or internal pressure exhibited fractured filaments (wires). Single and multiple fractures within filaments were observed. The degree of fracture was independent of filament direction in specimens TIP-1 and IP-1 (figure 88). The hoop wires of specimen T-1 (figure 86, view a) exhibited less severe fracture than did the helical wires (figures 86, view b, and 87, view a). The wires of the compression tested specimens were not fractured, which is to be expected.

The matrix of as-fabricated wire-wound tungsten material appears as an uneven structure (figure 87, view b). The lamellae are a maximum of 1 mil thick and run perpendicular to the material thickness. Numerous small voids approximately 0.002 in. in diameter are dispersed throughout the matrix. Larger voids, 0.003 to 0.010-in. in cross-section diameter, are located near the filaments (figure 88, views a and b). These large voids (shadows) result from wires blocking the deposition of the plasma-arc-sprayed matrix.

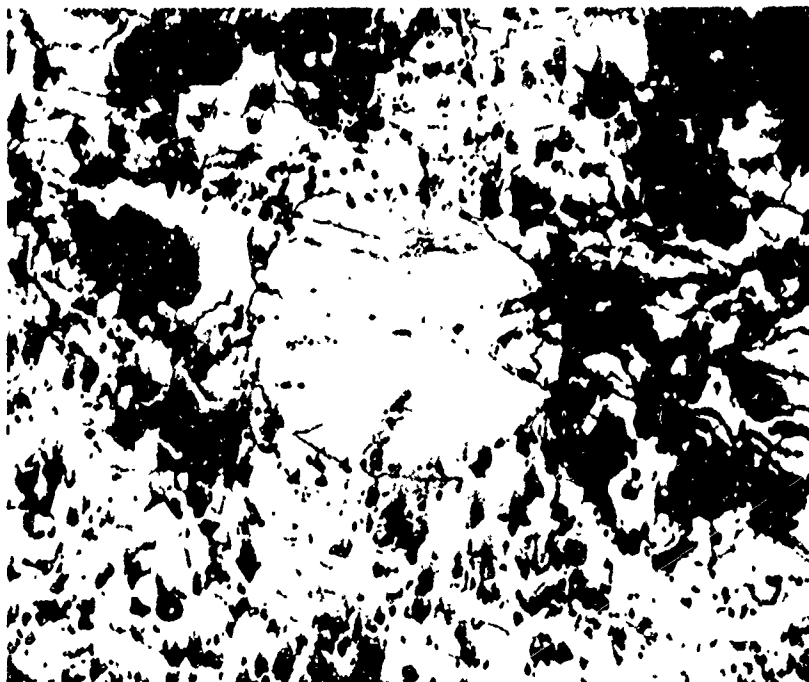
The elevated temperature tested specimens had some basic differences from the room temperature tested material:

- A. The filaments were not fractured in specimen T-4, which was tensile tested at 3,000°F, as shown by the helical wire in figure 89, view b.
- B. The filaments recrystallized, as shown by the grain boundaries in figures 89 and 90.
- C. The matrix has become more dense by the sintering action of elevated temperature and has a less pronounced lamellar structure.

Excluding the sintering reaction in the matrix, a limited reaction occurs between the filament and the matrix (figure 89, view b). Specimens C-3 and T-4 were exposed to 3,000°F (1,650°C) for less than 10 min. THE-1A was exposed to 3,000°F (1,650°C) in excess of 4 hr; and THE-3A was sintered at 3,600°F (1,980°C) for 1 hr and then was exposed in excess of 4 hr at 3,000°F (1,650°C). However, no significant difference between the structures of these specimens was apparent. This indicates that reaction effects are primarily temperature-controlled, rather than time-at-temperature dependent. This was shown in the density measurements in table XVI.



a. Hoop Wire
Magnification: 250
Unetched

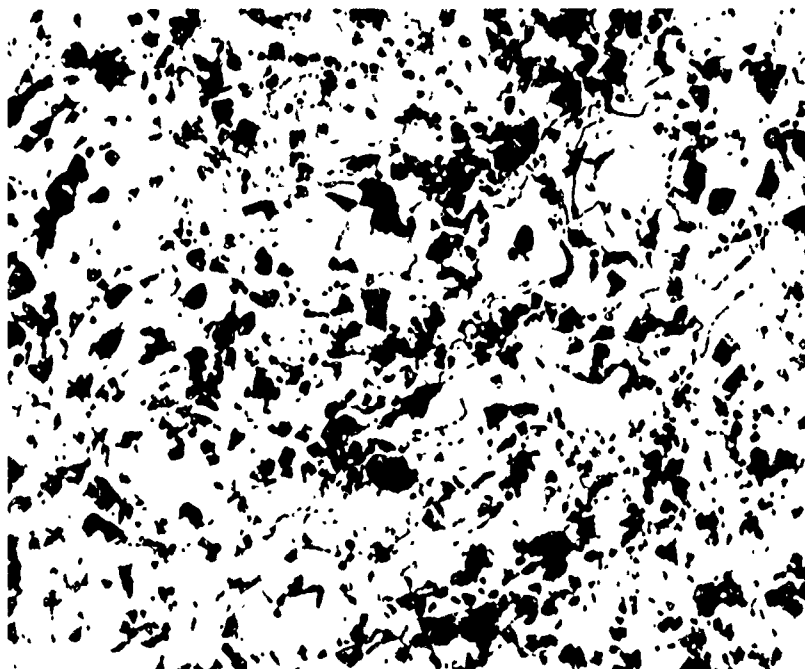


b. Helical Wire
Magnification: 250
Unetched

Figure 86. Metallographic Longitudinal Section (Specimen T-1)



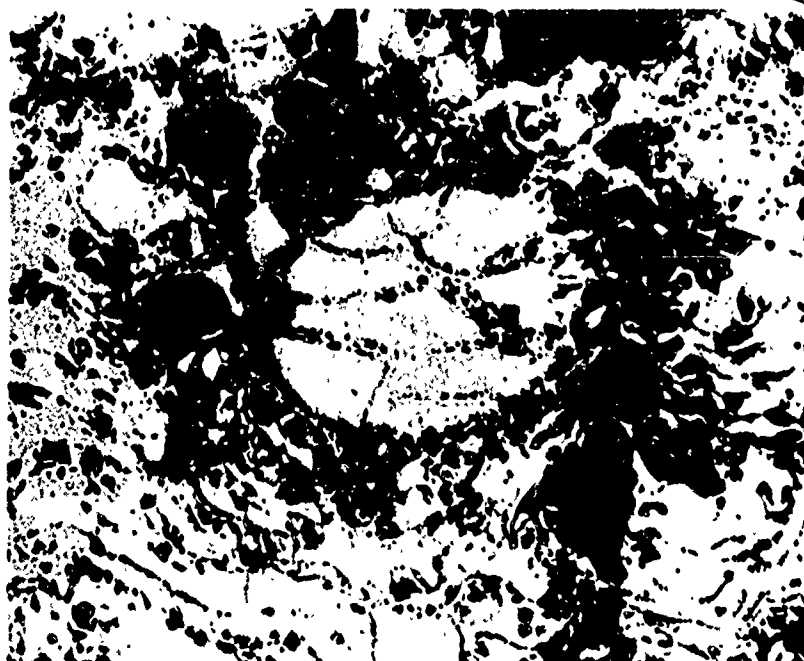
a. Magnification: 250
Etchant: HAc + HNO₃ + HF



b. Magnification: 250
Etchant: HAc + HNO₃ + HF

Figure 87. Optical Micrographs of a Transverse Section (Specimen T-1)

Reproduced from
best available copy.



a. Specimen: TIP-1
Magnification: 250

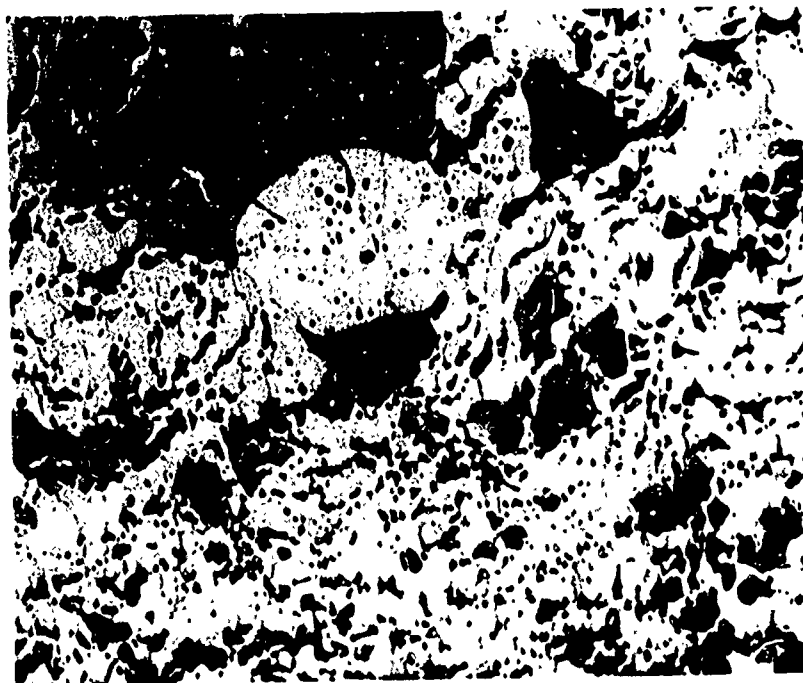
Section: Transverse
Unetched



b. Specimen: IP-1
Magnification: 250

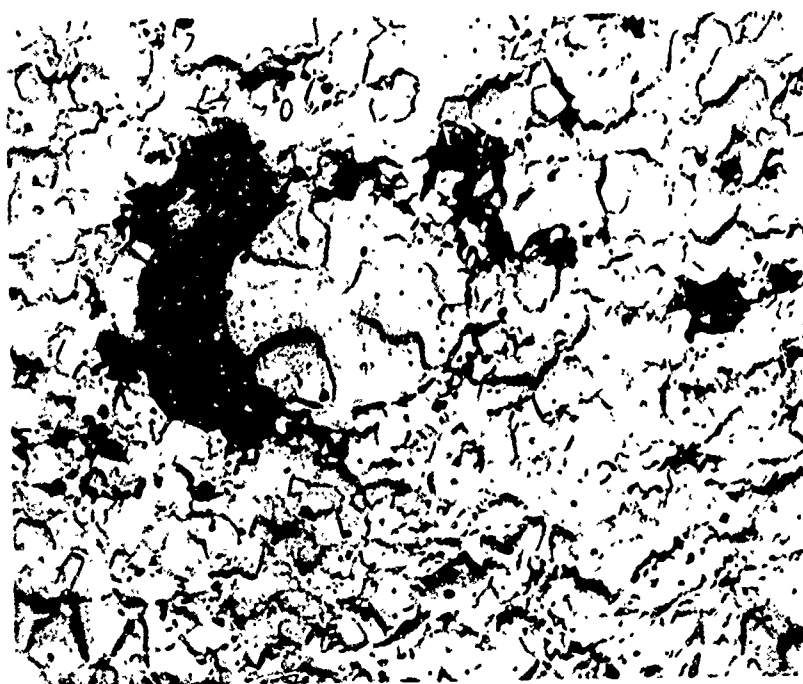
Section: Transverse
Etchant: $\text{HAc} + \text{HNO}_3 + \text{HF}$

Figure 88. Optical Micrographs of Metallographic Sections
(Specimens TIP-1 and IP-1)



a. Specimen: C-3
Magnification: 250

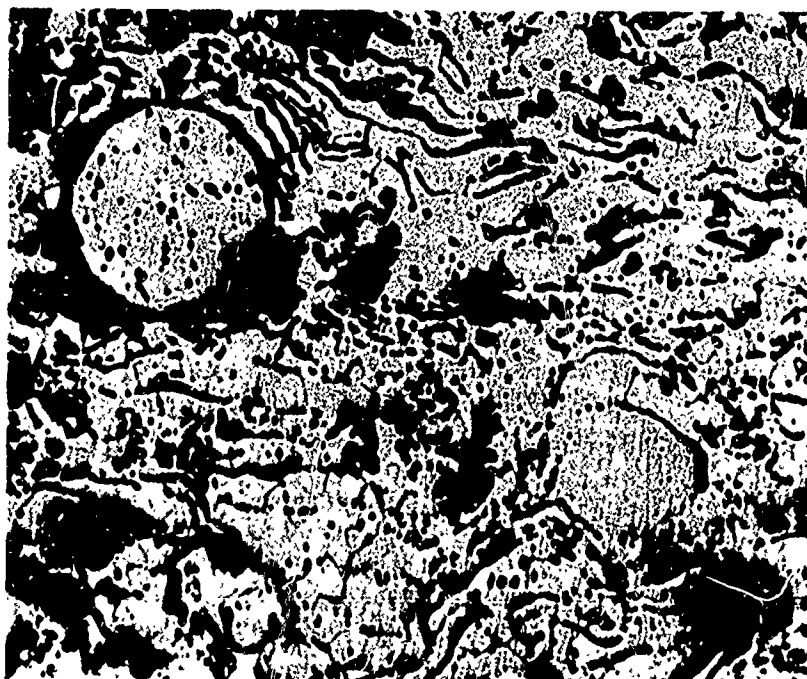
Section: Longitudinal
Unetched



b. Specimen: T-4
Magnification: 250

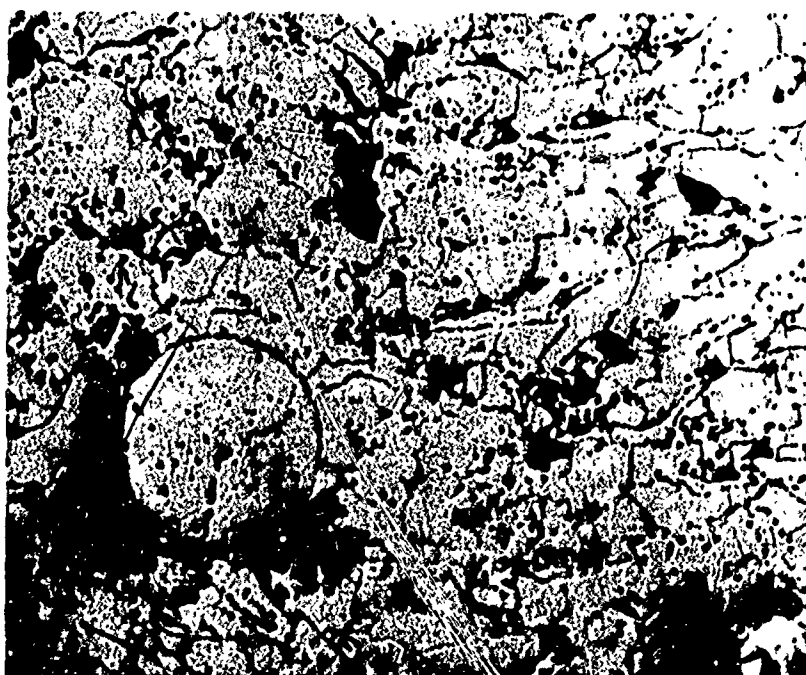
Section: Transverse
Etchant: HAc + HNO₃ + HF

Figure 89. Optical Micrographs (Specimens C-3 and T-4)



a. Specimen: THE-1A
Magnification: 250

Section: Longitudinal
Unetched



b. Specimen: THE-3A
Magnification: 250

Section: Longitudinal
Etchant: HAc + HNO₃ + HF

Figure 90. Optical Micrographs (Specimens THE-1A and THE-3A)

(2) Electron Metallography

A JSM-2 scanning electron microscope having 250 angstrom resolution and operating at 25 kv was used to examine microstructures and fracture sections of several selected specimens. Magnifications from 100 to 10,000 were used; magnifications of 300, 1,000, and 3,000 were the most useful. Metallographic sections examined included samples of test specimens T-1, IP-1, T-4, T-7, and THE-3A. Fracture sections examined included samples of test specimens T-1, IP-2, T-4, T-7, C-3, THE-3A, and TIP-1. These were selected as typical of the fabricated and tested specimens.

Metallographic or microstructure samples were the same as those used in optical examinations. The higher magnification and better resolution of the scanning electron microscope also was used to confirm optical microscopy observations.

The fracture sections examined were of two types: (1) the surfaces of fractures which occurred during room temperature mechanical property tests and (2) the faces of prepared fractures, i.e., fractures made for examining the internal structure. Observations of the matrix, filaments, and their interrelationship were made.

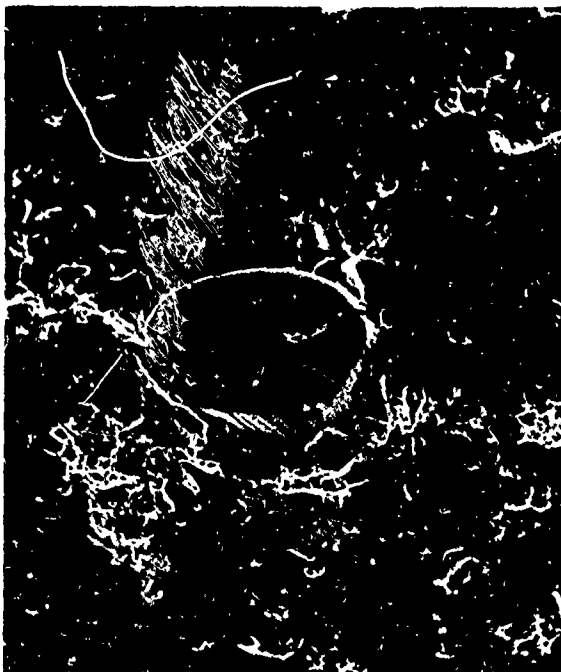
A micrograph of metallographically prepared specimen IP-1 (figure 91, views a and b) shows a fractured filament. At a magnification of 800, it appears that metal had been smeared into the larger fracture, and a very tight crack perpendicular to the large fracture was observed. Voids near the filament and in the matrix were noted, confirming previously observed optical microscopy examinations. The wire in the metallographic section of T-4 (figure 91, view c) appears to be attached to the matrix. At a magnification of 3,000 (figure 91, view d), it becomes uncertain whether this is a reaction zone or smeared metal.

The broken filament in the fracture section of specimen T-1 (figure 92, views a and b) has several small longitudinal fractures. These are similar to the fractures observed in the optical metallographic examinations. Note that the filament has necked down at the fracture indicating ductility. A void can be seen on one side of the filament.

The structure of the matrix as observed in the fracture section through specimen IP-2 (figure 92, views c and d) is in layers nominally 0.0005 to 0.001 in. in thickness. The fracture through the layers is typical of brittle material.

The micrographs of IP-2 in figure 93 include a hole from which a filament has pulled out during test. The matrix surface which outlines the hole and the surface of a filament (view d) are quite similar. This surface similarity illustrates the intimate contact that the matrix has with the filament.

Reproduced from
best available copy.



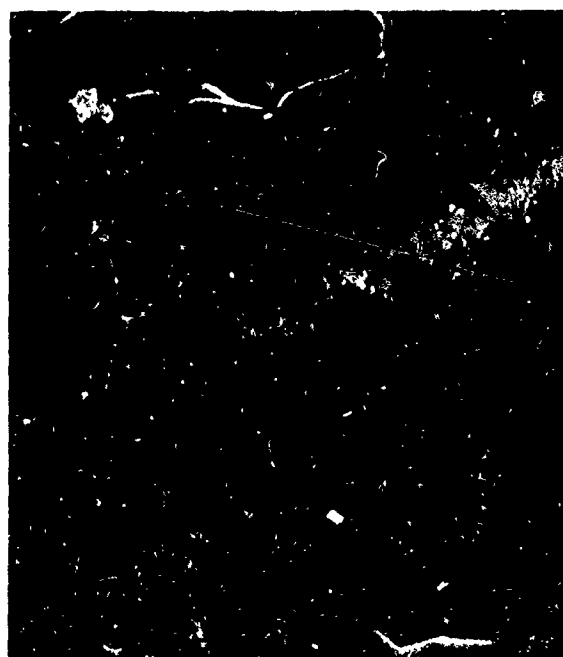
a. Specimen: IP-1
Magnification: 200



b. Magnification of a.:800



c. Specimen: T-4
Magnification: 200



d. Magnification of c.:3,000

Figure 91. SEM Micrographs of Metallurgical Sections
(Specimens IP-1 and T-4)



a. Specimen: T-1
Magnification: 200



b. Magnification of a.:3,000



c. Specimen: IP-2
Magnification: 1,000



d. Magnification of c.:3,000

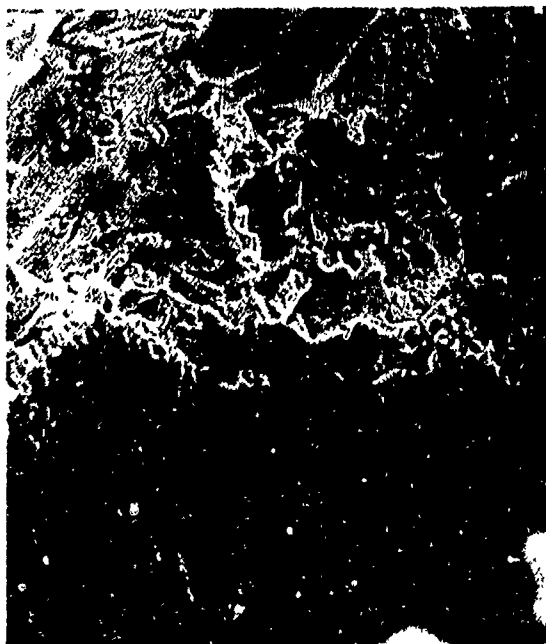
Figure 92. SEM Micrographs of Fracture Sections
(Specimens T-1 and IP-2)



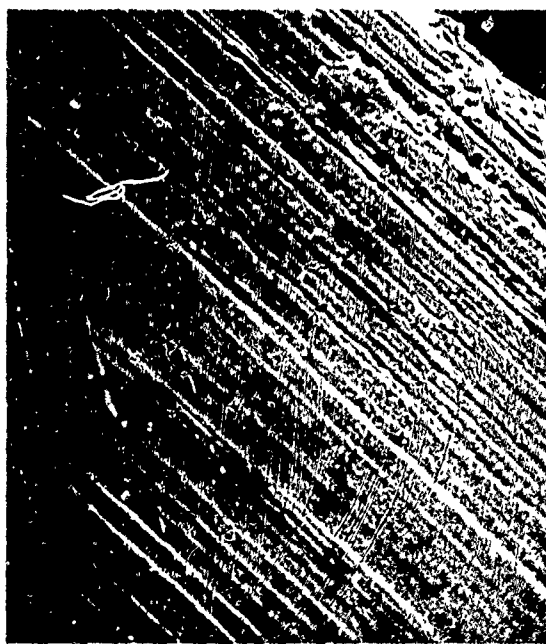
a. Specimen: IP-2
Magnification: 100



b. Magnification of a.:300



c. Magnification of b.:1,000



d. Specimen: IP-2 Filament
Magnification: 1,000

Figure 93. SEM Micrographs of a Fracture Section

Evidence of reaction zones between the matrix and filaments as the result of elevated test temperature exposure is shown in figures 94 and 95. The small protrusions (less than 0.001 in. across) on the wire surface (see arrows) are small amounts of the tungsten plasma-sprayed matrix bonded to the wire. Figure 94, view c, shows a reaction zone which has fractured on one side. Figure 95, views a and b, illustrates how matrix material reacts at the grain boundaries of recrystallized filaments.

Prepared fracture surfaces of a high-temperature exposed matrix are typified in figure 95, view c and d. The fractures are primarily of grain boundary separation with no evidence of lamellar separation. Recrystallization of the matrix material, with individually sprayed particles appearing to be crystal units, is established for short-time high-temperature exposed material. View d of figure 95 shows a reaction zone between the matrix particles.

A transverse-fractured filament in specimen T-7 is shown in figure 96. The recrystallized wire fractured along the grain boundaries and indicates no evidence of ductility.

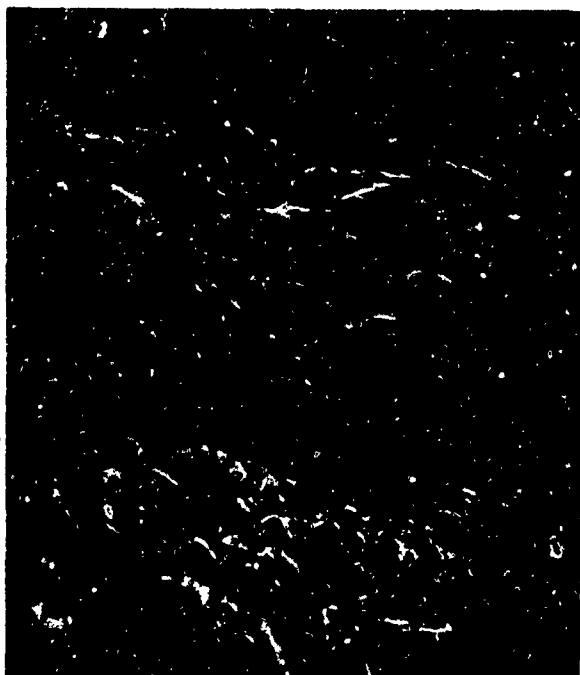
None of the specimens examined by scanning electron microscope methods contained evidence of contaminants or of reaction areas other than those of tungsten-to-tungsten. This corroborates the results of the chemical characterization studies.

d. Observations

The physical and chemical test results have provided surprising observations about the characteristics of wire-wound tungsten. It is apparent from the similarity of the density, chemical composition, and microstructure results that the composite is uniform and highly reproducible when fabricated under controlled conditions. Thus the mechanical and thermal properties can be assessed. Although exposure to elevated temperatures recrystallizes and embrittles the matrix and filaments, the composite retains its primary advantage of thermal shock resistance.

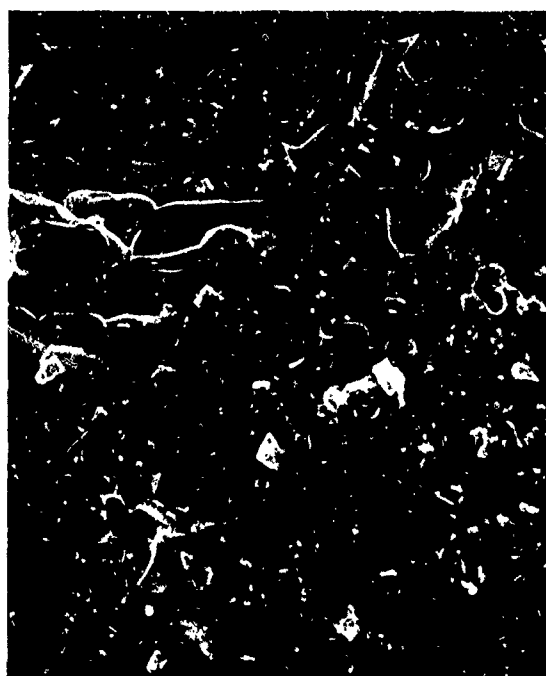
The composite is essentially free of any contaminating elements. Originally, it was assumed that "educated dirt" (i.e., oxides, nitrides, etc.) was, in part, responsible for the excellent performance of wire-wound tungsten. However, the chemical and electron microprobe analyses clearly showed this to be an incorrect assumption. Oxygen and nitrogen were present in the as-composited material as absorbed or adsorbed gases (trace oxides), but they did not react permanently with the tungsten upon elevated temperature exposure.

Microstructural characteristics verify the brittle nature of the composite and demonstrate that strength properties are matrix controlled. This substantiates UTC's previous design consideration that the composite should be used primarily in compression applications. Numerous metallographic comparisons of material exposed to elevated temperatures (3,000°F (1,650°C) to 4,000°F (2,200°C)) for various time periods (1 min to 5 hr)



a. Specimen: T-4
Magnification: 300

b. Magnification of the
Filament in a.:1,000



c. Magnification of b.:3,000

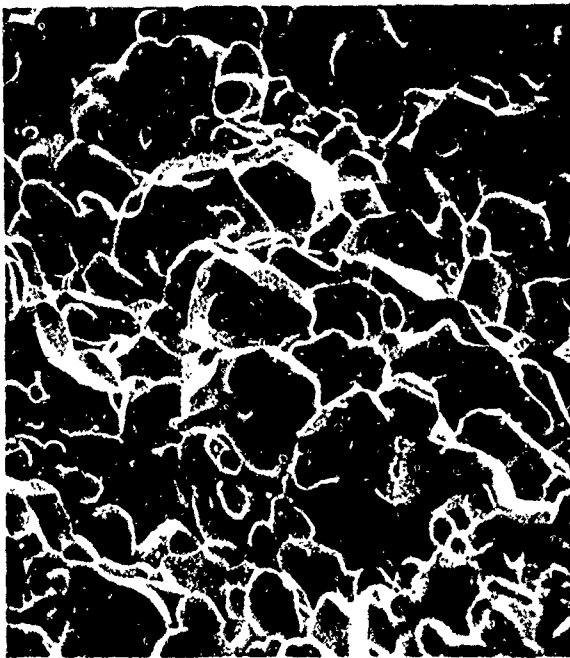
Figure 94. SEM Micrographs of a Fracture Section
Containing a Partially Exposed Filament



a. Specimen: T-7
Magnification: 1,000



b. Magnification of a.: 3,000

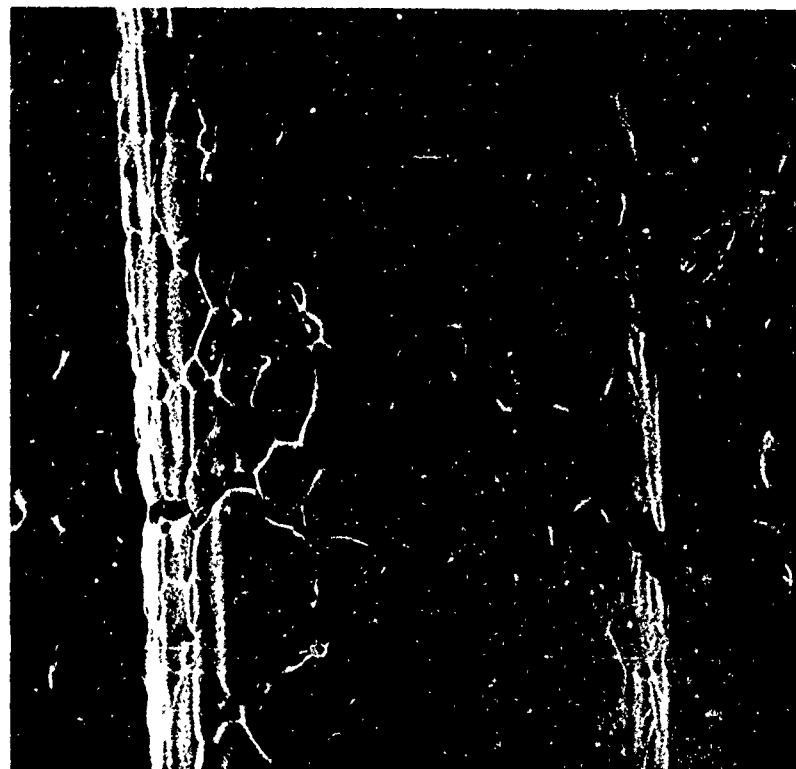


c. Specimen: T-7
Magnification: 1,000

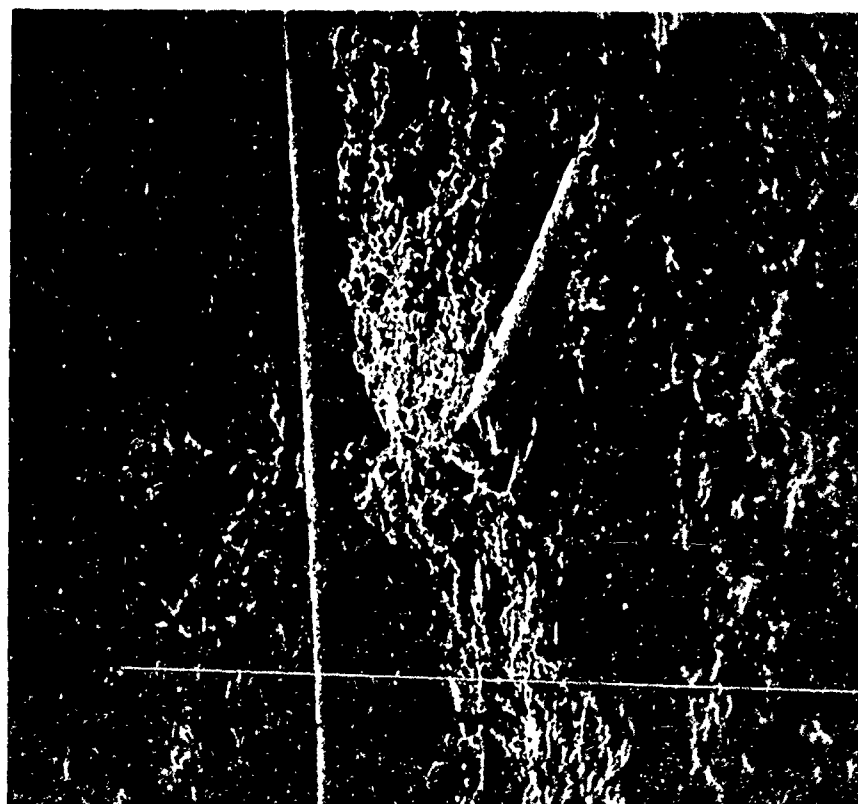


d. Magnification of c.: 3,000

Figure 95. SEM Micrographs of a Fracture Section (Specimen T-7)



b. Magnification of a.: 650



a. Specimen: T-7
Magnification: 100

Figure 96. SEM Micrographs of a Fracture Section (Specimen T-7)

show that sintering and reaction effects are primarily temperature-dependent rather than time-at-temperature dependent. This would indicate that the determined mechanical properties have value for nozzle throat design application where the temperature exposure is nearly instantaneous (measured in msec).

5. MATERIAL SPECIFICATION

A preliminary material specification for wire-wound tungsten composites was prepared and is presented in Appendix VI. This specification covers the procurement of raw materials, requirements for composite fabrication and expected characteristics, and the minimum inspection requirements to satisfy production of quality components. Data derived from the characterization program were used to develop the specification criteria.

The specification's requirements are slanted toward wire-wound-tungsten composites for rocket nozzle throat inserts, since that is the primary application for the material to date. Accordingly, the requirements reflect UTC's previous knowledge of wire-wound tungsten's performance in rocket nozzles where thermal shock resistance is needed and where the applied stress is compressive.

Raw material procurement limits are based on the specifications used to obtain tungsten powder and wire for fabrication of test specimens. Radiographic and visual examinations were the most acceptable means for detecting defects (according to the NDT evaluation); therefore, these methods formed the basis for NDT quality assurance provisions. Reproducibility from composite to composite is demonstrated by bulk density determinations and by an inexpensive compression test. These two tests are also indicative that plasma-arc-spraying and filament-reinforcing fabrication methods have been performed in the required manner.

SECTION IV

CONCLUSIONS

The results demonstrate that wire-wound tungsten composites have thermal, mechanical, and physical property characteristics which are unique to the material but suitable for design purposes. Further, it was shown that the composite can be fabricated so that its characteristics are uniform and reproducible and so that the resultant components are capable of evaluation by NDT inspection techniques.

Thermal property test results showed that thermal expansion is linear with temperature and nearly identical to that of tungsten. Likewise, the composite's specific heat is similar to tungsten (except for two lambda point variations). Thermal conductivity of as-composited material is extremely low (from room temperature to 1,110°F (600°C)) which is less than 10% of tungsten. However, as sintering commences with temperature, conductivity increases rapidly. The resultant curve is irreversible on cooling and assumes a configuration similar to typical curves for pressed and sintered tungsten. This characteristic will impose differing constraints in design for reuse of wire-wound tungsten. There was good agreement of data and, therefore, assurance that the properties are satisfactory for design.

The mechanical property test portion of the program provided some significant achievements in elevated temperature testing. In addition to wire-wound tungsten's mechanical properties, procedures and test apparatus were developed for rapid temperature testing and biaxial stress field application. The tests revealed that the composite has low strength under applied tensile loads and that failure is matrix dependent. The data indicate that wire-wound tungsten behaves in a nonlinear elastic manner at room temperature and as an elastic-plastic material at elevated temperature.

Wire-wound tungsten exhibited room temperature tensile properties of 2,800-psi ultimate strength and 6×10^6 psi tensile modulus. For comparison, pressed and sintered tungsten at an equivalent density (~85%) has values of 55,000 psi and 22×10^6 psi. The low strength is even more pronounced at elevated temperature; the ultimate strength at 3,000°F (1,650°C) was 310 psi. In compression, wire-wound tungsten exhibited room temperature ultimate strength of 30,000 psi and 6×10^6 psi elastic modulus. At 3,000°F (1,650°C) and 4,000°F (2,200°C), average compression ultimate strengths were 8,500 psi and 4,000 psi and elastic moduli were 0.45×10^6 psi and 0.16×10^6 psi, respectively. These data are indicative that wire-wound tungsten components are most useful in compression applications.

Room temperature mechanical property results of the specimens were in good agreement and are suitable for design approximations. However, too few specimens were evaluated to provide statistical design data. Elevated temperature results were more scattered, and the resultant data are limited because

of specimen breakage and initial difficulties with the testing equipment. Additional elevated temperature tests using larger specimens of a slightly modified configuration are needed to provide more useful design data.

Physical and chemical tests indicate that the material has reproducible and predictable characteristics. Density determinations show that significant void volume (10%) is retained after long-time elevated temperature exposure, thus indicating that thermal shock resistance may be satisfactory for reuse. The composite is surprisingly free of contaminating elements, and the only metallurgical reactions observed were those of tungsten to tungsten. Both the tungsten matrix and filaments underwent appreciable recrystallization upon exposure to 3,000°F (1,650°C) and 4,000°F (2,200°C) temperatures.

REFERENCES

1. Greening, T. A., "Advanced Wire-Wound Tungsten Nozzles," Final Report AFRPL-TR-67-181. United Technology Center, April 1967.
2. Stephen, W. A., "High-Chamber Pressure Evaluation of Wire-Wound Tungsten Nozzles," Technical Report AFRPL-TR-69-79, June 1969.
3. Askill, J., Fraser Diffusion Data for Metals, Alloys, and Simple Oxides, IFI-Plenum: New York, 1970, p. 39.
4. Alvarez, L. W., Thermodynamic Properties of Metals, U. S. Air Force Project Rand, Res. Mem. No. RM-4, February 18, 1947.
5. Touloukian, Y. S., Thermophysical Properties of High-Temperature Solid Materials, Purdue University, Vol. 1, 1967, p. 1023.
6. Salmassy, O. K., W. H. Duckworth, and A. D. Scharpe, "Behavior of Brittle State Materials," WADE Technical Report, Part I, June 1955, 53-58.
7. Matt, R. E., "Structural Defects in Infiltrated Tungsten Matrices," presented at the AIME Conference on Applied Aspects of Refractory Materials, Los Angeles, California, 9 and 10 December 1963.

APPENDIX I

PROCEDURES FOR PREPARATION OF MECHANICAL AND THERMAL PROPERTY SPECIMENS

#2380 - THE - Thermal Expansion

#2380 - TPSM - Thermal Properties

#2380 - IT - Tension

#2380 - TIP - Tension/Pressurization

#2380 - IPC - Internal Pressurization
and Compression

THERMAL EXPANSION SPECIMENS
Per Drawing No. JH-622 THE

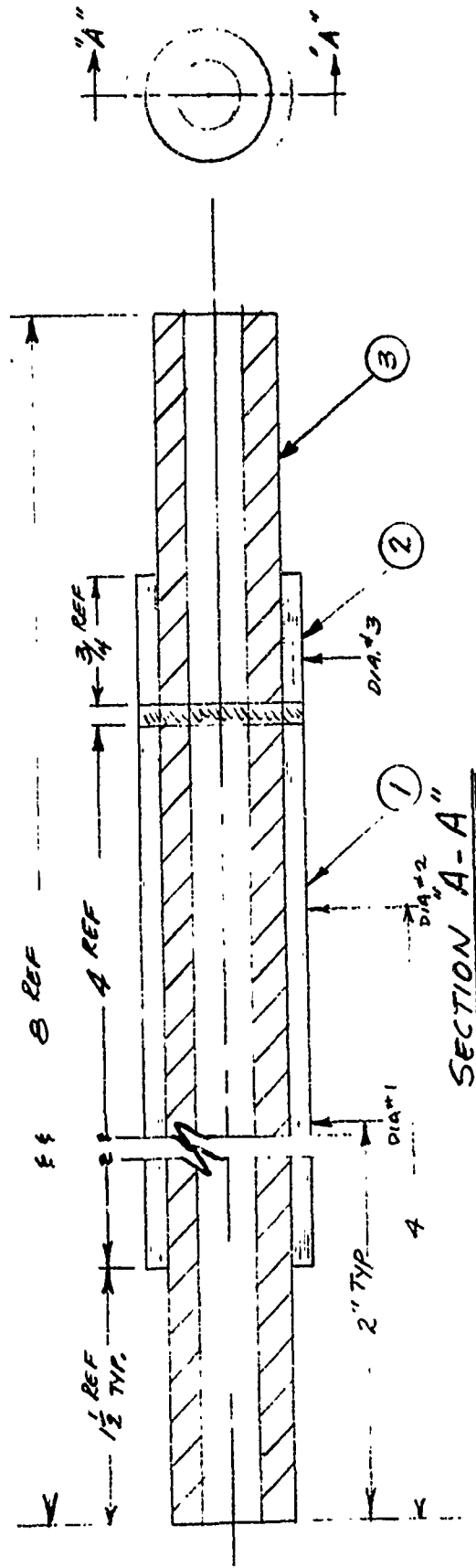
Procedure #2380-THE 9/16/70
Serial No.

<u>Operation</u>		<u>Operator Stamp</u>
1.	Receive Materials a) 10# W powder (-200, +325 mesh) b) 1/2# Ta powder (-200, +325 mesh) c) 1 graphite mandrel - Dwg - JH-916-M d) As required - 1% Thoriated Tungsten Wire (.004" dia)	
2.	Assemble mandrel on rotating spray fixture	
3.	Fabricate Wire-Wound tungsten specimen (JH-622-THE)(JH-970-FEX)	

Step	Layer	Type	Dia. #1		Dia. #2		Dia. #3		Op. Stamp
			Plan	Actual	Plan	Actual	Plan	Actual	
0	0	Op. #2	.750	---	.750	---	.750	---	---
1	1	W-.010	.760	---	.760	---	.760	---	---
2		(+)Helix							
3		W-.020	.780	_____	.780	_____	.780	_____	_____
4		(-)Helix							
5		W-.020	.800	_____	.800	_____	.800	_____	_____
6		Hoop							
7	2	W-.025	.825	_____	.825	_____	.825	_____	_____
8		(+)Helix							
9		W-.025	.850	_____	.850	_____	.850	_____	_____
10		(-)Helix							
11		W-.025	.875	_____	.875	_____	.875	_____	_____
12		Hoop							
13	3	W-.030	.905	_____	.905	_____	.905	_____	_____
14		(+)Helix							
15		W-.030	.935	_____	.935	_____	.935	_____	_____
16		(-)He							

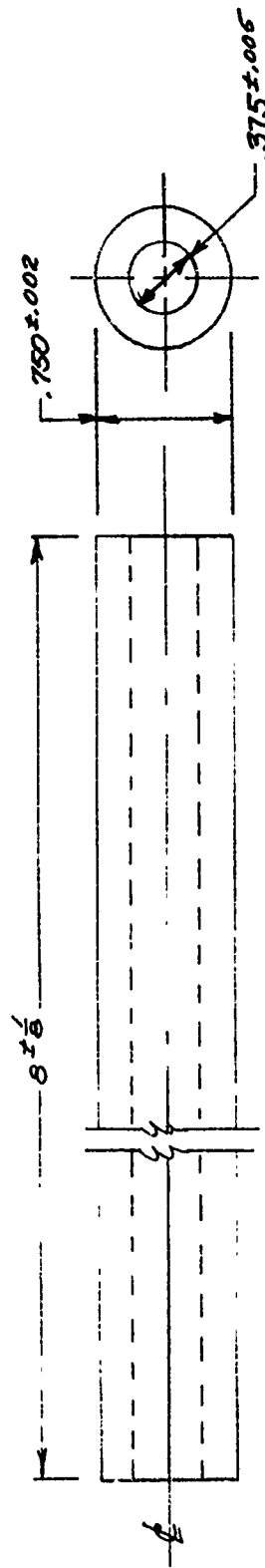
<u>Step</u>	<u>Layer</u>	<u>Type</u>	<u>Dia. #1</u>		<u>Dia. #2</u>		<u>Dia. #3</u>		<u>Op. Stamp</u>
			<u>Plan</u>	<u>Actual</u>	<u>Plan</u>	<u>Actual</u>	<u>Plan</u>	<u>Actual</u>	
17	,	W-.030	.965	_____	.965	_____	.965	_____	_____
18		Hoop							
20	4	W-.030	.995	_____	.995	_____	.995	_____	_____
21	5	Ta	1.000	_____	1.000	_____	1.000	_____	_____

4.	Inspect as sprayed specimen	_____	_____
5.	Cut to length - 4 in. axial .75 in. min radial	_____	_____
6.	Attach Serial No. (Ex. THE-1A for axial THE-IR for radial	_____	_____
7.	Remove graphite mandrels	_____	_____
8.	Inspect I.D. for irregularities	_____	_____
9.	Package and store for shipment	_____	_____



Schematic of
Thermal Expansion
Specimen Fabrication
No. JH-970-FEX

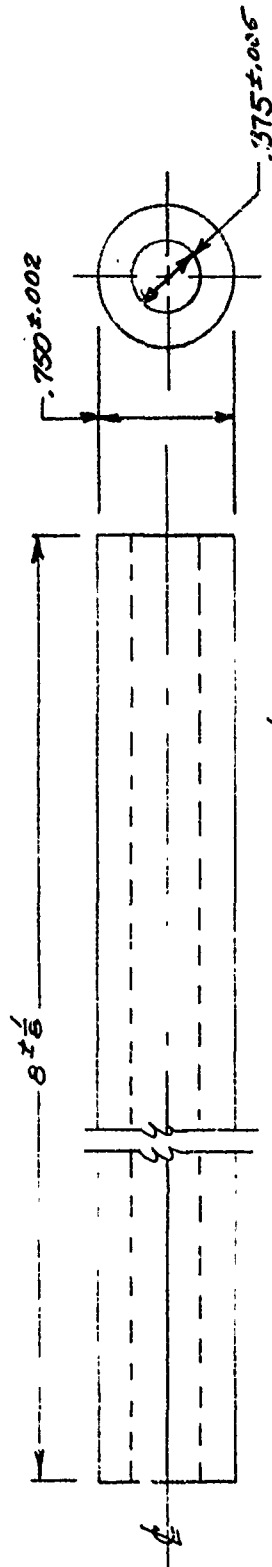
- 1 AXIAL SPECIMEN - JH-622-THE-ITEM 1
- 2 RADIAL SPECIMEN - JH-622-THE-ITEM 2
- 3 MANDREL - JH-916-M1



1. DIAMETERS TO BE CONCENTRIC TO ϕ WITHIN .002"
2. EXTERNAL SURFACE TO BE $\sqrt{32}$ OR BETTER
3. MAKE FROM ATJ OR 1 1/2-IN. DIA #8882 GRAPHITE BAR
(SPEER CARBON CO.)

MANDREL FOR
THERMAL EXP. SPEC.
LAB. DRAWING (UTC-MFP)
NO. JH-916-M

REV.	PROJ.
1	10/10/50
2	10/10/50
3	10/10/50
4	10/10/50
5	10/10/50
6	10/10/50
7	10/10/50
8	10/10/50
9	10/10/50
10	10/10/50



1. DIAMETERS TO BE CONCENTRIC TO ϕ WITHIN .002"
2. EXTERNAL SURFACE TO BE $\sqrt{32}$ OR BETTER
3. MAKE FROM ATJ OR 1-IN. DIA #8882 GRAPHITE BAR
(SPEER CARBON CO.)

MANDREL FOR
THERMAL EXP. SPEC.
LAB. DRAWING (UTC-M.F.P.)
NO. JH-916-M

REV.	PROJ.
1	1
2	2
3	3
4	4
5	5
6	6
7	7
8	8
9	9
10	10
11	11
12	12
13	13
14	14
15	15
16	16
17	17
18	18
19	19
20	20
21	21
22	22
23	23
24	24
25	25
26	26
27	27
28	28
29	29
30	30
31	31
32	32
33	33
34	34
35	35
36	36
37	37
38	38
39	39
40	40
41	41
42	42
43	43
44	44
45	45
46	46
47	47
48	48
49	49
50	50
51	51
52	52
53	53
54	54
55	55
56	56
57	57
58	58
59	59
60	60
61	61
62	62
63	63
64	64
65	65
66	66
67	67
68	68
69	69
70	70
71	71
72	72
73	73
74	74
75	75
76	76
77	77
78	78
79	79
80	80
81	81
82	82
83	83
84	84
85	85
86	86
87	87
88	88
89	89
90	90
91	91
92	92
93	93
94	94
95	95
96	96
97	97
98	98
99	99
100	100

PROCEDURE TO FABRICATE THERMAL PROPERTIES SPECIMENS

1 Receive Materials

- a) Mandrel (JH-TPSM) Speer 8882 Graphite
- b) Tungsten Powder (25#) P. O. _____
- c) Tungsten Wire - P. O. _____

2 Assemble Mandrel on Rotating Spray Fixture

3 JH-TPSM Spray and Wind According to the following schedule

<u>Step</u>	<u>Layer</u>	<u>Type</u>	<u>Dimension (Diameter Uniform) 2 Loc.</u>		<u>Op. Stamp</u>
			<u>P #1 A</u>	<u>P #2 A</u>	
0	0	Op #3	2.375	2.375	
1	1	.010 W	2.385	2.385	
2		(+)Helix			
3		.020 W	2.405	2.405	
4		(-)Helix			
5		.020 W	2.425	2.425	
6		Hoop			
7	2	.025 W	2.450	2.450	
8		(+)Helix			
9		.025 W	2.475	2.475	
10		(-)Helix			
11		.025 W	2.500	2.500	
12		Hoop			
13	3	.025 W	2.575	2.575	
14		(+)Helix			
15		.025 W	2.600	2.600	
16		(-)Helix			
17		.025W	2.625	2.625	
18		Hoop			

Procedure 2380-TPSM
10/15/70

<u>Step</u>	<u>Layer</u>	<u>Type</u>	<u>Dimension (Diameter Uniform) 2 Loc.</u>		<u>Op. Stamp</u>
			<u>P #1 A</u>	<u>P #2 A</u>	
19	4	.025 W	2.650	2.650	
20		(+)Helix			
21		.025 W	2.675	2.675	
22		(-)Helix			
23		.025 W	2.700	2.700	
24		Hoop			
25	5	.025 W	2.725	2.725	
26		(+)Helix			
27		.025 W	2.750	2.750	
28		(-)Helix			
29		.025 W	2.775	2.775	
30		Hoop			
31	6	.030 W	2.805	2.805	
32		(+)Helix			
33		.030 W	2.835	2.835	
34		(-) Helix			
35		.030 W	2.865	2.865	
36		Hoop			
37	7	.030 W	2.895	2.895	
38		(+)Helix			
39		.030 W	2.925	2.925	
40		(-)Helix			
41		.030 W	2.955	2.955	
42		Hoop			
43	8	.030 W	2.985	2.985	
44		(+)Helix			

Procedure 2380-TPSM
10/15/70

<u>Step</u>	<u>Layer</u>	<u>Type</u>	<u>Dimension (Diameter Uniform) 2 Loc.</u>		<u>Op. Stamp</u>
			<u>P #1 A</u>	<u>P #2 A</u>	
45		.030 W	3.015	3.015	
46		(-)Helix			
47		.030 W	3.045	3.045	
48		Hoop			
49	9	.030 W	3.075	3.075	
50		(+)Helix			
51		.030 W	3.105	3.105	
52		(-)Helix			
53		.020 W	3.125	3.125	
54		.010 Ta	3.135	3.135	

- 4 JH-TPSM Inspect as-sprayed specimen
- 5 Section (abrasive cut-off saw) into Specimen Blanks
- 6 JH-TPSM Grind (Machine) (-1) thermal diffusivity specimens (3 required)
- 7 JH-TPSM Grind (-2) thermal conductivity (6 required)
- 8 JH-TPSM Grind Specific heat specimens (-3) (5 required)
- 9 Inspect Specimens
- 10 Package and Store for Shipment

TENSION SPECIMENS - # 1T Through 7T
Per Drawing No. JH-622 T, Rev. A

Procedure # 2380 - 1T - 9/4/70

	Serial No. _____		
	<u>Operation</u>		<u>Operator Stamp</u>
	Description	M&P	Q.A.
1.	Receive Materials:		
	Qty		
a.	12#	Tungsten Powder - (-200, +325 mesh)	
b.	1/4#	Tantalum Powder	
c.	1 ea.	Graphite Mandrel - Drawing: JH-9170-M; ITEM 1	
d.	2 ea.	Stainless Steel Inserts - Drawing: JH-828-G, ITEM 1	
e.	As Req'd	1% Thoriated Tungsten Wire (.004" dia)	
2.	Assemble inserts & mandrel - JH-9470-F in rotating spray fixture		
3.	Fabricate Wire-Wound Tungsten Specimens - As Below		

Step	Layer	Type	Dia. #1		Dia. Gage		Dia. #2		Operator Stamp
			Plan	Actual	Plan	Actual	Plan	Actual	
0	0	^{op} #2	1.325		1.000		1.325		
1	1	W.010	1.335		1.010		1.335		
2		+Helix							
3		W.020	1.355		1.030		1.355		
4		-Helix							
5		W.020	1.375		1.050		1.375		
6		Hoop							
7	2	W.025	1.400		1.075		1.400		
8		+Helix							
9		W.025	1.425		1.100		1.425		
10		-Helix							
11		W	.050 1.475		.025 1.125		.050 1.475		
12		Hoop							

Step	Layer	Type	Dia. #1		Dia: Gage		Dia. #2		M&P Oper. Stamp
			Plan	Act.	Plan	Act.	Plan	Act.	
13	3	W	1.525		1.150		1.525		
14		+Helix							
15		W	1.575		1.175		1.575		
16		-Helix							
17		W	1.625		$\pm .010$ 1.200		1.625		
18		Hoop	Only In Grip Area						
19	4	W	1.675		---		1.675		
20		Hoop	Only In Grip Area						
21	5	W	1.700				1.700		
22		Hoop	Only In Grip Area						
23	6	W	1.725				1.725		
24		Hoop	Only In Grip Area						
25	7	W	1.750 (*)				1.750 (*)		
26	8	Ta	1.755 (*)		1.205 (*)		1.755 (*)		

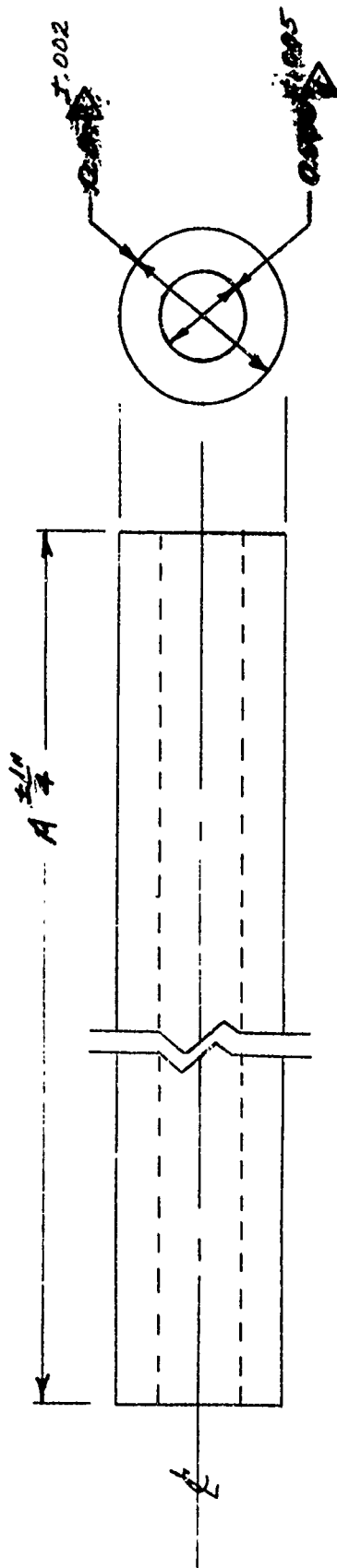
M&P

Q.A.

4. Inspect As-sprayed specimen
- (2)
5. Cut to $5-1/2 \pm 1/8$ Length (Mill ends to expose S. Steel)
6. Attach Serial Number to grip end
7. Remove Graphite Mandrel (subcontract)
8. Inspect inside diameter for machine nicks
9. Package and store for shipment

(1) It is intended that these diameters remain as sprayed!

(2) Save Ends



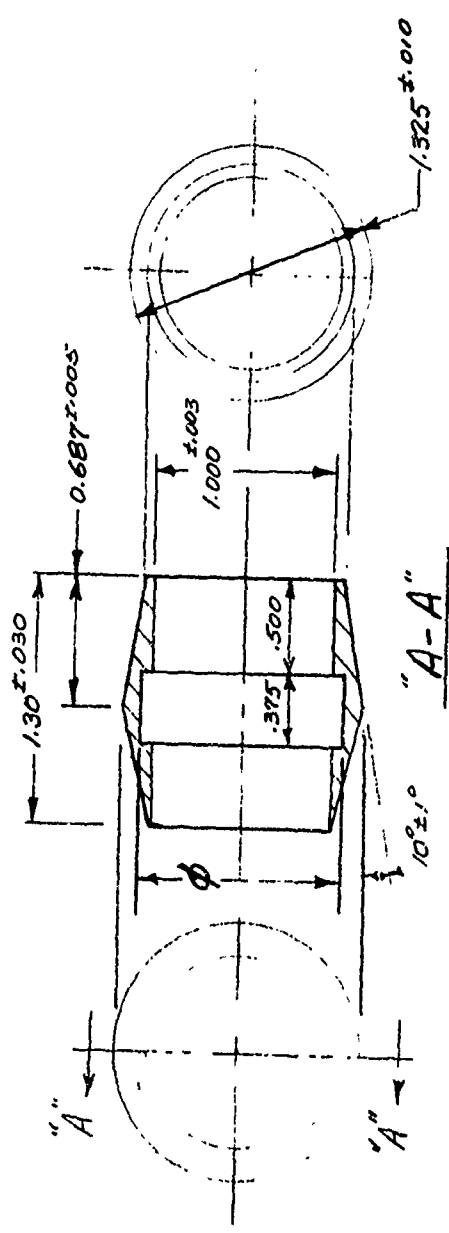
▽ DIAMETERS CONCENTRIC TO ϕ 0.002"

ITEM	O.D.	A	
-3	2.000	8	INTERNAL PRESS SPEC. - JH-622 IP
-2	1.625	11	TENSION/PRESS. SPEC. - JH-622 TIP
-1	1.000	8	TENSION SPECIMEN - JH 622 T

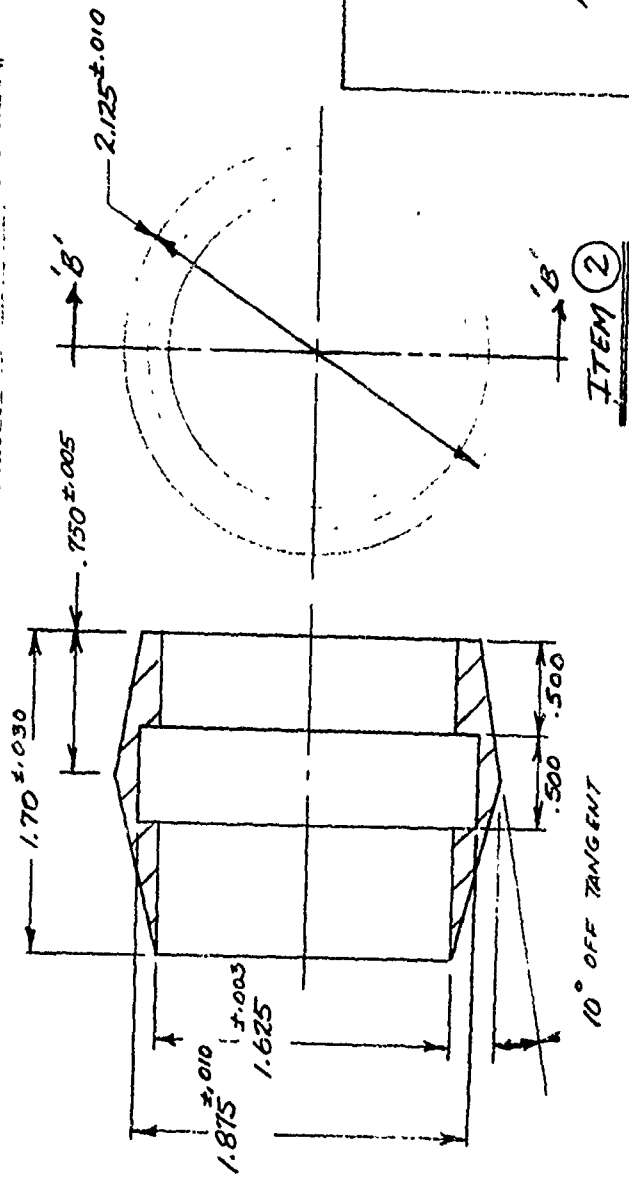
NOTE: 1) MAKE FROM ATJ GRAPHITE,
OR SPEER CARBON NO. 8882 GRAPHITE
2) SURFACE OF EXTERNAL DIAMETER
TO BE $\sqrt{32}$ OR BETTER.

MANDREL FOR W^3
MECHANICAL SPECIMENS
LAB. DWG.: (UTC MFP)
NO. JH-9170-M

ITEM 1



$\phi - 1.125 \pm .005$ DIAMETER



SECTION "B-B"

MATERIAL FOR BOTH ITEMS:
 304 STAINLESS STEEL
 OR EQUIVALENT

NOTE: 1. ITEM 1 USED ON
 JH-622 T

2. ITEM 2 USED ON
 JH-622 TIP

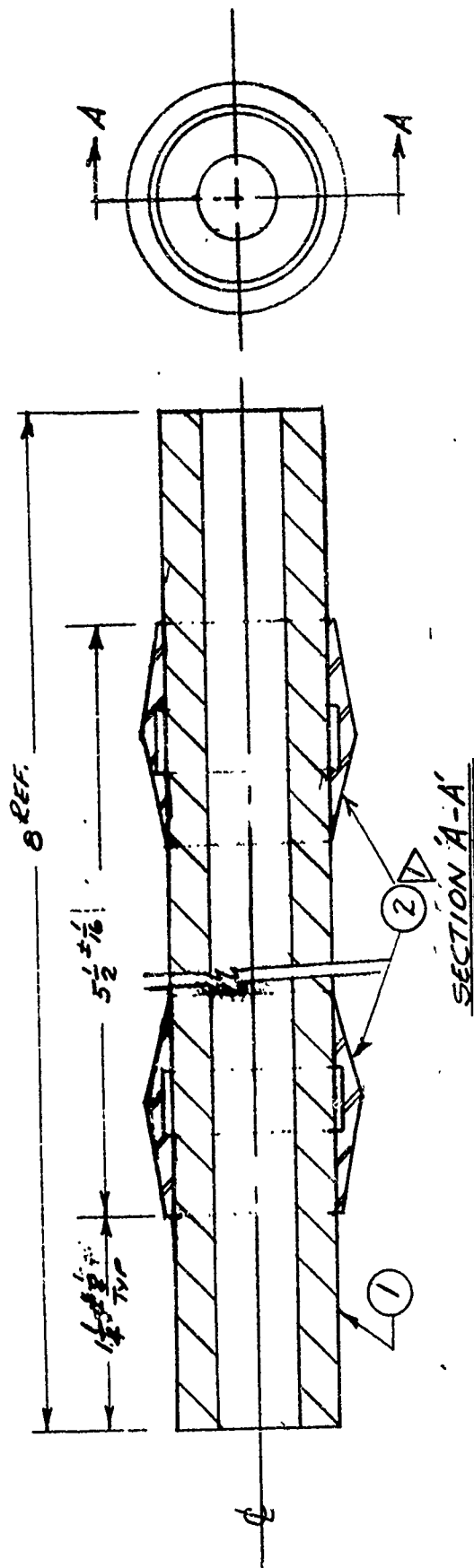
3. 63 FINISH ALL OVER

GRIP INSERT
 FOR WIRE-WOUND
 TUNGSTEN SPECIMENS

LAB. DRAWING (UTC-MFP)

NO. JH-828-S

REV.



NOTE REVERSE END LOCATION OF INSERTS

ITEM NO	QTY	DESCRIPTION
2	2	GRIP INSERT - PER JH-828-B ITEM ①
1	1	GRAPHITE MANDREL - PER UTC-MFP NO. JH-9170

MANDREL ASSY
for
W³ TENSION SPEC.
DWG.
No. JH-9470-F

Procedure 2380-T1P
9/8/70

PROCEDURE TO FABRICATE TENSION/INTERNAL PRESSURIZATION

Specimen^s No. T1P-1 thru T1P

Reference: Fab. Dwg. No. JH-622-T1P, Rev. A

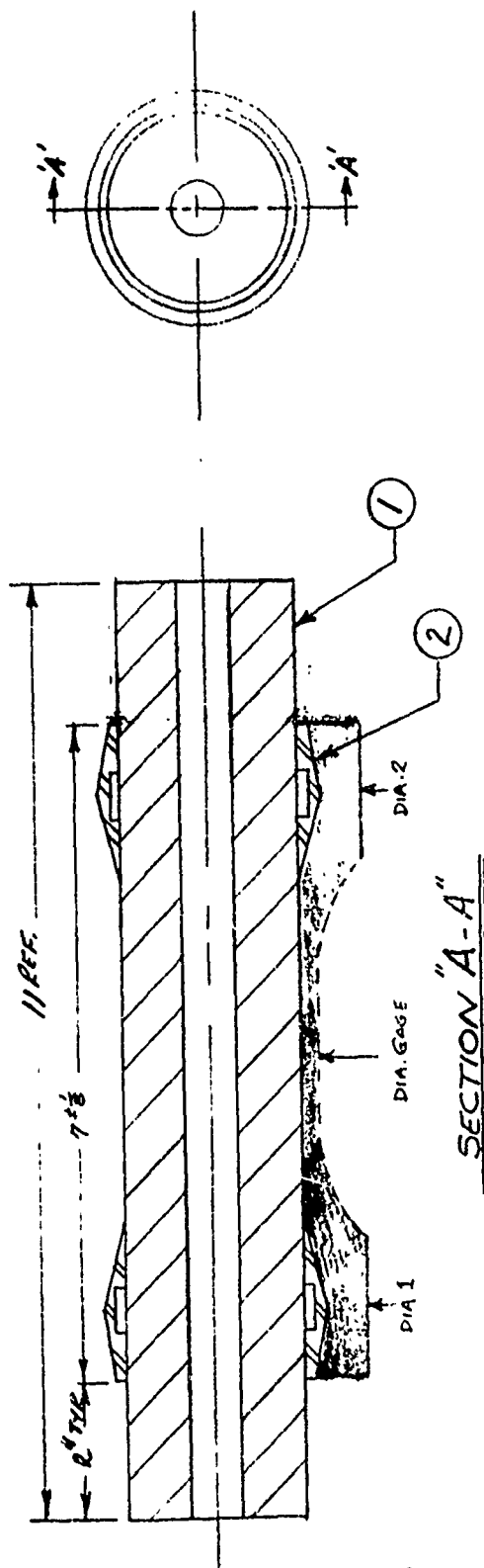
Serial No. _____

No.		Operation Description	Operator Sig.
1		Receive Materials	
	1	a) Mandrel per JH-9170-M; ITEM 2	
	2	b) Grip Inserts per Item 2 of JH-828G	
	~15#	c) Tungsten Powder (-200, +325 mesh)	
	~2#	d) Tantalum Powder (-200, +325 mesh)	
	As Req'd	e) Tungsten Wire (.004" dia Sylvania)	
2		Q.C. Approval _____	
3	JH-987F	Assemble grip inserts and mandrel	
4	JH-622T1P	Spray and Wind Specimen According to following schedule:	

Step	Layer	Type	Dia. #1		Dia. Gage		Dia. #2		Op. Stamp
			Plan	Act.	Plan	Act.	Plan	Act.	
0	0	Op. #3	2.125		1.625		2.125		
1	1	W.010	2.135		1.635		2.135		
2		(+)Helix	Wire						
3		W.020	2.155		1.655		2.155		
4		(-)H	Wire						
5		W.020	2.175		1.675		2.175		
6		Hoop	Wire						
7	2	W.025	2.200		1.700		2.200		
8		(+)H	Wire						
9		W	.050 2.250		.025 1.725		.050 2.250		

Step	Layer	Type	Dia. #1		Dia. Gage		Dia. #2		Op. Stamp
			Plan	Act.	Plan	Act.	Plan	Act.	
10	2	(-)Helix							
11		W	.050 2.300		.025 1.750		.050 2.300		
12		Hoop							
13	3	W	2.350		1.775		2.350		
14		(+)Helix							
15		W	2.400		1.800		2.400		
16		(-)Helix							
17		W	2.450		1.825		2.450		
18		Hoop							
19	4	W	2.500		1.850		2.500		
20		(+)Helix							
21		W	2.550		$\pm .010$ 1.875		2.550		
22		Hoop		Grip Area Only					
23	5	W	2.575				2.575		
24		Hoop		Grip Area Only					
25	6	W	2.600				2.600		
26	7	Ta	2.605		1.890		2.605		

4	JH-622T1P	Inspect As-Sprayed Specimen _____ Q.A.
5	JH-622T1P	Abrasive saw cut to $7 \pm 1/8$ length (save ends) _____ M&P
6		Attach Serial No. to grip end and scrap ends
7		Remove Graphite Mandrel
8		Inspect I.D. for Machine Defects
9		Package and Store for Shipment



NOTE: (1) 7 1/8" DIM. LOCATES SPECIMEN LENGTH.
 ESTABLISH REF. SURFACE FROM END OF
 MANDREL FOR SUBSEQUENT SECTIONING
 TO PRODUCE SPECIMEN.
 (2) SHADED AREA SHOWS SPEC. OUTLINE AND
 LOCATION OF SPRAY FAB. REF. DIA'S.

MANDREL ASS'Y
 FOR
 W³- TENSION/PRESS.
 SPECIMEN
 LAB. DWG. (UTC M&P)
 No. JH-987-F

2	2	GRIP INSERT PER JH-820-G; ITEM 2
1	1	MANDREL PER JH-9170-M, ITEM 2
ITEM QTY		

Procedure 2380-1PC
9/9/70

Title: PROCEDURE TO FABRICATE INTERNAL PRESSURIZATION/COMPRESSION

Specimens No: 1PC-1 Thru 1PC-7

Reference: Fabrication Drawing JH-622-1P

Schematic Drawing JH-FS-1PC

Serial No. _____

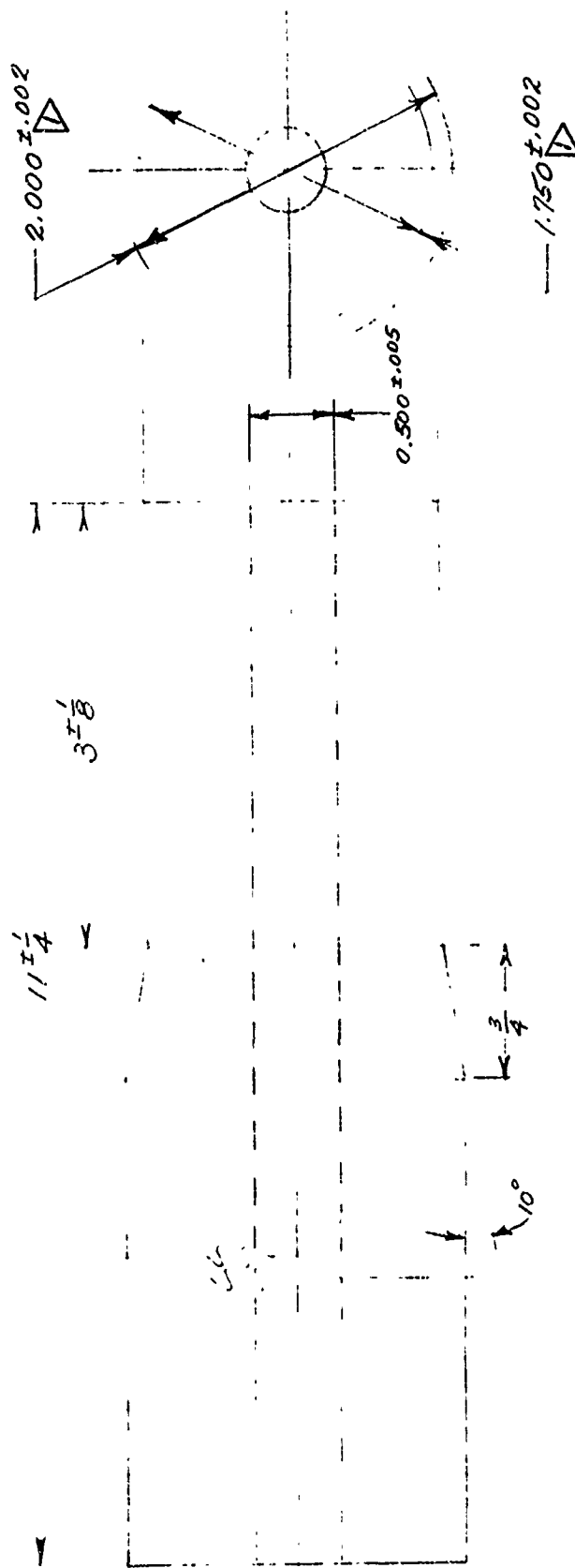
No.		Operation Description	Op. Stamp
1		Receive Materials	
	1 ea. JH-997M-	Spray Mandrel	
	~12#	Tungsten Powder (-200, +325)	
	~1#	Tantalum Powder (-200, +325)	
	As Req'd	1% Thoriated Tungsten Wire (.004" dia)	
2		Q.C. Approval	
3		Assemble Mandrel on Rotating Spray Fixture	
4	JH-622-1P	Spray & Wind Specimen According to following Schedule	

Step	Layer	Type	Dia. #1		Dia. #2		Dia. #3		Op. Stamp
			Plan	Act.	Plan	Act.	Plan	Act.	
0	0	Op. #3	2.000	_____	2.000	_____	1.750	_____	
1	1	W-.010	2.010	_____	2.010	_____	1.760	_____	
2		(+)Helix							
3		W-.020	2.030	_____	2.030		1.780		
4		(-)Helix							
5		W-.020	2.050		2.050		1.800		
6		Hoop							
7	2	W-.025	2.075	_____	2.075		1.825	_____	
8		(+)Helix							
9		W-.025	2.100	_____	2.100	_____	1.850		
10		(-)Helix							
11		W-.025	2.125		2.125	_____	1.875		
12		Hoop							

Step	Layer	Type	Dia. #1		Dia. #2		Dia. #3		Op. Stamp
			Plan	Act.	Plan	Act.	Plan	Act.	
13	3	W-.025	2.150	_____	2.150	_____	1.900	_____	_____
14		(+)Helix							
15		W-.025	2.175	_____	2.175	_____	1.925	_____	_____
16		(-)Helix							
17		W-.025	2.200	_____	2.200	_____	1.950	_____	_____
18	4	Hoop							
19		W-.025	2.225	_____	2.225	_____	1.975	_____	_____
20		(+)Helix							
21		W-.025	2.250	_____	2.250	_____	2.000	_____	_____
22		Hoop							
23		W-.020	2.270	_____	2.270	_____	2.020	_____	_____
24		Ta-.010	2.280	_____	2.280	_____	2.030	_____	_____

M&P - Q.A.

5	JH-622-1P	Inspect As-Sprayed Specimen	
6	JH-FS-1PC	Abrasive Saw Cut to Separate Int-Nut Press and Compression Specimens	
7		Attach Serial No.	
8		Remove Graphite Mandrels	
9		Inspect Inside Diameter for Nicks	
10		Package & Store for Shipment	

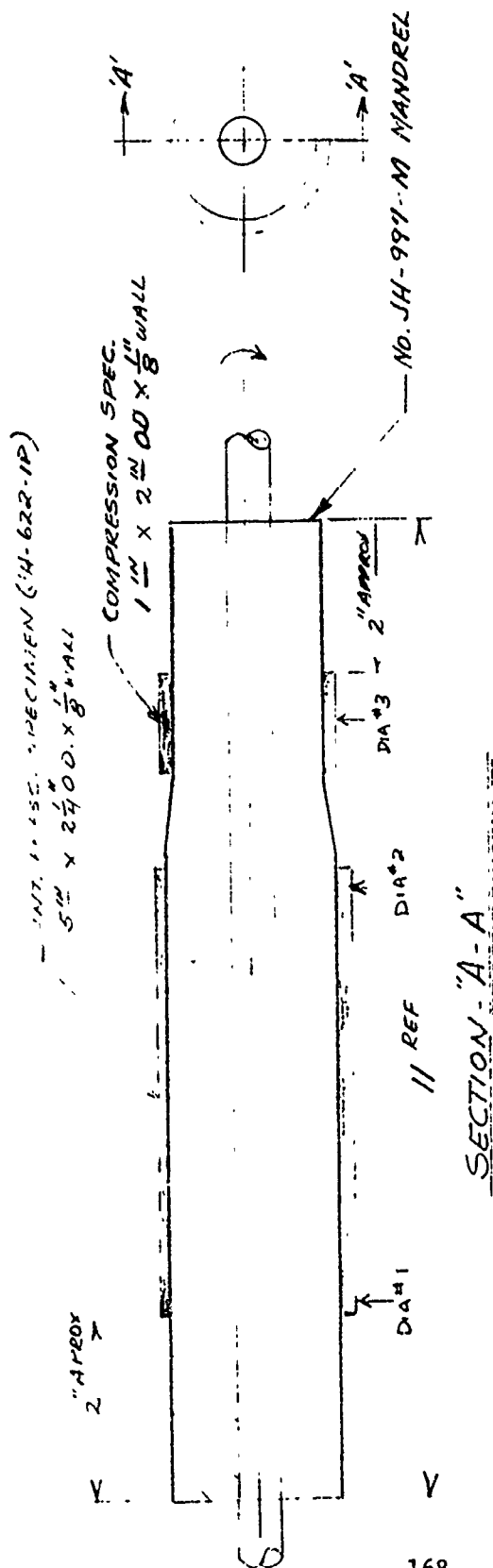


NOTE: ∇ THESE DIA'S CONCENTRIC TO ϕ WITHIN 0.002"

2. MAKE FROM ATJ GRAPHITE OR SPEER CARBON NO. 8882 GRAPHITE
3. SURFACE OF EXTERNAL DIA'S TO BE $\nabla 32$ OR BETTER

MANDREL: COMBINATION
INT. PRESS/COMPRESSION
SPECIMENS
LAB DWG. (UTC M&P)
No: JH-997-M

Revised by
JSA, 7/8/70



SHADED AREAS REPRESENT DESIRED SPECIMEN'S
 DIA'S #1, 2, 3 ARE IN-PROCESS MEASUREMENT LOCATIONS
 (SEE - 2380-1PC - FAB. PROCEDURE)

Repaired,
 JGD, 9/10/70

SCHEMATIC OF
 SET-UP TO PRODUCE
 W³ INT. PRESS. &
 COMPRESSION SPEC.'S

No. JH-FS-1PC

APPENDIX II

THERMAL CONDUCTIVITY MEASUREMENT BY THE SELF-GUARDING DISK TECHNIQUE

This is a steady-state technique which is appropriate for solids having low-to-moderate thermal conductivities. It has been developed and used at Battelle-Columbus for measurements over the range from -190 C to 2500 C, and is particularly appropriate for anisotropic material, because it features one-dimensional heat flow.

In this technique, a heat flow is established from a source through a specimen and a heat flow meter in series, to a sink. Under equilibrium conditions, temperatures in the specimen and meter are recorded and conductivity is calculated from the one-dimension relation

$$k = \frac{q}{A} \frac{L}{\Delta T}$$

where

k = thermal conductivity

q/A = heat flow per unit area

L = axial distance between temperature measurement points

ΔT = temperature difference across L .

The temperatures can be determined with good accuracy with thermocouples or optical pyrometer. Pertinent dimensions can also be measured accurately. The heat flow meter is constructed of a material which is appropriate as a thermal conductivity standard, and has a conductivity not greatly different from that of the specimen being measured. The meter materials used at Battelle include Pyroceram 9606, Type 347 stainless steel, and Armco iron.

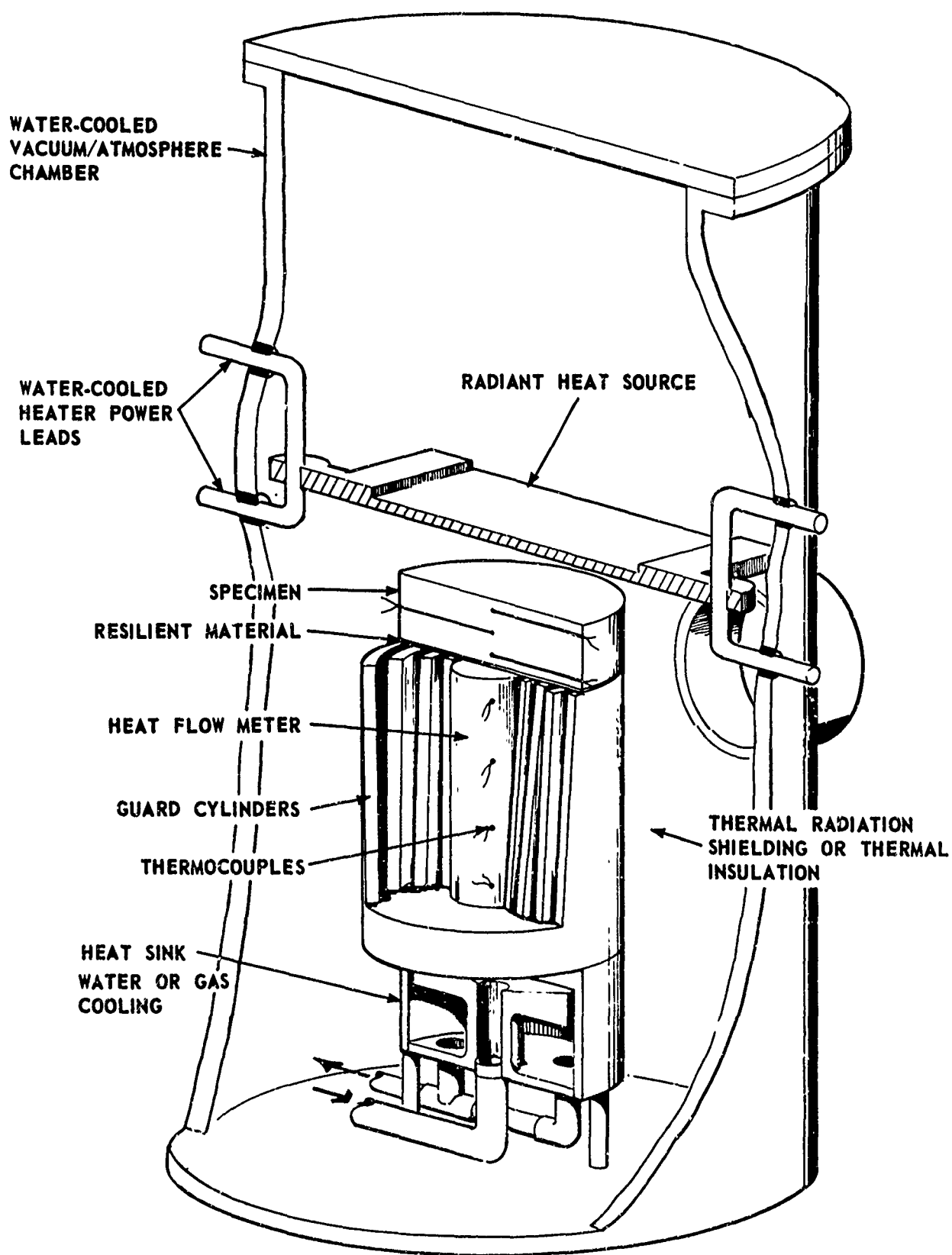
The specimen is a 3-in.-diameter disk; the disk thickness is selected on the basis of anticipated conductivity and desired measurement conditions. During measurement, heat is introduced uniformly over one face of the disk, and removed uniformly from the opposite face; i.e., axial heat flow.

However, only the central 1-in. diameter is considered to be the heat section; the remaining part guards against radial heat flow from this section. Specimen temperatures, hot face and cold face, are measured with either thermocouples or optical pyrometer. The arrangement varies with specimen material and estimated conductivity.

The meter is constructed so that heat flow along its axis will also be one-dimensional. The meter proper, the central 1-in.-diameter section, is surrounded by guard walls which are part of the one-piece structure. Thermocouples measure temperatures along the axis of the meter, and also at corresponding elevations in the guard walls; the former permit calculation of heat flow through the meter, and specimen, and the latter confirm one-dimension heat flow in the meter assembly.

The heat source is a resistance element selected on the basis of temperature range and compatibility with the specimen. The heat sink can be cooled with liquids or gases, or can be resistance heated to achieve desired thermal conditions. The entire assembly is contained in a vacuum-atmosphere chamber. Figure 1 shows the arrangement schematically; the various alternate arrangements of heat sources and sinks which are possible are, of course, not illustrated. Also not shown is the insulation which surrounds the assembly inside the chamber.

The net potential error in absolute value of the conductivity measured by this technique usually does not exceed ± 10 percent, and can be held to ± 5 percent if relatively ideal conditions (choice of meter, temperature measurement, etc.) can be employed. Errors in relative values are usually within ± 5 percent. These error estimates are based on results of measurements of "standard" materials.



HIGH-TEMPERATURE, THERMAL- CONDUCTIVITY APPARATUS FOR DISK SPECIMEN

FIGURE 1

APPENDIX III

THERMAL DIFFUSIVITY MEASUREMENT

Laser Pulse Technique

Thermal diffusivity measurements were made by the flash-laser technique. The technique employed was to position a thin disk-shaped specimen in the isothermal zone of a furnace and irradiate the front face by a short-duration laser pulse. As the heat pulse travels through the specimen, the back face temperature rise is recorded as a function of time. A dimensionless plot of the rear-surface temperature history is shown in Figure 1. The thermal diffusivity is given by

$$\alpha = \frac{0.48 L^2}{\pi^2 t_x} \quad , \quad (B-1)$$

where

α = thermal diffusivity

L = specimen thickness

t_x = time-axis intercept of straight-line
portion of time-temperature history.

Figure 2 is a photograph of the Battelle-Columbus thermal diffusivity apparatus. Figure 3 is a section drawing showing some internal details.

The specimen and heater were protected by an atmosphere of argon at atmospheric pressure. The specimens were held in a tantalum holder inside a double-walled tantalum tube heater. Specimen temperatures were measured with a thermocouple, the bead of which was placed adjacent to the specimen. Thermal-radiation shielding surrounds the heater.

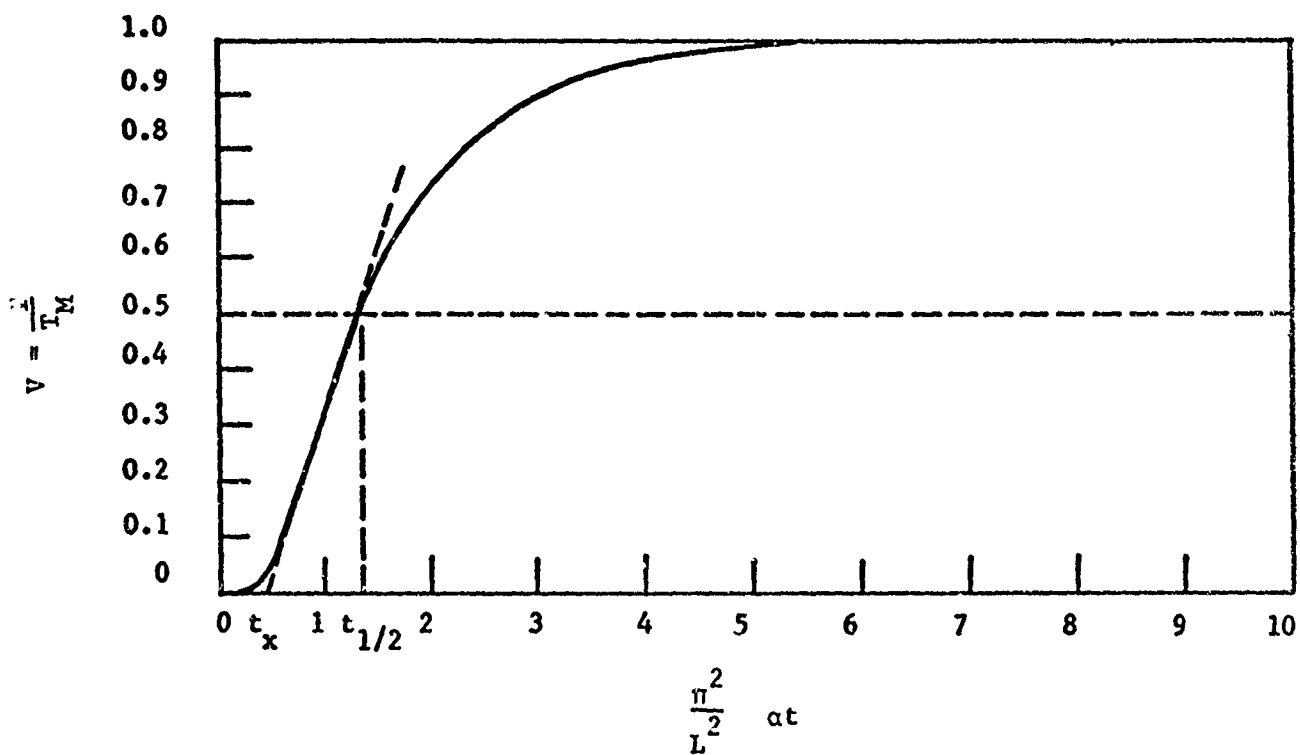


FIGURE 1. DIMENSIONLESS PLOT OF REAR-SURFACE TEMPERATURE HISTORY

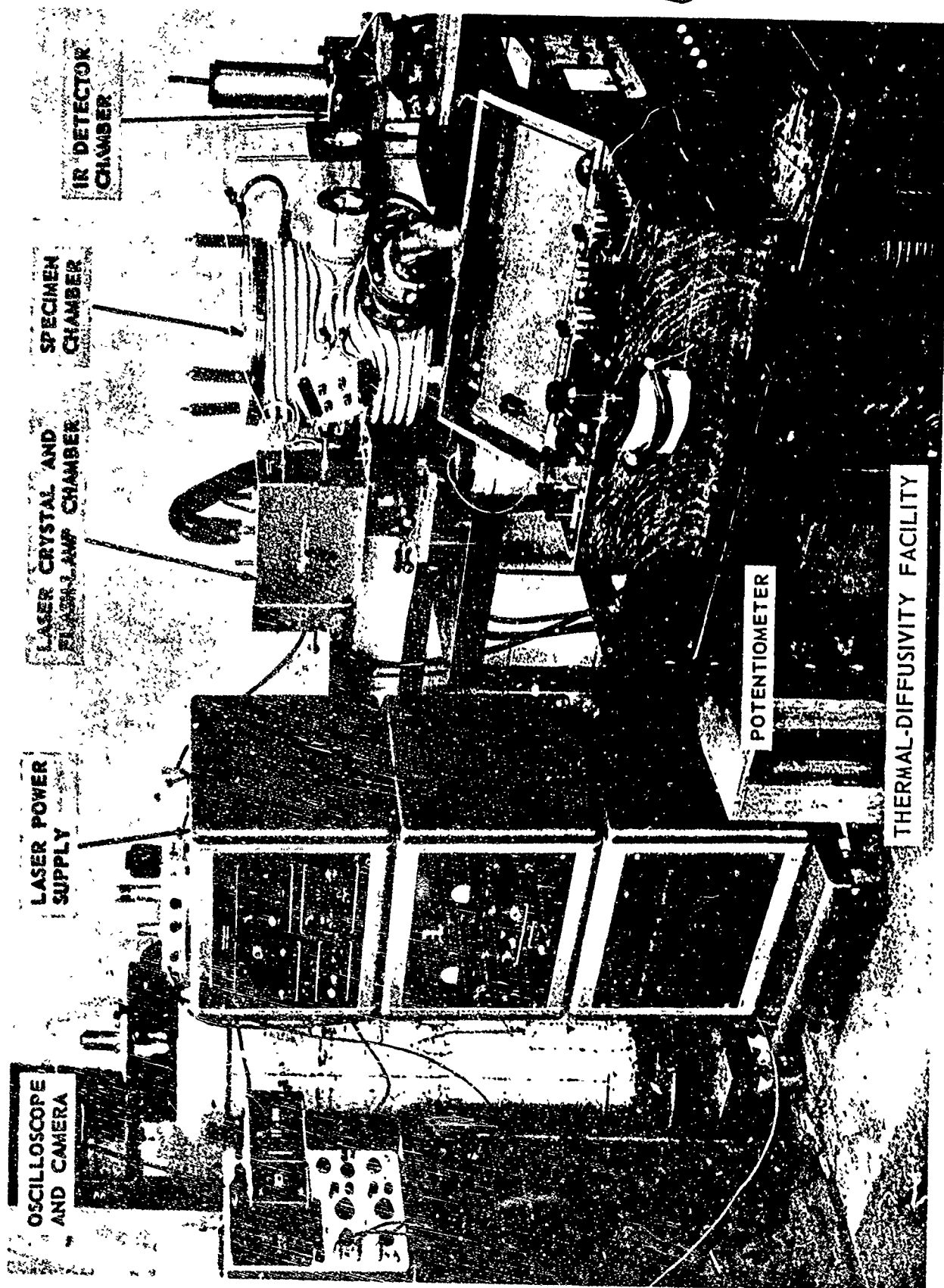


FIGURE 2

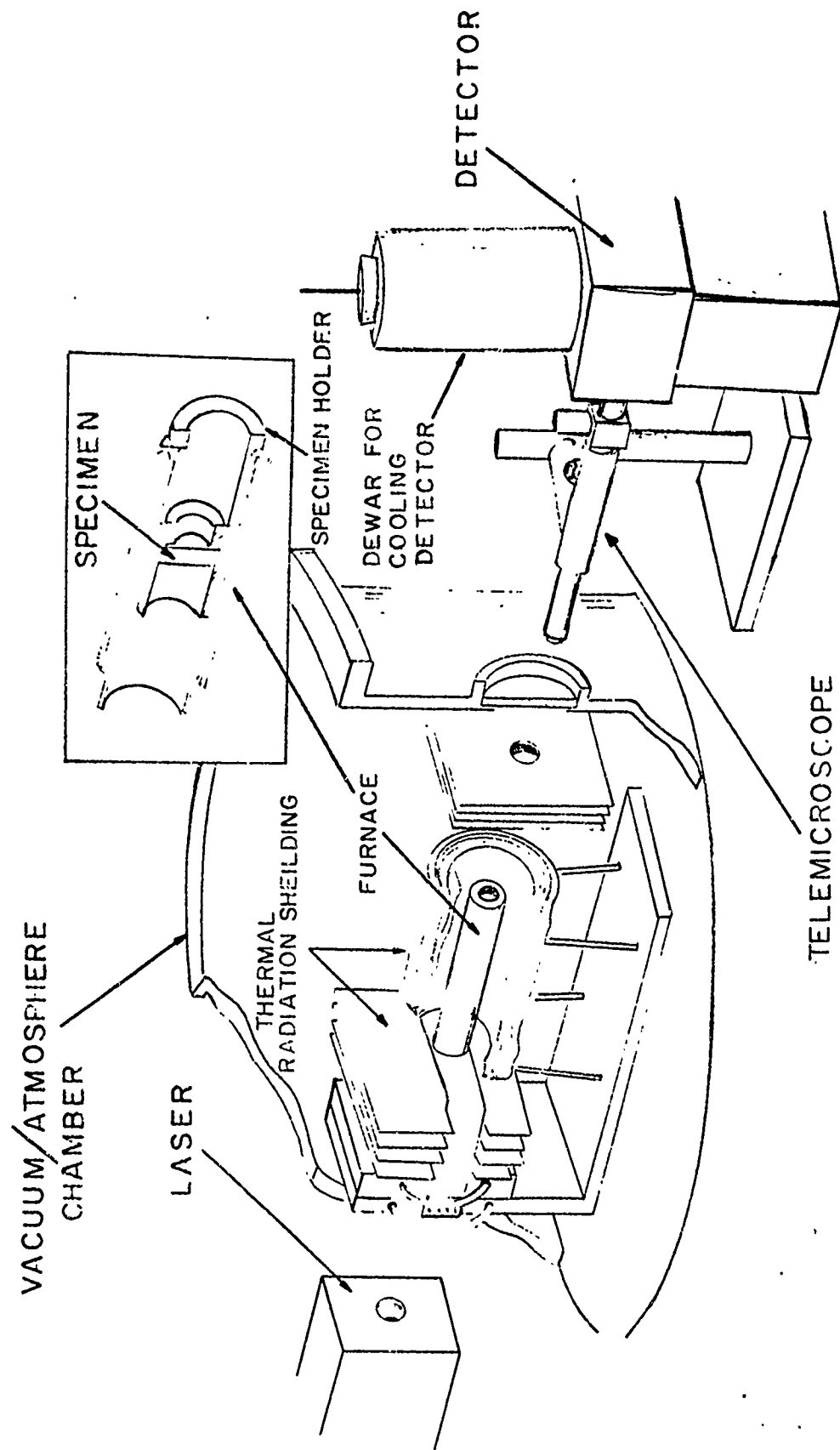


FIGURE 3. THERMAL DIFFUSIVITY APPARATUS

The radiation detector is shown in position to view the back face of the specimen. A lead sulfide cell is presently being used as the radiation detector. The detector is placed in one arm of a bridge circuit, the unbalance of which is shown on an oscilloscope and photographed by a camera. This provides a record of the rear-face time-temperature history from which t_x is read.

The error of thermal diffusivity values measured by the method described is estimated not to exceed ± 5 percent below 1800 C and ± 8 percent above 1800 C. These estimates are based on a weighted average of standard materials over a wide temperature range. Both the directly determined diffusivity values and derived thermal conductivity values have been compared with accepted literature values to arrive at these estimates.

APPENDIX IV

SPECIFIC HEAT MEASUREMENT

Ice Calorimeter Technique

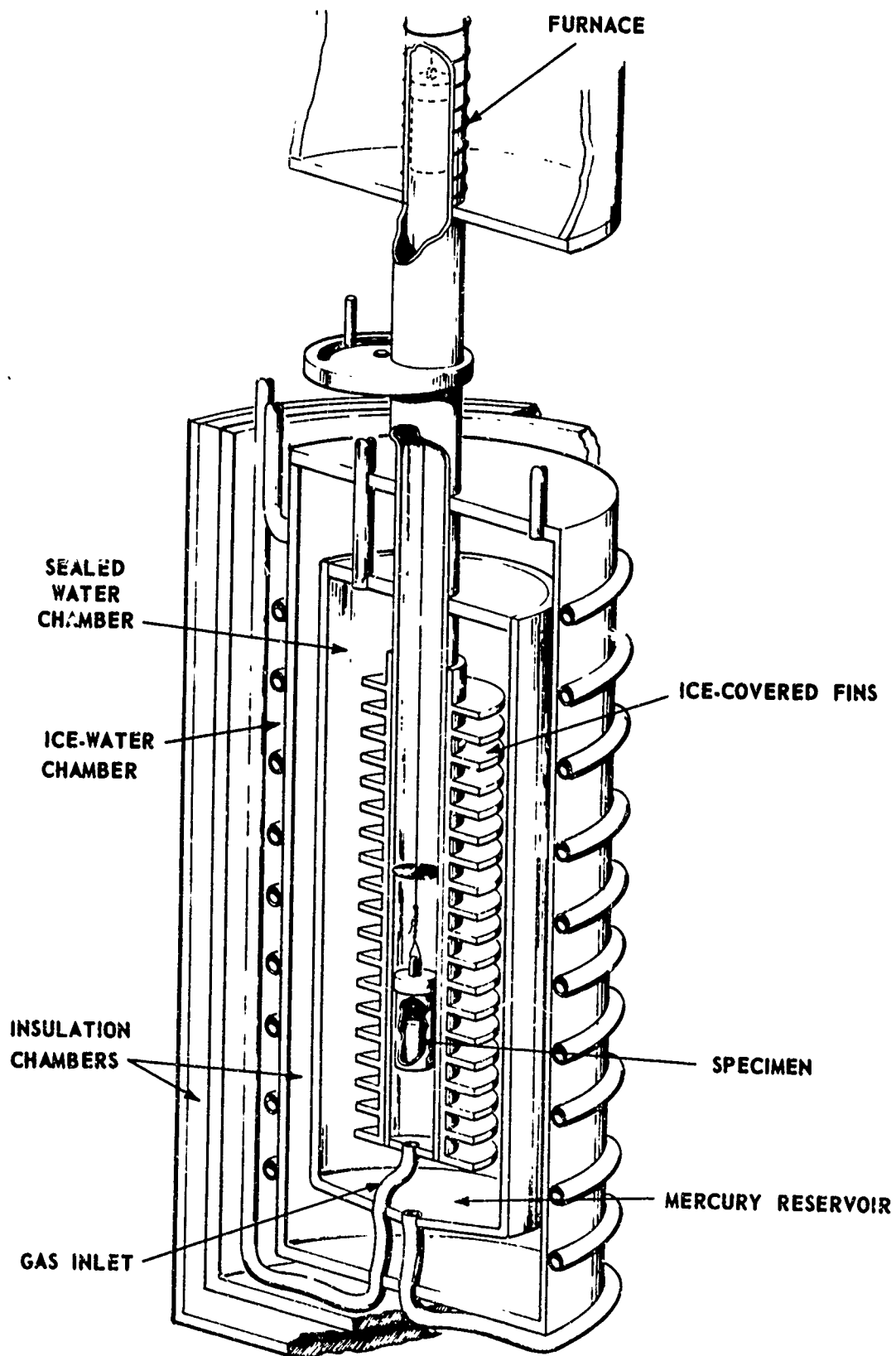
In this technique, specific heat is determined from graphical and analytical treatment of enthalpy data measured in a Bunsen-type ice calorimeter. Heat given up by a specimen in cooling from a preheated temperature to the ice point is measured in terms of the quantity of ice melted in a sealed water-ice system at 0 C. The quantity transfer agent is mercury; the amount transferred to or from the sealed system is determined by difference weighings. The constant for the system has been carefully determined, it is 270.48 joules per gram of mercury. Since all heat transfer is measured at the ice point, there is no need to measure temperatures in the calorimeter.

Figure 1 shows schematically the calorimeter arrangement. The specimen to be measured is encapsulated and heated to a desired temperature in a furnace above the well. It is then dropped into the well. Separate drops of an empty capsule of the same material and surface emittance determine the contribution of heat by the specimen by difference, and also virtually eliminate problems of heat loss by radiation from the specimen before it enters the well. The process is repeated through the temperature range of interest to establish an enthalpy-temperature curve. Specific heat is then calculated as the slope of this curve.

Specimen temperatures are measured by thermocouple or optical pyrometer. Calibration of the apparatus is checked frequently, using National Bureau of Standards Al_2O_3 as the standard. Agreement with NBS values is routinely within 1 percent.

For measurements below the ice point, the specimen is cooled to the desired temperature before dropping it into the well.

The present operating temperature range of the ice calorimeter is -190 C to 2200 C.



ICE CALORIMETER

FIGURE 1

APPENDIX V

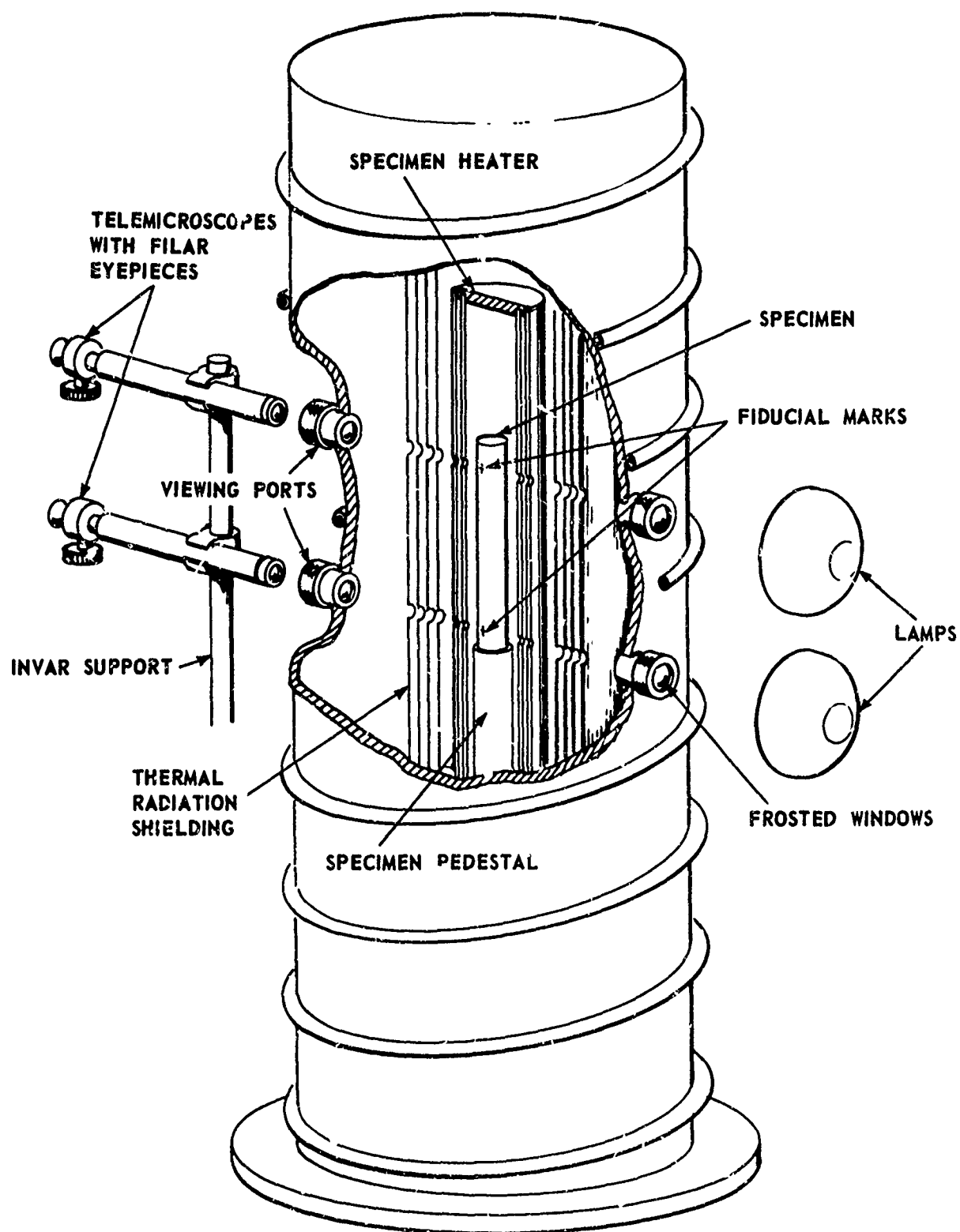
THERMAL EXPANSION MEASUREMENT

Direct View Dilatometer Technique

In this technique, the expansion or contraction of solids is measured directly by tracking, during heating or cooling, the relative displacement of fiducial marks on a specimen with telemicroscopes fitted with filar eyepieces.

Figure 1 schematically illustrates the measurement apparatus. The specimen, suitably marked, is supported within a tube furnace enclosed in an insulated vacuum/atmosphere chamber. Dilation on heating or cooling is tracked manually with the microscopes; specimen temperature is measured by either thermocouple or optical pyrometer. Figure 2 is a photograph of the apparatus.

Dilations of the order of 7×10^{-6} in. can be measured with this equipment; the nominal specimen length is 2-3/4 in. The temperature range currently covered is from room temperature to 2500 C.



HIGH-TEMPERATURE DILATOMETER AS USED FOR
DIRECT-VIEW EXPANSION MEASUREMENTS

FIGURE 1

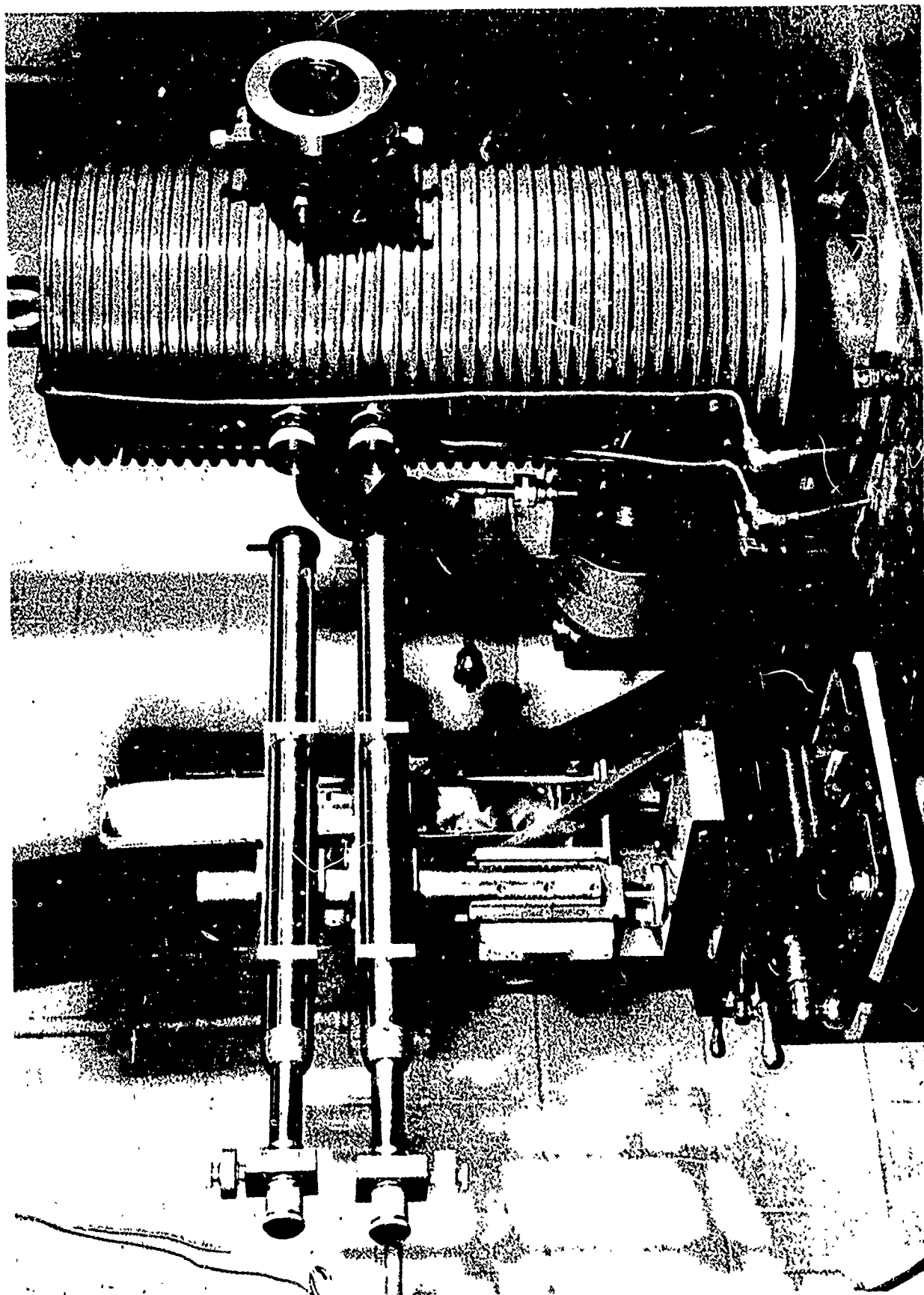


FIGURE 2. HIGH-TEMPERATURE RECORDING DILATOMETER

APPENDIX VI
SPECIFICATION

WIRE-WOUND-TUNGSTEN COMPOSITE

1. SCOPE. This specification covers the preparation of tungsten composites consisting of a plasma-arc sprayed tungsten matrix reinforced by filament windings of tungsten wire.

2. APPLICABLE DOCUMENTS

2.1 Government documents. The following documents of the issue in effect on date of invitation for bids form a part of this specification to the extent specified herein.

SPECIFICATIONS

Military

MIL-R-11470	Radiographic Inspection, Qualification of Equipment, Operators, and Procedures
-------------	--

STANDARDS

Federal

FED-STD-157	Metals, Test Methods
-------------	----------------------

Military

MIL-STD-453	Inspection, Radiographic
-------------	--------------------------

MIL-STD-129	Marking for Shipment and Storage
-------------	----------------------------------

(Copies of documents required by suppliers in connection with specific procurement functions should be obtained from the procuring activity or as directed by the contracting officer.)

2.2 Other publications. The following documents form a part of this specification to the extent specified herein. Unless otherwise indicated, the issue in effect on date of invitation for bids shall apply.

AMERICAN SOCIETY FOR TESTING AND MATERIALS (ASTM)

Standard

ASTM-B-311	Standard Method of Test for Density of Cemented Carbides
------------	--

(Application for copies should be addressed to American Society for Testing and Materials, 1916 Race Street, Philadelphia, Pennsylvania).

3. REQUIREMENTS

3.1 Materials. The materials of composite construction shall consist of tungsten powder and 1% thoriated tungsten wire in accordance with the requirements herein.

3.1.1 Tungsten powder. Tungsten powder as determined by a check analysis of the deliverable product shall conform to the chemical and physical requirements of Table I.

Table I

Physical and Chemical Requirements of Tungsten Powder

A. <u>Element</u>	Wt. %
tungsten (W)	99.7 minimum
molybdenum (Mo)	0.15 maximum
All other elements	0.15 maximum
B. <u>Physical Characteristics</u>	
bulk density (Scott)	100 - 175 gms/cu. in
flow rate (Hall)	15 seconds (max.)
Fisher No.	44 microns
Screen size	+200 - 5% max -200 +325 - 65% min -325 - 30% max

3.1.2 1% Thoriated Tungsten Wire. The wire as determined by a check analysis of the deliverable product shall conform to the chemical and physical requirements of Table II.

Table II

Requirements for Tungsten Wire

A. Chemical Analysis

Element	Wt. %
tungsten (W)	98.90 minimum
thoria (as tungsten metal powder)	0.95-1.05
all other elements	0.15-max

B. Physical Characteristics

tensile strength	65,000 psi \pm 5000 psi
end to end wire tolerance	1% max
out-of-round	4% max
wire size	30.15 mg/200 mm (.004-inches dia)

3.2 Mandrels. Mandrels required for fabrication of wire-wound tungsten composites shall be machined from graphite which conforms to the physical requirements of Table III. The surface of machined mandrels shall be 32 rms or finer.

Table III

Physical Requirements for Graphite Mandrels

Apparent density (g/cc)	- 1.75 ± .05
Specific resistance (ohm-inches)	- .00045 ± .00005
Coefficient of Thermal Exp (10^{-6} in/in $^{\circ}$ C)	-
with grain	- 3.2 ± .1
across grain	- 5.2 ± .1
Ash content (%)	- .06 max
Flexural Strength (psi min)	
with grain	- 4200
across grain	- 3800

3.3 Process. Using the materials of construction wire-wound-tungsten composites shall be processed in accordance with procedures developed for the required component configurations. The composite shall consist of individual layers of plasma-arc-sprayed tungsten and windings of tungsten filament. Filament orientation and percent loading shall be in accordance with design structural requirements.

3.3.1 Plasma Arc Gas. The plasma arc gas used in plasma-arc-spraying the tungsten powder matrix, shall be a mixture of 95% argon and 5% hydrogen.

3.3.2 Powder gas. The powder gas used to carry the tungsten powder to the plasma flame, shall be commercially pure argon (99.5%).

3.4 Mandrel Removal. Mandrels shall be removed from the composite in a manner which shall not produce imperfections at the composite interface.

3.5 Density. The bulk density shall be determined in accordance with ASTM-B-311 and shall be 85% ± 3% of the theoretical density of pure tungsten (19.3 g/cc).

3.6 Chemical composition. The chemical composition of the processed composite shall be essentially tungsten, except that the following impurity maximums, as determined by vacuum fusion shall be allowed:

Oxygen	- 3000 ppm
Nitrogen	- 300 ppm

3.7 Defect Limits. The processed composite when visually inspected shall be free of injurious surface discontinuities, such as cracks, laps, edge delaminations, and exposed filaments. When subjected to radiographic inspection the composites shall be free from injurious internal imperfections, such as cracks, delaminations and mis-oriented filaments.

3.7.1 Internal defects. When required by drawing requirement wire-wound tungsten composites shall be radiographed for evaluation of internal defects. Composites less than 0.250 inch-thick shall be radiographed by a 3000 rhm Cobalt 60 source (or equivalent) using techniques and operators qualified in accordance with MIL-R-11470. Composites greater than 0.250-inch thick shall be radiographed by neutron radiography with a neutron flux capability of 3.5×10^9 . For either method, the radiographic procedures established on a known defect-containing wire-wound-tungsten standard shall be used.

3.8 Mechanical properties. When specified by drawing requirement, the composite shall meet the following mechanical properties (sec 4.2.4 and 4.3.2) as determined by a compression test.

- a) Ultimate compressive strength, psi-30,000 min
- b) Elastic modulus ($\times 10^6$ psi)-5.8 min
- c) Poisson's ratio (record for reference)

3.9 Identification. Materials used in the preparation of wire-wound tungsten composites shall be identified with the following information as applicable:

- a) Number and revision letter of this specification
- b) Supplier identification
- c) Supplier heat (or lot) number

3.10 Reports. Three copies of the certified test report covering the test results for each heat shall accompany each shipment of raw material. This report shall include the following:

- a) Name of the supplier
- b) Serial and part number
- c) The testing laboratory used for tests
- d) Purchase order number
- e) This specification number and applicable revision letter
- f) Physical dimensions or referenced engineering document
- g) Quantity from each heat or lot.

3.11 Exceptions to Requirements. Any departure from the stated requirements herein must have written UTC approval prior to manufacturing.

4. QUALITY ASSURANCE PROVISIONS

4.1 Classification of tests. Inspection and testing of the bars and forgings shall be classified as:

- a) Acceptance tests (see 4.1.1)

4.1.1 Acceptance tests. The acceptance tests shall consist of all the inspections and tests specified herein.

4.2 Sampling. Sampling shall be accomplished in accordance with the following.

4.2.1 Chemical. At least one sample for chemical analysis shall be taken from each heat (lot) of material to be used in the composite construction and for each fabricated composite component. Chemical analysis of the fabricated composite shall be obtained from excess ends provided for in the fabrication procedure. Each sample shall consist of not less than two ounces of material.

4.2.2 Density. Each fabricated composite shall be tested for bulk density. Density shall meet the requirements of 3.5.

4.2.3 Defects. Each fabricated composite shall be inspected for surface defects, and when required by design specification for internal defects. Defect limits shall meet the requirements of 3.7.

4.2.4 Compression Specimens. Two or more compression specimens shall be prepared for each design application of a wire-wound-tungsten composite component. The specimens shall be 2-in O.D. by 1.75-inch I.D. by 1 in long and shall be prepared by plasma-arc spraying and filament reinforcement in a manner which duplicates the composite construction.

4.3 Test methods. The following test methods shall be used to determine that the materials of construction and the fabricated composite meets the requirements of this specification.

4.3.1 Chemical Composition. Chemical analysis shall be accomplished in accordance with FED-STD-151, method 112.1 (Spectro-chemical), except for oxygen and nitrogen which shall be by the vacuum fusion method.

4.3.2 Compression test. Compression specimens shall be tested in accordance with method 211.1 of FED-STD-151, except that the load shall be applied in compression and shall be normal to the centerline of the specimen. Elastic modulus shall be determined from a plot of stress vs. strain as recorded by strain gauges bonded to the specimen surface.

4.3.3 Test for Internal Defects. Composite components shall be inspected for internal defects by radiographic techniques. Photon radiography shall be used for composites less than 0.250-inch thick and neutron radiography shall be used for composites greater than 0.250-inch thick. Radiographic techniques shall be approved by the customer and shall be capable of revealing internal defects as contained in a standard sample. This standard shall be used in each radiograph in the manner of a penetrameter.

5. PREPARATION FOR DELIVERY

5.1 Packing. All material shall be packed in water tight containers and shall be further protected from damage by polyethylene bags or liners.

5.2 Marking. Interior packages and exterior shipping containers shall be marked in accordance with MIL-STD-129, and shall include, but not be limited to, the following information:

- a) Supplier's name
- b) Product designation
- c) Lot number or heat number
- d) Date of manufacture
- e) Number of pieces
- f) Purchase order number